TECHNICAL SOLUTIONS TO IMPROVE

Cardiac Regenerative Therapy

F.J. VAN SLOCHTEREN

Technical Solutions to Improve Cardiac Regenerative Therapy

ISBN: 978-90-8891-862-9
Vormgeving en Lay-out: wenz iD I Wendy Schoneveld, www.wenziD.nl
Printed by: BOXPress BV II Proefschriftmaken.nl
Published by: Uitgeverij BOXpress, 's-Hertogenbosch

Technical Solutions to Improve Cardiac Regenerative Therapy

Nieuwe technieken ter verbetering van cardiale regeneratieve therapie
(met een samenvatting in het Nederlands)

Proefschrift

ter verkrijging van de graad van doctor aan de Universiteit Utrecht
op gezag van de rector magnificus, prof.dr. G.J. van der Zwaan,
ingevolge het besluit van het college voor promoties in het openbaar
te verdedigen op woensdag 23 april 2014
des middags te 4.15 uur

door

Frebus Jan van Slochteren
geboren op 3 september 1977
te Oldekerk

Promotor: Prof. dr. P.A.F.M Doevendans

Co-promotoren: Dr. S.A.J. Chamuleau
Dr. Ir. C.L. de Korte

Financial support by the Heart & Lung Foundation Utrecht and Dutch Heart Foundation for the publication of this thesis is gratefully acknowledged.

Publication of this thesis was additionally supported by Stichting Cardiovasculaire Biologie, Volcano, Chipsoft, Biologics Delivery Systems™; a Johson and Johnson Medical Company

Contents

CHAPTER 1

General introduction and outline of the thesis

Cardiovascular disease is the number one cause of death throughout the world. Worldwide nearly 17 million people died in 2011 due to cardiovascular disease representing 30% of all global deaths. Ischemic heart disease (IHD) is the predominant contributor to cardiovascular morbidity and mortality. Seven million people died of ischemic heart disease in 2011 (WHO website July 2013). In the USA approximately 1 million myocardial infarctions (MIs) occur per year and more than 5 million patients suffer from chronic heart failure (HF)[1]. In combination with increasing incidence of cardiac risk factors such as obesity, hypertension and diabetes, IHD will remain to be a leading course of morbidity and mortality worldwide, and consequently a huge burden for society.

Ischemic heart disease

Ischemic heart disease (IHD) is a general term used to appoint cardiac diseases related to the mismatch between the supply and the demand for oxygen and nutrients of the heart to fulfill its function. IHD leads to a decreased left ventricular (LV) pump function, causing severe clinical symptoms. Clinically, three phases of the disease can be distinguished: Acute myocardial infarction (AMI), refractory angina pectoris (RAP), and heart failure (HF). During AMI a coronary artery is blocked due to a thromboembolic event caused by the rupture of a plaque in the artery. Consequently the blood flow to the cardiac muscle is decreased or totally blocked, leading to loss of cardiomyocytes. When the patient is transported timely to the hospital for a revascularization procedure via a percutaneous coronary intervention (PCI), coronary blood flow is restored[2], left ventricular function is improved, infarct size is limited, and clinical symptoms are reduced[3-5]. Paradoxically, the acute and complete restoration of blood flow also leads to mitochondrial re-energization, reactive oxygen species, intracellular Ca^{2+} overload and inflammation. It leads to so-called reperfusion injury and reduces the beneficial effect of the revascularization[6-8]. Currently PCI is the best available treatment for AMI patients. Despite the intervention, patients can develop clinical symptoms related to the ischemic event.

In patients suffering from RAP the coronary- and micro- vasculature and the myocardium are unable to adapt to the increased demand for oxygen and nutrients during exercise, leading to severe chest pain[9]. Pharmacological treatment of these patients with vasodilators, ACE inhibitors, and beta blockade aims to improve cardiac function, and relieve clinical symptoms[10]. Furthermore, antiplatelet drugs and statins are applied for preventive purposes. Due to the success of interventional and pharmacological treatment, IHD progresses to a chronic state in an increasing group of patients[10].

In current clinical practice treatment options for chronic heart failure patients are medication and revascularization through PCI or Coronary Artery Bypass Grafting (CABG) of chronically obstructed coronaries to establish full revascularization[11] and cardiac resynchronization therapy (CRT) to maximize the efficiency of cardiac work reduced by asynchronous contraction of the cardiac muscle[12]. Eventually a left ventricular assist device (LVAD) can be implanted to mechanically support the systemic blood circulation[13]. This latter option is most often used as a temporal bridge to a heart transplantation which is the last option for a HF patient[14]. It should be noted that yearly only a very limited number (30-35) of heart transplantations are performed in the Netherlands. Despite all the above mentioned therapeutic options, IHD remains the leading cause of death in the world. New therapies to treat IHD are therefore of great interest.

Myocardial healing

The pathogenesis of ischemic injury is a series of processes comprising cell death, inflammation and extracellular matrix (ECM) turnover. The loss of structure and mechanical integrity locally weakens the myocardium and leads to a high mechanical load, and local wall stress since cardiac function is necessarily maintained to conserve the systemic blood pressure. The high local wall stress triggers new matrix deposition in the ischemic area, and thereby cardiac remodeling overall[15-17]. Initially this cascade is started by the massive cell loss after an ischemic event[18]. Preventing the loss of cardiomyocytes or replacing cardiomyocytes with newly generated counterparts therefore is the most desirable therapy[19,20]. Although received with initial skepticism, the recent finding that the mammalian heart is a self-renewing organ capable of mobilizing progenitor cells to control the physiological turnover of cardiac cells has exposed a new perspective[21,22]. However these studies used different techniques to measure the rate of cardiomyocyte turnover under physiological conditions, both studies showed the existence of a progenitor cell niche in adult mammalian hearts. Interestingly, if this capacity to a limited extent is available in the mammalian heart, artificial enhancement of this capacity to protect cardiomyocytes, and thereby restore cardiac function after injury might be applicable as a new therapy for ischemic heart disease. This tempting alternative therapy has been the basis for many hypothesis of studies aiming at cardiac regeneration after ischemic heart disease in the last decade.

Cardiac regenerative therapy

In the last decade studies have focused on cardiac regeneration by means of transplantation of stem cells[23] or stem cell derived products from different stem cell sources[24] or the application of biomaterials[25] that can be loaded with stem cells for simultaneous local matrix stabilization[26,27]. Despite the dedication of researchers worldwide the therapeutic effects in both preclinical and clinical studies are still modest[28]. Both clinical and pre-clinical meta-analysis show ~3-4% improvement of LVEF after 6 months[29-31]. The remaining challenges are of biological, medical, and technical nature. Close collaboration of these three working areas is therefore necessary to improve cardiac regenerative therapy and make it suitable for clinical application[32] (Figure 1).

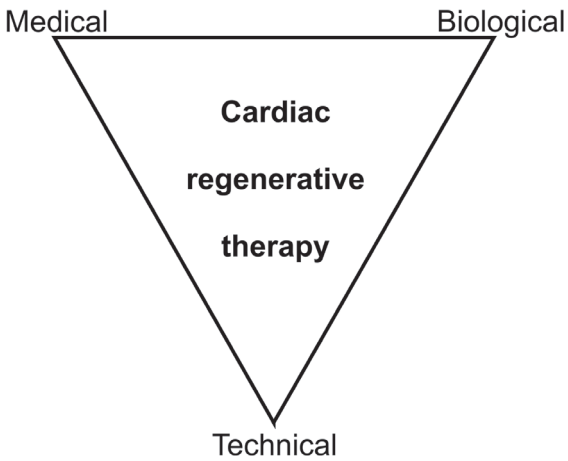

Figure 1. Multidisciplinary approach of cardiac regenerative therapy

Medical challenges

The promising initial pre-clinical results of cardiac stem cell therapy in the early 2000's, and the strong need for alternative therapies for IHD have led to the early initiation of clinical trials. It can be debated whether sufficient basic knowledge was available at the beginning of these trials. Fact is that in the last 13 years thousands of patients were enrolled in clinical cardiac stem cell trials. Due to these studies a lot is learned about cardiac stem cell therapy. Nevertheless a lot of issues remain as was outlined by the European Society of Cardiology taskforce on stem cells and repair of the heart[33]. The main medical challenge concerns the optimal time point to inject stem cells into the heart after ischemic injury, and which patients can benefit most from cardiac regenerative therapy, and should be treated. Once a patient group is selected, a specific task for medical doctors in the development of cardiac regenerative therapy is the translation between the bench and the bedside and vice versa[34,35]. The medical doctor is also responsible to clearly explain the pro's, con's, and uncertainties related to cell therapy, and then decide together with the patient which strategy to follow. Finally, the medical doctor is responsible for the patient safety during and after the therapy. In particular in the clinical trial phase of the therapy this aspect requires special attention.

Biological challenges

Cardiac regenerative therapy focuses on the improvement of outcome of patients with MI by protection of cardiomyocyte apoptosis, prevent adverse remodeling, and ultimately the replacement of damaged tissue with new functional tissue. The cell sources that are clinically being used for this purpose, or are the most promising to be used in future applications, are schematically shown in Figure 2 and briefly discussed here.

Bone marrow derived stem cells (BMC)

An easy accessible cell source is bone marrow (BM). Within the BM several cellular subsets can be observed, including mononuclear cells, hematopoetic progenitors, mesenchymal stem cells, and endothelial progenitor cells. After publication by Orlic et al[36] showing that large numbers of BMCs could successfully be differentiated in functionally contracting cardiomyocytes, BMCs were used in numerous pre-clinical trials. Recent meta-analyses

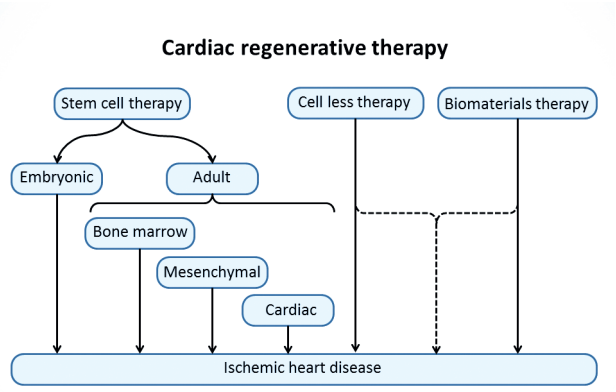

Figure 2. Schematic overview of the currently used cardiac regenerative therapeutics

have shown that the effect of BMC therapy increases the LVEF with ~3% compared to placebo treated patients[30,37]. The actual differentiation into cardiomyocytes could not be reproduced by other researchers[38]. Anyway, clinical studies have shown that BMC therapy for the injured heart is at least safe in the clinical setting, since no major side effects were noted. Since BMC therapy was shown to stimulate neovascularization, protect apoptosis, and activate the endogenous cardiac stem cell niche, the working mechanism is believed to be paracrine[39-42]. This means that via secretion of a variety of cytokines, growth factors, and small strands of non-coding RNA BMCs are able to modulate and improve the myocardium. This is further elaborated upon in the section about cell-less therapy.

Mesenchymal stem cells (MSC)

Mesenchymal stem cells can be isolated from different types of tissues, including adipose tissue, and are identified based on cell surface markers[43]. Moreover MSCs are seen as immunomodulatory cells that interact with a wide range of immune cells as they are a potent inhibitor of T cell activation[44]. Although there is a lack of a clear definition of which markers indicate full differentiation into functional cells, the ability of MSCs to differentiate into a variety of cell lineages, and their immune modulatory effect makes them an attractive therapeutic tool for cardiac regeneration[45-48]. After direct injection of MSCs into infarcted porcine myocardium engrafted MSCs cannot differentiated to cardiomyocytes, but since there is evidence of improved cardiac function and reduced post MI thinning, mechanisms are explained by the secretion of paracrine factors that induce angiogenesis and cardiomyogenesis[49]. With their immunosuppressive capacity and potent paracrine action MSCs clinically are also eligible for allogeneic therapy for IHD.

Cardiac stem/progenitor cells (CSC)

At the moment the most potent cell source for cardiac repair are cardiac stem cells, which can efficiently be differentiated into cardiomyocytes, endothelial and smooth muscle cells[50]. In addition upon induction of differentiation transplanted cardiomyocytes integrate electrically and metabolically with neighboring host cardiomyocytes. Different groups have isolated different human CSCs which were obtained from cardiac explant derived cardiospheres, or based on expression of the transcription factor islet-1, surface antigen expression of c-kit, or an unidentified protein cross-reacting with the mouse stem cell antigen-1 (Sca-1)[19,51]. Infusion of various CSC sources have been shown to significantly limit infarct size, attenuate LV remodeling and improve cardiac performance in different experimental models. Since the initial discovery of CSCs in 2003 two phase I safety trials have been published and show that autologous CSC transplantation is safe and feasible. Functional results showed an impressive increase in LVEF at 2 years in the SCIPIO trial[52], and a decrease of the infarct size without an increase of LVEF in the CADUCEUS trial[53].

Embryonic stem cells (ESC) and induced pluripotent stem cells (iPS)

Embryonic stem cells have the ability to divide indefinitely, and are able to differentiate into all cell types of the body, thereby making it the cell most suitable for cardiac stem cell therapy. This great potential on the other side is a disadvantage because it can lead to uncontrolled tumor formation[54]. Moreover ethical and political issues play a role in the use of embryonic material. To overcome these issues recently progenitor or pluripotent cells have been derived from brown adipose tissue, and induced pluripotent stem cells (iPS cells) have been derived from reprogrammed skin fibroblasts. The iPS cells exhibit the

essential characteristics of ESCs by inserting four different genes. In cardiology this development has led to the reprogramming of cardiac fibroblast to cardiac myocytes[55,56]. Much more information about the safety of this technique is mandatory prior to further clinical application.

Cell less therapy

Since for both BMCs and MSCs the working mechanisms is believed to be via paracrine signaling, it is obvious that via direct secretion or injection of cytokines, growth factors, or small strands of non-coding RNA the effects of the stem cell therapy can be mimicked. This so called 'cell less' cardiac regenerative therapy has been investigated in the last years[57,58]. The delivery of microvesicles like exosomes to the myocardium via stem cell derived conditioned medium has shown to play a cardio protective role after injury[59]. As shown by Vrijsen et al. the contents of the exosomes is thought to be cell type and state specific, and can be growth factors, mRNAs, miRNAs, MMP-9, and EMMPRIN[24]. Although the first *in-vivo* experiments have shown promising results with respect to angiogenesis more studies are necessary to prove the beneficial effects of cell less therapy in IHD.

Biomaterials

Besides transplantation of biologics, the injection or infusion of biomaterials has been applied to support the local extracellular matrix after an ischemic injury in order to enhance matrix integrity and prevent adverse remodeling after myocardial injury[60-62]. Although not much is known about the mechanisms of action, and the materials must be optimized, in both small and large animals this approach has shown to significantly increase wall thickness, vascularization, LV volumes, and, most importantly, cardiac function[26,27,63]. Moreover, the combination of biomaterials and stem cells or stem cell derived factors forms a delivery platform for slow release of paracrine factors in the heart after injection[25].

Engineering challenges

All cardiac regenerative therapeutics share that they ultimately need to be applied to the most optimal location in the myocardium to fulfill their task. Accurate delivery to the region of interest is necessary for two reasons. In the first place the diffusion of the stem cells or biologics into the infarcted myocardium is complex and still limited[64], and therefore must be delivered close to the injured myocardium. The second reason is the discovery that the retention of stem cells after injection is low. Approximately 10% of the cells remaining after 4 hours[65], regardless of the delivery route used. Besides aiming for improved delivery efficiency it therefore is a challenge to at least deliver the cells at the optimal location. Currently used delivery routes are: intracoronary infusion, intramyocardial injection, endoscopic guided pericardial injection, retrograde intravenous injection, and surgical injection or application of endocardial cell sheets[66-68]. When focusing on the clinical application of cardiac regenerative therapy in HF patients, the most suitable delivery route is intramyocardial injection. Both surgical and pericardial injection require surgery, and are therefore more demanding and risky for the patient. Intramyocardial injection is a minimal invasive percutaneous procedure, and can be applied to patients in which the coronary arteries are chronically obstructed, whereas the intracoronary infusion technique requires patent coronaries. Various catheter systems are available to perform intramyocardial injections, using different needle types[69]. The NOGA®XP intramyocardial injection system[70] provides a three dimensional (3D) magnetic tracking technology and allows for the

assessment of local electrical and mechanical tissue characteristics. Local unipolar (UV) and bipolar (BV) depolarization potentials and relative catheter tip displacements (Linear Local Shortening, LLS) are measured at multiple locations on the left ventricular (LV) endocardium. These measurements are interpolated to obtain a three-dimensional reconstruction which is used to guide stem cell injections[71-75]. Ultimately the NOGA®XP system guides injections to the hibernating myocardium being electrical viable (measured by UV and BV) and mechanically dead (measured by LLS). In practice however hibernating tissue is very hard to designate, and injections are often performed based on the a priori knowledge of the physician based on cardiovascular imaging (e.g. MRI, SPECT, echo). Gold standard infarct assessment techniques based on MRI are however available. It is an engineering challenge to put this information into a format which can be used to guide injections in real time. Another engineering challenge faced in cardiac regenerative therapy is to establish a relevant measure of local cardiac function to provide the most optimal feedback to optimize the therapy. Since cardiac regenerative therapy aims at local interaction with the injured myocardium, it is most suitable to use local measures of cardiac function as a feedback measure of the therapy. Primary clinical endpoints used in clinical trials often are all cause mortality (BAMI-trial, clinicaltrials.gov: NCT01569178), or the progression of the disease to cardiac failure. Since there is such a strong need for new therapies for IHD, it has been tempting to use clinical endpoints for pre-clinical studies as well. Surrogate endpoints used in cardiac regenerative therapy studies are: LV volumes, ejection fraction (EF), myocardial perfusion, quality of life questionnaires, exercise capacity (VO_2 max, 6 minute walk test). Since these surrogate endpoints are well known amongst physicians, and correlate well with disease prognosis and mortality, they have been used to show the positive effects of cardiac regenerative therapies. Yet, the common surrogate endpoints provide no further insights into the therapeutic mechanisms of action, and therefore provide incomplete feedback to optimize the therapy[76-78]. Current technological developments have created the possibility to design new local measures of cardiac function to specifically assess the therapeutic effects of cardiac regenerative therapy[79,80]. The establishment of new local cardiac function measurement techniques to optimize the therapy in a highly constructive manner is a typical engineering challenge.

Addressed engineering challenges

The remaining challenges of cardiac regenerative therapy are multiple, and require a multidisciplinary approach. Close collaboration of biologists, medical doctors and medical engineers is mandatory to design solutions to existing problems and bring the therapy to the next level. In this thesis two engineering challenges are addressed:

1. Development of the optimal injection technique for application of cardiac regenerative therapy: targeting and guidance to the optimal injection location.
2. Development of the optimal measurement technique of local cardiac function to establish constructive feedback for optimizing cardiac regenerative therapy.

Engineering in the clinic

In daily clinical practice physicians treat patients according to the latest evidence based knowledge. Thereby it is assured that the therapy given is the best possible therapy for the patient based on the historical response of the population, and the use of a potentially harmful therapy or drug is prevented. The provided therapy however not necessarily is the

best therapy for the individual patient. The fact that 'non responders' exist in multiple medical disciplines is caused by the fact that the therapy given might have been the best with regard to the population, but not the best for the individual patient. The patient may not be suited for the therapy of choice, either because the pathophysiology of the patient has progressed too far to be sensitive to the therapy, or because the therapy just is not the most suitable therapy. Clinicians deal with dilemma's on this subject every day. The establishment of new therapies to better treat a smaller subgroup of the population, or ideally individual patients, requires an approach that is open to new insights or technologies. Hereby a medical engineer can play an important role. Different from a medical doctor, a medical engineer comprises profound knowledge of the biologic and patho-physiologic side of the problem and has the capabilities to understand the physical processes and the way these processes can be measured, intervened upon, and described using mathematical models. The Department of Biomedical Engineering of the Eindhoven University of Technology educates medical engineers. Besides engineering skills, like designing new diagnostic or interventional techniques, performing and evaluating scientific experiments, a medical engineer learns to quantify and objectify patient data as well. Thereby a medical engineer is excellently qualified to answer medical research questions ensuing from daily clinical practice. For successful embedment of a medical engineer in a multidisciplinary team consisting of biologists and medical doctors open communication is required to effectively translate medical research questions into engineering ones and vice versa. For the non-responders of the therapy of choice as mentioned above, it is desirable to design new treatment options. Especially in large patient populations. In such research projects, the medical engineer can establish or re-design the optimal therapeutic or diagnostic technique to apply and assess the therapy. Moreover, the use of new therapeutic and diagnostic techniques can lead to new insights in patho-physiology, which can lead to new therapeutic targets. Besides the scientific interests the current societal tendency to not only translate research findings into scientific output, but also into social and commercial value, has created another task for medical engineers. Based on scientific findings the medical engineer can introduce new ideas that are eligible for valorization.

Technical solutions to improve cardiac regenerative therapy

Hypothesis

1. Infarct transmurality measured by the gold standard late gadolinium enhancement MRI can be co-visualized during the injection procedure using the clinical standard NOGA®XP intramyocardial injection system based on electromechanical mapping (EMM).
2. The target area selection based on the gold standard imaging technique of infarct transmurality provides valuable additional information during the injection procedure.
3. Respiratory motion affects the registration accuracy of the electromechanical mapping datasets and the data obtained from MRI.
4. Cardiac deformation assessment based on radiofrequency ultrasound analysis can be used to accurately measure myocardial strain, and provides new insights in cardiac biomechanics regarding to the local effects of cardiac regenerative therapy.

Outline of this thesis

So far, cardiac regenerative therapy has been a field of interest for biologists and medical doctors. Using the standard techniques available in clinical practice to both perform the therapy, and measure the therapeutic effects, progression of the therapy has been modest. In this thesis the focus is on the smart use of novel techniques in order to create new tools to improve the therapy.

Part I. Addressing the technical challenges of cardiac regenerative therapy

The (pre)-clinical studies of cardiac regenerative therapy that are performed so far all have used different methods, and merely EF as a primary and clinically relevant endpoint. **Chapter 2** is a review of the studies that performed a secondary endpoint measurement being an invasive (hyperemic micro vascular resistance index (HMRi), electromechanical mapping) or non-invasive (perfusion, viability, fibrosis, deformation imaging) measure of local cardiac function. The relations between these parameters and the working mechanisms of cardiac regenerative therapy are identified. Finally suggestions are done for a more optimal feedback parameter to improve cardiac regenerative therapy.

Part II. Advanced delivery

In **Chapter 3** the in house developed 3D CartBox image registration toolbox to register the electromechanical mapping data on cine MRI and co-visualize late gadolinium enhanced MRI images during the cardiac injection procedures is described. Besides the guidance of the catheter on the gold standard MRI data, this toolbox allows treatment planning based on the exact determination of the border zone of the infarct with a distinct infarct transmurality. **Chapter 4** describes the first results of a retrospective study using the treatment planning and 3D CartBox image registration toolbox in a cohort of 17 pigs after a chronic myocardial infarction. The registration of the MRI and the EMM by 3D CartBox is affected by respiratory induced motion of the heart. **Chapter 5** describes a pilot study of a newly developed algorithm to compensate the respiratory induced motion of the heart during the EMM procedure. In **Chapter 6** the business plan of the spin-off company CARTcare is presented. CARTcare exploits the 3D CartBox image registration toolbox developed in this PhD project and discussed in Chapter 3 of this thesis.

Part III. Advanced assessment of local cardiac function

In current clinical practice there are no clinical techniques available to measure local cardiac deformation in a highly detailed fashion. In **Chapter 7** radiofrequency ultrasound based deformation analysis is suggested as a novel measure of local cardiac deformation to assess the local effects of cardiac regenerative therapy, and create a robust feedback measure to optimize the therapy. The study was performed using infarcted and healthy regions of a porcine model of chronic myocardial infarction. Validation was done by histology and a geometrical model of the LV. In **Chapter 8** the RF ultrasound compounding technique was used to obtain the strain in the longitudinal direction with a higher accuracy. Since the frame rate decreases while using the compounding technique and the performance of strain imaging is highly dependent on the ration between frame rate and the velocity of the tissue, it was first tested in a finite element model of LV mechanics. This was necessary to correctly interpret the results from the data that were acquired *in vivo*.

References

1. Go AS, Mozaffarian D, Roger VL, Benjamin EJ, Berry JD, Borden WB, Bravata DM, Dai S, Ford ES, Fox CS, Franco S, Fullerton HJ, Gillespie C, Hailpern SM, Heit Ja, Howard VJ, Huffman MD, Kissela BM, Kittner SJ, Lackland DT, Lichtman JH, Lisabeth LD, Magid D, Marcus GM, Marelli A, Matchar DB, McGuire DK, Mohler ER, Moy CS, Mussolino ME, Nichol G, Paynter NP, Schreiner PJ, Sorlie PD, Stein J, Turan TN, Virani SS, Wong ND, Woo D, Turner MB. Heart disease and stroke statistics--2013 update: a report from the American Heart Association. Circulation. 2013;127:6-245
2. Levine GN, Bates ER, Blankenship JC, Bailey SR, Bittl Ja, Cercek B, Chambers CE, Ellis SG, Guyton Ra, Hollenberg SM, Khot UN, Lange Ra, Mauri L, Mehran R, Moussa ID, Mukherjee D, Nallamothu BK, Ting HH. 2011 ACCF/AHA/SCAI Guideline for Percutaneous Coronary Intervention: executive summary: a report of the American College of Cardiology Foundation/American Heart Association Task Force on Practice Guidelines and the Society for Cardiovascular Angiography and Interventions. Catheterization and cardiovascular interventions: official journal of the Society for Cardiac Angiography & Interventions. 2012;79:453-495
3. de Roos A, Matheijssen NAA, Doornbos J, van Dijkman PRM, van Voorthuisen E, van der Wall EE. Myocardlal infarct size after reperfusion therapy: assessment with Gd-DTPA-enhanced MR Imaging. Cardiac Radiology. 1990;176:517-521
4. Kleiman NS, White HD, Ohman EM, Ross AM, Woodlief LH, Califf RM, Holmes DR, Bates E, Pfisterer M, Vahanian A. Mortality within 24 hours of thrombolysis for myocardial infarction. The importance of early reperfusion. The GUSTO Investigators, Global Utilization of Streptokinase and Tissue Plasminogen Activator for Occluded Coronary Arteries. Circulation. 1994;90:2658-2665
5. Fishman DL, Leon MB, Baim DS, Schatz RA, Savage MP, Penn I, Detre K, Veltri L, Ricci D, Nobuyoshi M, Cleman M, Heuser R, Almond D, Teirstein PS, Fish DR, Colombo A, Brinker J, Moses J, Shaknovich A, Hirshfeld J, Bailey S, Ellis S, Rake R, Goldberg S. A randomized comparison of coronary-stent placement and balloon angioplasty in the treatment of coronary artery disease. New England Journal of Medicine. 1994;331:496-501
6. Braunwald E, Kloner RA. The stunned myocardium: prolonged, postischemic ventricular dysfunction. Circulation. 1982;66:1146-1149
7. Manning AS, Hearse DJ. Reperfusion-induced arrhythmias: Mechanisms and Prevention. Journal of Cellular Cardiology. 1984;16:497-518
8. Krug A, Du Mesnil de Rochemont R, Korb G. Blood supply of the myocardium after temporary occlusion. Circulation Research. 1966;19:57-62
9. Henry TD, Satran D, Hodges JS, Johnson RK, Poulose AK, Campbell AR, Garberich RF, Bart BA, Olson RE, Boisjolie CR, Harvey KL, Arndt TL, Traverse JH. Long-term survival in patients with refractory angina. European Heart Journal. 2013;34:2683-2688
10. Jessup M, Abraham WT, Casey DE, Feldman AM, Francis GS, Ganiats TG, Konstam MA, Mancini DM, Rahko PS, Silver MA, Stevenson LW, Yancy CW. 2009 focused update: ACCF/AHA Guidelines for the Diagnosis and Management of Heart Failure in Adults: a report of the American College of Cardiology Foundation/American Heart Association Task Force on Practice Guidelines: developed in collaboration with the International Society for Heart and Lung Transplantation. Circulation. 2009;119:1977-2016
11. Stecher D, van Slochteren FJ, Hoefer IE, Pasterkamp G, Tulleken CAF, van Herwerden LA, Buijsrogge MP. The nonocclusive laser-assisted coronary anastomotic connector in an off-pump porcine bypass model. The Journal of thoracic and cardiovascular surgery. 2013;In Press:1-8
12. Leenders GE, Cramer MJ, Bogaard MD, Meine M, Doevendans PA, De Boeck BW. Echocardiographic prediction of outcome after cardiac resynchronization therapy: conventional methods and recent developments. Heart failure reviews. 2011;16:235-250
13. Kirkels JH, de Jonge N, Lahpor JR. Assist devices in the new decade: from technical developments to political decisions. European journal of heart failure. 2010;12:217-218

14. Lund LH, Edwards LB, Kucheryavaya AY, Dipchand AI, Benden C, Christie JD, Dobbels F, Kirk R, Rahmel AO, Yusen RD, Stehlik J. The Registry of the International Society for Heart and Lung Transplantation: thirtieth official adult heart transplant report--2013; focus theme: age. The Journal of heart and lung transplantation: the official publication of the International Society for Heart Transplantation. 2013;32:951-964
15. Holmes JW, Borg TK, Covell JW. Structure and mechanics of healing myocardial infarcts. Annual review of biomedical engineering. 2005;7:223-253
16. Holmes JW, Nunez JA, Covell JW. Functional implications of myocardial scar structure. American Journal Of Physiology Heart and Crculation Physiology. 1997;41:2123-2130
17. Holmes JW, Yamashita H, Waldman LK, Covell JW. Scar Remodeling and Transmural Deformation After Infarction in the Pig. Circulation. 1994;90:410-420
18. Reinecke H, Minami E, Zhu W-Z, Laflamme MA. Cardiogenic differentiation and transdifferentiation of progenitor cells. Circulation research. 2008;103:1058-1071
19. Koudstaal S, Jansen of Lorkeers SJ, Gaetani R, Gho JMIH, van Slochteren FJ, Sluijter JPG, Doevendans PA, Ellison GM, Chamuleau SAJ. Concise Review: Heart Regeneration and the Role of Cardiac Stem Cells. Stem cells translational medicine. 2013;2:0-0
20. Jakob P, Landmesser U. Current status of cell-based therapy for heart failure. Current heart failure reports. 2013;10:165-176
21. Kajstura J, Gurusamy N, Ogórek B, Goichberg P, Clavo-Rondon C, Hosoda T, D'Amario D, Bardelli S, Beltrami AP, Cesselli D, Bussani R, del Monte F, Quaini F, Rota M, Beltrami Ca, Buchholz Ba, Leri A, Anversa P. Myocyte turnover in the aging human heart. Circulation research. 2010;107:1374-1386
22. Bergmann O, Bhardwaj RD, Bernard S, Zdunek S, Barnabé-Heider F, Walsh S, Zupicich J, Alkass K, Buchholz BA, Druid H, Jovinge S, Frisen J. Evidence for Cardiomyocyte Renewal in Humans. Science. 2010;324
23. Smits AM, Laake LWV, Ouden KD, Schreurs C, Szuhai K, van Echteld CJ, Mummery CL, Doevendans PA, Goumans M-J. Human cardiomyocyte progenitor cell transplantation preserves long-term function of the infarcted mouse myocardium. Cardiovascular Research. 2009;83:527-535
24. Vrijsen KR, Sluijter JPG, Schuchardt MWL, van Balkom BWM, Noort WA, Chamuleau SAJ, Doevendans PAFM. Cardiomyocyte progenitor cell-derived exosomes stimulate migration of endothelial cells. Journal of cellular and molecular medicine. 2010;14:1064-1070
25. Bastings MM, Koudstaal S, Kieltyka RE, Nakano Y, Pape AC, Feyen DA, van Slochteren FJ, Doevendans PA, Sluijter JP, Meijer EW, Chamuleau SAJ, Dankers PY. A Fast pH-Switchable and Self-Healing Supramolecular Hydrogel Carrier for Guided, Local Catheter Injection in the Infarcted Myocardium. Advanced healthcare materials. 2014;3:70-78
26. Landa N, Miller L, Feinberg MS, Holbova R, Shachar M, Freeman I, Cohen S, Leor J. Effect of Injectable Alginate Implant on Cardiac Remodeling and Function After Recent and Old Infarcts in Rat. Circulation. 2008;117:1388-1396
27. Leor J, Tuvia S, Guetta V, Manczur F, Castel D, Willenz U, Petnehazy Ö, Landa N, Feinberg MS, Konen E, Goitein O, Tsur-gang O, Shaul M, Klapper L, Cohen S. Intracoronary Injection of In Situ Forming Alginate Hydrogel Reverses Left Ventricular Remodeling After Myocardial Infarction in Swine. Journal of the American College of Cardiology. 2009;54:1014-1023
28. Malliaras K, Kreke M, Marbán E. The stuttering progress of cell therapy for heart disease. Clinical pharmacology and therapeutics. 2011;90:532-541
29. van der Spoel TIG, Jansen of Lorkeers SJ, Agostoni P, van Belle E, Gyöngyösi M, Sluijter JPG, Cramer MJ, Doevendans PAFM, Chamuleau SAJ. Human relevance of pre-clinical studies in stem cell therapy: systematic review and meta-analysis of large animal models of ischaemic heart disease. Cardiovascular research. 2011;91:649-658
30. Jeevanantham V, Butler M, Saad A, Abdel-Latif A, Zuba-Surma EK, Dawn B. Adult Bone Marrow Cell Therapy Improves Survival and Induces Long-Term Improvement in Cardiac Parameters: A Systematic Review and Meta-Analysis. Circulation. 2012:551-568

31. Zimmet H, Porapakkham P, Porapakkham P, Sata Y, Haas SJ, Itescu S, Forbes A, Krum H. Short- and long-term outcomes of intracoronary and endogenously mobilized bone marrow stem cells in the treatment of ST-segment elevation myocardial infarction: a meta-analysis of randomized control trials. European journal of heart failure. 2011
32. Bursac N. Stem Cell Therapies for Heart Disease: Why Do We Need Bioengineers? IEEE Engineering in Medicine and Biology Magazine. 2007;26:76-79
33. Bartunek J, Dimmeler S, Drexler H, Fernández-Avilés F, Galinanes M, Janssens S, Martin J, Mathur A, Menasche P, Priori S, Strauer B, Tendera M, Wijns W, Zeiher A. The consensus of the task force of the European Society of Cardiology concerning the clinical investigation of the use of autologous adult stem cells for repair of the heart. European heart journal. 2006;27:1338-1340
34. Kwon SU, Yeung AC, Ikeno F. The role of large animal studies in cardiac regenerative therapy concise review of translational stem cell research. Korean circulation journal. 2013;43:511-518
35. Frey-Vasconcells J, Whittlesey KJ, Baum E, Feigal EG. Translation of stem cell research: points to consider in designing preclinical animal studies. Stem cells translational medicine. 2012;1:353-358
36. Orlic D, Kajstura J, Chimenti S, Bodine DM, Leri A, Anversa P. Bone marrow stem cells regenerate infarcted myocardium. Nature. 2001;410:701-705
37. Clifford DM, Fisher SA, Brunskill SJ, Doree C, Mathur A, Watt S, Martin-Rendon E. Stem cell treatment for acute myocardial infarction (Review). The Cochrane Library. 2012
38. Murry CE, Soonpaa MH, Reinecke H, Nakajima H, Nakajima HO, Rubart M, Pasumarthi KBS, Virag JI, Bartelmez SH, Poppa V, Bradford G, Dowell JD, Williams DA, Field LJ. Haematopoietic stem cells do not transdifferentiate into cardiac myocytes in myocardial infarcts. Nature. 2004;428:13-15
39. Dimmeler S, Zeiher AM, Schneider MD. Unchain my heart: the scientific foundations of cardiac repair. The Journal of Clinical Investigation. 2005;115:572-583
40. Chimenti I, Smith RR, Li TS, Gerstenblith G, Messina E, Giacomello A, Marban E. Relative roles of direct regeneration versus paracrine effects of human cardiosphere-derived cells transplanted into infarcted mice. Circ Res. 2010;106:971-980
41. Li TS, Cheng K, Malliaras K, Smith RR, Zhang Y, Sun B, Matsushita N, Blusztajn A, Terrovitis J, Kusuoka H, Marban L, Marban E. Direct comparison of different stem cell types and subpopulations reveals superior paracrine potency and myocardial repair efficacy with cardiosphere-derived cells. J Am Coll Cardiol. 2012;59:942-953
42. Crisostomo PR, Abarbanell AM, Wang M, Lahm T, Wang Y, Meldrum DR. Embryonic stem cells attenuate myocardial dysfunction and inflammation after surgical global ischemia via paracrine actions. Am J Physiol Heart Circ Physiol. 2008;295:1726-1735
43. Dominici M, Le Blanc K, Mueller I, Slaper-Cortenbach I, Marini F, Krause D, Deans R, Keating A, Prockop D, Horwitz E. Minimal criteria for defining multipotent mesenchymal stromal cells. The International Society for Cellular Therapy position statement. Cytotherapy. 2006;8:315-317
44. van den Akker F, Deddens JC, Doevendans PA, Sluijter JP. Cardiac stem cell therapy to modulate inflammation upon myocardial infarction. Biochimica et biophysica acta. 2013;1830:2449-2458
45. Williams AR, Hare JM. Mesenchymal stem cells: biology, pathophysiology, translational findings, and therapeutic implications for cardiac disease. Circulation research. 2011;109:923-940
46. Hare JM, Fishman JE, Gerstenblith G, DiFede Velazquez DL, Zambrano JP, Suncion VY, Tracy M, Ghersin E, Johnston PV, Brinker JA, Breton E, Davis-Sproul J, Schulman IH, Byrnes J, Mendizabal AM, Lowery MH, Rouy D, Altman P, Wong Po Foo C, Ruiz P, Amador A, Da Silva J, McNiece IK, Heldman AW, George R, Lardo A. Comparison of allogeneic vs autologous bone marrow–derived mesenchymal stem cells delivered by transendocardial injection in patients with ischemic cardiomyopathy: the POSEIDON randomized trial. JAMA: the journal of the American Medical Association. 2012;308:2369-2379
47. Amado LC, Schuleri KH, Saliaris AP, Boyle AJ, Helm R, Oskouei B, Centola M, Eneboe V, Young R, Lima JAC, Lardo AC, Heldman AW, Hare JM. Multimodality noninvasive imaging demonstrates in vivo cardiac regeneration after mesenchymal stem cell therapy. Journal of the American College of Cardiology. 2006;48:2116-2124

48. Schuleri KH, Amado LC, Boyle AJ, Centola M, Saliaris AP, Gutman MR, Hatzistergos KE, Oskouei BN, Zimmet JM, Young RG, Heldman AW, Lardo AC, Hare JM. Early improvement in cardiac tissue perfusion due to mesenchymal stem cells. American journal of physiology. Heart and circulatory physiology. 2008;294:2002-2011
49. Gnecchi M, Zhang Z, Ni A, Dzau VJ. Paracrine mechanisms in adult stem cell signaling and therapy. Circulation research. 2008;103:1204-1219
50. Dawn B, Stein AB, Urbanek K, Rota M, Whang B, Rastaldo R, Torella D, Tang XL, Rezazadeh A, Kajstura J, Leri A, Hunt G, Varma J, Prabhu SD, Anversa P, Bolli R. Cardiac stem cells delivered intravascularly traverse the vessel barrier, regenerate infarcted myocardium, and improve cardiac function. Proc Natl Acad Sci U S A. 2005;102:3766-3771
51. Chamuleau SAJ, Vrijsen KR, Rokosh DG, Tang XL, Piek JJ, Bolli R. Cell therapy for ischaemic heart disease: focus on the role of resident cardiac stem cells. Netherlands Heart Journal. 2009;17:200-208
52. Bolli R, Chugh AR, D'Amario D, Loughran JH, Stoddard MF, Ikram S, Beache GM, Wagner SG, Leri A, Hosoda T, Sanada F, Elmore JB, Goichberg P, Cappetta D, Solankhi NK, Fahsah I, Rokosh DG, Slaughter MS, Kajstura J, Anversa P. Cardiac stem cells in patients with ischaemic cardiomyopathy (SCIPIO): initial results of a randomised phase 1 trial. Lancet. 2011;378:1847-1857
53. Malliaras K, Makkar RR, Smith RR, Cheng K, Wu E, Bonow RO, Marban L, Mendizabal A, Cingolani E, Johnston PV, Gerstenblith G, Schuleri KH, Lardo AC, Marban E. Intracoronary cardiosphere-derived cells after myocardial infarction: evidence for therapeutic regeneration in the final 1-year results of the CADUCEUS trial. J Am Coll Cardiol. 2013
54. Nussbaum J, Minami E, Laflamme MA, Virag JA, Ware CB, Masino A, Muskheli V, Pabon L, Reinecke H, Murry CE. Transplantation of undifferentiated murine embryonic stem cells in the heart: teratoma formation and immune response. FASEB journal: official publication of the Federation of American Societies for Experimental Biology. 2007;21:1345-1357
55. Zhang J, Wilson GF, Soerens AG, Koonce CH, Yu J, Palecek SP, Thomson JA, Kamp TJ. Functional cardiomyocytes derived from human induced pluripotent stem cells. Circulation research. 2009;104:30-41
56. Carpenter L, Carr C, Yang CT, Stuckey DJ, Clarke K, Watt SM. Efficient differentiation of human induced pluripotent stem cells generates cardiac cells that provide protection following myocardial infarction in the rat. Stem cells and development. 2012;21:977-986
57. Chamuleau SAJ, van Belle E, Doevendans PAFM. Enhancing cardiac stem cell differentiation into cardiomyocytes. Cardiovascular research. 2009;82:385-387
58. Vrijsen KR, Chamuleau SAJ, Noort WA, Doevendans PA, Sluijter JPG. Stem cell therapy for end-stage heart failure: indispensable role for the cell? Current opinion in organ transplantation. 2009;14:560-565
59. Lai RC, Arslan F, Lee MM, Sze NSK, Choo A, Chen TS, Salto-Tellez M, Timmers L, Lee CN, El Oakley RM, Pasterkamp G, de Kleijn DPV, Lim SK. Exosome secreted by MSC reduces myocardial ischemia/reperfusion injury. Stem cell research. 2010;4:214-222
60. Christman KL, Lee RJ. Biomaterials for the treatment of myocardial infarction. Journal of the American College of Cardiology. 2006;48:907-913
61. Rane AA, Christman KL. Biomaterials for the treatment of myocardial infarction: a 5-year update. Journal of the American College of Cardiology. 2011;58:2615-2629
62. Johnson TD, Christman KL. Injectable hydrogel therapies and their delivery strategies for treating myocardial infarction. Expert opinion on drug delivery. 2013;10:59-72
63. Christman KL, Fok HH, Sievers RE, Fang Q, Lee RJ. Fibrin Glue Alone and Skeletal Myoblasts in a Fibrin Scaffold Preserve Cardiac Function after Myocardial Infarction. Tissue Engineering. 2004;10
64. Taghavi S, George JC. Homing of stem cells to ischemic myocardium. American journal of translational research. 2013;5:404-411
65. van der Spoel TIG, Vrijsen KR, Koudstaal S, Sluijter JPG, Nijsen JFW, de Jong HW, Hoefer IE, Cramer MJM, Doevendans PA, van Belle E, Chamuleau SAJ. Transendocardial cell injection is not superior to intracoronary infusion in a porcine model of ischemic cardiomyopathy: A study on delivery efficiency. Journal of cellular and molecular medicine. 2012:2768-2776

66. Fukushima S, Sawa Y, Suzuki K. Choice of cell-delivery route for successful cell transplantation therapy for the heart. Future cardiology. 2013;9:215-227
67. van der Spoel TIG, Chun-Tsu Lee J, Vrijsen KR, Sluijter JPG, Cramer MJM, Doevendans PA, Belle EV, Chamuleau SAJ. Non-surgical stem cell delivery strategies and in vivo cell tracking to injured myocardium. International Journal of Cardiovascular Imaging. 2012;16:2768-2776
68. Campbell NG, Suzuki K. Cell delivery routes for stem cell therapy to the heart: current and future approaches. J Cardiovasc Transl Res. 2012;5:713-726
69. Kumar A, Haralampus CA, Hughes M, Rouy D, Cresswell N, Braun R, Turner D, Amrani D, Motlagh D, Schaer GL. Assessment of safety, accuracy, and human CD34+ cell retention after intramyocardial injections with a helical needle catheter in a porcine model. Catheterization and cardiovascular interventions: official journal of the Society for Cardiac Angiography & Interventions. 2013;81:970-977
70. Ben-Haim SA, Osadchy D, Schuster I, Gepstein L, Hayam G, Josephson ME. Nonfluoroscopic, in vivo navigation and mapping technology. Nature Medicine. 1996;2:1393-1395
71. Ramshorst JV, Antoni ML, Beeres SL, Roes SD, Delgado V, Rodrigo SF, Roos AD, Holman ER, Fibbe WE, Lamb HJ, Zwaginga JJ, Boersma E, van der Wall EE, Schalij MJ, Atsma DE, Bax JJ. Intramyocardial Bone Marrow-Derived Mononuclear Cell Injection for Chronic Myocardial Ischemia: the Effect on Diastolic Function. Circulation Cardiovascular Imaging. 2011;4:122-129
72. Ramshorst JV, Atsma DE, Beeres SLMA, Mollema SA, Ajmone Marsan N, Holman ER, van der Wall EE, Schalij MJ, Bax JJ. Effect of intramyocardial bone marrow cell injection on left ventricular dyssynchrony and global strain. Heart. 2009;95:119-124
73. Gyöngyösi M, Dib N. Diagnostic and prognostic value of 3D NOGA mapping in ischemic heart disease. Nature Reviews Cardiology. 2011;8:393-404
74. Perin EC, Silva GV, Sarmento-Leite R, Sousa ALS, Howell M, Muthupillai R, Lambert B, Vaughn WK, Flamm SD. Assessing Myocardial Viability and Infarct Transmurality With Left Ventricular Electromechanical Mapping in Patients With Stable Coronary Artery Disease: Validation by Delayed-Enhancement Magnetic Resonance Imaging. Circulation. 2002;106:957-961
75. Gyöngyösi M, Lang I, Dettke M, Beran G, Graf S, Sochor H, Nyolczas N, Charwat S, Hemetsberger R, Christ G, Edes I, Balogh L, Krause KT, Jaquet K, Kuck K-H, Benedek I, Hintea T, Kiss R, Préda I, Kotevski V, Pejkov H, Zamini S, Khorsand A, Sodeck G, Kaider A, Maurer G, Glogar D. Combined delivery approach of bone marrow mononuclear stem cells early and late after myocardial infarction: the MYSTAR prospective, randomized study. Nature clinical practice. Cardiovascular medicine. 2009;6:70-81
76. van Slochteren FJ, Teske AJ, van der Spoel TIG, Koudstaal S, Doevendans PA, Sluijter JPG, Cramer MJM, Chamuleau SAJ. Advanced measurement techniques of regional myocardial function to assess the effects of cardiac regenerative therapy in different models of ischaemic cardiomyopathy. European heart journal cardiovascular Imaging. 2012;13:808-818
77. Tendera M, Wojakowski W. How to measure the effects of the intracoronary stem cell therapy ? European Journal of Echocardiography. 2010;11:438-439
78. Traverse JH, Henry TD, Moye LA. Is the measurement of left ventricular ejection fraction the proper end point for cell therapy trials? An analysis of the effect of bone marrow mononuclear stem cell administration on left ventricular ejection fraction after ST-segment elevation myocardia. American heart journal. 2011;162:671-677
79. Couade M, Pernot M, Messas E, Bel A, Ba M, Hagege A, Fink M, Tanter M. In vivo quantitative mapping of myocardial stiffening and transmural anisotropy during the cardiac cycle. IEEE transactions on medical imaging. 2011;30:295-305
80. Pernot M, Couade M, Mateo P, Crozatier B, Fischmeister R, Tanter M. Real-time assessment of myocardial contractility using shear wave imaging. Journal of the American College of Cardiology. 2011;58:65-72

PART ONE

Addressing the technical challenges of cardiac regenerative therapy

Frebus J. van Slochteren[1], Arco J. Teske[1], Tycho I.G. van der Spoel[1], Stefan Koudstaal[1,2], Pieter A. Doevendans[1,2], Joost P.G. Sluijter[1,2], Maarten J.M. Cramer[1], Steven A.J. Chamuleau[1,2]

[1] Department of Cardiology, University Medical Centre Utrecht, The Netherlands
[2] Interuniversity Cardiology Institute of the Netherlands (ICIN), Utrecht, The Netherlands

CHAPTER **2**

Advanced measurement techniques of regional myocardial function to assess the effects of cardiac regenerative therapy in different models of ischemic cardiomyopathy

Published in the European Heart Journal Cardiovascular Imaging, May 2012

Abstract

Cardiac regenerative therapy is still not used in daily clinical practice. A reason for this might be the modest effect on relevant global clinical endpoints (i.e. ejection fraction (EF)) in pre-clinical studies. To introduce proper improvement strategies it is important to extend the focus from clinical endpoints to more detailed local measures of cardiac function. In this review, we discuss the measurement principles of all invasive and non invasive techniques that are used to assess the local effects of cardiac regenerative therapy in order to improve feedback to researchers unraveling the dominant pathways that lead to effective cardiac regeneration. Generally adopted mechanisms of cardiac regenerative therapy are: 1) vasculogenesis, 2) cardiomyogenesis, and 3) matrix assisted myocardium stabilization. Since direct in vivo measures of these mechanisms don't exist, we discuss the measurement techniques of local microvascular resistance, myocardial perfusion, viability, fibrosis, and deformation imaging. The ability of these techniques to reflect the mechanisms of cardiac regenerative therapy, and the results of applications in stem cell studies are discussed, and critically commented upon. Special attention is given to applications of deformation imaging since this has recently been suggested and used as a potential new technique to assess local changes of cardiac biomechanics, which requires special knowledge about cardiac physiology. We conclude that besides the clinically relevant EF measurements, detailed measures of local cardiac function provide information about the local changes induced by cardiac regenerative therapy. In particular, combination of deformation imaging, by ultrasound or MRI, with simultaneously measured local geometry and pressure measurements is a promising approach to assess the effects of cardiac regenerative therapy on local cardiac biomechanics. This approach provides information about local tissue contractility, stiffness, and thereby remodeling. We recommend that researchers use this comprehensive approach in future studies.

Introduction

Myocardial infarction (MI) leads to irreversible damage of tissue caused by prolonged ischemia or reperfusion-induced injury. The broad spectrum of ischemic heart disease (IHD) consists of acute IHD, i.e. acute MI (AMI), and chronic IHD, i.e. refractory angina pectoris (RAP), and heart failure (HF). In addition to pharmacological therapies, catheter based and surgical interventions are applied to limit the infarct size by reperfusing the myocardium at risk, and thereby prevent further deterioration of left ventricular (LV) function. Recently, stem cell therapy was introduced as an additional therapy for patients that suffer from acute or chronic IHD. Via cell fusion or paracrine signaling between injected and native cells, this therapy targets cardiomyogenesis and vasculogenesis, and limits adverse remodeling. Despite the promising initial results obtained in preclinical research[1], recent clinical and preclinical research has been disappointing in terms of global LV function[2,3]. The importance of measuring global LV function (LV volumes, ejection fraction (EF), dp/dt_{max}, maximal elastance) has been well established as it is closely related to prognosis. Unfortunately these measures are most likely inappropriate to detect the relatively small and local functional changes in the myocardium induced by cardiac regenerative therapy. Consequently several fundamental questions addressing the working mechanisms of cardiac regenerative therapy are still unanswered, thereby hampering the introduction of proper strategies to (further) improve cell therapy. Besides optimization of the therapeutic medium and delivery methods[4,5], optimal selection of the techniques to assess regional cardiac function should therefore also receive increasing attention[6,7]. However, no optimal assessment strategy is proposed so far. To assess the local changes in the myocardium by cardiac regenerative therapy, non invasive imaging of perfusion, viability, tissue fibrosis, and regional function assessment by deformation imaging could be applied. Invasive measurements encompass intracoronary flow and pressure, endocardial surface potentials, and linear local shortening. In this review, we summarize local measurement techniques and assess their diagnostic values in cardiac regenerative therapy. We believe that this is necessary to choose the optimal endpoints for future clinical studies and improve feedback to researchers determining the dominant pathways that lead to effective cardiac regeneration.

Cardiac regenerative therapy

IHD is the result of acute or chronic insufficient blood supply to meet myocardial metabolic needs. At a cellular and tissue level this results in cardiomyocyte apoptosis and necrosis, inflammation, and fibrosis formation. Consequently this will lead to loss of cardiomyocytes, scar formation, and finally ventricular remodeling[8]. Clinically this can eventually result in RAP or HF. At organ level this process is successively characterized by the causes and effects stated in Table 1.

In order to improve or prevent deterioration of cardiac function cardiac regenerative therapy is suggested to affect 3 different processes causing distinct structural constitutional changes in the myocardium:

1. *Vasculogenesis* aims at the repair of the microvasculature in the myocardium. In cases of chronic ischemia it restores blood supply to the ischemic hibernating cardiomyocytes, thereby restoring their contractile function and passive mechanical properties (Ref. A in Table 1). Preclinical studies have shown increased vessel growth in infarcted areas after treatment with autologous mesenchymal stem cells[9,10]. Another possible, but probably

modest effect of vasculogenesis, is the increase of tissue stiffness due to the mechanical contribution of perfused arteries[8] (Ref. C in Table 1).
2. *Cardiomyogenesis* aims at the replenishment of cardiomyocytes within the infarcted area that are both electrically and mechanically coupled to the native myocardium, addressing the effect of ref A in Table 1. Although cardiomyogenesis has been proven in vitro[1], evidence of in vivo cardiomyogenesis with clinically used cells is scarce[11]. Since noticeable improvement of contractile function and tissue stiffness (Ref. B and C in Table 1) requires ingrowth of coupled functional cardiomyocytes on a large scale, it is unexpected with currently used cells. Nevertheless cytoprotection, suppression of inflammation, or enhancement of endogenous repair through paracrine signaling have been suggested to prevent apoptosis. This consequently alters tissue constitution and thereby reduce stiffness and increase function after transplantation of mesenchymal stem cells[12].
3. *Matrix assisted myocardium stabilization* (MAMS) aims at mechanical support of the ischemic and infarcted tissue by biomaterial injections. When applied in the optimal amount, timing, and location, these biomaterials have been shown to intervene in the remodeling process[13]. Finite element modeling studies of LV mechanics have shown that both isotropic[14] and anisotropic[15] alteration of local tissue stiffness can have a beneficial effect on global ventricular function. During extra cellular matrix (ECM) degradation MAMS leads to reduced compliance (Ref. B in Table 1)[13]. During ECM deposition and cross linking MAMS leads to reduced infarct stiffness (Ref. C in Table 1)[13]. Interactions between these approaches and the biological response need to be investigated further in vivo.
Ultimately all abovementioned constitutional changes in the myocardium will result in limitation of ECM degradation and improvement of cardiomyocyte survival in the myocardium[16]. This will lead to a reduction of adverse myocardial remodeling with concomitantly increasing wall thickness, reduction of infarct stiffness, and increased contractile function (Ref. A, B, and C in Table 1). The three mechanisms of repair and subsequent constitutional changes in the myocardium are illustrated in Figure 1.

Table 1. The myocardial infarction cascade

Ref.	Time	Cause	Effect
A	Hours	Reduced myocardial perfusion	Reduced contractile function
B	Days	Degradation of the ECM framework	Increased tissue compliance
C	Weeks	Deposition and cross linking of a newly developed collagen network	Gradually increasing infarct stiffness

Measurement techniques for cardiac regenerative therapy

It is currently not possible to directly measure any of the three repair mechanisms of stem cell therapy outlined in Figure 1. Therefore alternative measures must be chosen that reflect the abovementioned effects of the therapy. Myocardial perfusion imaging or intracoronary pressure and flow measurements could be used to quantify local blood supply to the myocardium. Myocardial viability imaging or endocardial surface potentials can serve as a measure of tissue viability. Myocardial fibrosis imaging reflects the local extent of adverse remodeling. Deformation imaging parameters are related to local cardiac biomechanics, and can potentially be used to assess local constitutional changes. Several invasive and non invasive techniques are currently available to assess these different aspects of

functional outcome in cardiac regenerative therapy with respect to regional function. Each technique has its own strengths and limitations, and thorough knowledge of this will consequently lead to a better definition of clinical endpoints and will further enhance our understanding of the potential effects of cardiac regenerative therapy. In the following section different invasive and non-invasive techniques are outlined in terms of available derived parameters and results of recent clinical trials when available. Since multiple studies have employed echocardiography for functional assessment of outcome after cardiac regenerative therapy, this imaging technique will be discussed more thoroughly.

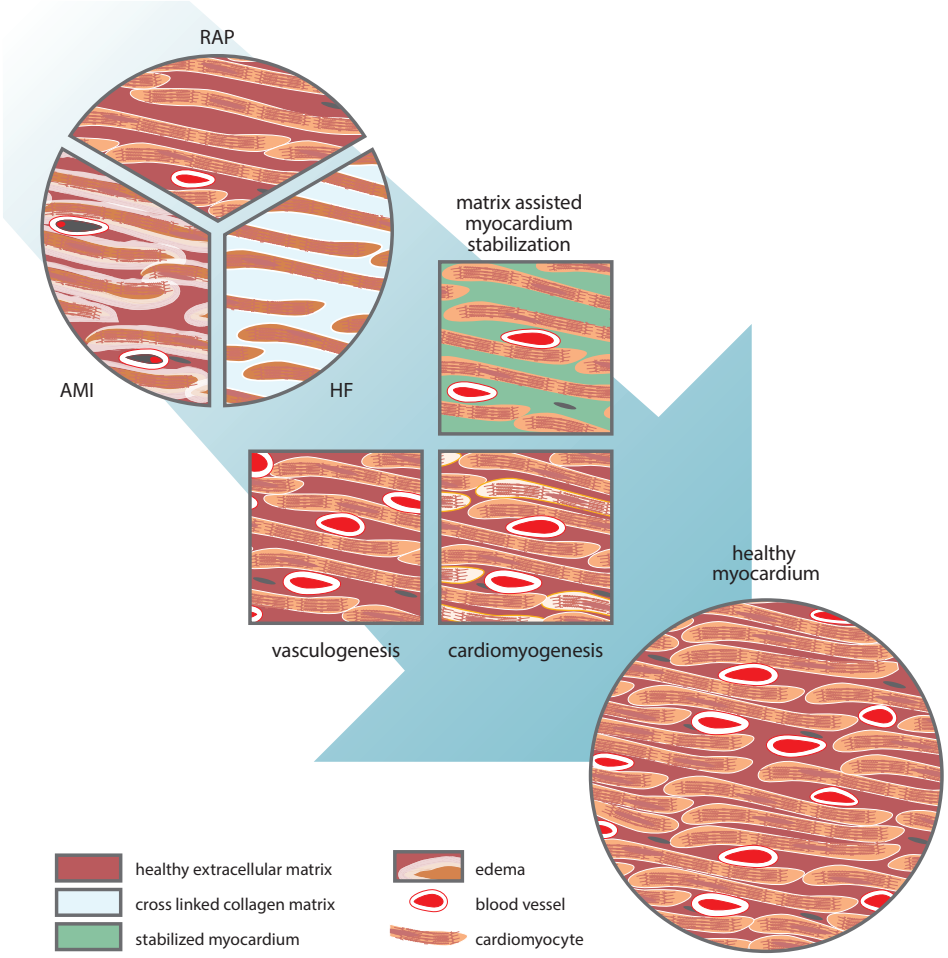

Figure 1. Schematic representation of mechanisms of repair by cardiac regenerative therapy. RAP = refractory angina pectoris, AMI = acute myocardial infarction, HF = heart failure

Invasive assessment

Intracoronary pressure and velocity measurements in coronary stenosis are used to calculate the severity of the stenosis from the hyperemic stenotic resistance index (HSRi), fractional flow reserve (FFR), and coronary flow velocity reserve (CFVR) that are determined during pharmacologically established hyperemia[17]. For these measurements a microwire equipped with a pressure and Doppler sensor is fluoroscopically guided into the vessel of interest as is depicted in Figure 2. The ratio of the pressure difference caused by the stenosis and the distal average peak velocity represents the HSRi. The ratio of the microvascular pressure difference and distal average peak velocity, measured during pharmacologically established hyperemia, represents the hyperemic microvascular resistance index (HMRi)[18] (Figure 2). Both blood pressure and velocity are taken into account in this parameter.

Non invasive coronary flow velocity reserve measurements can be done by transthoracic Doppler echocardiography[19]. Because this measure does not account for pressure differences affecting the tissue perfusion, and has not been used to assess the effects of cardiac regenerative therapy in vivo so far, this technique is not discussed further.

Both the REPAIR-AMI trail[20] and the HEBE trail[21] used HMRi to assess the angiogenic capacity of bone marrow derived progenitor cell (BMC), bone marrow mononuclear cell (BMMC) and peripheral blood mononuclear cell (PBMC) therapy after coronary infusion, 4 days after percutaneous coronary intervention (PCI) in ST-segment elevation myocardial infarction (STEMI) patients. In a study by Bax et al.[22] normal HMRi values of approximately 1.8 increased to 3.2 during infarction and normalize again after PCI. The HEBE trial reported no additional reduction of HMRi in all study groups, whereas the REPAIR-AMI trail reported a significant decrease of the HMRi in the BMC group to a value below normal: 1.2. An overview of these results is presented in Table 2. The origin of the large improvement in the REPAIR-AMI trail compared to the HEBE trial could be the longer interval between the onset of symptoms and reperfusion in the REPAIR-AMI trail, causing a larger infarct as suggested by the HEBE investigators. Differences in the adenosine dosages (intravenous infusion of 140µg/kg body weight (REPAIR-AMI) versus intracoronary bolus of 20 to 40µg (HEBE)) might also have affected the results since they can cause a different degree of hyperemia.

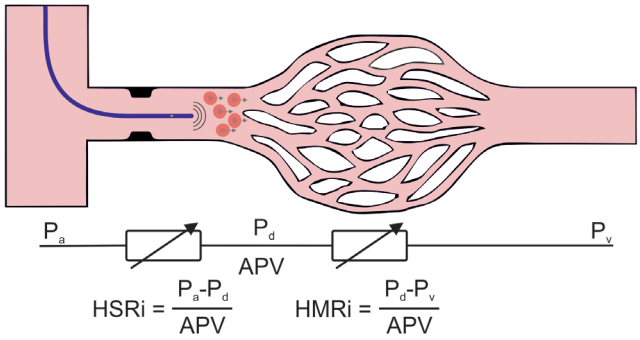

Figure 2. The HSRi and HMRi measurement principles. Pa = aortic pressure, Pd = distal pressure, Pv = venous pressure, APV = average peak velocity

Table 2. Baseline and follow up values of the hyperemic microvascular resistance index (HMRi)

		HMRi (mmHg·s/cm) Infarct related artery		HMRi (mmHg·s/cm) Reference artery	
		Baseline	Follow-up	Baseline	Follow-up
Bax et al.[22]	Time after PCI	Immediately	6 months	Immediately	6 months
	PCI (n=73)	3,2 ± 1,7	1,8 ± 0,6	2,2 ± 0,6	1,8 ± 0,7
Hebe trial[21]	Time after PCI	6 days	132 days	6 days	132 days
	PBMC (n=18)	1,9 ± 0,8	1,8 ± 0,6	1,7 ± 0,6	1,6 ± 0,4
	BMMC (n=23)	2,0 ± 0,5	1,8 ± 0,6	1,7 ± 0,6	1,7 ± 0,5
	placebo (n=19)	1,9 ± 0,5	1,7 ± 0,5	1,8 ± 0,4	1,5 ± 0,5
Repair-AMI[20]	Time after PCI	Immediately	4 months	Immediately	4 months
	BMC (n=28)	1,86 ± 1,0	1,20 ± 0,6	1,64 ± 0,6	2,28 ± 2,8
	placebo (n=26)	1,77 ±0,6	1,52 ± 0,8	1,59 ±0,6	1,55 ± 0,5

HMRi in the infarct related coronary artery and a reference coronary artery after acute PCI (Bax et al.), PBMC, BMMC, and placebo injections (HEBE), and BMC and placebo infusion (Repair-AMI)

Since vasculogenesis induced changes of distal pressure and flow in an individual patient might be very small compared to the measurement noise caused by sub optimal catheter positioning, HMRi cannot be used to assess the vasculogenesis in a single patient. In a patient population however HMRi can provide insight into local changes of fluid resistance. Since HMRi quantifies the microvascular resistance, it might be affected by the extent of the microvasculature as well as the mechanical pressure exerted by the (infarcted) myocardium. Besides vasculogenesis, reduced tissue stiffness might therefore also cause reduction of HMRi. Inevitable for this measurement is its invasiveness and therefore patency of the coronary arteries. A special remark must be made about the use of the aortic pressure to calculate the HMRi in both studies mentioned above. To prevent the overestimation of HMRi due to residual stenosis, measurement of the distal pressure is more appropriate to calculate the HMRi.

Electromechanical mapping (EMM) in the LV is done with a catheter mapping technique simultaneously records the electrical unipolar (UP) and bipolar (BP) depolarization voltages on the LV endocardium. The positions of the measurements are recorded by a magnetic tracking system. The relative motion between neighboring measurement points during the cardiac cycle is a measure of local tissue deformation, expressed as linear local shortening (LLS). Multiple studies have shown a good sensitivity and specificity of the peak UP and BP values, and peak LLS values, to distinguish viable from non viable myocardium as determined by fibrosis, perfusion, and viability imaging techniques or histological analysis[23,24]. Theoretically, cardiac regenerative therapy induced substitution of infarcted areas by healthy tissue would lead to normalization of UP, BP, and LLS values. Hereby EMM becomes an alternative method to assess the therapeutic effects.

Application of electromechanical mapping for the assessment of cardiac regenerative therapy has shown a non significant increase of UP and a significant increase of LLS after trans endocardial autologous bone marrow cell transplantation in patients with chronic IHD[25]. Moreover a significant increase of both UP and LLS was observed after intracoronary infusion of autologous bone marrow mesenchymal stem cells in patients with acute MI[26].

Initially EMM was intended as a method to perceive the myocardial scar and guide injections to the border zone of the scar during cardiac catheterization based upon visualization of local depolarization potentials and LLS on a 3D surface mesh. Limitations for local therapeutic effect assessment are the low spatial resolution and inhomogeneous distribution of mapping points. This requires interpolation between the measurements and thereby does not reliably represent the true spatial distribution of depolarization potentials and LLS. In addition to that, the endocardial surface potentials do reflect scar transmurality but do not reflect the complex 3D scar geometry[27]. This method is invasive and requires at least one hour of mapping time by an experienced physician. In summary, based on these limitations we conclude that this method is suboptimal to assess the small regional effects targeted by cardiac regenerative therapy.

Non invasive imaging

Magnetic resonance imaging (MRI) can be used to assess regional tissue perfusion, viability, scarring, and deformation. Perfusion and scarring assessment rely on the first passage and late uptake of gadolinium contrast respectively. Perfusion measurements use the upslope of the signal intensity in the myocardium when a gadolinium based contrast agent (GBCA) is injected[28]. Transient differences in perfusion during rest and exercise (or pharmacological increased oxygen demand), reflects the reversibility of the perfusion defect. Currently MRI late Gadolinium enhancement (LGE) is the gold standard for myocardial fibrosis imaging. It uses the delayed increase of signal intensity caused by the delayed washout of injected GBCA from the greatly expanded extracellular space of the myocardial scar[9]. Contractile reserve can be assessed by dobutamine stress MRI. Hereby the improvement of local systolic function by wall motion analysis in ischemic segments after positive inotropic stimulation by dobutamine infusion is a measure of local contractile reserve. Myocardial deformation, reflecting regional function, can be performed by a technique labeled tagging MRI which has been discussed in previous articles[29,30]. Quantification of deformation can possibly be used to assess local changes of cardiac biomechanics caused by cardiac regenerative therapy[9,31-35]. An overview of studies using tagging MRI to assess the effects of cardiac regenerative therapy is listed in Table 3. A practical disadvantage of MRI in the clinical setting is the exclusion of patients with an ICD or patients that suffer from claustrophobia that cannot be inserted into the MRI system.

MR perfusion measurements showed an improved perfusion 15 months after cardiac regenerative therapy compared to control[36]. Several studies that reported scar size measured by LGE after cardiac regenerative therapy showed a marked reduction in infarct size compared to control[37-42] after follow up periods of 3 to 18 months. Recently Leistner et al.[43] reported scar volumes after 5 years follow up, and showed a decreased infarct volume / LV wall volume ratio. Unfortunately there was no control group in this study. In contrast to that, other studies showed no effect on infarct mass after 6 weeks follow up in animals[44], or after 15 months follow up in humans[36]. Even a higher reduction of infarct mass and scared segments in the control group compared to the therapy group after 6 months follow up is also reported[45]. Since infarct size also tends to decrease naturally[8,46], and results in literature are not unequivocal, it is very difficult to draw conclusions from these studies about the mechanisms involved.

Nuclear imaging is most often used to assess tissue perfusion, viability, fibrosis, and wall motion. Single photon emission computed tomography (SPECT)[47] and positron emission tomography (PET)[48] quantify tissue perfusion from the early tissue uptake of a perfusion tracer. Multi slice computer tomography (MSCT)[49] is a radiography technique by which tissue perfusion can be quantified from the early tissue uptake of a perfusion tracer with addition of anatomical information. Whereas SPECT quantifies the relative perfusion compared to the region with the highest tracer uptake, PET imaging allows quantification of the absolute perfusion in the myocardium. In both modalities, different tracers can be used that have different uptake mechanisms and supply different radiation exposure to the patient[50]. Perfusion difference during rest and exercise (or pharmacological increased oxygen demand), reflects the reversibility of the perfusion defect. Viability assessment by SPECT imaging uses the signal increase caused by the persisting tracer uptake in the myocardium due to an intact cell membrane. Viability imaging by [^{18}F]-FDG PET uses the transfer of fatty acid metabolism in normal myocardium to glucose metabolism in dysfunctional but viable myocardium. Cellular uptake of ^{18}F labeled glucose indicates cell viability. Since the spatial resolution of SPECT and PET is low, wall motion assessment by these imaging modalities only provide coarse deformation information. At the expense of severe radiation exposure, myocardial fibrosis imaging by MSCT showed similar results as the gold standard LGE MRI[49].

Many studies use nuclear techniques to assess changes of perfusion and viability after cardiac regenerative therapy in AMI, chronic MI, and RAP patients. As was already outlined in a review by Beeres et al.[51] most of these studies using SPECT report a decrease of the perfusion defect 3 to 12 months after bone marrow cell therapy[52-60]. Of interest, two studies using PET did not show any improvement in regional perfusion[39,44]. The cause of this difference could be the relative (SPECT) versus the absolute (PET) quantification of perfusion, or different attenuation correction methods, but this remains speculative. Studies using glucose utilization to assess tissue viability reported equal or increased viability in ischemic segments[26,52,54,55,57-59,61]. Studies assessing contractile reserve[53,56,62] showed a less pronounced improvement. From this, the authors conclude that this difference might possibly be caused by extensive cellular damage induced reduction of contractile reserve, but preserved glucose utilization. A study to reveal the mechanism underlying this difference could provide valuable insight in interpretation of viability and contractile reserve data.

Ultrasound imaging (US) supplies methods to quantify perfusion, viability, and deformation. Perfusion measurements by US[63] rely upon the uptake of an ultrasound contrast agent consistent of microbubbles in the myocardium, which opacifies the myocardium. Perfusion defects show as a less bright or non opacified area. Perfusion difference during rest and exercise (or pharmacological increased oxygen demand), reflects the reversibility of the perfusion defect. Local contractile reserve assessment by US[64] is done by dobutamine stress echocardiography (DSE), where improvement of local systolic wall motion in ischemic segments after positive inotropic stimulation by dobutamine infusion reflects local contractile reserve. Assessment of regional cardiac deformation is another novel application within the US examination. For correct interpretation of these measures knowledge of deformation imaging technology, physiology, and physics is necessary. These are extensively discussed in previous articles[65,66]. Although cardiac deformation indices have been used in cardiac regenerative therapy, there is no unequivocal relation between cardiac regenerative therapy and indices of cardiac deformation. Applications of

Table 3. Overview of cardiac regeneration studies using deformation imaging as an endpoint. Unless otherwise stated, the treatment effect represents the changes in the infarcted area of all therapy groups with respect to the control group for all follow up time points

1st Author	No. of Patients	Setting/Study design	Delivery route	Cell Type	FU-weeks	Strain	Treatment	Strain Rate	Treatment	Method
Beitnes et al.[72]	50 vs. 50 ctrl	AMI/randomized/ctrl -	intracoronary	68×10^6 BMNC	24, 3y	$\varepsilon L_{peak\ systolic}$	→→			STE
Herbots et al.[67]	33 vs. 34 ctrl	AMI/randomized/ctrl -	intracoronary	304×10^6 BMC + 172×10^6 BMNC	16	$\varepsilon L_{end\ systolic}$	↑	$d\varepsilon L/dt_{\ peak\ systolic}$	↑	TDI
Hopp et al.[45]	15 vs. 13 ctrl	AMI/randomized/ctrl -	intracoronary	68×10^6 BMC	24	$\varepsilon C_{end\ systolic}$	↓			MRT
Karatasakis et al.[68]	10	IHD	intracoronary	1.6×10^7 BMC	24	εL_{max} $\varepsilon L_{ejection\ time}$ $\varepsilon L_{post\ systolic}$	↑[1] ↑ →	$d\varepsilon L/dt_{\ peak\ systolic}$	↑	TDI
Lebrun et al.[69]	11	IHD	intracoronary	250×10^6 BMNC	16	$\varepsilon L_{max\ systolic}$	→[1]	$d\varepsilon L/dt_{\ peak\ systolic}$	→	TDI STE
Plewka et al.[70]	40 vs. 20 ctrl	STEMI/randomized/ctrl -	intracoronary	1.44×10^8 BMC	24	$\varepsilon L_{systolic}$	↑			
Ruan et al.[73]	9 vs. 11 ctrl	AMI/double-blinded randomized/ctrl -	intracoronary	BMC	12, 24	$\varepsilon L_{peak\ systolic}$	↑→			TDI
van Ramshorst et al.[71]	14 vs. 10 ctrl	Chronic IHD/non-randomised/ctrl -	intramyocardial	93×10^6 BMC	12	$\varepsilon L_{global\ peak\ systolic}$	↑			STE
Williams et al.[35]	8	Chronic IHD/non-randomised	intramyocardial	BMNC & MSC	12, 24, 1y	εC_{peak}	↑→→[1]			MRT
1st Author	**No. of Animals**	**Setting/Study design**	**Delivery route**	**Cel Type**	**FU-weeks**	**Strain**	**Treatment effect**	**Strain Rate**	**Treatment effect**	**Method**
Amado et al.[31]	6 vs. 6 ctrl	3 days post IR of RCA\ctrl -	intramyocardial	2×10^8 allogenic MSC	1, 4, 8	εC_{peak}	↑↑↑			MRT
Rickers et al.[32]	5 vs 5. pl	4 weeks post LAD ligation\ctrl -	surgical	1×10^6/inj autologous MAPCs	8, 16	εC_{peak}	↑↑			MRT

Table 3. Continued

Quevedo et al.[33]	6 vs. 4 pl	4 weeks post IR of LAD\ctrl -	intramyocardial	2×10^8 allogenic MSC	1, 4, 8, 12	εC_{peak}	↑↑↑		MRT
Schuleri et al.[34]	6 vs. 3 vs 6 pl	12 weeks post IR of LAD\ctrl -	surgical	20×10^6 allogenic MSC 200×10^6 allogenic MSC	24	εC_{peak}	$\uparrow\uparrow^2$		MRT
Schuleri et al.[10]	10 vs. 6 pl vs. 8 ctrl	2 days post IR of LAD\ctrl -	intramyocardial	200×10^6 allogenic MSC	8	εC_{peak}	↑		MRT
Schneider et al.[74]	5 vs. 4 vs. 6 vs. 8 pl	2 weeks post LCX ligation\ctrl -	intramyocardial	2.5×10^7 autologous MSC 2.9×10^7 allogenic MSC 1.7×10^7 autologous BMNC	4	$\varepsilon R_{systolic}$ $\varepsilon R_{post\ systolic}$	$\rightarrow\rightarrow\rightarrow^2$ $\rightarrow\rightarrow\rightarrow^2$	$dER/dt_{\substack{peak \\ systolic}}$	→	TDI

BMC = bone marrow cell, BMNC = bone marrow mononuclear cell, CAD = coronary artery disease, CABG = coronary artery bypass grafting, ctrl = controle group included, ctrl- = negative control group included, ctrl+ = positive control group included, εL = longitudinal strain, εC = circumferential strain, εR = radial strain, FU = follow up, IR = ischemia reperfusion, LAD = left descending coronary artery, LCX = left coronary artery, MAPC = multipotent adult progenitor cell, MRT = magnetic resonance tagging, MSC = mesenchymal stem cell, RCA = right coronary artery, STE = speckle tracking echocardiography, TDI = tissue Doppler imaging, treatment effect = effect with respect to control groupunless otherwise stated, y = year, 1 = with respect to baseline measurements, 2 = effects of all therapy groups

US derived indices of cardiac deformation to assess the effects of cardiac regenerative therapy[67-74] are summarized in Table 3. Here we shortly introduce deformation imaging in ischemic cardiomyopathies and cardiac regenerative therapy, and discuss the results of the studies that are done with it so far.

Cardiac deformation can be measured by US and tagging MRI. It is always the result of the local stress on a segment of myocardium and the sum of the active and passive stresses within the segment[75]. It is typically measured in the cardiac coordinate system with components: longitudinal, circumferential, and radial and expressed as a one dimensional parameter: strain (ε) and its time derivative strain rate (SR)[76]. Since the heart is a complex structure of interconnected myofibers, we hypothesize that improvement of global cardiac function must inevitably be preceded or accompanied by improvement of local cardiac mechanics in the region targeted with stem cell therapy. Although these local changes are small, and the relations between changes in the deformation pattern and the pathology are complex, proper application of local myocardial deformation assessment might provide insights into the therapeutic mechanisms of cardiac regenerative therapy. When assessing small changes of cardiac deformation, physiological determinants and confounders of deformation become important. Cardiac contractility[77], ventricular geometry[78-80], and the interaction between tissue segments with a different elasticity are important physiological determinants of deformation[79,81]. Changing inotropy and pre-afterload

have shown that strain correlates to ejection fraction and strain rate correlates to contractility[77,80,82]. In deformation imaging studies of normal, ischemic, and scarred myocardium systolic radial (thickening) and longitudinal and circumferential (shortening) peak strain values, and strain rate values are lower in ischemic segments (Ref. A in Table 1)[79].

As ischemic time elapses and tissue elasticity increases (Ref. B in Table 1) these are increasingly replaced by dyskinetic radial thinning, longitudinal and circumferential lengthening, and postsystolic radial thickening (PST), and longitudinal and circumferential shortening (PSS)[83]. When ventricular remodeling progresses, the increased fibrosis enhances tissue stiffness and replaces dyskinetic lengthening by isometric motion during systole and decreased longitudinal and circumferential lengthening and radial thinning during diastole (Ref. C in Table 1). Eventually there is no deformation left in transmurally infarcted tissue, ultimately resulting in constrictive LV filling and progression towards both systolic and diastolic dysfunction.

Besides the inotropic properties of individual cardiomyocytes, cardiac contractility depends on the amount of cardiomyocytes that contribute to contraction. Since all mechanisms of repair aim at preservation of cardiomyocytes they can all affect contractility, and can be best assessed by strain rate. Passive tissue elasticity is targeted by all mechanisms of stem cell therapy. It will first act upon the diastolic tissue velocity, or diastolic strain (rate), and quantitatively depend on LV geometry, tissue anisotropy, and the pressure-volume relationship. Secondary it might affect systolic deformation due to stiffness induced preload changes. Preload and the excitation pattern inevitably affect deformation via the Frank Starling mechanism[84]. Afterload affects local wall stress, and thereby local deformation. Since pre-afterload and the excitation pattern are not expected to change due to cardiac regenerative therapy they are considered physiological confounders when assessing cardiac deformation. Ventricular geometry plays a key role in the stress distribution in the myocardium, affecting local deformation and ventricular remodeling[79,85]. Ventricular geometry should therefore always be considered in the interpretation of deformation measures. To exclude changes induced by geometry and other physiology or physics related deformation imaging confounders (e.g. image quality, through plane motion, reduced wall thickness), they must either be controlled or measured simultaneously.

Different indices of systolic myocardial deformation have been reported to assess the effects of stem cell therapy. Table 3 provides an overview of 15 stem cell studies in patients and large animals with deformation imaging endpoints. Since 5 studies have used one dimensional tissue Doppler imaging (TDI), 3 studies have used two-dimensional speckle tracking echocardiography (STE), and 7 studies have used two-dimensional MRI tagging, all techniques are described. All studies report unchanged or increased longitudinal (εL), circumferential (εC), and radial (εR) peak or systolic strain and strain rate after the therapy. In studies using a one dimensional technique the directions of acquisition are limited to the longitudinal and radial direction. Although cardiac deformation is affected by multiple physiological interactions as is described in detail above, influential parameters are not reported by all studies. Despite the fact that loading changes are not targeted by the therapy, it cannot be assumed that no loading changes occur during the follow up period. In particular, the geometric alterations caused by (natural) scar size reduction or scar stiffening might induce significant loading alterations. The absence of indices of geometry, volume, and pressure therefore make it difficult to state that the reported improvements are caused by the therapy. In addition, the different study designs, and the use of different

methods to distinguish infarcted from healthy tissue prevent further unraveling of the underlying mechanisms of repair from these studies. Herbots et al[67] reported the EDV, LV sphericity index, and estimated the systolic pressure from the cuff pressure before the ultrasound examination to estimate preload, geometry, and afterload. Since the sphericity index and EDV did not differ before and after therapy, authors concluded the absence of preload changes. Systolic arterial blood pressure however was significantly lower in the treated group. This would most likely also effect local myocardial deformation, but was not investigated further.

Use of deformation imaging to assess the effects of cardiac regenerative therapy is understandable since all physiological determinants of deformation: contractility, geometry, and elasticity are targeted by stem cell therapy. However, interpretation of these results remains difficult due to the interactions between physiological determinants and confounders: dyssynchronous contraction, pre- and afterload, infarct size reduction, and natural infarct stiffening. Only when the interaction of multiple physiologic mechanisms is controlled, a single parameter can be measured. Furthermore, assessment of contractility via the peak strain is doubtful since this more or less reflects local EF, and is less related to contractility and stiffness. Here for the use of strain rate seems to be more appropriate as described above[82]. The use of strain (rate) patterns to assess the relation between systolic and postsystolic deformation might also be of interest since this changes in response to ischemia, passive stiffness, and contractility of the tissue[75]. Although the sphericity index[86] is a simple global 2D measure of ventricular shape it can be used as a reference of ventricular shape. For local assessment, measurement of local ventricular shape is desired[85].

Discussion

The different invasive and non-invasive quantitative techniques and their derivatives discussed in this review reflect different aspects of cardiac function. Distinct relations between the measures, effects, and mechanisms of cardiac regenerative therapy unlikely exist. Presumable relations however exist between the measurement techniques and the three typical mechanisms of cardiac regenerative therapy: vasculogenesis, cardiomyogenesis, and matrix assisted myocardium stabilization (MAMS).

	Invasive		Non invasive imaging			
	Hyperemic Microvascular Resistance index	Electromechanical mapping	Perfusion	Viability	Fibrosis	Deformation
Vasculogenesis	■	■	■	■	■	■
Cardiomyogenesis	■	■	■	■	■	■
MAMS	■	■	■	■	■	■

Figure 3. Relations between measurement techniques and mechanisms of repair by cardiac regenerative therapy. MAMS = matrix enhanced myocardium stabilization, ■ = relation presumed, ■ = no direct relation expected, ■ = no relation.

These relations are visualized by means of a color scale in Figure 3. Intracoronary pressure and velocity derived HMRi is likely to reflect vasculogenesis.
This can either be induced by direct vasculogeneic stimuli, or stimuli originating from increased metabolic demand induced by cardiomyogenesis or matrix assisted myocardium stabilization. Mechanical effects caused by altered tissue stiffness can also affect HMRi. Therefore HMRi is not able to differentiate between mechanisms unequivocally. Although electromechanical mapping is suitable to guide intramyocardial injections, its application to assess the changes induced by cardiac regenerative therapy does not provide insight into the mechanisms involved. Myocardial perfusion is related to the myocardial microvasculature. Besides vasculogenesis, the other mechanisms of cardiac regenerative therapy can also induce changes of perfusion. Both cardiomyogenesis and MAMS aim to prevent cell death and change the local stiffness of the tissue. Thereby these processes can affect tissue perfusion as well. It must also be recalled that increased perfusion or viability does not inherently imply improved LV function. In summary, increase of perfusion and viability does not provide conclusive evidence for a single mechanism underlying these changes. Since the extent of myocardial fibrotic scaring is also subjected to biologically largely varying natural scar size reduction, the additional effects of cardiac regenerative therapy mechanisms on scar size are difficult to assess. Cardiac deformation imaging parameters reflect elements of cardiac biomechanics. We state that in a setting of synchronous contraction with stable pre- and afterload, when physiological determinants and confounders of deformation are measured (geometry), or controlled (pre- afterload, inotropy), deformation imaging becomes a tool to assess the local contractility (active) or tissue stiffness (passive). Such a comprehensive approach allows distinction between the physiological determinants, confounders, and ultimately the therapeutic alterations of deformation. Despite these positive considerations, deformation imaging most likely cannot conclusively distinguish the mechanism of repair of cardiac regenerative therapy, but can provide a unique insight in the local active and passive properties of both contractile and ischemic or infarcted tissue. Moreover, since there is a different response to ischemia and remodeling between endo and epicardium[46], measurement of this difference might be very interesting and relevant. As a first step, these approaches must be tested in fully equipped animal experiments. Knowledge gained from this can be used in clinical applications. Since these measurements are non-invasive and feasible in human subjects they can add importantly to the understanding of the mechanisms involved in cardiac stem cell therapy.

Future perspective

All discussed techniques to assess the local functional effects of cardiac regenerative therapy have been clinically available for the last decade. Especially in the field of the computational intense deformation imaging techniques, technological progress has created applicable new possibilities to reliably and accurately assess local cardiac function. For example: the newest STE tracking algorithms have the possibility to assess the local differences between the sub epicardial, and sub endocardial wall. Furthermore, vector velocity imaging (VVI), and real time three dimensional transthoracic echocardiography techniques allow determination of regional EF and motion. We would like to emphasize that these sophisticated quantification techniques mainly rely on sophisticated post processing algorithms. We believe that results obtained by these techniques must therefore

be critically reviewed to prevent interference of the data by these algorithms. Application of these techniques to assess local effects of cardiac regenerative therapy might provide additional insights, but this first need extensive validation in both preclinical (animal studies) and clinical studies.

Conclusion

Despite the progress in preclinical studies with different cell types, delivery methods, and timing of delivery, translation of cardiac regenerative therapy to clinical applications is still hampered. Main reason for this might be the modest effect on clinical endpoints that are closely correlated to survival rate and cardiac events (i.e. EF), in these studies. To introduce proper improvement strategies and extend our knowledge about the working mechanisms of cardiac regenerative therapy, it is important to extend the focus from clinical endpoints to detailed local measures of cardiac function as is suggested by different authors[6,7]. In this review, we have discussed measurement techniques of local microvascular resistance, myocardial perfusion, viability, fibrosis, and deformation. All independent measures lack specificity to uniquely assess the 3 proposed repair mechanisms of stem cell therapy. Combinations of measurements provide more insight. In particular, combination of deformation imaging, by ultrasound or MRI, with simultaneously measured local geometry and pressure measurements is a promising approach to assess the effects of cardiac regenerative therapy on local cardiac biomechanics. This comprehensive approach provides information about local tissue contractility, stiffness, and thereby remodeling. We recommend that researchers use this comprehensive approach in future studies.

Acknowledgements

This research is part of the Project P1.04 SMARTCARE of the research program of the BioMedical Materials institute, co-funded by the Dutch Ministry of Economic Affairs, Agriculture and Innovation. The financial contribution of the Nederlandse Hartstichting is gratefully acknowledged.

References

1. Smits AM, van Vliet P, Metz CH, Korfage T, Sluijter JPG, Doevendans PA. Human cardiomyocyte progenitor cells differentiate into functional mature cardiomyocytes: an in vitro model for studying human cardiac physiology and pathophysiology. Nature Protocols. 2009;4:232-243
2. Segers VFM, Lee RT. Stem-cell therapy for cardiac disease. Nature. 2008;451:937-942
3. Malliaras K, Kreke M, Marbán E. The stuttering progress of cell therapy for heart disease. Clinical pharmacology and therapeutics. 2011;90:532-541
4. Gyöngyösi M, Lang I, Dettke M, Beran G, Graf S, Sochor H, Nyolczas N, Charwat S, Hemetsberger R, Christ G, Édes I, Balogh L, Krause KT, Jaquet K, Kuck K-h, Benedek I, Hintea T, Kiss R, Préda I, Kotevski V, Pejkov H, Zamini S, Khorsand A, Sodeck G, Kaider A, Maurer G, Glogar D. Combined delivery approach of bone marrow mononuclear stem cells early and late after myocardial infarction: the MYSTAR prospective, randomized study. Nature Clinical Practice. 2008;6:70-81
5. Van Der Spoel TIG, Chun-Tsu Lee J, Vrijsen KR, Sluijter JPG, Cramer MJM, Doevendans PA, Belle EV, Chamuleau SAJ. Non-surgical stem cell delivery strategies and in vivo cell tracking to injured myocardium. International Journal of Cardiovascular Imaging. 2010;27:367-383
6. Tendera M, Wojakowski W. How to measure the effects of the intracoronary stem cell therapy? European Journal of Echocardiography. 2010;11:438-439
7. Traverse JH, Henry TD, Moye LA. Is the measurement of left ventricular ejection fraction the proper end point for cell therapy trials? An analysis of the effect of bone marrow mononuclear stem cell administration on left ventricular ejection fraction after ST-segment elevation myocardial infarction when evaluated by cardiac magnetic resonance imaging. American heart journal. 2011;162:671-677
8. Holmes JW, Borg TK, Covell JW. Structure and Mechanics of Healing Myocardial Infarcts. Annual Reviews of Biomedical Engineering. 2005;7:223-253
9. Schuleri KH, Amado LC, Boyle AJ, Centola M, Saliaris AP, Gutman MR, Hatzistergos KE, Oskouei BN, Zimmet JM, Young RG, Heldman AW, Lardo AC, Hare JM. Early improvement in cardiac tissue perfusion due to mesenchymal stem cells. American Journal Of Physiology Heart and Circulation Physiology. 2008;294:2002-2011
10. Gavira JJ, Nasarre E, Abizanda G, Pérez-Ilzarbe M, de Martino-Rodriguez A, García de Jalón JA, Mazo M, Macias A, García-Bolao I, Pelacho B, Martínez-Caro D, Prósper F. Repeated implantation of skeletal myoblast in a swine model of chronic myocardial infarction. European heart journal. 2010;31:1013-1021
11. Murry CE, Soonpaa MH, Reinecke H, Nakajima H, Nakajima HO, Rubart M, Pasumarthi KBS, Virag JI, Bartelmez SH, Poppa V, Bradford G, Dowell JD, Williams DA, Field LJ. Haematopoietic stem cells do not transdifferentiate into cardiac myocytes in myocardial infarcts. Nature. 2004;428:13-15
12. Williams AR, Hare JM. Mesenchymal Stem Cells: Biology, Pathophysiology, Translational Findings, and Therapeutic Implications for Cardiac Disease. Circulation research. 2011;109:923-940
13. Leor J, Tuvia S, Guetta V, Manczur F, Castel D, Willenz U, Petnehazy Ö, Landa N, Feinberg MS, Konen E, Goitein O, Tsur-gang O, Shaul M, Klapper L, Cohen S. Intracoronary Injection of In Situ Forming Alginate Hydrogel Reverses Left Ventricular Remodeling After Myocardial Infarction in Swine. Journal of the American College of Cardiology. 2009;54:1014-1023
14. Wall ST, Walker JC, Healy KE, Ratcliffe MB, Guccione JM. Theoretical Impact of the Injection of Material A Finite Element Model Simulation. Circulation. 2006;114:2627-2635
15. Fomovsky GM, Macadangdang JR, Ailawadi G, Holmes JW. Model-Based Design of Mechanical Therapies for Myocardial Infarction. Journal of Cardiovascular Translational Research. 2011;4:82-91
16. Smits AM, Laake LWV, Ouden KD, Schreurs C, Szuhai K, van Echteld CJ, Mummery CL, Doevendans PA, Goumans M-J. Human cardiomyocyte progenitor cell transplantation preserves long-term function of the infarcted mouse myocardium. Cardiovascular Research. 2009;83:527-535
17. Meuwissen M, Siebes M, Chamuleau SAJ, Tijssen JGP, Spaan JAE, Piek JJ. Intracoronary pressure and flow velocity for hemodynamic evaluation of coronary stenoses. Expert review of cardiovascular therapy. 2003;1:471-479

18. Meuwissen M, Chamuleau SAJ, Siebes M, Schotborgh CE, Koch KT, De Winter RJ, Bax M, De Jong A, Spaan JAE, Piek JJ. Role of Variability in Microvascular Resistance on Fractional Flow Reserve and Coronary Blood Flow Velocity Reserve in Intermediate Coronary Lesions. October. 2001;103:184-187
19. Murata E, Hozumi T, Matsumura Y, Fujimoto K, Sugioka K, Takemoto Y, Watanabe H, Yamagishi H, Yoshiyama M, Iwao H, Yoshikawa J. Coronary Flow Velocity Reserve Measurement in Three Major Coronary Arteries Using Transthoracic Doppler Echocardiography. Echocardiography. 2006;23:279-286
20. Erbs S, Linke A, Schächinger V, Assmus B, Thiele H, Diederich K-W, Hoffmann C, Dimmeler S, Tonn T, Hambrecht R, Zeiher AM, Schuler G. Restoration of Microvascular Function in the Infarct-Related Artery by Intracoronary Transplantation of Bone Marrow Progenitor Cells in Patients With Acute Myocardial Infarction. Circulation. 2007;116:366-374
21. van der Laan AM, Hirsch A, Haeck JDE, Nijveldt R, Delewi R, Biemond BJ, Tijssen JGP, Marques KMJ, Zijlstra F, van Rossum AC, Piek JJ. Recovery of microcirculation after intracoronary infusion of bone marrow mononuclear cells or peripheral blood mononuclear cells in patients treated by primary percutaneous coronary intervention the Doppler substudy of the hebe trial. JACC. Cardiovascular interventions. 2011;4:913-920
22. Bax M, de Winter RJ, Koch KT, Schotborgh CE, Tijssen JGP, Piek JJ. Time course of microvascular resistance of the infarct and noninfarct coronary artery following an anterior wall acute myocardial infarction. The American journal of cardiology. 2006;97:1131-1136
23. Gyöngyösi M, Dib N. Diagnostic and prognostic value of 3D NOGA mapping in ischemic heart disease. Nature Reviews Cardiology. 2011;8:393-404
24. Psaltis PJ, Carbone A, Leong DP, Lau DH, Nelson AJ, Kuchel T, Jantzen T, Manavis J, Williams K, Sanders P, Gronthos S, Zannettino ACW, Worthley SG. Assessment of myocardial fibrosis by endoventricular electromechanical mapping in experimental nonischemic cardiomyopathy. International Journal of Cardiovascular Imaging. 2011;27:25-37
25. Perin EC, Dohmann HFR, Borojevic R, Silva SA, Sousa ALS, Mesquita CT, Rossi MID, Carvalho AC, Dutra HS, Dohmann HJF, Silva GV, Belém L, Vivacqua R, Rangel FOD, Esporcatte R, Geng YJ, Vaughn WK, Assad JAR, Mesquita ET, Willerson JT. Transendocardial, Autologous Bone Marrow Cell Transplantation for Severe, Chronic Ischemic Heart Failure. Circulation. 2003;107:2299-2302
26. Chen S-L, Fang W-W, Ye F, Liu Y-H, Qian J, Shan S-J, Zhang J-J, Chunhua RZ, Liao L-M, Lin S, Sun J-P. Effect on Left Ventricular Function of Intracoronary Transplantation of Autologous Bone Marrow Mesenchymal Stem Cell in Patients With Acute Myocardial Infarction. American Journal of Cardiology. 2004;94:92-95
27. Wijnmaalen AP, Van Der Geest RJ, Van Huls Van Taxis CFB, Siebelink H-MJ, Kroft LJM, Bax JJ, Reiber JHC, Schalij MJ, Zeppenfeld K. Head-to-head comparison of contrast-enhanced magnetic resonance imaging and electroanatomical voltage mapping to assess post-infarct scar characteristics in patients with ventricular tachycardias: real-time image integration and reversed registration. European Heart Journal. 2010;32:104-114
28. Heydari B, Jerosch-Herold M, Kwong RY. Assessment of myocardial ischemia with cardiovascular magnetic resonance. Progress in cardiovascular diseases. 2011;54:191-203
29. Axel L, Dougherty L. MR Imaging of Motion with Spatial Modulation of Magnetization. Radiology. 1989;171:841-845
30. Shehata ML, Cheng S, Osman NF, Bluemke DA, Lima JAC. Myocardial tissue tagging with cardiovascular magnetic resonance. Journal of Cardiovascular Magnetic Resonance. 2009:11-55
31. Amado LC, Schuleri KH, Saliaris AP, Boyle AJ, Helm R, Oskouei B, Centola M, Eneboe V, Young R, Lima JAC, Lardo AC, Heldman AW, Hare JM. Multimodality Noninvasive Imaging Demonstrates In Vivo Cardiac Regeneration After Mesenchymal Stem Cell Therapy. Journal of the American College of Cardiology. 2006;48:2116-2124
32. Rickers C, Gallegos R, Seethamraju RT, Wang X, Swingen C, Jayaswal A, Rahrmann EP, Kastenberg ZJ, Clarkson CE, Bianco R, O'Brian T, Verfaillie C, Bolman III RM, Wilke N, Jerosch-Herold M. Applications of Magnetic Resonance Imaging for Cardiac Stem Cell Therapy. Journal of Interventional Cardiology. 2004;17:37-46

33. Quevedo HC, Hatzistergos KE, Oskouei BN, Feigenbaum GS, Rodriguez JE, Valdes D, Pattany PM, Zambrano JP, Hu Q, McNiece I, Heldman AW, Hare JM. Allogeneic mesenchymal stem cells restore cardiac function in chronic ischemic cardiomyopathy via trilineage differentiating capacity. Proceedings of the national acedemy of science. 2009;106:14022-14027
34. Schuleri KH, Feigenbaum GS, Centola M, Weiss ES, Zimmet JM, Turney J, Kellner J, Zviman MM, Hatzistergos KE, Detrick B, Conte JV, McNiece I, Steenbergen C, Lardo AC, Hare JM. Autologous mesenchymal stem cells produce reverse remodelling in chronic ischaemic cardiomyopathy. European Heart Journal. 2009;30:2722-2732
35. Williams AR, Trachtenberg B, Velazquez DL, McNiece I, Altman P, Rouy D, Mendizabal AM, Pattany PM, Lopera GA, Fishman J, Zambrano JP, Heldman AW, Hare JM. Intramyocardial Stem Cell Injection in Patients With Functional Recovery and Reverse Remodeling. Circulation research. 2011;108:792-796
36. Thiele H, Schuster A, Erbs S, Linke A, Lenk K, Adams V, Hambrecht R, Schuler G. Cardiac magnetic resonance imaging at 3 and 15 months after application of circulating progenitor cells in recanalised chronic total occlusions. International journal of cardiology. 2009;135:287-295
37. Meyer GP, Wollert KC, Lotz J, Steffens J, Lippolt P, Fichtner S, Hecker H, Schaefer A, Arseniev L, Hertenstein B, Ganser A, Drexler H. Intracoronary bone marrow cell transfer after myocardial infarction: eighteen months' follow-up data from the randomized, controlled BOOST (BOne marrOw transfer to enhance ST-elevation infarct regeneration) trial. Circulation. 2006;113:1287-1294
38. Erbs S, Linke A, Adams V, Lenk K, Thiele H, Diederich K-W, Emmrich F, Kluge R, Kendziorra K, Sabri O, Schuler G, Hambrecht R. Transplantation of blood-derived progenitor cells after recanalization of chronic coronary artery occlusion: first randomized and placebo-controlled study. Circulation research. 2005;97:756-762
39. Janssens S, Dubois C, Bogaert J, Theunissen K, Deroose C, Desmet W, Kalantzi M, Herbots L, Sinnaeve P, Dens J, Maertens J, Rademakers F, Dymarkowski S, Gheysens O, Van Cleemput J, Bormans G, Nuyts J, Belmans A, Mortelmans L, Boogaerts M, Van de Werf F. Autologous bone marrow-derived stem-cell transfer in patients with ST-segment elevation myocardial infarction: double-blind, randomised controlled trial. Lancet. 2006;367:113-121
40. Britten MB, Abolmaali ND, Assmus B, Lehmann R, Honold J, Schmitt J, Vogl TJ, Martin H, Schächinger V, Dimmeler S, Zeiher AM. Infarct remodeling after intracoronary progenitor cell treatment in patients with acute myocardial infarction (TOPCARE-AMI): mechanistic insights from serial contrast-enhanced magnetic resonance imaging. Circulation. 2003;108:2212-2218
41. Schächinger V, Assmus B, Britten MB, Honold J, Lehmann R, Teupe C, Abolmaali ND, Vogl TJ, Hofmann W-K, Martin H, Dimmeler S, Zeiher AM. Transplantation of progenitor cells and regeneration enhancement in acute myocardial infarction: final one-year results of the TOPCARE-AMI Trial. Journal of the American College of Cardiology. 2004;44:1690-1699
42. Lunde K, Solheim S, Aakhus S, Arnesen H, Abdelnoor M, Egeland T, Endresen K, Ilebekk A, Mangschau A, Fjeld JG, Smith HJ, Taraldsrud E, Grøgaard HK, Bjørnerheim R, Brekke M, Müller C, Hopp E, Ragnarsson A, Brinchmann JE, Forfang K. Intracoronary injection of mononuclear bone marrow cells in acute myocardial infarction. The New England Journal of Medicine. 2006;355:1199-1209
43. Leistner DM, Fischer-Rasokat U, Honold J, Seeger FH, Schächinger V, Lehmann R, Martin H, Burck I, Urbich C, Dimmeler S, Zeiher AM, Assmus B. Transplantation of progenitor cells and regeneration enhancement in acute myocardial infarction (TOPCARE-AMI): final 5-year results suggest long-term safety and efficacy. Clinical research in cardiology. 2011;100:925-934
44. de Silva R, Raval AN, Hadi M, Gildea KM, Bonifacino AC, Yu Z-X, Yau YY, Leitman SF, Bacharach SL, Donahue RE, Read EJ, Lederman RJ. Intracoronary infusion of autologous mononuclear cells from bone marrow or granulocyte colony-stimulating factor-mobilized apheresis product may not improve remodelling, contractile function, perfusion, or infarct size in a swine model of large myocardial. European heart journal. 2008;29:1772-1782
45. Hopp E, Lunde K, Solheim S, Aakhus S, Arnesen H, Forfang K, Edvardsen T, Smith H-J. Regional myocardial function after intracoronary bone marrow cell injection in reperfused anterior wall infarction - a cardiovascular magnetic resonance tagging study. Journal of cardiovascular magnetic resonance. 2011;13:22-22

46. Holmes JW, Yamashita H, Waldman LK, Covell JW. Scar Remodeling and Transmural Deformation After Infarction in the Pig. Circulation. 1994;90:410-420
47. Beller GA, Heede RC. SPECT imaging for detecting coronary artery disease and determining prognosis by noninvasive assessment of myocardial perfusion and myocardial viability. Journal of cardiovascular translational research. 2011;4:416-424
48. Machac J. Cardiac positron emission tomography imaging. Seminars in nuclear medicine. 2005;35:17-36
49. Mahnken AH, Koos R, Katoh M, Wildberger JE, Spuentrup E, Buecker A, Günther RW, Kühl HP. Assessment of myocardial viability in reperfused acute myocardial infarction using 16-slice computed tomography in comparison to magnetic resonance imaging. Journal of the American College of Cardiology. 2005;45:2042-2047
50. Baggish AL, Boucher CA. Radiopharmaceutical agents for myocardial perfusion imaging. Circulation. 2008;118:1668-1674
51. Beeres SLMA, Bengel FM, Bartunek J, Atsma DE, Hill JM, Vanderheyden M, Penicka M, Schalij MJ, Wijns W, Bax JJ. Role of Imaging in Cardiac Stem Cell Therapy. Journal of the American College of Cardiology. 2007;49:1137-1148
52. Strauer BE, Brehm M, Zeus T, Bartsch T, Schannwell C, Antke C, Sorg RV, Kögler G, Wernet P, Müller H-W, Köstering M. Regeneration of Human Infarcted Heart Muscle by Intracoronary Autologous Bone Marrow Cell Transplantation in Chronic Coronary Artery Disease The IACT Study. Journal of the American College of Cardiology. 2005;46:1651-1658
53. Strauer BE, Brehm M, Zeus T, Köstering M, Hernandez A, Sorg RV, Kögler G, Wernet P. Repair of Infarcted Myocardium by Autologous Intracoronary Mononuclear Bone Marrow Cell Transplantation in Humans. Circulation. 2002;106:1913-1918
54. Döbert N, Britten M, Assmus B, Berner U, Menzel C, Lehmann R, Hamscho N, Schächinger V, Dimmeler S, Zeiher AM, Grünwald F. Transplantation of progenitor cells after reperfused acute myocardial infarction: evaluation of perfusion and myocardial viability with FDG-PET and thallium SPECT. European journal of nuclear medicine and molecular imaging. 2004;31:1146-1151
55. Bartunek J, Vanderheyden M, Vandekerckhove B, Mansour S, De Bruyne B, De Bondt P, Van Haute I, Lootens N, Heyndrickx G, Wijns W. Intracoronary injection of CD133-positive enriched bone marrow progenitor cells promotes cardiac recovery after recent myocardial infarction: feasibility and safety. Circulation. 2005;112:I178-183
56. Katritsis DG, Sotiropoulou PA, Karvouni E, Karabinos I, Korovesis S, Perez SA, Voridis EM, Papamichail M. Transcoronary transplantation of autologous mesenchymal stem cells and endothelial progenitors into infarcted human myocardium. Catheterization and cardiovascular interventions. 2005;65:321-329
57. Beeres SLMA, Aakhus S, Bax JJ, Dibbets P, Stokkel MPM, Zeppenfeld K, Fibbe WE, van der Wall EE, Schalij MJ, Atsma DE. Effect of intramyocardial injection of autologous bone marrow-derived mononuclear cells on perfusion, function, and viability in patients with drug-refractory chronic ischemia. Journal of nuclear medicine: official publication, Society of Nuclear Medicine. 2006;47:574-580
58. Beeres SLMA, Bax JJ, Dibbets-Schneider P, Stokkel MPM, Fibbe WE, van der Wall EE, Schalij MJ, Atsma DE. Sustained effect of autologous bone marrow mononuclear cell injection in patients with refractory angina pectoris and chronic myocardial ischemia: twelve-month follow-up results. American heart journal. 2006;152:684.e611-686
59. Beeres SLMA, Bax JJ, Kaandorp TAM, Zeppenfeld K, Lamb HJ, Dibbets-Schneider P, Stokkel MPM, Fibbe WE, de Roos A, van der Wall EE, Schalij MJ, Atsma DE. Usefulness of intramyocardial injection of autologous bone marrow-derived mononuclear cells in patients with severe angina pectoris and stress-induced myocardial ischemia. The American journal of cardiology. 2006;97:1326-1331
60. Kang H-J, Kim H-S, Zhang S-Y, Park K-W, Cho H-J, Koo B-K, Kim Y-J, Soo Lee D, Sohn D-W, Han K-S, Oh B-H, Lee M-M, Park Y-B. Effects of intracoronary infusion of peripheral blood stem-cells mobilised with granulocyte-colony stimulating factor on left ventricular systolic function and restenosis after coronary stenting in myocardial infarction: the MAGIC cell randomised clinical. Lancet. 2004;363:751-756

61. Assmus B, Schächinger V, Teupe C, Britten M, Lehmann R, Döbert N, Grünwald F, Aicher A, Urbich C, Martin H, Hoelzer D, Dimmeler S, Zeiher AM. Transplantation of Progenitor Cells and Regeneration Enhancement in Acute Myocardial Infarction (TOPCARE-AMI). Circulation. 2002;106:3009-3017
62. Fernández-Avilés F, San Román JA, García-Frade J, Fernández ME, Peñarrubia MJ, de la Fuente L, Gómez-Bueno M, Cantalapiedra A, Fernández J, Gutierrez O, Sánchez PL, Hernández C, Sanz R, García-Sancho J, Sánchez A. Experimental and clinical regenerative capability of human bone marrow cells after myocardial infarction. Circulation research. 2004;95:742-748
63. Galiuto L, Locorotondo G, Paraggio L, De Caterina AR, Leone AM, Fedele E, Barchetta S, Porto I, Natale L, Rebuzzi AG, Bonomo L, Crea F. Characterization of microvascular and myocardial damage within perfusion defect area at myocardial contrast echocardiography in the subacute phase of myocardial infarction. European Journal of Echocardiography. 2011;13:174-180
64. Buckley O, Di Carli M. Predicting benefit from revascularization in patients with ischemic heart failure: imaging of myocardial ischemia and viability. Circulation. 2011;123:444-450
65. Teske AJ, Boeck BWLD, Melman PG, Sieswerda GT, Doevendans PA, Cramer MJM. Echocardiographic quantification of myocardial function using tissue deformation imaging, a guide to image acquisition and analysis using tissue Doppler and speckle tracking. Cardiovascular Ultrasound. 2007;5:1-19
66. Støylen A, Heimdal A, Bjørnstad K, Wiseth R, Vik-Mo H, Torp H, Angelsen B, Skjaerpe T. Strain Rate Imaging by Ultrasonography in the Diagnosis of Coronary Artery Disease. Journal Of The American Society Of Echocardiography. 2000;13:1053-1064
67. Herbots L, D'hooge J, Eroglu E, Thijs D, Ganame J, Claus P, Dubois C, Theunissen K, Bogaert J, Dens J, Kalantzi M, Dymarkowski S, Bijnens B, Belmans A, Boogaerts M, Sutherland G, Werf FVD, Rademakers F, Janssens S. Improved regional function after autologous bone marrow-derived stem cell transfer in patients with acute myocardial infarction: a randomized, double-blind strain rate imaging study. European Heart Journal. 2009;30:662-670
68. Karatasakis G, Leontiadis E, Peristeri I, Manginas A, Goussetis E, Graphakos S, Papadakis E, Cokkinos DV. Intracoronary infusion of selected autologous bone marrow stem cells improves longitudinal myocardial strain and strain rate in patients with old anterior myocardial infarction without recent revascularization. European Journal of Echocardiography. 2010;11:440-445
69. Lebrun F, Berchem GUY, Delagardelle C, Beissel J, Rouy D, Wagner DR. Improvement of Exercise-Induced Cardiac Deformation After Cell Therapy for Severe Chronic Ischemic Heart Failure. Journal of Cardiac Failure. 2006;12:108-113
70. Plewka M, Krzeminska-Pakula M, Lipiec P, Zbigniew Peruga J, Jezewski T, Kidawa M, Wierzbowska-Drabik K, Korycka A, Robak T, Damian Kasprzak J. Effect of Intracoronary Injection of Mononuclear Bone Marrow Stem Cells on Left Ventricular Function in Patients With Acute Myocardial Infarction. Journal of Cardiology. 2009;104:1336-1342
71. Ramshorst JV, Atsma DE, Beeres SLMA, Mollema SA, Ajmone Marsan N, Holman ER, van der Wall EE, Schalij MJ, Bax JJ. Effect of intramyocardial bone marrow cell injection on left ventricular dyssynchrony and global strain. Heart. 2009;95:119-124
72. Beitnes JO, Gjesdal O, Lunde K, Solheim S, Edvardsen T, Arnesen H, Forfang K, Aakhus S. Left ventricular systolic and diastolic function improve after acute myocardial infarction treated with acute percutaneous coronary intervention, but are not influenced by intracoronary injection of autologous mononuclear bone marrow cells: a 3 year serial echocardiographic sub-study of the randomized-controlled ASTAMI study. European Journal of Echocardiography. 2011;12:98-106
73. Ruan W, Pan C, Huang G, Li Y, Ge J, Shu X. Assessment of left ventricular segmental function after autologous bone marrow stem cells transplantation in patients with acute myocardial infarction by tissue tracking and strain imaging. Chin Med J (Engl). 2005;118:6
74. Schneider C, Krause K, Jaquet K, Geidel S, Malisius R, Boczor S, Rau T, Zienkiewicz T, Hennig D, Kuck K-H. Intramyocardial Transplantation of Bone Marrow-Derived Stem Cells: Ultrasonic Strain Rate Imaging in a Model of Hibernating Myocardium. Journal of Cardiac Failure. 2008;14:861-872

75. Skulstad H, Edvardsen T, Urheim S, Rabben SI, Stugaard M, Lyseggen E, Ihlen H, Smiseth OA. Postsystolic Shortening in Ischemic Myocardium: Active Contraction or Passive Recoil? Circulation. 2002;106:718-724
76. Heimdal A, Støylen A, Torp H, Skjærpe T. Real-Time Strain Rate Imaging of the Left Ventricle by Ultrasound. Journal Of The American Society Of Echocardiography. 1998;11:1013-1019
77. Weidemann F, Jamal F, Sutherland GR, Claus P, Kowalski M, Hatle L, Scheerder ID, Bijnens B, Rademakers FE. Myocardial function defined by strain rate and strain during alterations in inotropic states and heart rate. American Journal Of Physiology Heart and Crculation Physiology. 2002;283:792-799
78. Burkhoff D, Mirsky I, Suga H. Assessment of systolic and diastolic ventricular properties via pressure-volume analysis: a guide for clinical, translational, and basic researchers. American Journal Of Physiology Heart and Crculation Physiology. 2005;289:501-512
79. Bijnens B, Claus P, Weidemann F, Strotmann J, Sutherland GR. Investigating Cardiac Function Using Motion and Deformation Analysis in the Setting of Coronary Artery Disease. Circulation. 2007;116:2453-2464
80. Burns AT, Gerche AL, D´hooge J, Macisaac AI, Prior DL. Left ventricular strain and strain rate: characterization of the effect of load in human subjects. European Journal of Echocardiography. 2010;11:283-289
81. Claus P, Weidemann F, Dommke C, Bito V, Heinzel FR, D'hooge J, Sipido KR, Sutherland GR, Bijnens B. Mechanisms of Postsystolic thickening in ischemic myocardium: mathematical modelling and comparison with experimental ischemic substrates. Ultrasound. 2007;33:1963-1970
82. Ferferieva V, Van den Bergh A, Claus P, Jasaityte R, Veulemans P, Pellens M, La Gerche A, Rademakers FE, Herijgers P, D'hooge J. The relative value of strain and strain rate for defining intrinsic myocardial function. American journal of physiology. Heart and circulatory physiology. 2011;302:H188-195
83. Weidemann F, Dommke C, Bijnens B, Claus P, D'hooge J, Mertens P, Verbeken E, Maes A, Werf FVD, Scheerder ID, Sutherland GR. Defining the Transmurality of a Chronic Myocardial Infarction by Ultrasonic Strain-Rate Imaging. Circulation. 2003;107:883-888
84. Boeck BWLD, Kirn B, Teske AJ, Hummeling RW, Doevendans PA, Cramer MJ, Prinzen FW. Three-dimensional mapping of mechanical activation patterns, contractile dyssynchrony and dyscoordination by two-dimensional strain echocardiography: Rationale and design of a novel software toolbox. Cardiovascular Ultrasound. 2008:6-22
85. Zhong L, Su Y, Yeo S-Y, Tan R-S, Ghista DN, Kassab G. Left ventricular regional wall curvedness and wall stress in patients with ischemic dilated cardiomyopathy. American journal of physiology. Heart and circulatory physiology. 2009;296:H573-584
86. Di Donato M, Dabic P, Castelvecchio S, Santambrogio C, Brankovic J, Collarini L, Joussef T, Frigiola A, Buckberg G, Menicanti L. Left ventricular geometry in normal and post-anterior myocardial infarction patients: sphericity index and 'new' conicity index comparisons. European journal of cardio-thoracic surgery. 2006;29:S225-S230

PART TWO

Advanced delivery

F.J. van Slochteren[1], R. van Es[1], S. Koudstaal[1,5], T.I.G. van der Spoel[1], J.P.G. Sluijter[1,5], J. Verbree[2], R.H.R. Pruim[2], J.P.W. Pluim[3], T. Leiner[4], P.A. Doevendans[1,5], S.A.J. Chamuleau[1,5]

[1] Department of Cardiology, University Medical Centre Utrecht, The Netherlands
[2] Department of Technical Medicine, University of Twente, Enschede, The Netherlands
[3] Imaging Sciences Institute, University Medical Centre Utrecht, The Netherlands
[4] Department of Radiology, University Medical Centre Utrecht, The Netherlands
[5] Interuniversity Cardiology Institute of the Netherlands (ICIN), Utrecht, The Netherlands

CHAPTER **3**

Multimodality infarct identification for optimal image guided intramyocardial cell injections

Submitted

Abstract

Background

Intramyocardial cell injections in the context of cardiac regenerative therapy can currently be performed using electromechanical mapping (EMM) provided by the NOGA®XP catheter injection system. The gold standard technique to determine infarct size and location however is late gadolinium enhanced magnetic resonance imaging (LGE-MRI). In this article we describe a practical and accurate technique to co-register LGE-MRI and NOGA®XP dataset during the injection procedures to ultimately perform image guided injections to the border zone of the infarct determined by LGE-MRI.

Materials and methods

LGE-MRI and EMM were obtained in 3 pigs with chronic myocardial infarction. MRI and EMM datasets were registered using the in-house developed 3D CartBox image registration toolbox consisting of three steps: 1) landmark registration, 2) surface registration, and 3) manual optimization. The apex and the coronary ostia were used as landmarks.

Results

Image registration was successful in all datasets, and resulted in a mean registration error of 3.22 ± 1.86mm between the MRI surface mesh and EMM points. Visual assessment revealed that the locations and the transmural extent of the infarctions measured by LGE-MRI only partly overlap with the infarct areas identified by the EMM parameters.

Conclusions

The 3D CartBox image registration toolbox enables registration of the EMM on pre-procedurally acquired MRI during the catheter injection procedure. This allows the operator to perform real-time image guided cell injections into the border zone of the infarct as assessed by LGE-MRI. 3D CartBox thereby for the first time enables standardization of the injection location for cardiac regenerative therapy.

Introduction

Previous studies have shown that injection of stem/progenitor cells into the border zone of the infarcted area in the context of cardiac regenerative therapy helped to stimulate cardiac repair and protection via cell-to-cell contact and secretion of paracrine factors[1-6]. However, therapeutic effects may rely on the delivery and retention of the regenerative therapeutics on a location where oxygen and nutrients are available to enable survival[7]. Hence, accurate identification of viable tissue in proximity of the infarct is of great importance. Via intramyocardial injection catheters stem/progenitor cells or biomaterials can be injected minimally invasive into the myocardium. Injection locations can be chosen based on tissue viability measures obtained from electromechanical mapping (EMM), or a-priori knowledge about the infarct location[8]. The NOGA®XP intramyocardial injection system[9] provides a three dimensional (3D) magnetic tracking technology and allows for the assessment of local electrical and mechanical tissue characteristics. Local unipolar (UV) and bipolar (BV) depolarization potentials and relative catheter tip displacements (Linear Local Shortening, LLS) are measured at multiple locations on the left ventricular (LV) endocardium. These measurements are interpolated to obtain a three-dimensional reconstruction which is used to guide cell injections. This technique is currently used in clinical practice[10-15]. Measurements can however not be performed in regions that are susceptible for arrhythmias and measurements are interpolated in regions where no measurements are taken. Furthermore, cut-off values of EMM parameters to identify areas with different viability/perfusion/transmurality vary greatly between studies[14]. Altogether this approach is not reproducible, and prone to errors regarding accurate and detailed identification of the infarct border zone. Since the non transmural border zone of the infarction is believed to be the preferred delivery site of the stem cell therapeutics[1], it is crucial for it to by optimally defined during the injection procedure. We hypothesize that combining the gold standard measure of infarct size and location by late gadolinium enhanced magnetic resonance imaging (LGE-MRI) and practical guidance (NOGA®XP) would further optimize the cell delivery location, and lead to a uniform injection strategy. This approach enables accurate selection and targeting of the infarct border zone with a distinct infarct transmurality with a value between 0 and 100%. In this study we describe the development of a practical software toolbox (3D CartBox) that enables real-time image guided cell injections. 3D CartBox registers NOGA®XP catheter positions on pre-procedurally acquired MRI images to perform intramyocardial injections to locations with an a priori identified distinct infarct transmurality. In addition 3D CartBox can be used to further specify the definition of border zone of the infarct[7].

Materials and methods

3D CartBox is a Matlab based software toolbox to register NOGA®XP catheter positions on an endocardial surface mesh derived from MRI. Prior to registration two image processing steps are necessary: 1) Data acquisition, and 2) Data pre-processing as illustrated in Figure 1. 3D CartBox is used for the registration and consists of three phases: 1) initial registration, 2) Iterative Closest Point (ICP) registration, and 3) manual registration. After the registration process post processing is performed to visualize the data in bullseye plots. In the development process described in this study the 3D CartBox toolbox was applied

to data of 3 pigs with a chronic myocardial infarction. The study design is illustrated in Figure 2. The algorithms used in 3D CartBox and in the pre- and post-processing steps are explained in detail in the supplementary data.

Animals

All experiments were performed in accordance with the "Guide for the Care and Use of Laboratory Pigs" prepared by the Institute of Laboratory Animal Resources and with prior approval by the Animal Experimentation Committee of the Faculty of Medicine, Utrecht University, the Netherlands. Three 6-month old female Dalland Landrace pigs (60-70 kg; Instituut voor dierhouderij en diergezondheid (IDDLO), Lelystad, the Netherlands) were pre-treated with clopidogrel 75 mg/day for 3 days and amiodarone 400mg/day for 10 days. In all pigs myocardial infarction (MI) was induced by 75 minutes of percutaneous balloon occlusion of the proximal left circumflex coronary artery as previously described[16]. Eight weeks after MI the experiments were performed as shown in Figure 2.

Data acquisition

The *in vivo* MRI images were acquired using a 1.5 Tesla Philips Medical Systems Achieva scanner. The MRI sequences for the CINE and the LGE MRI acquisitions are described in the supplementary data. The NOGA®XP system (Biosense Webster, Cordis, Johnson & Johnson, USA) version 1.1.43 was used equipped with a 7 French NOGA mapping catheter (Biosense Webster, Cordis, Johnson & Johnson, Diamond Bar, USA) for the mapping. The LV was entered via the left carotid artery, and retrograde passage through the aortic valve. Readout of the catheter tip location was done in end-diastole using R-wave triggering. Thereby providing only end-diastolic tip locations for registration. Electrocardiograms were filtered at 30–400 Hz (bipolar) and 1–240 Hz (unipolar). The EMM datasets were acquired in consideration of the criteria for good electromechanical mapping[14]. Points acquired in

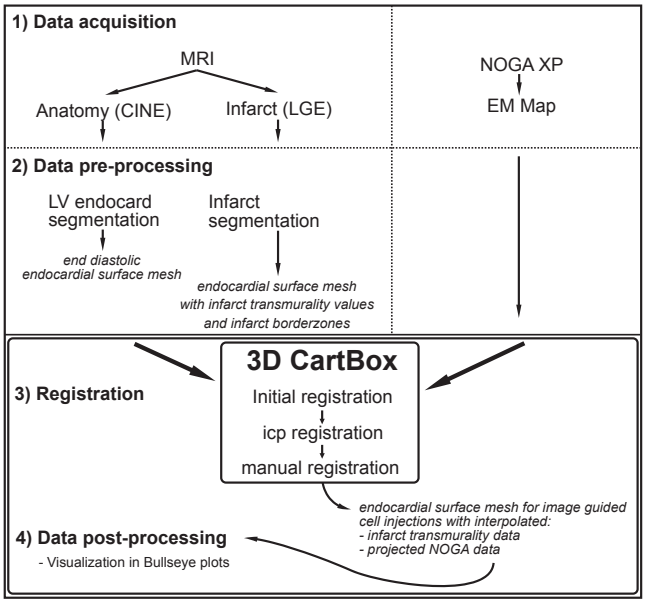

Figure 1. Workflow of the image processing steps that are necessary to use the 3D CartBox toolbox.

the left and right coronary ostia and the apex served as anatomical landmarks and are used for the first registration step. The apex location was taken as the most outward point that was reached in the apical region confirmed by fluoroscopy. To obtain data from the NOGA®XP system in a real time fashion, the system was modified to enable read-only access from an external computer running 3D CartBox.

Data pre-processing

Data pre-processing consists of 1) segmentation of the left ventricle using the CINE images, 2) segmentation of the infarct using the LGE images, 3) calculation of the infarct transmurality, 4) projection of the infarct transmurality on the endocardial surface mesh derived from the end diastolic CINE images, and 5) calculation of the infarct transmurality border zone preferred to use for cell injections. The details of the pre-processing steps are described in the supplementary data.

Registration

During initial registration the raw NOGA®XP dataset and the MRI datasets are registered coarsely based on the anatomical landmarks using a closed-form least squares approach[17,18]. Used anatomical landmarks are the left and the right coronary ostia and the apex as previously described[19]. After acquiring points in all regions of the left ventricular endocardium, an iterative closest point (ICP) algorithm[20] was applied to optimize the registration. If necessary the registration was manually optimized by adjusting the registration interactively. The algorithms used for the registration are explained in detail in the supplementary data. The accuracy of the registration was expressed by the registration error being the mean ± standard deviation of the shortest distance from each EMM point to the cine mesh surface as previously described[19]. The relevance of the used registration error measure is pointed out in the supplementary data. To prevent interference by EMM points that were not located in the cine mesh (e.g. LV outflow tract), these points were excluded for ICP registration, error calculation, and further processing.

Perioperative image guidance

In this study perioperative registration is performed in two animals. After initial registration the acquired EMM points are visualized in the freely rotatable 3D endocardial surface mesh with projected infarct transmurality data. In addition the MR images are displayed as shown in Figure 3 E and F. Newly acquired NOGA®XP measurement points appear on the screen. Free rotation of the mesh and the MR images during the image guided procedure assures correct positioning of the needle before cell injection.

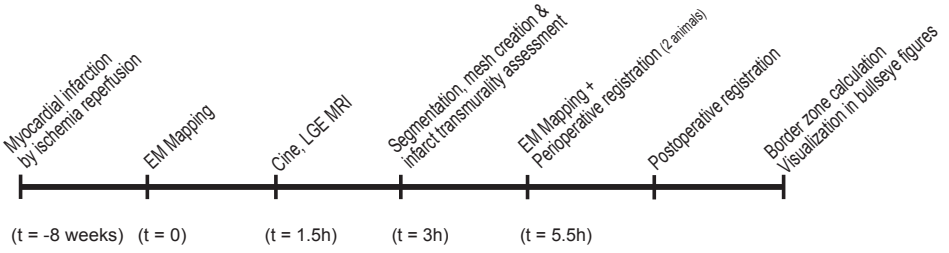

Figure 2. Time line of the experiments. The second mapping procedure was performed in two pigs.

Post-processing

For visualization purposes both the infarct transmurality values and the infarct border zones, as well as the EMM data were projected on the 3D endocardial surface mesh and bullseye plots using customized software.

Statistical analysis

All data is presented as mean ± standard deviation (SD). A one-way ANOVA test was used to assess difference between the number of points/cm^2 in the different infarct transmurality areas. $P < 0.05$ was considered significant.

Results

Data pre-processing

MRI findings are listed in Table 1. The mean LV ejection fraction was 42 ± 1%. All LGE datasets showed a clear fibrotic area as shown in Figure 3b. The LV ejection fraction shows that 8 weeks after MI the pigs had mild heart failure, and a similar infarct size (27.5 ± 3.5% of total LV area). The 75-100% infarct transmurality area was the smallest, and was absent in one pig. Infarct transmurality was assessed and subdivided in areas with 0, 0-25, 25-50, 50-75, and 75-100% transmurality as illustrated in Figure 3d. The mean endocardial surface areas in these subdivisions respectively were: 73.6 ± 19.7, 7.2 ± 1.0, 9.5 ± 2.6, 5.8 ± 2.8, and 4.6 ± 5.2 cm^2, thereby covering 72.5 ± 5.1,

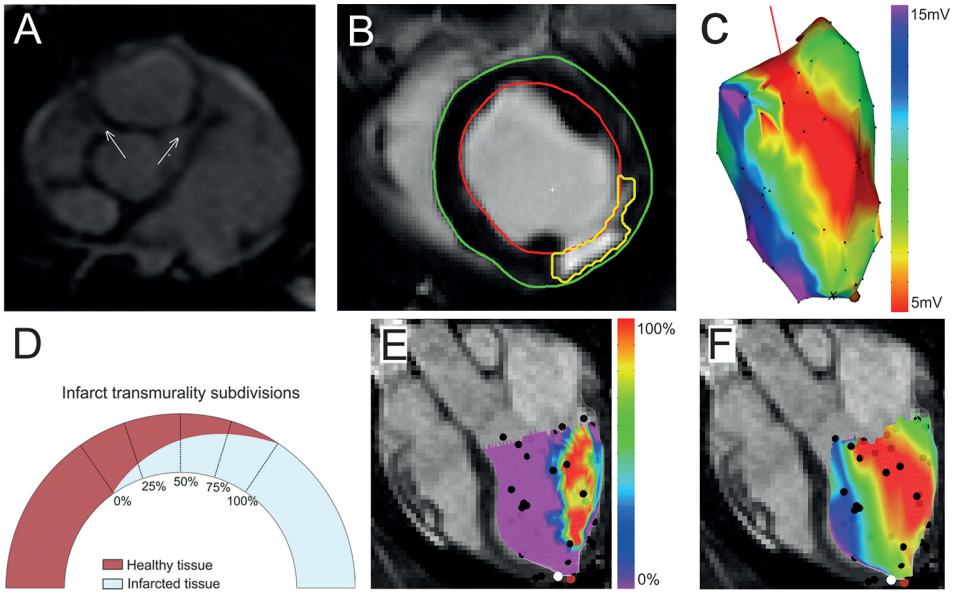

Figure 3. Short axis BTFE image with coronary ostia (A). Segmentation of the epicardium (green), endocardium (red), scar area (yellow) on the short axis LGE scans (B). NOGA®XP representation of unipolar voltage map (C). Subdivision of infarct transmurality (D). Infarct transmurality superimposed on cine mesh (E). Unipolar voltage projection superimposed on cine mesh (F). Colored dots are: NOGA measurement points (black), the apex (white), annotated location (brown).

Table 1. Results of cine and late enhancement magnetic resonance imaging of 3 animals. Data are expressed as mean ± SD.

LV end-diastolic volume (ml)	128 ± 19
LV end-systolic volume (ml)	75 ± 11
LV ejection fraction (%)	42 ± 1
Myocardium volume (ml)	118 ± 18
Infarct volume (ml)	17 ± 3
LV area (cm^2)	101 ± 21
Infarct area 0 % transmurality (cm^2)	73.6 ± 19.7 (72.5 ± 5.1%)
Infarct area 0 - 25 % transmurality (cm^2)	7.2 ± 1.0 (7.2 ± 0.5 %)
Infarct area 25 - 50 % transmurality (cm^2)	9.5 ± 2.6 (9.6 ± 2.9 %)
Infarct area 50 - 75 % transmurality (cm^2)	5.8 ± 2.8 (6.4 ± 4.4 %)
Infarct area 75 - 100 % transmurality (cm^2)	4.6 ± 5.2 (4.3 ± 4.3 %)

7.2 ± 0.5, 9.6 ± 2.9, 6.4 ± 4.4, and 4.3 ± 4.3 % of the total LV endocardial surface area. The locations of the coronary ostia could be identified on the cine images (Figure 3a). In all three pigs we were able to acquire EMM points in, or in the vicinity of the coronary ostia. The mean number of EMM points was 66.3 ± 14.2.

Registration

The registration results are listed in Table 2. Perioperative registration was performed in two pigs to test the real time use of the 3D CartBox toolbox (Figure 2). During the real time EMM procedures the cine mesh was successfully merged with the EMM based upon the anatomical landmarks and ICP. After application of ICP the mean surface registration error was 3.27 ± 1.93 mm. No manual optimization of the registration was applied to the datasets. After exclusion of points located outside the cine mesh the mean registration error was 3.22 ± 1.86 mm. A cine mesh with projected infarct transmurality and UV are shown in Figure 3e and 3f. Figure 3c shows the corresponding NOGA®XP EMM. The average coverage of EMM points in the different infarct transmurality areas was 0.76 ± 0.44 points/cm2. There was no significant difference between the number of points/cm2 in each infarct transmurality area of all the different animals (p=0.96).

Post processing

To evaluate the projection of the EMM data on the endocardial surface mesh Figure 4 shows bulls eye figures of the UV and BV as represented by the NOGA®XP system (a, d) and after projection on the cine mesh (b, e). From the comparison with the infarct transmurality depicted in Figure 4 c it can be observed that there is limited agreement between the EMM values and infarct transmurality. In Figure 5 the 50% infarct transmurality border zone determined by LGE-MRI is projected on the bullseye figures of the infarct transmurality (a), UV (b), BV (d), and LLS (e). From these images it can be observed that only low UV and BV values show some alignment with the 50% infarct transmurality border zone. Figure 5 c and f show the projection of the 50% infarct transmurality border zone on the endocardial surface mesh as it is visualized during image guided cell injection procedures.

Table 2. Three dimensional electromechanical mapping and image registration results of 3 animals. Data are expressed as mean ± SD.

Electromechanical mapping points			
Total number of points	192		
Points per animal	66.3 ± 14.2		
Distance EMM points to MRI mesh surface (mm)			
All EMM points	3.27 ± 1.93 mm based on 192 points		
All EMM points in cine mesh	3.22 ± 1.86 mm based on 183 points		
Points per infarct transmurality area			
0%	53.3 ± 11.7	0.8 ± 0.3 points/cm^2	
0 - 25%	6.0 ± 3.6	0.8 ± 0.5 points/cm^2	
25 – 50%	6.0 ± 3.0	0.7 ± 0.4 points/cm^2	ns (p=0.96)
50 – 75%	2.6 ± 1.5	0.4 ± 0.1 points/cm^2	
75 – 100%	4.5 ± 4.1	0.9 ± 1.2 points/cm^2	

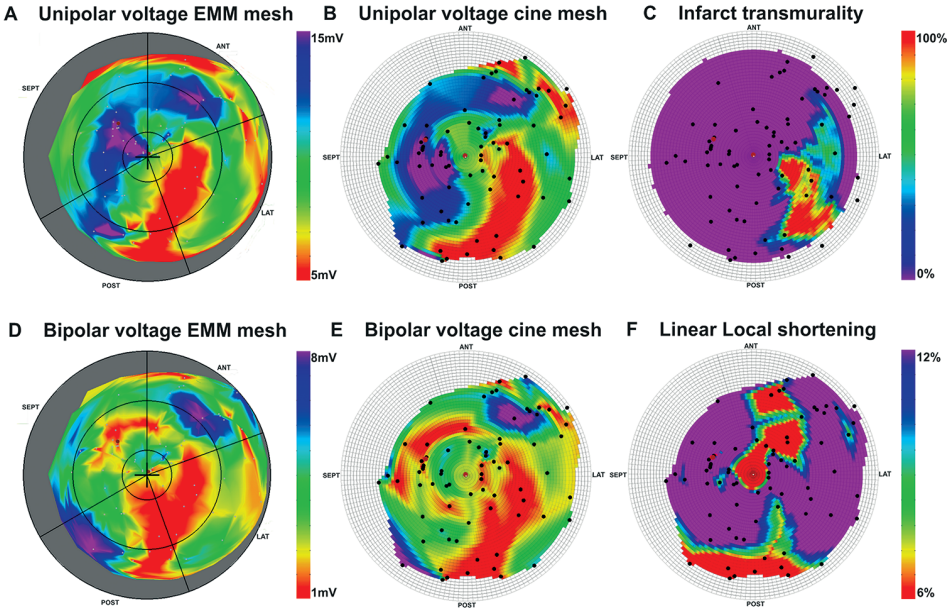

Figure 4. Typical bullseye plots of the NOGA system: Unipolar voltage (A), Bipolar voltage (D). And data projected on the cine mesh: Unipolar voltage (B), Bipolar voltage (E). Infarct transmurality based on LGE-MRI (C), and linear local shortening (F). Colored dots are: NOGA measurement points (black), the apex (white), annotated location (brown).

Discussion

In this study, the feasibility of perioperative integration of electromechanical data acquired with the NOGA®XP system with MRI data was shown for the first time. The in-house developed 3D CartBox image registration toolbox has allowed us to register the EMM dataset on a surface mesh derived from end-diastolic CINE MRI images in real time with a mean surface registration error of 3.27 ± 1.93mm. The three main findings of this study were: 1) real-time use of the toolbox was feasible. 2) Visually a discrepancy was found between infarct assessment by EMM and LGE-MRI. 3) The 3D CartBox toolbox can be of additional value for infarct assessment during cardiac cell injection procedures.

Data acquisition and pre-processing

The LV ejection fraction in Table 1 showed that 8 weeks after MI the pigs had mild heart failure, and a similar infarct size. The absence of a transmural infarction in one pig is most likely induced by the different response to the ischemia reperfusion procedure due to biological variation. The number of points in the EMM (66.3 ± 14.2) just fulfilled the criteria for good electromechanical mapping as published[14]. During the mapping procedure the EMM points were acquired homogeneously spread over the endocardium, as was confirmed by the number of points/cm^2 in each area with a distinct infarct transmurality presented in Table 2, and as can be observed from the distribution of EMM points in Figure 4 and 5.

Registration

However acquiring more EMM points might have been beneficial for the registration, the homogeneous distribution of EMM points over the endocardium has assured a correct registration. Due to the longer acquisition time of the LGE images, gated LGE scans did not exactly represent the end diastolic phase. To assure use of the end diastolic ventricular shape for registration we chose to use the end diastolic frame of the cine images for mesh creation, registration and projection of the EMM data. The exclusion of EMM points that were not located in the cine mesh was done to prevent registration based on EMM points that were located in areas of the LV that were not visualized with MRI. Of the three cases in this study totally 9 mapping points were discarded for this reason. Consequently the registration using all EMM points has a slightly higher registration error: 3.27 ± 1.93mm compared to 3.22 ± 1.86mm for the map without the excluded points. However this difference does not affect registration, it does prevent erroneous projection of EMM parameters on the cine mesh. The 10 times higher weighing of the apex during landmark registration and restriction of the ICP algorithm to 10 degrees in the sagittal plane, and 20 degrees in the transverse and coronal planes were chosen empirically. The resulting surface registration error of 3.22 ± 1.86mm was less than the value reported in research were CARTO merge was used[19]. The remaining error can be caused by respiratory induced motion of the heart during the EMM procedure. The NOGA®XP system does not compensate for this.

Post-processing

A high similarity is observed between the EMM maps produced by the NOGA®XP system and the EMM data projected on the cine mesh. The projection of the EMM data on the endocardial surface mesh via linear interpolation results in an accurate projection of the

true endocardial surface measurements (Figure 4 a-b, and d-e). Based on visual assessment in Figure 5 agreement between the infarct identification by EMM and LGE-MRI is the best with UV, and poor with both BV and LLS. However it cannot be ruled out completely, the small registration error makes it unlikely that this was the main origin of the poor agreement. Another explanation might be the occurrence of endocardial conducting tissue in regions with an infarct, mimicking normal tissue, or extension of the low voltage regions to neighboring areas of non-transmural infarction through interpolation. Acquiring more points during the mapping procedure in the border zone may solve this problem, provided that this area is known, and not susceptible to arrhythmias due to catheter manipulation. Based on the rationale that 100% transmurally infarcted myocardium is not a location where the stem cells are supplied with sufficient oxygen and nutrients[1], and in regions with 0% transmurality there is no use for stem cells, we have chosen to show the 50% infarct transmurality border zone on the bullseye figures in Figure 5. Visual assessment shows that the EMM parameters only partly identify the 50% infarct transmurality border zone assessed by the gold standard LGE-MRI infarct assessment technique. The 3D CartBox toolbox enables accurate targeting of infarct border zones with a distinct infarct transmurality at any percentage between 0 and 100% transmurality determined by LGE-MRI. Thereby 3D CartBox for the first time enables objective specification of the target locations for intramyocardial injections in the context of cardiac regenerative therapy.

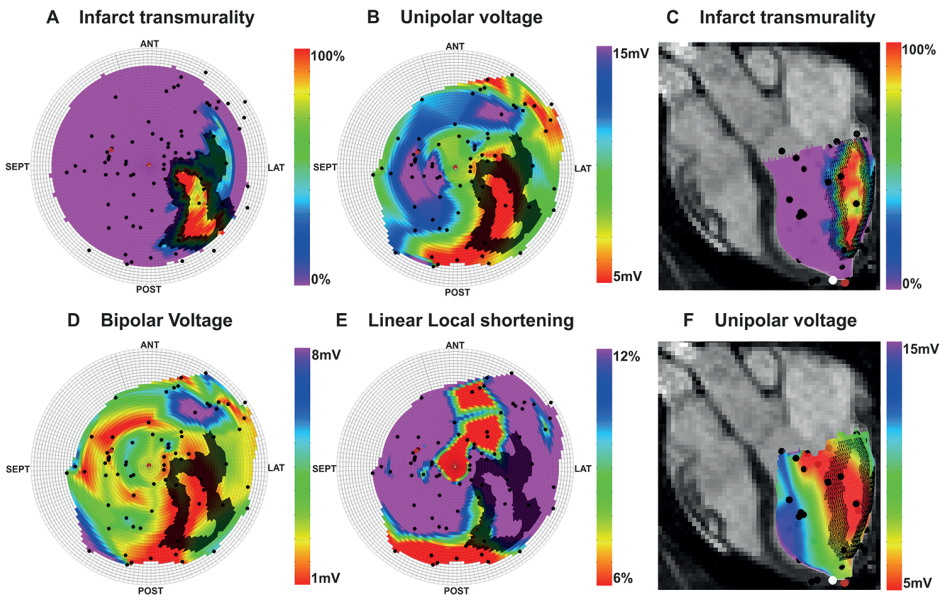

Figure 5. Bullseye plots with in black the overlay of the 50% infarct border zone. Infarct transmurality based on LGE-MRI (A), Unipolar voltage (B), Bipolar voltage (D) and linear local shortening (E). The infarct transmurality (C) and unipolar voltage (F) projected on the endocardial surface mesh in an end diastolic long axis cine MRI image illustrates the operator view during the image guided injection procedure. Colored dots are: NOGA measurement points (black), the apex (white), annotated location (brown).

Clinical implications

Incorrect injections of stem cells into the myocardium might importantly restrain the success of cardiac regenerative therapy[7]. The combination of the gold standard fibrosis imaging technique for infarct and infarct border zone identification, and a catheter navigation technique to guide injections is a crucial step to target the infarct border zone more accurately. This approach could lead to shorter injection procedures, less necessity for the use of fluoroscopy to confirm the injection location, and less radiation for the patient and the physician. The workflow of 3D CartBox includes: MRI, segmentation, and EMM. Altogether this approximately takes 3 hours. Thereby it is a clinically feasible solution. Real-time integration of LGE-MRI during cardiac cell injection procedures could be a key to harnessing the full therapeutical effects of cardiac stem cell therapy. The 3D CartBox toolbox enables the use of all parameters (perfusion, fibrosis, myocardial wall thickening, myocardial tissue tagging) from a pre-procedural acquired MRI or other imaging modality (SPECT/CT) to guide the cell injection procedures. The 3D CartBox toolbox for image guided cardiac cell injections is rewarded with the BMM valorization grant, and will be made commercially available via the newly founded spin-off company CARTcare: 'Technical solutions to improve cardiac regenerative therapy'.

Limitations

The use of the coronary ostia for landmark registration is potentially dangerous for the patient and therefore not suitable for clinical use of the toolbox, although it has been reported in literature[19]. For clinical application of the toolbox in the future we aim to use other fiducial points. The 3 pigs used in this study was found not to be sufficient to perform a quantitative analysis of the overlap between the infarct areas identified by EMM and LGE-MRI or perform a detailed analysis of the thresholds of the NOGA parameters in the areas with different infarct transmurality. A new study must be performed to explore these aspects by applying 3D CartBox to a larger dataset. Although during all procedures the criteria for good electromechanical mapping were adhered to, acquiring more points might have resulted in a lower registration error. During the mapping procedure small respiratory induced excursions of the catheter tip could be observed. Since the NOGA®XP system did not compensate for respiratory induced motion of the cathetertip, this most likely affected the registration. Compensation for respiratory motion might be beneficial for future applications.

Conclusion

We have developed the 3D CartBox toolbox for real time registration of EMM and MRI data that combines the gold standard diagnostic imaging techniques and highly accurate cardiac navigation to guide cardiac cell injection procedures. The 3D CartBox toolbox shows promising results but more research is necessary to specify the optimal injection location in order to maximize the improvement of cardiac function by cardiac regenerative therapy.

Acknowledgements

Authors would like to acknowledge Merel Schurink, Marlijn Jansen, Maringa Emons and Joyce Visser for excellent technical assistance and animal care, and Thijs Dijkgraaf for his assistance with the read-only access to the NOGA system from an external computer. Many thanks as well for Dries Feyen for reading and correcting the manuscript.

Funding sources
This work was supported by the Netherlands Heart Foundation '[2003B07304 and 2010T025]', BSIK program "Dutch Program for Tissue Engineering", '[grant 6746]', and a Bekalis price (PD). This research is part of the Project P1.04 SMARTCARE of the research program of the BioMedical Materials institute, co-funded by the Dutch Ministry of Economic Affairs and the Nederlandse

References

1. Orlic D, Kajstura J, Chimenti S, Bodine DM, Leri A, Anversa P. Bone marrow stem cells regenerate infarcted myocardium. Nature. 2003;410:701-705
2. Smits AM, Laake LWV, Ouden KD, Schreurs C, Szuhai K, Van Echteld CJ, Mummery CL, Doevendans PA, Goumans M-J. Human cardiomyocyte progenitor cell transplantation preserves long-term function of the infarcted mouse myocardium. Cardiovascular Research. 2009;83:527-535
3. Beltrami AP, Barlucchi L, Torella D, Baker M, Limana F, Chimenti S, Kasahara H, Rota M, Musso E, Urbanek K, Leri A, Kajstura J, Nadal-Ginard B, Anversa P. Adult cardiac stem cells are multipotent and support myocardial regeneration. Cell. 2003;114:763-776
4. Loffredo FS, Steinhauser ML, Gannon J, Lee RT. Bone marrow-derived cell therapy stimulates endogenous cardiomyocyte progenitors and promotes cardiac repair. Cell stem cell. 2011;8:389-398
5. Quevedo HC, Hatzistergos KE, Oskouei BN, Feigenbaum GS, Rodriguez JE, Valdes D, Pattany PM, Zambrano JP, Hu Q, McNiece I, Heldman AW, Hare JM. Allogeneic mesenchymal stem cells restore cardiac function in chronic ischemic cardiomyopathy via trilineage differentiating capacity. Proceedings of the national acedemy of science. 2009;106:14022-14027
6. Dimmeler S, Zeiher AM, Schneider MD. Unchain my heart: the scientific foundations of cardiac repair. The Journal of Clinical Investigation. 2005;115:572-583
7. Duran JM, Taghavi S, Berretta RM, Makarewich CA, Sharp III T, Starosta T, Udeshi F, George JC, Kubo H, Houser SR. A characterization and targeting of the infarct border zone in a Swine model of myocardial infarction. Clinical and translational science. 2012;5:416-421
8. Kumar A, Haralampus CA, Hughes M, Rouy D, Cresswell N, Braun R, Turner D, Amrani D, Motlagh D, Schaer GL. Assessment of safety, accuracy, and human CD34+ cell retention after intramyocardial injections with a helical needle catheter in a porcine model. Catheterization and Cardiovascular Interventions. 2013;81:970-977
9. Ben-Haim SA, Osadchy D, Schuster I, Gepstein L, Hayam G, Josephson ME. Nonfluoroscopic, in vivo navigation and mapping technology. Nature Medicine. 1996;2:1393-1395
10. van Ramshorst J, Atsma DE, Beeres SLMA, Mollema SA, Ajmone Marsan N, Holman ER, van der Wall EE, Schalij MJ, Bax JJ. Effect of intramyocardial bone marrow cell injection on left ventricular dyssynchrony and global strain. Heart (British Cardiac Society). 2009;95:119-124
11. van Ramshorst J, Antoni ML, Beeres SLMA, Roes SD, Delgado V, Rodrigo SF, de Roos A, Holman ER, Fibbe WE, Lamb HJ, Zwaginga JJ, Boersma E, van der Wall EE, Schalij MJ, Atsma DE, Bax JJ. Intramyocardial bone marrow-derived mononuclear cell injection for chronic myocardial ischemia: the effect on diastolic function. Circulation. Cardiovascular imaging. 2011;4:122-129
12. Perin EC. Assessing Myocardial Viability and Infarct Transmurality With Left Ventricular Electromechanical Mapping in Patients With Stable Coronary Artery Disease: Validation by Delayed-Enhancement Magnetic Resonance Imaging. Circulation. 2002;106:957-961
13. Gyöngyösi M, Lang I, Dettke M, Beran G, Graf S, Sochor H, Nyolczas N, Charwat S, Hemetsberger R, Christ G, Edes I, Balogh L, Krause KT, Jaquet K, Kuck K-H, Benedek I, Hintea T, Kiss R, Préda I, Kotevski V, Pejkov H, Zamini S, Khorsand A, Sodeck G, Kaider A, Maurer G, Glogar D. Combined delivery approach of bone marrow mononuclear stem cells early and late after myocardial infarction: the MYSTAR prospective, randomized study. Nature clinical practice. Cardiovascular medicine. 2009;6:70-81
14. Gyöngyösi M, Dib N. Diagnostic and prognostic value of 3D NOGA mapping in ischemic heart disease. Nature Reviews Cardiology. 2011;8:393-404
15. van Ramshorst J, Bax JJ, Beeres SLMA, Dibbets-Schneider P, Roes SD, Stokkel MPM, de Roos A, Fibbe WE, Zwaginga JJ, Boersma E, Schalij MJ, Atsma DE. Intramyocardial bone marrow cell injection for chronic myocardial ischemia: a randomized controlled trial. Journal of the American Medical Association. 2009;301:1997-2004

16. van Slochteren FJ, Teske AJ, van der Spoel TIG, Koudstaal S, Doevendans PA, Sluijter JPG, Cramer MJM, Chamuleau SAJ. Advanced measurement techniques of regional myocardial function to assess the effects of cardiac regenerative therapy in different models of ischaemic cardiomyopathy. European heart journal cardiovascular Imaging. 2012;13:808-818
17. Arun KS, Huang TS, Blostein SD. Least squares fitting of two 3D point sets. IEEE Transactions on Pattern Analysis and Machine intelligence. 1987;PAMI-9:698-700
18. Umeyama S. Least-squares estimation of transformation parameters between two point patterns. IEEE Transactions on Pattern Analysis and Machine intelligence. 1991;13:376-380
19. Wijnmaalen AP, Van der Geest RJ, Van Huls Van Taxis CFB, Siebelink H-MJ, Kroft LJM, Bax JJ, Reiber JHC, Schalij MJ, Zeppenfeld K. Head-to-head comparison of contrast-enhanced magnetic resonance imaging and electroanatomical voltage mapping to assess post-infarct scar characteristics in patients with ventricular tachycardias: real-time image integration and reversed registration. European Heart Journal. 2010;32:104-114
20. Besl PJ, McKay ND. A Method for Registration of 3-D Shapes. IEE transactions on pattern analysis and machine intelligence. 1992;14
21. Heiberg E, Sjögren J, Ugander M, Carlsson M, Engblom H, Arheden H. Design and validation of Segment--freely available software for cardiovascular image analysis. BMC medical imaging. 2010;10:1-13
22. Heiberg E, Engblom H, Engvall J, Hedström E, Ugander M, Arheden H. Semi-automatic quantification of myocardial infarction from delayed contrast enhanced magnetic resonance imaging. Scandinavian cardiovascular journal: SCJ. 2005;39:267-275
23. Bergström P. Iterative Closest Point Method. Matlab Central. 13 Oct 2006 (Updated 26 Nov 2007)

Supplementary data

In this supplementary data we describe the workflow and the technology that is used to perform image guided cell injections using the 3D CartBox image registration toolbox. The subsequent steps of 3D CartBox that are discussed are illustrated in figure 1 of the main text. All steps of the workflow were applied to an *in vivo* dataset and a phantom dataset was used to assess the registration. Of each step both the purpose and the algorithms used are discussed and Illustrated with images.

Data acquisition

The *in vivo* MRI images were acquired using a 1.5 Tesla Philips Medical Systems Achieva scanner with a commercially available 5 channel phased array cardiac coil. All scans were made using ECG gating. The cine and LGE scans were respectively made with 25 and 1 (end diastolic) phases per cardiac cycle, at the same slice positions and with the same slice orientation. The cine scans were made using Balanced Fast Field Echo (BTFE) with repetition time [TR]/echo time [ET] = 2.9 ms/1.45 ms. Flip angle = 55°, Voxel size = 2.43 x 2.43 mm, field of view [FOV] = 35 x 35 cm, 144 x 144 matrix, 5mm slice thickness, 30 phases/R to R interval. LGE scans were made with [TR]/[ET] = 4.61ms/1.41 ms, Flip angle = 15°, Voxel size = 1.36 x 1.36 mm, field of view [FOV] = 35 x 35 cm, 256 x 256 matrix, 5mm slice thickness. The phantom study was performed using a deformed water bottle. MR images were acquired using a 3.0T scanner (Philips Medical Systems). Short axis images were made, repetition time [TR]/ echo time [ET] = 2.84ms/1.42 ms. Flip angle = 55°, Voxel size = 1.36x1.36 mm, field of view [FOV] = 35x35 cm, 256x256 matrix, 5 mm slice thickness.

1. *Data preprocessing*

Purpose

To assess the infarct transmurality from the LGE scans and project infarct transmurality values on the endocardial surface mesh of the left ventricle in order to guide catheter injections based on infarct transmurality data. Assign an infarct transmurality border zone to use for cell injections.

Method

Segmentation of the left ventricle on the short axis CINE and LGE MRI data is done in the end diastolic phase in approximately 20 slices located from apex to base. The segmentations are done automatically and checked on the long axis images using the freely available software Segment version 1.9 R2507 (http://segment.heiberg.se)[21] available for Matlab (MATLAB 2012a, The MathWorks Inc., Natick, MA, 2012). Segmentations are done to create a 3D surface mesh (cine mesh) of the left ventricular endocardium for surface registration and projection of the acquired data. Subsequently the myocardial infarct was segmented on the LGE images using the area based semi-automatic segmentation[22]. If necessary both the left ventricle and the infarct segmentations were manually adjusted by an experienced radiologist (TL). The results of the infarct segmentation process in one slice is illustrated in Figure S1 A. Area based infarct transmurality values are calculated in 80 circumferential segments of all slices using the bullseye function of segment. The results of the infarct transmurality assessment are illustrated in figure S1 B. The infarct transmurality data was projected on the CINE derived endocardial surface mesh using the

TriScatteredInterp function of Matlab. The CINE derived surface mesh with projected infarct transmurality data is illustrated in figure S1 C. The infarct transmurality projected on the endocardial surface mesh is used to calculate the infarct border zone using an in house developed treatment planning algorithm. The infarct border zone is defined as a 1 cm wide rim over the 50% infarct transmurality isoline. Furthermore the endocardial surface mesh is used for registration of the EMM points, image guided injection procedures, and post processing. Landmark locations used for initial registration are the coronary ostia and apex locations. These locations were selected manually in the end-diastolic frames of the cine images using customized Matlab software.

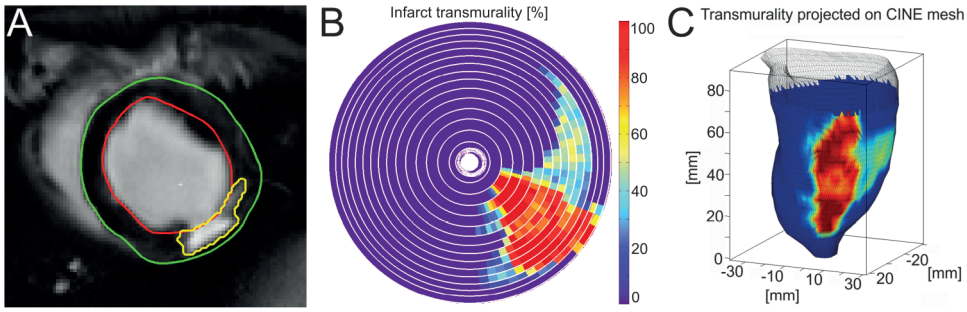

Figure S1. Infarct transmurality segmentation of a single slice (A). The result of the area based infarct transmurality assessment by Segment (B). The transmurality projection on the CINE mesh (C).

2. Registration

Purpose

To combine the EMM dataset and the MRI dataset in order to 1) guide the EMM catheter based on the transmurality values derived from LGE MRI data and 2) combine the EMM and the LGE dataset for comparison and optimize the threshold values of the EMM parameters for areas with a different infarct transmurality. The initial registration step is used for a coarse alignment of the EMM and CINE MRI mesh. The Iterative closest point registration is used to fit the EMM points to the endocardial surface.

Method

Initial registration

Two sets of three 3D points consisting of the two locations of the coronary ostia and the apex measured from CINE MRI (p_{MRI}) and EMM (p_{EMM}) serve as registration landmarks, and are used as input for the initial registration algorithm. The order of the landmarks in both sets of points is the same. The initial registration algorithm is adapted from algorithms published[17,18] and consists of nine steps:

1: Calculate the centroid (c) of each point set:

$$p_{cMRI} = \frac{1}{3}\sum_{i=1}^{3} p_{MRI\,i} \qquad p_{cEMM} = \frac{1}{3}\sum_{i=1}^{3} p_{EMM\,i}$$

2: Translate both sets of points to the origin:

$$q_{MRI} = p_{MRI_i} - p_{cMRI} \qquad q_{EMM} = p_{EMM_i} - p_{cEMM}$$

3: Calculate the 3x3 matrix H:

$$H = \sum_{i=1}^{3} q_{MRI_i} \cdot q_{EMM_i}^{T}$$

4: Calculate the singular value decomposition of H:

$$H = UDV^T$$

5: Multiply the determinants of V and U:

$$X = det\,(V) \cdot det\,(U)$$

6: Determine the S matrix dependent of X:

$$S = \begin{cases} I & if\ X = 1 \\ diag(1,1,-1) & if\ X = -1 \end{cases}$$

7: Determine the Rotation matrix:

$$R = USV^T$$

8: Determine the translation vector:

$$T = p_{EMM} - R \cdot p_{MRI}$$

9: Apply R and T to the EMM dataset:

$$allpoints_{EMM} = (R \cdot allpoints_{EMM}) + T$$

For optimal registration of the apex the algorithm was adapted to apply 10 times higher weighing of the apex compared to the coronary ostia by adding points to the apex location. After applying the rotation matrix and translation vector to (p_{EMM}) and the complete set of all the EMM points ($allpoints_{EMM}$), the orientation and location of(p_{EMM}) and ($allpoints_{EMM}$) is similar to the(p_{MRI}) point set. The result of the initial registration of an *in vivo* EMM dataset is illustrated in figure S4 A and can be used as input for the second step of 3D CartBox.

Iterative closest point registration

The second registration step incorporated in 3D CartBox is the Iterative Closest Point Method[20,23] (ICP). In this method the coarsely registered 3 x n point set of the CINE MRI (p_{MRI}) and a 3 x m point set of the EMM (p_{EMM}) are used as input. The ICP algorithm consists of three steps that are iteratively executed.

1: For all points in the EMM dataset compute the closest point in the MRI dataset using the distance function d:

$$\mathrm{d}(\mathrm{MRI}, \mathrm{p}_{EMM_i}) = \min_{j\in\{1,\ldots,n\}} \left\| \mathrm{p}_{MRI_j} - \mathrm{p}_{EMM_i} \right\|$$

Let C be the resulting set of m closest points for each of the points in the EMM set. To align the EMM to the MRI dataset a transformation (T) consisting of both a rotation (R) and a translation (*T*) is necessary. For each point the transformation is: $\mathrm{T}(p_{EMM}) = R \cdot p_{EMM} + T$, and per set of closest points the resulting distance after the transformation can be calculated: $p_{MRI_i} - \mathrm{T}(p_{EMM_i}) = p_{MRI_i} - (R \cdot p_{EMM_i} + T)$.
To calculate the rotation and translation to minimize the registration error, an error function needs to be optimized:

2: Optimize error function: $argmin_{R,T}\, f(R,T) = \frac{1}{m}\sum_{i=1}^{m} \left\| p_{MRI_i} - (R \cdot p_{EMM_i} + T) \right\|^2$

3: Apply the translation to the EMM dataset: $p_{EMM_{new}} = R \cdot p_{EMM} + T$

After the third step of the ICP process the first step of the ICP process is executed again using the results of the third step. These three steps are iteratively executed until the criteria to finish the process are reached. In 3D CartBox the finalization criteria are set to a maximum number of iterations (100) or a resulting sum squared error (SSE) below $1{\cdot}10^{-15} mm$. Using ICP the registration is based upon the points in the (p_{EMM}) point set that are closest to the points in the (p_{MRI}) point set. The results of the ICP registration in an *in vivo* dataset are shown in figure S2, and cross sectional views of the registration are shown in figure S4.

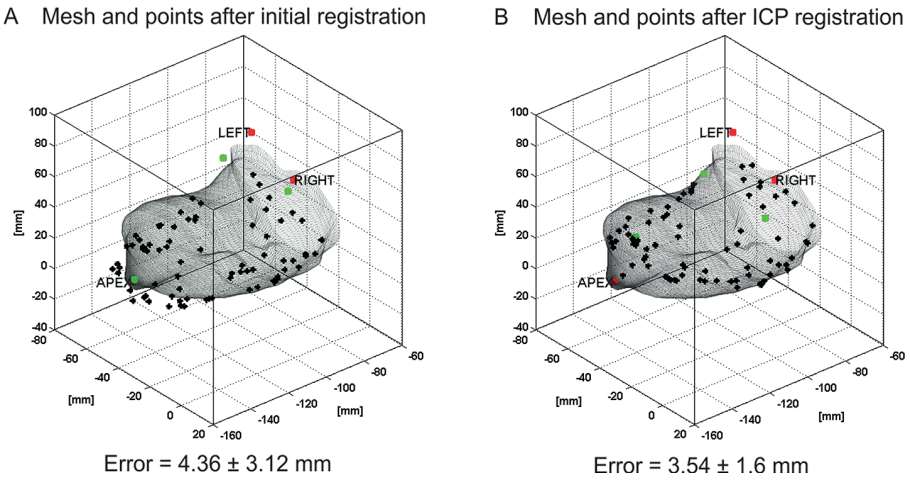

Figure S2. 3D endocardial surface meshes with EMM points show the results after initial registration of an *in vivo* dataset using the apex and left and right coronary ostia as landmarks (A). And ICP registration (B).

Manual registration

Because ICP does not take into account the anatomical correctness of the registration the results of the ICP algorithm need to be checked and approved by the user. This is incorporated into the 3D CartBox workflow. In this way the rotations and translations that are suggested by the ICP algorithm are controlled to be correct and beneficial for the registration. To allow experienced physicians to optimize the registration based on anatomy or additional landmarks that are acquired during the EMM procedure, 3D CartBox facilitates a manual manipulation of the registration. This can be done by adjusting the rotation and translation of (p_{EMM}) interactively with six degrees of freedom. These are rotation and translation in the sagittal, coronal, and transverse plane. Rotations were limited to respectively 10, 20 and 20 degrees to prevent excess rotations. The final registration result of a phantom dataset after manual registration is shown in figure S3.

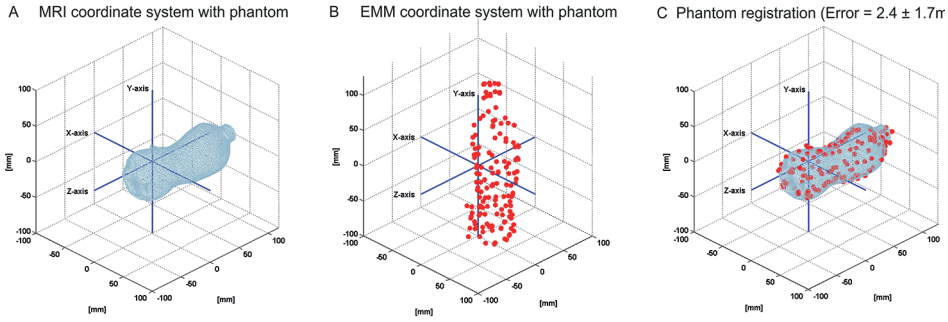

Figure S3. Final registration results of a phantom dataset

3. Post processing

Purpose

Present data using clinical standard visualization techniques.

Method

Create bullseye plots.

Error assessment

The accuracy of the registration was expressed by the registration error being the mean ± standard deviation of the shortest distance from each EMM point to the cine mesh surface. To show the relevance of this measure a cross sectional view of the registration is shown in figure S4. The registration error of the registration shown in figure S4 is 3.54 ± 1.6 and was based on 79 EMM points.

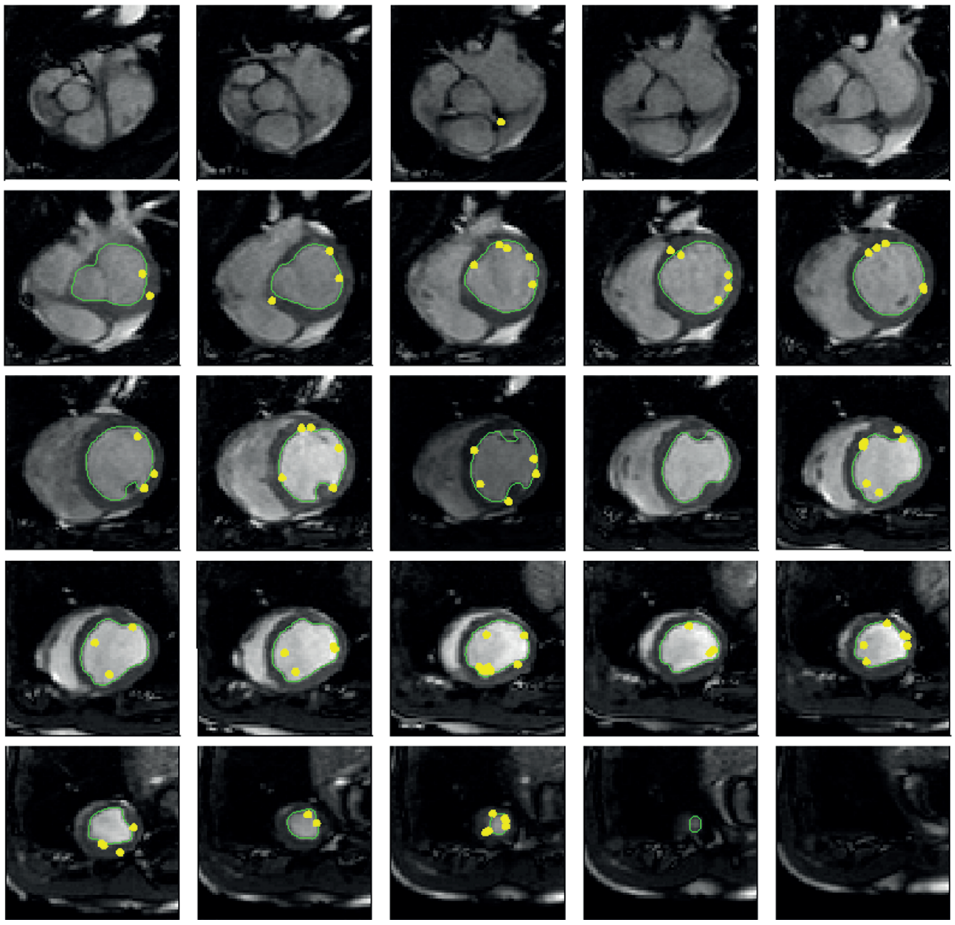

Figure S4. Cross sectional view of the final registration results of an in vivo dataset. The green line represents the endocardial surface mesh and the yellow points are the EMM points.

PART TWO

Advanced delivery

F.J. van Slochteren[1], R. van Es[1], M. Gyöngyösi[2], T.I.G. van der Spoel[1], S. Koudstaal[1], T. Leiner[3], P.A. Doevendans[1,4], S.A.J. Chamuleau[1,4]

[1] Department of Cardiology, University Medical Centre Utrecht, The Netherlands
[2] Department of Cardiology, Medical University of Vienna, Vienna, Austria
[3] Department of Radiology, University Medical Centre Utrecht, The Netherlands
[4] Interuniversity Cardiology Institute of the Netherlands (ICIN), Utrecht, The Netherlands

CHAPTER 4

Accurate infarct border zone identification by combined electromechanical mapping and MRI to improve the targeting of intramyocardial stem cell injections in a porcine model of chronic myocardial infarction

Submitted

Abstract

Objectives

For optimal success of cardiac regenerative therapy intramyocardial catheter guided stem cell transplantations are performed in infarct border zone areas i.e. the closest region of viable myocardium in the vicinity of the infarct area.

Background

The gold standard technique to determine the infarct border zone is late gadolinium enhanced magnetic resonance imaging (LGE-MRI). Nevertheless, the NOGA®XP electromechanical mapping (EMM) catheter guided injection system is used to guide injections to the infarct border zone. We have developed a practical and accurate technique to fuse the NOGA®XP electromechanical maps with LGE-MRI. Besides performing image guided stem cell injections in the true border zone of the infarct these techniques allow us to perform a highly accurate multimodality analysis of the myocardium.

Methods

LGE-MRI and EMM were obtained in 17 pigs with chronic myocardial infarction. MRI and EMM datasets were registered using our in-house developed 3D CartBox image registration software toolbox. Comparisons between MRI and EMM were performed to assess 1) the overlap between infarcted areas identified by EMM and LGE-MRI. The overlap was expressed by the match ratio. 2) The EMM values measured in the areas with a distinct infarct transmurality. 3) The highest sensitivity and specificity of the EMM to assess infarct transmurality. 4) The EMM specification of the true infarct border zone.

Results

Registration was successful in all datasets, and resulted in a mean error of 3.01±1.94mm between the MRI mesh and EMM points. The best match ratio (>60%) was found between areas with infarct transmurality ≥25% and UV≤8.8±1.9mV. The highest sensitivity and specificity to identify infarct transmuralities were found for UV <9mV and BV <1.2mV to respectively identify infarct transmurality of ≥10% and ≥90%. The EMM parameters in the border zones have a large variance.

Conclusion

Our 3D CartBox image registration toolbox enables registration of the EMM on pre-acquired MRI during the catheter injection procedure. Although EMM is used to guide injections in clinical practice and can distinguish healthy from infarcted myocardium, this in depth multimodality analysis showed that infarct transmurality assessment by EMM is not so accurate. Dedicated real-time cell injections into the true border zone of the infarct using 3D CartBox might be key to harnessing the full therapeutical effects of cardiac stem cell therapy.

Introduction

Cardiac regenerative therapy for ischemic heart disease (IHD) targets local cardiac protection and regeneration by means of vasculogenesis, cardiomyogenesis, and matrix support[1]. Previous studies have shown that injection of stem/progenitor cells into the border zone of the infarcted area, stimulates cardiac repair via cell-to-cell contact and secretion of paracrine factors[2-5]. Therapeutic effects may importantly rely on the delivery and retention of the regenerative therapeutics on a location where oxygen and nutrients are available to enable survival. Hence, accurate identification of viable tissue in proximity of the myocardial infarct (MI) (infarct border zone) is therefore of great importance. The gold standard technique to assess infarct size and location is Late Gadolinium Enhancement (LGE-MRI). Currently cell injections are however performed using the NOGA®XP electromechanical mapping (EMM) technique. This technique measures local unipolar (UV) and bipolar (BV) electrical depolarization potentials and relative catheter tip displacements (Linear Local Shortening, LLS), to assess the local electrical and mechanical tissue characteristics and guide minimal invasive intramyocardial injections. A 3D magnetic tracking technique is used to perform measurements and injections at multiple locations on the endocardium guided by a three-dimensional interpolated reconstruction of the LV endocardium[6]. Prior studies have investigated the relations between myocardial viability/perfusion/infarction and NOGA®XP parameters[7,8] using bullseye matching techniques. Other studies in the field of electrophysiology have shown beneficial effects of the integration of electroanatomical mapping (EAM) and LGE-MRI for ventricular arrhythmia ablations[9-11]. Different from the ablations, the injection locations in the context of cardiac regenerative therapy have no built-in control of the correct location, and strongly determine the therapeutic effects. Since the infarcted myocardium is highly susceptibility for arrhythmias upon catheter contact, and the mapping procedure is time-consuming, EMM measurements do not completely cover the endocardium and data is interpolated in regions where no measurements are done. Moreover, in the prior studies to assess the relation between viability/perfusion/infarction and NOGA®XP parameters, different definitions of viability/perfusion/transmurality are used, leading to a large variance between the threshold values found[7]. The most accurate identification of the infarct therefore is LGE-MRI. Since the non transmural border zone of the infarction is believed to be the preferred delivery site of the stem cell therapeutics[2], it is crucial for it to by optimally defined during the injection procedure. We have developed the 3D CartBox image integration toolbox to fuse NOGA®XP EMM and MRI data in a real time fashion[12]. Furthermore we have developed an automatic algorithm to assign infarct areas and border zones with a distinct infarct transmurality[12]. Besides performing image guided stem cell injections in the true border zone of the infarct these techniques allow us to perform a highly accurate multimodality analysis of the myocardium. With this technique we can combine the gold standard infarct imaging technique and local measures of myocardial electrical activity in order to more specifically assess areas and border zones most suitable for stem cell injections. In this study we perform a retrospective in depth multimodality analysis of the myocardial infarction areas and border zones with different infarct transmuralities in a porcine model of chronic myocardial infarction.

Methods

Animals

For this study 2 animal models were used. In model 1 (LCX) myocardial infarction (MI) was induced by 75 minutes of proximal left circumflex coronary artery (LCX) balloon occlusion as previously described[13]. Three 6-month old female Dalland Landrace pigs (60-70 kg; IDDLO, Lelystad, the Netherlands) were pre-treated with clopidogrel 75 mg/day for 3 days and amiodarone 400mg/day for 10 days. Experiments were performed accordance with the "Guide for the Care and Use of Laboratory Pigs" prepared by the Institute of Laboratory Animal Resources and with prior approval by the Animal Experimentation Committee of the Faculty of Medicine, Utrecht University, the Netherlands. In model 2 (LAD) MI was induced in 14 3-months old domestic pigs by 90 minutes of percutaneous balloon occlusion of the left anterior descending coronary artery (LAD) after the second diagonal branch, followed by reperfusion. Pigs were pre-treated with clopidogrel (300 mg) and aspirin (250 mg) one day before procedure, and treated with daily dose of 75 mg clopidogrel and 100 mg aspirin. The experiments were performed in accordance with the "Guide for the Care and Use of Laboratory Pigs" prepared by the Institute of Laboratory Animal Resources and with prior approval by The Experimental Animal Care and Use Committee at the Faculty of Animal Science of the University of Kaposvar (Hungary). In all pigs the experiments as shown in Figure 1 were performed.

Data acquisition

In the University Medical Center Utrecht MRI images were acquired using a 1.5T Philips Medical systems Achieva scanner with a surface cardiac array coil. BFFE Cine scans were made to assess cardiac function, and for registration of the NOGA map on the end diastolic endocardium. The settings during the MRI acquisitions were as follows. BFFE: repetition time [TR]/echo time [ET] /∞ = 2.9 ms/1.45 ms. Flip angle = 55°, Voxel size = 2.43 x 2.43 mm, field of view [FOV] = 35 x 35 cm, 144 x 144 matrix, 5mm slice thickness, 30 phases/R to R interval, electrocardiographic gated. LGE: repetition time [TR]/echo time [ET]/∞ = 4.61ms/1.41 ms, Flip angle = 15°, Voxel size = 1.36 x 1.36 mm, field of view [FOV] = 35 x 35 cm, 256 x 256 matrix, 5mm slice thickness. In the University of Kaposvar MRI images were acquired using a 1.5T Siemens Avanto scanner with a body surface coil. BFFE: repetition time [TR]/echo time [ET] /∞ = 41.85 ms/1.18 ms. Flip angle = 68°, Voxel size = 1.4 x 1.4 mm, field of view [FOV] = 35 x 25 cm, 256 x 176 matrix, 8mm slice thickness, 25 phases/R to R interval, electrocardiographic gated. LGE: repetition time [TR]/echo time [ET]/∞ = 577ms/1.18 ms, Flip angle = 50°, Voxel size = 1.4 x 1.4 mm, field of view [FOV] = 35 x 25 cm, 256 x 180 matrix, 8mm slice thickness. Cine and LGE scans were made at the same positions with the same orientation.

The NOGA® XP system (Biosense Webster, Cordis, Johnson & Johnson, USA) version 1.1.43 was used equipped with a 7 French NOGA mapping catheter (Biosense Webster, Cordis, Johnson & Johnson, Diamond Bar, USA) for the mapping procedure. The LV was entered via the left carotid artery and the femoral artery (LAD), and retrograde passage through the aortic valve. The catheter tip location is tracked throughout the complete cardiac cycle. Data storage is triggered on the R-wave, providing only end diastolic measurement values and points for registration. Electrocardiograms were filtered at 30–400 Hz (bipolar) and 1–240 Hz (unipolar). The EMM datasets were acquired in consideration of the criteria for good electromechanical mapping[7].

Data pre-processing

Segmentation of the left ventricle on the short axis CINE and LGE MRI data is done in the end diastolic phase in approximately 20 slices located from apex to base. The segmentations are done automatically and checked on the long axis images using the freely available software Segment version 1.9 R2507 (http://segment.heiberg.se)[14] available for Matlab (MATLAB 2012a, The MathWorks Inc., Natick, MA, 2012). Segmentations are done to create a 3D surface mesh (cine mesh) of the left ventricular endocardium for surface registration and projection of the acquired data. Subsequently the myocardial infarct was segmented on the LGE images using the area based semi-automatic segmentation[15]. If necessary both the left ventricle and the infarct segmentations were manually adjusted by an experienced radiologist. Area based infarct transmurality values are calculated in 80 circumferential segments of all slices using the bullseye function of segment[15]. The infarct transmurality data was projected on the CINE derived endocardial surface mesh using the TriScatteredInterp function of Matlab. The CINE derived surface mesh with projected infarct transmurality data is illustrated in Figure 2A. The infarct transmurality projected on the endocardial surface mesh is used to calculate the infarct border zone using an in house developed treatment planning algorithm. The infarct border zone is defined as a 1cm wide rim over the 50% infarct transmurality isoline. Furthermore the endocardial surface mesh is used for registration of the EMM points, image guided injection procedures, and post processing.

Image registration

Registration of the NOGA®XP and the MRI datasets was performed using a modified 3D CartBox image integration toolbox[12]. Instead of using anatomical landmarks for registration, we applied a standard rotation which aligns the NOGA®XP and the MRI coordinate systems. Hereafter we performed a rigid body translation of the NOGA®XP dataset based on the apex location. The remaining error now was caused by the slightly altered orientation of the animals with respect to the NOGA®XP and MRI coordinate systems. Since the pigs were in supine position during both the EMM and MRI procedures the orientation of the animal in during the EMM and MRI procedures could be standardized to minimize the remaining registration error. The registration error was minimized further by an iterative closest point (ICP) algorithm[16]. The ICP algorithm was restricted to small rotations around the apex in the sagittal, coronal, and transverse plane of respectively 10, 20 and 20 degrees to prevent excess rotations. If necessary the registration was manually optimized by adjusting the registration interactively with six degrees of freedom. These are rotation and translation in the sagittal, coronal, and transverse planes. The registration error was expressed by the mean and standard deviation of the closest distance between the EMM points and the cine mesh surface as previously described[11]. To prevent interference by EMM points that were not located in the cine mesh (e.g. LV outflow tract), these points were excluded for registration, error calculation and further processing.

Analysis

Multiple analysis were done in order to perform a thorough in depth multimodality analysis of the LGE-MRI and EMM data. At first the overlap between the infarct areas indicated by EMM and the infarct transmurality measured by LGE-MRI was calculated by means of the 'match ratio'. The match ratio was defined as:

$$\text{Match ratio} = \frac{\text{overlap area between LGE and EMM (A)}}{\text{LGE area (B)}} \cdot \frac{\text{overlap area between LGE and EMM (A)}}{\text{EMM area (C)}}$$

Herein A represents the overlap between the LGE area and the EMM area. B represents the LGE area and C represents the EMM area. The match ratio is 1 when the LGE and EMM areas perfectly overlap, and 0 when the LGE and EMM areas are completely separated. A match ratio ≥0.6 was considered a match between the LGE and EMM parameters[17]. Calculation of the match ratio is illustrated in Figure 2. Match ratios were calculated for 5 infarct transmurality areas increasing from 0 to 100%, and EMM parameters that increased from the minimum value to the maximum value in 6 discrete steps. Furthermore the infarct was divided in 5 areas with [0], <0,25], <25,50], <50,75], <75,100] % infarct transmurality to make a comparison between the infarct transmurality areas and the locally measured NOGA® XP parameters. We have calculated the sensitivity and specificity of the NOGA® XP parameters to identify areas with a different infarct transmurality. The highest area under the curve (AUC) of the resulting ROC curves was taken as the best predictor. To assess the theorem that the border zone of the infarct is characterized by a reduced LLS and a maintained UV or BV, we compared the local WT and LLS values in order to validate LLS as a measure of local cardiac tissue deformation. To prevent a wrong interpretation of low voltage areas in the valvular plane with no infarct, and therefore no LGE contrast, we excluded the basal layers that were not infarcted from the analysis. Finally we have identified the true infarct border zones by defining a 1cm wide border over infarct transmurality isolines of 0, 25, 50, 75, 100%, and characterized these true border zones in terms of the EMM parameters. For identification of the border zone best used for cardiac regenerative therapy injections we suggest 50% infarct transmurality[18].

Statistics

All data is presented as mean ± standard deviation (SD). A Kruskall-Wallis test was used to assess the difference between the number of points in the different infarct transmurality areas. An independent samples Mann-Whitney U-test was used to test the difference between the two animal models, and the values of the EMM parameters in the different infarct transmurality areas. $P < 0.05$ was considered significant.

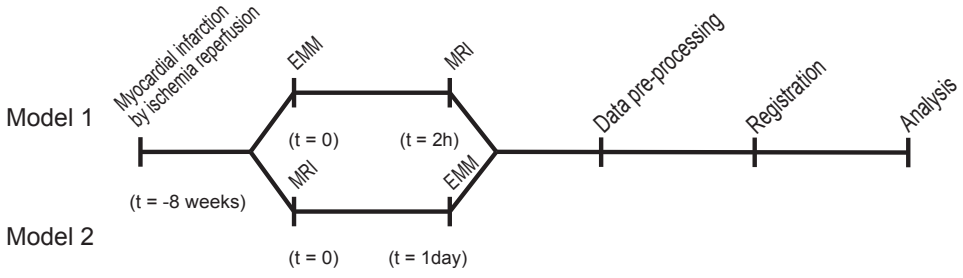

Figure 1. Time line of the experiments of model 1 (LCX), and model 2 (LAD)

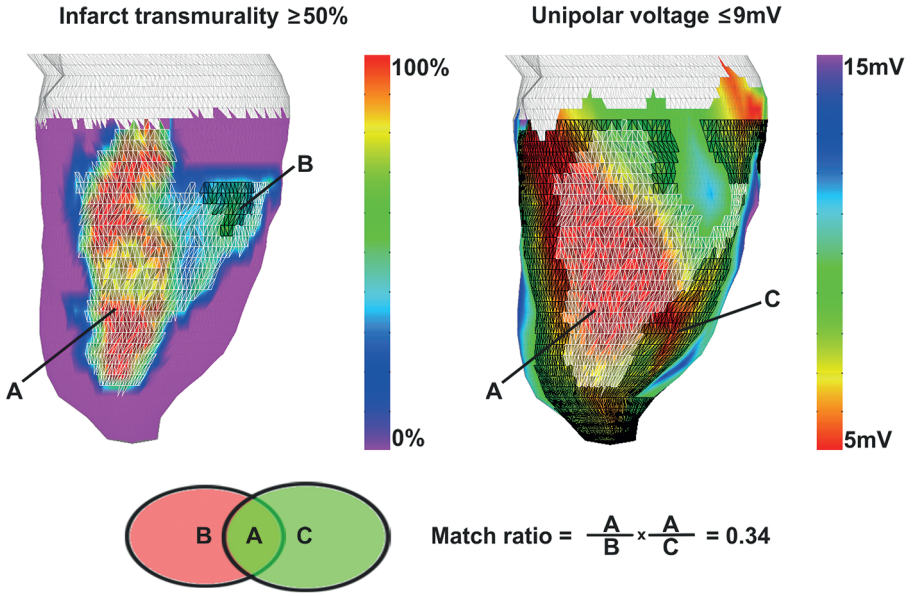

Figure 2. The match ratio. Overlap (A) between the infarct area with transmurality ≥50% (B) and unipolar voltage ≤9mV (C) is expressed by the match ratio. In this case the match ratio is 0.34.

Results

Animals

In the animals that underwent an LCX occlusion the infarct was located in the midlateral wall (3 animals). In this group MRI and EMM were performed within 2 hours. In the animals that underwent an LAD occlusion the infarct was located apicoseptally and mid-apical anterior (14 animals). In this group MRI and EMM were performed within 1 day. All LGE datasets showed a clear fibrotic area on LGE-MRI.

Data acquisition

MRI findings are collected in Table 1. The mean LV ejection fraction was 42 ± 8.7%. The mean endocardial surface area in the [0], <0,25], <25,50], <50,75], <75,100] % infarct transmurality subdivisions respectively was: 68.2 ± 12.8cm^2, 10.6 ± 3.2cm^2, 6.5 ± 3.5cm^2, 6.4 ± 2.2cm^2, and 10.9 ± 7.3cm^2 thereby covering 66.1 ± 6.1%, 10.5 ± 3.3%, 6.3 ± 3.4%, 6.4 ± 2.6% and 10.5 ± 6.3% of the total LV endocardial surface area. A significant difference in infarct size was found between ischemia reperfusion models performed in the LCX and LAD in the 25-50%, and 75-100% infarct transmurality areas p=0.03 and 0.04 respectively. The mean number of EMM points in each map was 152.3 ± 55.

Image registration

The registration data is summarized in Table 2. The total number of points of the 17 datasets that are used for registration, and projection of EMM parameters on the endocardial surface mesh for comparison is 2590. The EMM points that were acquired during the mapping

procedure were homogeneously distributed over the endocardial surface to assure optimal registration of the EMM and MRI cine mesh. The resulting registration error was 3.01±1.94mm. The EMM points were not homogeneously distributed over the areas with a distinct infarct transmurality ($p < 0.05$). The point density was highest in the regions with 25-50% and 75-100% infarct transmurality.

Analysis

Match ratios of the EMM parameters are shown in Figure 3. It can clearly be appreciated that of all EMM parameters UV has the highest match ratio for all transmurality values. Nevertheless the match ratio only is ≥0.6 for areas with infarct transmurality ≥25% and UV≤8.8±1.9mV. Both the BV and LLS have a match ratio ≥0.6, only for areas with a infarct transmurality ≥0%. This is the definition of the match ratio. Match ratios of BV and LLS are <0.6 in all areas with infarct transmurality ≥25%, indicating that there is a poor overlap of areas with low BV and LLS values and areas with ≥25% infarct transmurality. To determine the cause of the low match ratios we have visualized the distribution of the EMM parameters in the areas with a distinct infarct transmurality as shown in Figure 4. The highest UV and BV values were found in areas with 0% infarct transmurality as is shown in Figure 4A and B, in all other infarct transmurality areas the UV and BV values were lower, but did not show a strong relation to infarct transmurality. The LLS is poorly related to the infarct transmurality as is shown in Figure 4C. The green line and a grey band in Figure 4 respectively show the threshold values for which the highest sensitivity and specificity was found (shown in Figure 5) and the threshold values of the EMM parameters to identify core infarct that are reported in literature[7]. The differences between the UV, BV, LLS values in the different infarct transmurality areas are statistically assessed in Table 3, 4 and 5 respectively. The highest sensitivity and specificity of all the EMM parameters to detect areas with infarct transmurality ≥0% are shown in Figure 5. The highest AUC (0.76) for UV is found for an infarct transmurality of ≥10%. For UV <9mV; sensitivity = 0.81 and specificity = 0.64. The highest AUC (0.76) for BV is found for infarct transmurality ≥90%.

Table 1. Results of cine and late enhancement magnetic resonance imaging of 17 animals. Data are expressed as mean ± SD.

LV end-diastolic volume (ml)	123.6 ± 32.6	
LV end-systolic volume (ml)	72.8 ± 26.4	
LV stroke volume (ml)	50.7 ± 11.5	
LV ejection fraction (%)	42.0 ± 8.7	
Heart rate	92.7 ± 20.7	
Myocardium volume (ml)	111 ± 15.6	
Infarct volume (ml)	15.6 ± 4.1	
LV area (cm2)	102.7 ± 13.8	
Infarct area 0 % transmurality (cm^2)	68.2 ± 12.8	(66.1 ± 6.1 %)
Infarct area 0 - 25 % transmurality (cm^2)	10.6± 3.2	(10.5 ± 3.3 %)
Infarct area 25 - 50 % transmurality (cm^2)	6.5 ± 3.5	(6.3 ± 3.4 %)
Infarct area 50 - 75 % transmurality (cm^2)	6.4 ± 2.2	(6.4 ± 2.6 %)
Infarct area 75 - 100 % transmurality (cm^2)	10.9 ± 7.3	(10.5 ± 6.3 %)

Table 2. Three dimensional electromechanical mapping and image registration results of 17 animals. Data are expressed as mean ± SD. The differences between the points/cm2 of each area are calculated using the Kruskall Wallis test.

Electromechanical mapping points			
Total number of EMM points	2867		
EMM points used for registration	2590		
Points per animal	152.3 ± 55		
Registration error (mm)	3.01 ± 1.94		
Points used for projection and analysis			
Total number of EMM points	1581		
Points per animal	93 ± 27.2		
Points per infarct transmurality area used for projection and analysis			
0%	50.2 ± 18.4	0.7 ± 0.3 points/cm^2	
0 - 25%	9.7 ± 6.2	0.9 ± 0.5 points/cm^2	
25 – 50%	8.0 ± 4.3	1.4 ± 0.7 points/cm^2	($p < 0.05$)
50 – 75%	6.3 ± 5.6	0.9 ± 0.6 points/cm^2	
75 – 100%	18.7 ± 14.2	1.5 ± 0.8 points/cm^2	

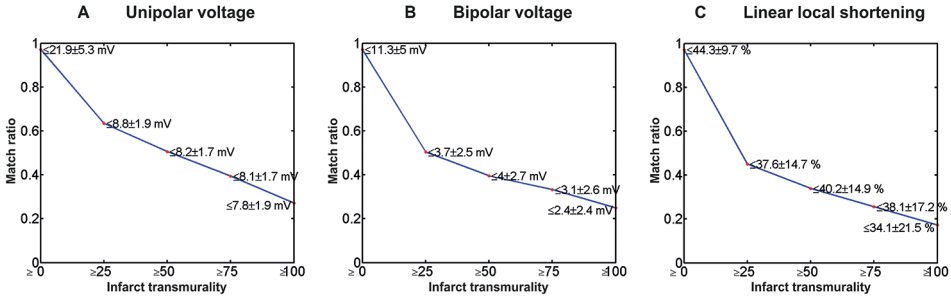

Figure 3. Maximal match ratios (y-axis) of the unipolar voltage (A), bipolar voltage (B), linear local shortening (C) for each infarct transmurality area (x-axis). The numbers in the graph annotate the mean±SD of the threshold values of the corresponding parameters that result in the highest match ratios of the parameter.

For BV <1.2mV; sensitivity = 0.7 and specificity = 0.68. The worst AUC is found for LLS (AUC = 0.48). Infarct transmurality ≥90%, for LLS <8.75% (sensitivity = 0.58, specificity = 0.6). Furthermore we have assessed the relations between the infarct transmurality and both WT, and LLS. Although the whiskers of both WT and LLS in Figure 6B and C are large, it can be appreciated that in contrast to LLS, WT is related to infarct transmurality. The ROC curve in Figure 6A shows that WT<2.5% distinguishes infarct transmurality ≥10% with sensitivity = 0.8 and specificity = 0.69. Figure 7 depicts the different border zones of the infarct as calculated by our in house developed treatment planning algorithm which can be used for cell injections. Electromechanical characterization of the tissue in the infarct transmurality border zones is shown in Figure 8. As could be expected, this is comparable to the relation between the infarct areas and the EMM parameters as shown in Figure 4.

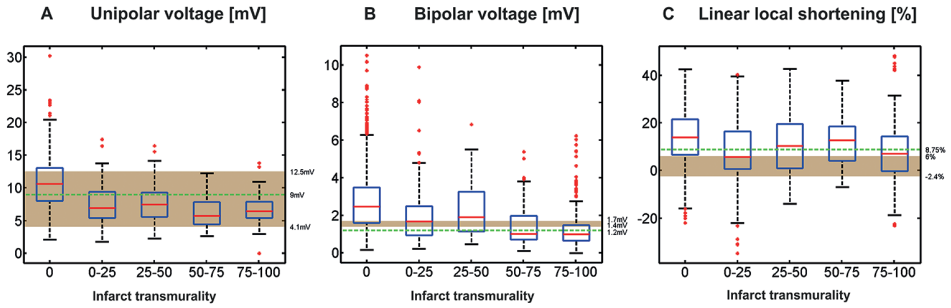

Figure 4. Box plots of the distribution of the unipolar voltage (A), bipolar voltage (B) linear local shortening (C) values over the areas with a distinct infarct transmurality. Boxes represent the 25-75% percentiles and the red line in the boxes represents the median value. Red dots are outliers (>3 x SD from the mean value). The green line represents the value with the highest AUC as shown in figure 5. The grey area represents the range of the threshold values reported in literature to distinguish core infarct. Numbers on the right annotate the range of the threshold values and the value of the green line.

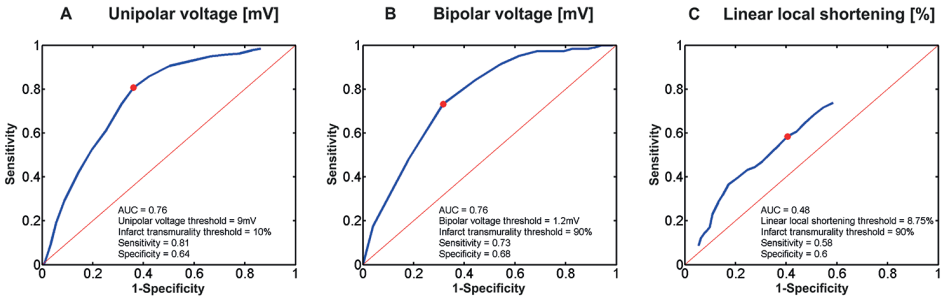

Figure 5. ROC curves for the unipolar voltage (A), bipolar voltage (B), linear local shortening (C) with the highest AUC. The corresponding thresholds of the respective parameters, and the infarct transmurality are annotated in the figures. The red dot marks the highest sensitivity and specificity.

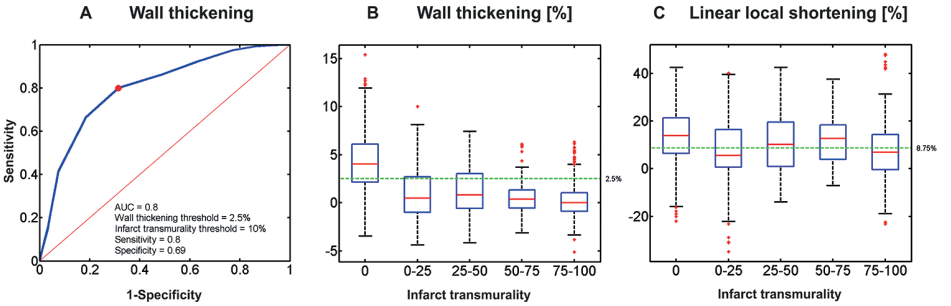

Figure 6. ROC curve for wall thickening (A) with the highest AUC. The corresponding thresholds for wall thickening and infarct transmurality are annotated in the figure. Box plots of the distribution of the wall thickening (B) and linear local shortening (C). Boxes represent the 25-75% percentiles and the red line in the boxes represents the median value. Red dots are outliers (>3 x SD from the mean value). The green line represents the value with the highest AUC.

Table 3. P-values of the differences between the unipolar voltages of the different infarct transmurality groups calculated with the Mann-Whitney U-test.

	0%	0-25%	25-50%	50-75%	75-100%
0%		<0.01	<0.01	<0.01	<0.01
0 - 25%	<0.01		0.43	<0.01	<0.01
25 – 50%	<0.01	0.43		<0.01	<0.01
50 – 75%	<0.01	<0.01	<0.01		0.05
75 – 100%	<0.01	<0.01	<0.01	0.05	

Table 4. P-values of the differences between the bipolar voltages of the different infarct transmurality groups calculated with the Mann-Whitney U-test.

	0%	0-25%	25-50%	50-75%	75-100%
0%		<0.01	<0.01	<0.01	<0.01
0 - 25%	<0.01		0.22	<0.01	<0.01
25 – 50%	<0.01	0.22		<0.01	<0.01
50 – 75%	<0.01	<0.01	<0.01		0.17
75 – 100%	<0.01	<0.01	<0.01	0.17	

Table 5. P-values of the differences between the linear local shortening values of the different infarct transmurality groups calculated with the Mann-Whitney U-test.

	0%	0-25%	25-50%	50-75%	75-100%
0%		<0.01	<0.01	0.09	<0.01
0 - 25%	<0.01		0.09	<0.01	0.75
25 – 50%	<0.01	0.09		0.26	0.02
50 – 75%	0.09	<0.01	0.26		<0.01
75 – 100%	<0.01	0.75	0.02	<0.01	

Discussion

In this study we have applied the 3D CartBox image integration toolbox on a dataset of 17 pigs with a chronic MI. For the first time we have registered NOGA® XP EMM data on a surface mesh derived from end-diastolic CINE MRI images in real time with a mean surface registration error of 3.01 ± 1.94mm. In contrast to earlier studies using a manual segmental comparison[7], this technique enabled an accurate in depth analysis of the electromechanical properties of infarct areas. The four main findings of this study were: 1) The overlap between infarct areas identified by low EMM values and infarct areas identified by LGE-MRI is poor. 2) UV and BV do distinguish infarcted and healthy tissue, but lack the sensitivity to make a distinction between different infarct transmurality values. 3) LLS and WT are differently affected by infarct transmurality. 4) Our treatment planning algorithm can be used to identify the true infarct border zone based on LGE-MRI. In the true border zone a wide range of EMM parameters is found.

Animals

This study was conducted in a multicenter fashion using 2 different animal models. In the LCX model there was one pig with no 75-100% infarct transmurality area 8 weeks after MI. Most likely this was caused by the biological varying response to an ischemia time of 75 minutes. In the 90 minutes LAD occlusion model all pigs had a transmural infarct 6 weeks after MI. The different times between the MI and the data acquisition has not influenced the analysis since the infarct is known to be established 3 weeks after MI[19].

Data acquisition

Although data in Utrecht and Kaposvar were recorded using different equipment, data acquisition protocols were identical, and therefore image registration and analysis could be easily performed using our 3D CartBox toolbox using standard image formats for MRI (DICOM) and NOGA®XP (SQL database).

Image registration

EMM and MRI were performed within 2 hours (LCX), and 1 day (LAD). This different time points could have affected the cardiac loading situation during the EMM and MRI procedures. However, since the NOGA®XP measurement points were not exactly obtained in the entire LV, and we did not observe large differences between the registration errors of the different models, we believe that this effect was minimal. In this study we have used the standard rotation to align the NOGA®XP and MRI coordinate systems, instead of initial registration based on anatomical landmarks[12]. To prevent erroneous rotations by the subsequent ICP and manual optimization steps of the registration, we have manually secured that rotations during these steps did not exceed 5 degrees. The resulting registration error is 3.01 ± 1.94mm, which is clinically relevant and comparable to the values reported in studies where Carto® was used: 3.83 ± 0.57mm[11] or 4.3 ± 3.2 mm[10]. The SD of the registration error is affected by the regularity of the heart rate during the EMM procedures resulting in end diastolic LV volume alterations, or respiratory induced motion of the heart. The NOGA®XP system does not compensate for this. From Table 2 it can be observed that the EMM points are not homogeneously distributed over the areas with a different infarct transmurality. The highest point density is found in the area with 75-100% infarct transmurality. This most likely is caused by the targeted search for the infarct area during the mapping procedure.

Analysis

As already visually noticed[9,11], areas that show a considerable infarct transmurality on LGE-MRI do not always overlap with infarct areas identified by EMM. To quantify the overlap between two areas we have established the match ratio. The threshold of the match ratio ≥0.6 indicating a sufficient overlap is adopted from Tokuda et al.[17]. We believe that the match ratio as shown in Figure 3 clearly quantifies the overlap between two areas. The poor match ratio values found however are caused by the low sensitivity of the EMM parameters to distinguish different infarct transmurality values as shown in Figure 4. In our data we found that EMM has the highest sensitivity and specificity to identify infarct transmuralities of ≥10% and ≥90% by electric signals UV <9mV and BV <1.2mV respectively as is shown in Figure 5. This most likely is caused by the pickup of depolarization signals from a larger area by a single electrode (UV), which are filtered out by the subtraction of two electrode signals that are placed within 2mm on the catheter (BV). Infarcted tissue in

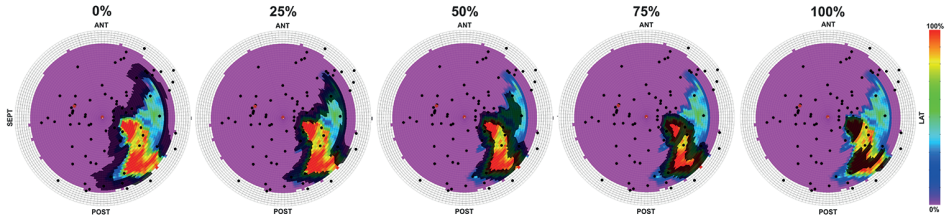

Figure 7. Bullseye figures of the infarct transmurality border zones of 0, 25, 50, 75, and 100%.

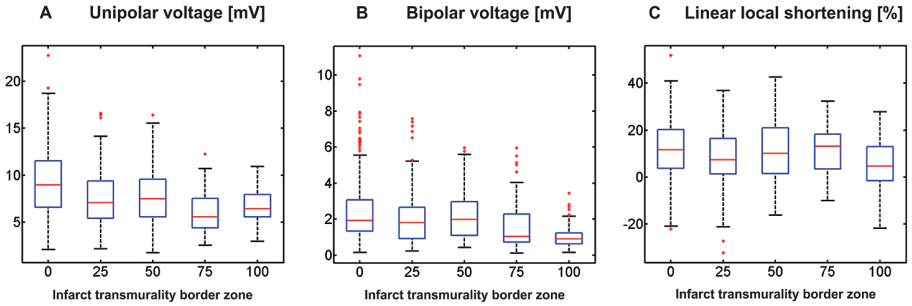

Figure 8. Box plots of the distribution of the unipolar voltage (A), bipolar voltage (B) linear local shortening (C) values over the 5 border zones with a different infarct transmurality as shown in figure 7. Boxes represent the 25-75% percentiles and the red line in the boxes represents the median value. Red dots are outliers (>3 x SD from the mean value).

the vicinity of the measurement decreases UV in a larger area whereas BV is only affected by the local tissue. UV therefor performs best to identify areas with infarct transmurality ≥10%, whereas BV is more eligible to identify areas with infarct transmurality ≥90%. Unfortunately neither area is off interest during cardiac regenerative therapy injections. In contrast to cell injection procedures EAM procedures in electrophysiology are used to identify the arrhythmogenic substrate. Therefore more points are acquired in the core infarct areas, resulting in a better core identification based on BV. Unfortunately studies using a comparable registration algorithm in the field of electrophysiology either did not calculate the ROC curves[11], or did not perform an detailed analysis of the areas with a different infarct transmurality[9,10]. The wide range of threshold values represented in literature[7] to identify core infarct as shown by the gray area in Figure 4 results from the use of different definitions of viability/perfusion/transmurality and the use of absolute (PET, echocardiography, histology) and relative (SPECT) techniques to identify this, in combination with a manual segmental comparison to EMM data. To be able to target the infarct border zone for stem cell injection procedures the LLS parameter was introduced to measure local relative cathetertip displacements caused by cardiac deformation. Areas with a severely depressed deformation (LLS) and a maintained UV or BV should present the hibernating tissue in the infarct border zone. Strikingly figure 6 illustrates that there is no relation between LLS (6C) and the local infarct transmurality in comparison to WT (6B). This is caused by the definition of LLS being: '*the change in distance between an index*

point and all its recorded surrounding points from late diastole to maximum systole'[20]. A weighing is applied to emphasize points within a distance of 8-15mm[20]. Consequently for a point in an area with small number of points or points moving due to tethering of the tissue, LLS is based on points located more distantly, or based on a false perception, causing erroneous LLS values. To correctly assess cardiac deformation by LLS therefore a higher point density is necessary. This has however never been investigated. In summary, the feasibility to accurately identify the infarct border zone by EMM is limited. We therefore have developed a treatment planning algorithm to identify infarct border zones with a distinct transmurality, in order to perform regenerative therapy injections in a distinct area[12]. The values of the EMM parameters found in the border zones depicted in Figure 7 are widely spread as shown in Figure[8]. The spread is even more pronounced in the border zones compared to the areas, because a border zone is defined as a 1cm wide border over distinct infarct transmurality isolines, causing it to overlay multiple infarct transmurality areas and consequently a wider range of EMM values.

Clinical implications

Conclusions drawn in this study about the targeting of the infarct area by EMM in a porcine model of chronic myocardial infarction has revealed that UV<9mV best targets the area with transmurality ≥10%. However since this might not be the true border zone[18], it is certainly in the vicinity of the infarct, and therefore preferred over injections based upon fluoroscopy solely. Combination of the gold standard infarct imaging technique for both infarct and infarct border zone identification, and a catheter navigation technique might be more accurate to guide injections targets the infarct border zone. This approach could lead to shorter injection procedures, less necessity for the use of fluoroscopy to confirm the injection location, and less radiation for the patient and the physician. Real-time integration of LGE-MRI during cardiac stem cell injection procedures could be a key to harnessing the full therapeutical effects of cardiac stem cell therapy. The treatment planning and 3D CartBox toolbox enables the use of all parameters (perfusion, fibrosis, myocardial wall thickening, myocardial tissue tagging) from a pre-procedural acquired MRI or other imaging modality (SPECT/CT) to guide the stem cell injection procedures. The 3D CartBox toolbox for image guided cardiac stem cell injections is rewarded with the BMM valorization grant, and will be made commercially available via the newly founded spin-off company CARTcare: 'Technical solutions to improve cardiac regenerative therapy'.

Limitations

For both the use of BV and LLS it was concluded that the acquiring of more measurement points might have been necessary to gain insight into the full potential of the BV and LLS parameters. Furthermore we did not perform a total comparison between EMM, LGE-MRI, and histology. In prior comparisons using coarse registration techniques a good agreement was found between EMM and histology[21] and between LGE-MRI and histology[22-24]. A similar comparison would have generated insight into the accuracy of our image registration technique. Such a study is necessary to assess the use of LGE-MRI guided injections and will be performed in the near future. During the mapping procedure small respiratory induced excursions of the catheter tip could be observed. Since the NOGA®XP system did not compensate for respiratory induced motion of the cathetertip, this most likely affected the registration. Compensation for respiratory motion might be beneficial for future applications.

Conclusion

We are the first to perform solid registration and an in depth comparison of the NOGA®XP EMM parameters and infarct transmurality measured by LGE-MRI. Based on our findings the infarct identification by EMM is determined by the used parameter and the amount of mapping points, and thereby operator dependent. Accurate infarct border zone identification therefore can better be based upon the gold standard imaging modality to assess infarct transmurality in combination with an image registration toolbox (3D CartBox) to guide injections in real time.

Funding sources

This work was supported by the Netherlands Heart Foundation '[2003B07304 and 2010T025]', BSIK program "Dutch Program for Tissue Engineering", '[grant 6746]', and a Bekalis price (PD). This research is part of the Project P1.04 SMARTCARE of the research program of the BioMedical Materials institute, co-funded by the Dutch Ministry of Economic Affairs and the Nederlandse Hartstichting.

References

1. Dimmeler S, Zeiher AM, Schneider MD. Unchain my heart: the scientific foundations of cardiac repair. The Journal of Clinical Investigation. 2005;115:572-583
2. Orlic D, Kajstura J, Chimenti S, Bodine DM, Leri A, Anversa P. Bone marrow stem cells regenerate infarcted myocardium. Nature. 2001;410:701-705
3. Smits AM, Laake LWV, Ouden KD, Schreurs C, Szuhai K, Van Echteld CJ, Mummery CL, Doevendans PA, Goumans M-J. Human cardiomyocyte progenitor cell transplantation preserves long-term function of the infarcted mouse myocardium. Cardiovascular Research. 2009;83:527-535
4. Beltrami AP, Barlucchi L, Torella D, Baker M, Limana F, Chimenti S, Kasahara H, Rota M, Musso E, Urbanek K, Leri A, Kajstura J, Nadal-Ginard B, Anversa P. Adult cardiac stem cells are multipotent and support myocardial regeneration. Cell. 2003;114:763-776
5. Loffredo FS, Steinhauser ML, Gannon J, Lee RT. Bone marrow-derived cell therapy stimulates endogenous cardiomyocyte progenitors and promotes cardiac repair. Cell Stem Cell. 2011;8:389-398
6. Gyöngyösi M, Lang I, Dettke M, Beran G, Graf S, Sochor H, Nyolczas N, Charwat S, Hemetsberger R, Christ G, Edes I, Balogh L, Krause KT, Jaquet K, Kuck K-H, Benedek I, Hintea T, Kiss R, Préda I, Kotevski V, Pejkov H, Zamini S, Khorsand A, Sodeck G, Kaider A, Maurer G, Glogar D. Combined delivery approach of bone marrow mononuclear stem cells early and late after myocardial infarction: the MYSTAR prospective, randomized study. Nature Clinical Practice. Cardiovascular Medicine. 2009;6:70-81
7. Gyöngyösi M, Dib N. Diagnostic and prognostic value of 3D NOGA mapping in ischemic heart disease. Nature Reviews Cardiology. 2011;8:393-404
8. Perin EC, Silva GV, Sarmento-Leite R, Sousa ALS, Howell M, Muthupillai R, Lambert B, Vaughn WK, Flamm SD. Assessing Myocardial Viability and Infarct Transmurality With Left Ventricular Electromechanical Mapping in Patients With Stable Coronary Artery Disease: Validation by Delayed-Enhancement Magnetic Resonance Imaging. Circulation. 2002;106:957-961
9. Codreanu A, Odille F, Aliot E, Marie P-Y, Magnin-Poull I, Andronache M, Mandry D, Djaballah W, Régent D, Felblinger J, de Chillou C. Electroanatomic characterization of post-infarct scars comparison with 3-dimensional myocardial scar reconstruction based on magnetic resonance imaging. Journal of the American College of Cardiology. 2008;52:839-842
10. Desjardins B, Crawford T, Good E, Oral H, Chugh A, Pelosi F, Morady F, Bogun F. Infarct architecture and characteristics on delayed enhanced magnetic resonance imaging and electroanatomic mapping in patients with postinfarction ventricular arrhythmia. Heart Rhythm. 2009;6:644-651
11. Wijnmaalen AP, Van Der Geest RJ, Van Huls Van Taxis CFB, Siebelink H-MJ, Kroft LJM, Bax JJ, Reiber JHC, Schalij MJ, Zeppenfeld K. Head-to-head comparison of contrast-enhanced magnetic resonance imaging and electroanatomical voltage mapping to assess post-infarct scar characteristics in patients with ventricular tachycardias: real-time image integration and reversed registration. European Heart Journal. 2010;32:104-114
12. Van Slochteren FJ, Van Es R, Koudstaal S, Van Der Spoel TIG, Sluijter JPG, Verbree J, Pruim RHR, Pluim JPW, Leiner T, Doevendans PA, Chamuleau SAJ. Multimodality infarct identification for optimal image guided intramyocardial cell injections. Submitted. 2014
13. van der Spoel TIG, Vrijsen KR, Koudstaal S, Sluijter JPG, Nijsen JFW, de Jong HW, Hoefer IE, Cramer M-JM, Doevendans PA, van Belle E, Chamuleau SAJ. Transendocardial cell injection is not superior to intracoronary infusion in a porcine model of ischaemic cardiomyopathy: a study on delivery efficiency. Journal of Cellular and Molecular Medicine. 2012;16:2768-2776
14. Heiberg E, Sjögren J, Ugander M, Carlsson M, Engblom H, Arheden H. Design and validation of Segment - freely available software for cardiovascular image analysis. BMC Medical Imaging. 2010;10:1-13
15. Heiberg E, Engblom H, Engvall J, Hedström E, Ugander M, Arheden H. Semi-automatic quantification of myocardial infarction from delayed contrast enhanced magnetic resonance imaging. Scandinavian Cardiovascular Journal. 2005;39:267-275
16. Umeyama S. Least-squares estimation of transformation parameters between two point patterns. IEEE Transactions on Pattern Analysis and Machine intelligence. 1991;13:376-380

17. Tokuda M, Tedrow UB, Inada K, Reichlin T, Michaud GF, John RM, Epstein LM, Stevenson WG. Direct comparison of adjacent endocardial and epicardial electrograms: implications for substrate mapping. Journal of the American Heart Association. 2013;2:e000215-e000215
18. Romero J, Kahan J, Kelesidis I, Makani H, Wever-Pinzon O, Medina H, Garcia MJ. CMR imaging for the evaluation of myocardial stunning after acute myocardial infarction: a meta-analysis of prospective trials. European Heart Journal Cardiovascular Imaging. 2013;14:1080-1091
19. Holmes JW, Borg TK, Covell JW. Structure and Mechanics of Healing Myocardial Infarcts. Annual Reviews of Biomedical Engineering. 2005;7:223-253
20. Psaltis PJ, Worthley SG. Endoventricular Electromechanical Mapping - The Diagnostic and Therapeutic Utility of the NOGA ® XP Cardiac Navigation System. Journal of Cardiovascular Translational Research. 2009;2:48-62
21. Wolf T, Gepstein L, Dror U, Hayam G, Shofti R, Zaretzky a, Uretzky G, Oron U, Ben-Haim SA. Detailed endocardial mapping accurately predicts the transmural extent of myocardial infarction. Journal of the American College of Cardiology. 2001;37:1590-1597
22. Pop M, Ghugre NR, Ramanan V, Morikawa L, Stanisz G, Dick AJ, Wright GA. Quantification of fibrosis in infarcted swine hearts by ex vivo late gadolinium-enhancement and diffusion-weighted MRI methods. Physics in Medicine and Biology. 2013;58:5009-5028
23. Kim RJ, Fieno DS, Parrish TB, Harris K, Chen EL, Simonetti O, Bundy J, Finn JP, Klocke FJ, Judd RM. Relationship of MRI delayed contrast enhancement to irreversible injury, infarct age, and contractile function. Circulation. 1999;100:1992-2002
24. Amado LC, Gerber BL, Gupta SN, Rettmann DW, Szarf G, Schock R, Nasir K, Kraitchman DL, Lima JA. Accurate and objective infarct sizing by contrast-enhanced magnetic resonance imaging in a canine myocardial infarction model. Journal of the American College of Cardiology. 2004;44:2383-2389

PART TWO

Advanced delivery

R. van Es1, F.J. van Slochteren[1], S.J. Jansen of Lorkeers[1], F. Vos1, R. Blankena[1], P.A. Doevendans[1,2], S.A.J. Chamuleau[1,2]

[1] Department of Cardiology, University Medical Centre Utrecht, The Netherlands
[2] Interuniversity Cardiology Institute of the Netherlands (ICIN), Utrecht, The Netherlands

CHAPTER **5**

Real-time correction of respiratory induced cardiac motion in endocardial mapping procedures

In preparation

Abstract

Introduction

Endocardial catheter interventions like cell injections or ablations are often based on endocardial surface maps (ESM). To target the location for the therapy a high precision is often required. Since ESM are created while the patient is breathing freely, respiratory induced cardiac motion artifacts can appear in the ESM. These artifacts can lead to mis-targeting of the optimal therapy delivery location, but also to a mismatch when registering the ESM with data from other 3D imaging modalities such as MRI.

Methods

We have developed a customized interface to connect a respiratory transducer to the NOGA®XP electromechanical mapping (EMM) system showing the respiratory signal as a baseline drift. A correction algorithm was designed to adjust the locations of all measured points to their location during end expiration. Here for correction vectors are determined based on the amplitude and slope of the respiratory signal measured from respiratory induced motion of a fiducial EMM point. The algorithm was evaluated in a phantom, in which motion was induced by a ventilator. Moreover, the results were validated in a large animal model. MRI was used to evaluate the registration error with the EMM data with and without correction of respiratory induced motion.

Results

The recording and analysis of the respiratory signal on a precordial ECG lead was successful. In the phantom model the registration error improved from 2.8±2.2mm before to 1.9±1.3mm after correction compared to 2.0±1.4mm in the nonmoving model. In the animal experiment the maximal apical displacement of 3.7±1.1mm was reduced to 2.3±0.5mm (35±17%, $p<0.05$) after correction. The improvement of the registration error with the MRI mesh in the animal model was minimal.

Conclusion

Respiratory induced cardiac motion correction during endocardial mapping procedures is feasible and can be incorporated in commercially available systems. Due to limited respiratory induced cardiac motion in pigs we could not proof the clinical relevance of respiratory correction. It is known that respiratory induced cardiac motion is larger in humans. It therefore stands to reason that in the clinical situation, respiratory correction can reduce artifacts and guide the operator to the optimal location to deliver the therapy.

Introduction

During endocardial catheter guided ablations or cell injections treatment planning often depends on detailed endocardial surface map (ESM) of locally measured electrical or mechanical tissue characteristics[1,2]. Different electro anatomical (EAM) or electromechanical (EMM) mapping systems are commercially available that can determine the exact 3D location of the catheter tip inside the heart in real time using electrical or magnetic fields[3-5]. The optimal location for the therapy is selected based on the ESM. Parameters stored in the ESM include the local depolarization potentials and relative cardiac motion induced displacement of the catheter tip. All data are stored with their respective 3D locations. Data is interpolated in the areas that are spatially located between the acquired mapping points to reconstruct the complete endocardial surface.
During the construction of an ESM the patient is usually awake and breathing freely. Respiratory induced cardiac motion (RICM) leads to spatial errors in the ESM. A low spatial resolution of EAM together with the RICM induced artifacts may subsequently lead to a misinterpretation of the exact location of preferred therapy delivery. Mis-targeting can happen during for example endocardial ablations or intramyocardial injections in the context of cardiac regenerative therapy. Furthermore, fusion of ESMs with pre-procedural acquired 3D image data from other imaging modalities (e.g. MRI, SPECT) has recently gained more interest in order to optimize catheter interventions[6-9] and described in chapter 3 and 4 of this thesis. By combining EAM with for example late enhancement MRI, it is possible to use high resolution scar data to guide real time catheter interventions. To enable the high spatial resolution, modern 3D imaging modalities of the heart are triggered both on ECG and respiration. The lack of respiratory triggering of the ESM poses a possible source of error when registering ESM with other imaging data. RICM correction of ESMs may reduce the mismatch and lead to less or smaller registration artifacts and to a more accurate use of information gathered from multiple systems to diagnose and treat. A sub-centimeter precision is often required to effectively perform therapies. However, clinical studies using 3D cardiac imaging show cardiac movement can range up to approximately a centimeter during free breathing[10-12]. It is therefore important to either take RICM into account or correct for it during the mapping procedure to guarantee the most optimal therapy.
In this study we introduce a novel technique to correct for the effect of RICM during EMM procedures in real time without the need for respiratory gating. Respiratory gating only facilitates the acquisition of EMM points at end-expiration and therefore is time consuming. We aimed to assess the effect of RICM on the ESM in a phantom and *in vivo* in two ways: 1) to measure the RICM induced artifacts in a reference point, and 2) to quantify the registration error after fusing of the ESM with an endocardial surface mesh derived from end expiratory acquired cine MRI, with and without use of RICM correction.

Methods

Respiration and NOGA®XP measurements

For the mapping procedures the NOGA®XP intramyocardial injection system (Biosense Webster, Cordis, Johnson & Johnson, USA) version 1.1.43 was used. The system provides a three dimensional (3D) magnetic tracking technology and allows for the assessment of local electrical and mechanical tissue characteristics. A customized interface was necessary to enable the measurement of the respiratory signal by the NOGA®XP system.

We developed a system to perform respiratory motion correction by connecting a piëzo respiratory belt transducer (UFI Model 1132 Pneumotrace II™) to the ECG inputs of the NOGA®XP system as shown in Figure 1. Hereby we were able to measure the respiratory signal as a baseline ECG shift in the connected channel. To control the amount of baseline shift and the impedance of both connected systems we used the interface shown in Figure 1. The 3D end-diastolic location of each acquired mapping point is stored in the local NOGA®XP database based using ECG R-wave triggering. The use of an ECG lead as an input for the respiratory signal ensures synchronicity of the stored signals and locations. The NOGA®XP system records a 12-lead ECG of 2.5s for each mapped point. Storage of the 3D location of the catheter-tip is triggered at t=2s in the stored ECG (R-wave). For the respiratory analysis, the ECG signal was fitted with a 5th order polynomial over the 1.5-2.5s interval to eliminate R-wave artifacts and signal noise. Both the amplitude and the slope of the respiratory signal at t=2s are used to determine the correction vector (value and direction) of each acquired mapping point to the end expiratory location. The data of the NOGA®XP system was accessed from an external computer.

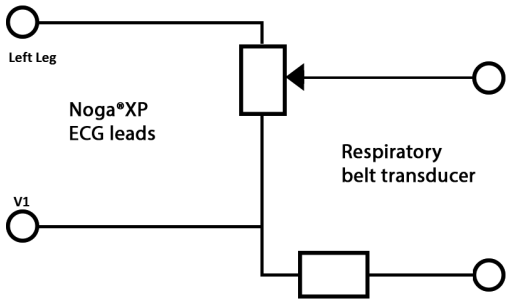

Figure 1. Circuit of system used to connect a respiratory belt transducer to the ECG leads of Noga®XP system to instigate ECG baseline drift in the V1 lead.

Phantom experiment

A non-rotational symmetric bottle was prepared to serve as a phantom and was mapped while lying still. Thereafter, the phantom was mounted on a test lung which was connected to a ventilator. The ventilator tidal volume was set to cause a 15mm motion of the phantom in primarily one direction. The mapping catheter was fixed to the phantom while ventilating the test lung to acquire a reference measurement of the motion of the phantom. Hereafter the phantom was mapped on the inside while ventilating the test lung. An ECG simulator was connected to the NOGA®XP system to enable triggered data acquisition and was set to simulate normal sinus rhythm at 80 beats/minute. The NOGA®XP ECG filter settings were optimized to allow visualization of respiratory signals in the 0.05-0.5Hz range.

Porcine experiments

All animal experiments were conducted in accordance with the national guidelines on animal care and with prior approval by the Animal Experimentation Committee of the Faculty of Medicine, Utrecht University, the Netherlands. Five female Dallas land race pigs were subjected to LAD balloon occlusion for 90 minutes and reperfusion 8 weeks before the measurements. The animals (83±6 kg) were used for the assessment of the respiratory motion correction algorithm.

A respiratory belt transducer was attached around the abdomen of the pig just below the ribs, where maximal respiratory induced movement could be measured. The transducer was connected to the NOGA®XP system as described before. The ventilator was set to a frequency of 12 breaths/minute with a tidal volume of 10 ml/kg and a 2:1 expiration to inspiration ratio. The LV was entered via the left carotid artery and retrograde passage through the aortic valves. First the RICM was measured in the apex by successively mapping at least 60 points. Secondly, in a new map, the LV was mapped according to the recommendations for EMM acquisition[4]. After the mapping procedure a MRI scan was made. The animals were euthanized after finishing the experiments.

MRI

In vivo MRI was performed under anesthesia on a clinical 3T scanner (Achieva TX, Philips Healthcare, Best, the Netherlands) with a 32-channel receive coil. ECG-gated CINE images were made with Voxel size = 1.25x125mm, Flip Angle = 45 degrees, Slice Thickness = 8mm, Matrix size = 256x256, Repetition time [TR] = 3.31ms, Echo Time [TE]= 1.65ms, and 30 Phases/R to R interval. Free breathing non-ECG-triggered images were made in short and long-axis frames to assess respiratory induced motion of the apex. Voxel size = 2.43x2.43mm, Flip Angle =30 degrees, [TR]=2.33ms, Matrix size = 128x128, [VOF]= 31x31cm. The end-diastolic CINE images are segmented using the freely available software Segment version 1.9 R3262 (http://segment.heiberg.se)[13]. The endocardial surface mesh is used for the registration with the NOGA®XP mapping points with and without RICM correction. In this way we were able to quantify the effects of RICM on the registration accuracy with a surface mesh derived from end expiratory recorded MRI data. The registration is performed using 3D CartBox and was based on a standard rotation and translation followed by an angle limited iterative closest point procedure, and manual correction if necessary as described in chapter 4 of this thesis[14].

Correction

The correction algorithm adjusts the locations of all measured points to their location during end expiration. Correction vectors are determined based on the amplitude and slope of the respiratory signal measured from respiratory induced motion of a fiducial EMM point. In the phantom experiment the catheter tip therefore is positioned at a fixed location on the surface of the phantom during ventilation of the lung, and during the *in vivo* measurements the catheter is positioned in the LV apex. The reference location is mapped at least at 60 increments throughout the respiratory cycle to assure position measurements at each instance of the respiratory cycle. Thereafter the cardiac motion pattern during the respiratory cycle is separated into an inspiratory and expiratory part. For each part a 2-dimensional second order polynomial function is fitted for each direction of the Cartesian coordinate system (3D) using a least squares approach. The six resulting functions are used to determine 3D correction vectors to correct the acquired 3D location of each point based on its position with respect to the respiratory cycle towards the point of maximum expiration.

Analysis and statistics

Corrections were performed towards the point at maximum expiration. To assess the effects of the RICM correction we calculated the root mean squared error (RMSE) of the distance from the point acquired at maximal expiration to every other point. The same

end-expiratory location is used for both the uncorrected and corrected RMSE. Maximal apical displacement represents the range of apical locations during respiration, and is measured as the distance between the point at maximal expiration and the point furthest from that during the reference measurement. Both the RMSE and the maximal apical displacement are expressed in mm. The registration error is calculated as mean distance of each mapping point to the MRI endocardial surface mesh after registration of the NOGA®XP ESM with MRI endocardial surface mesh. The registration expressed as mean ± standard deviation in millimeters. Paired T-tests were used to compare original with corrected data, $p<0.05$ was considered to be statistically significant.

Results

Respiratory Registration

The recording of the respiratory signal on a precordial ECG lead was successful. The respiratory signals of 10 EMM points registered by the baseline shift of ECG lead V1 in the phantom and *in vivo* experiment are shown in Figures 2A and 2D respectively.

Phantom experiment

The results of the phantom experiment are summarized in table 1. The motion of the phantom was 15mm in one (Z) direction and 2mm in the other (X and Y) directions (Figure 2B and 2C). The RMSE was 6.5mm before and 1.1mm after correction (Figure 4A) the effect of the correction algorithm on the motion of the reference location is shown in Figure 2C. The registration error of the ESM on the MRI mesh was 2.0±1.4mm when no simulated respiratory motion was applied to the phantom (Figure 3A). With induced motion, the registration error was 2.8±2.2m before and 1.9±1.3mm after correcting for the motion as shown in Figures 3B, 3C and 4B.

Porcine experiments

One animal was excluded from analysis due to technical failure in the acquisition of the respiratory signals. The results of the phantom experiment are summarized in table 1. On average 91±9 reference point were acquired at the apex, the left ventricular maps consisted of 80±9 points. The RICM correction algorithm was able to correct for the

Table 1. Results of the phantom and porcine experiments.

	Apex RMSE		Apex max displacement (mm)		Registration error (mm)	
	Original	Corrected	Original	Corrected	Original	Corrected
Animal#1	2.3	1.0	3.4	1.9	4.6±2.2	4.4±2.0
Animal#2	1.3	0.9	2.6	1.7	3.6±1.6	3.7±1.4
Animal#3	2.1	1.6	5.5	2.6	3.6±1.7	3.3±1.3
Animal#4	4.1	1.7	3.3	3.0	3.3±1.5	3.4±1.6

Apex RMSE quantifies the deviation of the apex position during breathing from the apex position at the end expiration. Apex max displacement quantifies the range of the range of apical locations during respiration. The registration error is the error remaining after registration on the surface mesh of the phantom and the LV cine mesh.

respiratory induced apical movement as shown in Figure 4A. The maximal apical displacement was 3.7±1.1mm before and 2.3±0.5mm after correction (P<0.05). This is a reduction of 35±17%. A representative example of acquired apical reference points is shown in Figure 2F.

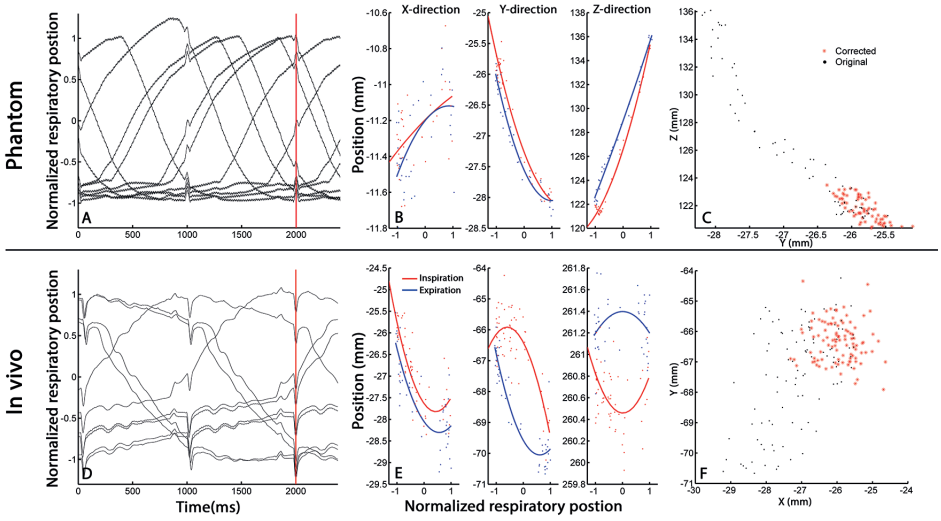

Figure 2. Example of 10 respiratory signals recorded during 10 EMM points in the phantom and *in vivo* experiments respectively (A and D). The respiratory position is determined at time point t=2000ms (red line), being the end-diastolic phase (R-wave). The recorded 3D (XYZ) data of all (n=77 and n=100) mapped reference positions of the fiducial point with the fitted 2nd order polynomial functions for inspiration (red) and expiration (blue) (B and E). Reference measurement before (black) and after correction (red) (C and F).

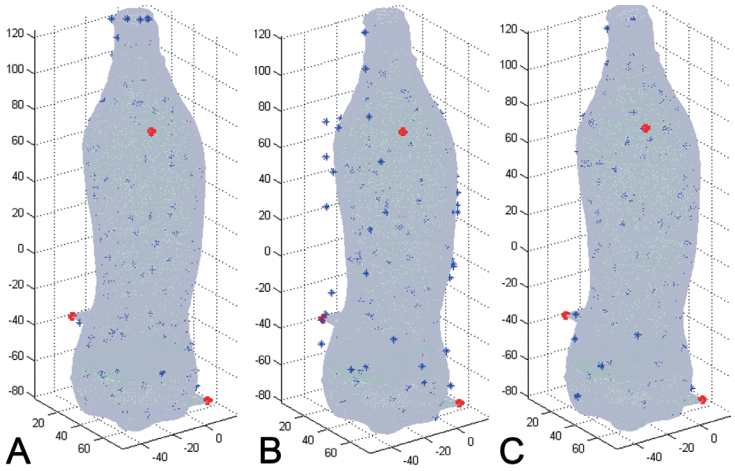

Figure 3. Shows the registration of acquired EAM points (blue) to the MRI derived surface mesh (light blue) were no motion was applied to the phantom. Landmark points (red) were fixed to the external surface of the phantom (registration error 2.0±1.4mm) (A). Shows the uncorrected registration with applied motion (registration error 2.8±2.2mm) (B). Shows the corrected registration with applied motion (registration error 1.9±1.3mm) (C).

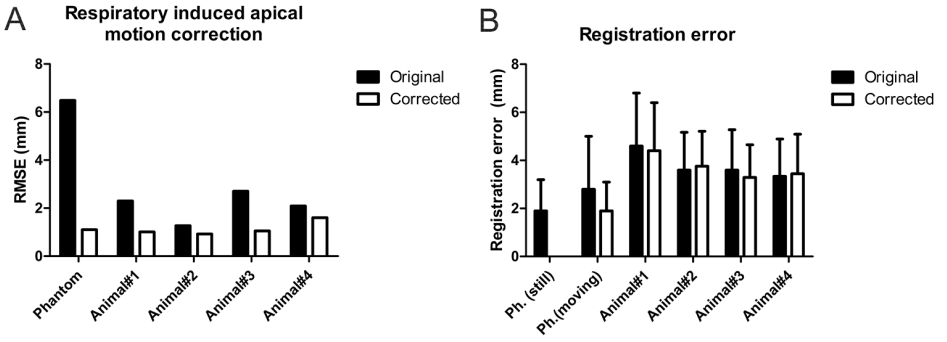

Figure 4. The RMSE error of the reference measurement before and after correction (A). The registration error of the EAM map to the MRI derived endocardial surface mesh before and after correction (B). The phantom were no motion was applied (Ph. still) was not corrected.

Discussion

Measuring respiratory induced cardiac motion with the NOGA®XP mapping system is feasible using our in-house developed customized interface. In a phantom experiment, the correction algorithm showed to be effective in reducing the registration error. In the porcine experiments respiratory induced motion of the left ventricular apex was measured and was smaller than values reported in human studies. Our correction algorithm is however capable to significantly reduce the apical displacement throughout the respiratory cycle from 3.7±1.1mm to 2.3±0.5mm (35±17%, $p<0.05$). The registration error of corrected ESM on the MRI segmentation showed minimal improvement, we believe that this due to the limited amount of RICM we observed in this porcine model. From the MRI acquisitions of the porcine experiments we found a maximal apical displacement of 3.7±1.1mm which is less than values reported in human studies[10-12]. To explore the RICM of pigs we setup a single experiment in which we increased the tidal volume. We observed a 120% increase (3.3 to 7.3mm) of RICM (maximal apical displacement) of the apex upon a 25% increase in tidal volume.

Multiple commercial systems offer the option to use respiratory gating next to ECG gating during EAM procedures. This inadvertently leads to longer procedures since mapping points are only acquired during a short phase of the respiratory cycle, usually the end-expiratory phase. Furthermore, respiratory gating in free breathing patients may be unreliable since respiratory cycles are never exactly the same. This can lead to different residual volumes and thus to different cardiac positions. Our respiratory correction algorithm allows the acquisition of mapping points during the whole respiratory cycle. By uncoupling inspiration and expiration, and take into account both the amplitude and velocity to determine the correction vector, the algorithm is able to circumvent previously mentioned difficulties. Since the algorithm depends on reference measurements, subject specific breathing characteristics, such as depth and rate of breathing, are considered in the algorithm. Additionally, using these characteristics, abnormal breaths during the mapping procedure can be identified and excluded if necessary. Correction of all the EMM points to the end-

expiratory location based on the respiratory induced motion of a single apical point assumes that respiration causes linear rigid body cardiac motion. This assumption might be too simple. When the motion is different in different parts of the heart, all parts of the heart should have a unique correction vector. To establish a comprehensive RICM correction algorithm it might be more efficient to establish a coarse RICM vector for all parts off the heart based on a non- respiratory gated cine MRI dataset, and optimize this for individual patients based on the catheter motion in the apex.

Data acquisition

Acquiring respiration data with the NOGA®XP system using one of the precordial leads that are not used during the procedure is feasible. To optimize the amount of baseline drift a voltage divider equipped with a potentiometer was implemented in the system. However, a dedicated respiratory input port is desirable in a clinical setting. We chose to use a respiratory belt to have a clear signal of the respiration. Measurement of the respiratory signal from the ECG leads via thoracic impedance alterations[15] might be more appropriate in future clinical applications.

Limitations

All experiments were performed with the pig connected to a ventilator, therefore respiration curves were predictable and similar throughout the entire procedure. RICM in the porcine model is limited, and as a result it is difficult to evaluate the effect of RICM on the registration error. An explanation for the difference between the RICM of pigs and humans might be found in the difference between thoracic anatomies. The thoracic cage of the pig is more cone shaped compared to humans, which we believe leads to reduced RICM. In retrospect, however we were able to affirm the basic principle of our correction algorithm, the used animal model might not have been the most appropriate for this study.

Conclusion

RICM correction during endocardial mapping procedures is feasible and can be incorporated in commercially available systems. In phantom experiments our correction algorithm showed good results. In the porcine experiments however, RICM was found to be limited, leading to minimal additional value of the correction algorithm. Higher RICM values are reported in patients. Clinically RICM correction will therefore most likely be of additional value to obtain an anatomical correct map or allow optimal registration on respiratory gated imaging data and guide the operator to the target location for therapy with higher accuracy.

References

1. de Groot NMS, Bootsma M, van der Velde ET, Schalij MJ. Three-dimensional catheter positioning during radiofrequency ablation in patients: first application of a real-time position management system. Journal of Cardiovascular Electrophysiology. 2000;11:1183-1192
2. Ben-Haim SA, Osadchy D, Schuster I, Gepstein L, Hayam G, Josephson ME. Nonfluoroscopic, in vivo navigation and mapping technology. Nature Medicine. 1996;2:1393-1395
3. Psaltis PJ, Worthley SG. Endoventricular Electromechanical Mapping - The Diagnostic and Therapeutic Utility of the NOGA ® XP Cardiac Navigation System. Journal of Cardiovascular Translational Research. 2009;2:48-62
4. Gyöngyösi M, Dib N. Diagnostic and prognostic value of 3D NOGA mapping in ischemic heart disease. Nature Reviews Cardiology. 2011;8:393-404
5. Wijnmaalen AP, Van Der Geest RJ, Van Huls Van Taxis CFB, Siebelink H-MJ, Kroft LJM, Bax JJ, Reiber JHC, Schalij MJ, Zeppenfeld K. Head-to-head comparison of contrast-enhanced magnetic resonance imaging and electroanatomical voltage mapping to assess post-infarct scar characteristics in patients with ventricular tachycardias: real-time image integration and reversed registration. European Heart Journal. 2010;32:104-114
6. Tao Q, Milles J, Van Huls Van Taxis C, Lamb HJ, Reiber JHC, Zeppenfeld K, Van Der Geest RJ. Toward Magnetic Resonance-Guided Electroanatomical Voltage Mapping for Catheter Ablation of Scar-Related Ventricular Tachycardia: A Comparison of Registration Methods. Journal of cardiovascular electrophysiology. 2011:1-7
7. Reddy VY, Malchano ZJ, Holmvang G, Schmidt EJ, D'Avila A, Houghtaling C, Chan RC, Ruskin JN. Integration of Cardiac Magnetic Resonance Imaging With Three-Dimensional Electroanatomic Mapping to Guide Left Ventricular Catheter Manipulation Feasibility in a Porcine Model of Healed Myocardial Infarction. Journal of the American College of Cardiology. 2004;44:12-12
8. Dickfeld T, Tian J, Ahmad G, Jimenez A, Turgeman A, Kuk R, Peters M, Saliaris A, Saba M, Shorofsky S, Jeudy J. MRI-Guided ventricular tachycardia ablation: integration of late gadolinium-enhanced 3D scar in patients with implantable cardioverter-defibrillators. Circulation. Arrhythmia and electrophysiology. 2011;4:172-184
9. Van Slochteren FJ, Van Es R, Koudstaal S, Van Der Spoel TIG, Sluijter JPG, Verbree J, Pruim RHR, Pluim JPW, Leiner T, Doevendans PA, Chamuleau SAJ. Multimodality infarct identification for optimal image guided intramyocardial cell injections. Submitted. 2014
10. Shechter G, Ozturk C, Resar JR, McVeigh ER. Respiratory motion of the heart from free breathing coronary angiograms. IEEE Trans Med Imaging. 2004;23:1046-1056
11. Jagsi R, Moran JM, Kessler ML, Marsh RB, Balter JM, Pierce LJ. Respiratory motion of the heart and positional reproducibility under active breathing control. International Journal of Radiation Oncology, Biology, Physics. 2007;68:253-258
12. Holland AE, Goldfarb JW, Edelman RR. Diaphragmatic and cardiac motion during suspended breathing: preliminary experience and implications for breath-hold MR imaging. Radiology. 1998;209:483-489
13. Heiberg E, Sjögren J, Ugander M, Carlsson M, Engblom H, Arheden H. Design and validation of Segment--freely available software for cardiovascular image analysis. BMC medical imaging. 2010;10:1-13
14. Van Slochteren FJ, Van Es R, Gyöngyösi M, Van der Spoel TIG, Koudstaal S, Leiner T, Doevendans PA, Chamuleau SAJ. Accurate infarct border zone identification by combined electromechanical mapping and MRI to improve the targeting of intramyocardial stem cell injections in a porcine model of chronic myocardial infarction. Submitted. 2014
15. Baker LE, Hill DW. The use of electrical impedance techniques for the monitoring of respiratory pattern during anaesthesia. British Journal of Anaesthesia. 1969;41:2-17

PART TWO

Advanced delivery

Frebus J. van Slochteren[1], René van Es[1], Marlene Végh[3], Theodoor Rutgers[3], Jalal Es-sbai[3], Henk Viëtor[3], Lucas Beekman[4], Pieter A. Doevendans[1,2], Steven A.J. Chamuleau[1,2]

[1] Department of Cardiology, University Medical Centre Utrecht, The Netherlands
[2] Interuniversity Cardiology Institute of the Netherlands (ICIN), Utrecht, The Netherlands
[3] Drug Discovery Factory Services, Bussum, The Netherlands
[4] Valorization office, University Medical Centre Utrecht, The Netherlands

CHAPTER **6**

Outline of the CARTcare business plan: 'Technical solutions to improve cardiac regenerative therapy'

Adopted from the original business plan of the spin-off company "CARTcare" rewarded with the BMM* valorization grant

* BioMedical Materials

Abstract

Background

With the growing numbers of cardiovascular morbidity and mortality, regenerative therapies are becoming increasingly important for the treatment of ischemic heart disease (IHD). Despite the excitement surrounding cardiac regenerative therapy, many challenges still remain. Besides selection of the appropriate cell type and appropriate timing of therapy, efficient and standardized methods to deliver the therapeutics are of great importance. We have developed a technology to standardize the injection strategy which is eligible for commercial exploitation.

Product development

We have developed (1) a treatment planning algorithm to define the optimal injection location (infarct border zone) based on infarct transmurality measured from LGE-MRI, and (2) a 3D image registration toolbox (3D CartBox) for real-time visualization of the optimal injection location during injection procedures using NOGA®XP. Combining these techniques will lead to a standardized delivery strategy and treatment. Our solution is easy to use and less operator dependent than current techniques.

Business idea and strategy

We aim at commercialization of our findings in an integrated valorization and exploitation process. Herein we investigate technical and economic opportunities, and set up a spin-off company: CArdiac Regenerative Therapy care (CARTcare). We plan to implement the valorization of the treatment planning and 3D CartBox toolbox in two phases: (1) core-lab service for treatment planning, and (2) use of the treatment planning toolbox to guide injections in real time.

Market and competition

The market for cardiac regenerative therapies is significant: Approximately 1 million myocardial infarctions (MIs) occur per year in the USA, while more than 5 million patients suffer from chronic heart failure (HF). Cardiac regenerative therapies have important potential for the treatment of IHD by improving cardiac function, quality of life and survival. The market value for cardiology and vascular regenerative therapy is estimated to reach a market value of $3.29 billion by 2019. Many clinical cardiac stem cell trials that are currently running or are being designed involve partnerships between large pharmaceutical and catheter companies. CARTcare intends to join such partnerships by being the first company offering a standardized injection technique.

Business organization

CARTcare originated from the research and development efforts for the treatment planning and 3D CartBox toolbox developed within the BMM SMARTCARE project by the department of Cardiology of the UMC Utrecht. Creating a spin-off company is a logical step to further develop and commercialize the technology platform. In addition, a spin-off company with strong academic bonds, is in a better position to establish partnerships with catheter and pharmaceutical companies for R&D collaboration and licensing. The management of CARTcare combines excellent scientific knowledge with extensive experience in business development and commercialization, which should ensure a successful development and exploitation of the treatment planning and 3D CartBox toolbox.

Introduction

The aim of the BioMedical Materials (BMM) SMARTCARE project is to develop micro tissues for cardiac regeneration. An overview of the BMM SMARTCARE consortium is presented in table 1. The objective of work package 5 of the SMARTCARE project is to test the developed micro tissues in large animal models (Figure 1). Within work package 5 we have developed a technique to integrate the gold standard measure of infarct transmurality derived from MRI and practical guidance by the NOGA®XP injection system to optimize the delivery of the micro tissues to the infarct border zone.
Here for we have developed an easy-to-use practical toolbox (3D CartBox), that allows real-time image guided intramyocardial injections based on visualization of the infarct border zone. This toolbox provides the possibility to guide injections with high accuracy to locations with a distinct infarct transmurality. The toolbox has been tested preclinical in a pig model of chronic myocardial infarction, in which we retrospectively applied the treatment planning algorithm to MRI datasets and calculated the match ratio of the target areas determined by NOGA®XP, and by our treatment planning. This study indicated that the treatment planning and 3D CartBox toolbox enables guidance of intramyocardial injections with high accuracy to locations with a distinct infarct transmurality.
The treatment planning and 3D CartBox toolbox developed within the BMM SMARTCARE project is a unique and intelligent solution for a targeted and standardized delivery strategy. This will solve current issues with the determination of, and guidance to the optimal delivery location, and will ultimately improve clinical outcome for patients.

Innovation & unique selling points

The treatment planning and 3D CartBox toolbox therefore have the following unique selling points:
Treatment planning:
- Standardized detection of infarct border zone and definition of injection locations
- Prevention of injection in potentially dangerous areas
- Less operator dependency

3D CartBox:
- Real-time visualization of the infarct border zone during injection procedures
- Improved delivery efficiency of cardiac regenerative therapy
- Improved injection accuracy
- Less operator dependency
- Shorter injection procedures

With the treatment planning and 3D CartBox toolbox we believe we can achieve an improved functional outcome of cardiac regenerative therapy at lower costs.

Market analysis

IHD is the predominant contributor to cardiovascular morbidity and mortality. Approximately 1 million myocardial infarctions (MIs) occur per year in the USA, while more than 5 million patients suffer from chronic heart failure (HF)[1]. Up to 74% of MIs lead to HF, with a 5-year-mortality of more than 60% in the affected population and average survival rate of less than 1,7 years after diagnosis. Regenerative therapies have potential for the treatment of IHD by improving cardiac function, quality of life and survival. The market for 3D CartBox focusses on regenerative therapy in these IHD patients. The total therapeutic market for

regenerative therapy will reach to over $35 billion by 2019. The cardiology and vascular market segment is estimated to reach a market value of $3.29 billion by 2019[2]. The past decade has resulted in major advancements in the clinical application of cardiac regenerative therapy[3-6]. Worldwide 475 clinical cardiac stem cell trials are being performed[7]. Although the evidence supports a significant beneficial effect of regenerative therapy[8], the technology remains immature. Lack of targeted and standardized delivery strategies have limited the interpretation of results, and makes comparison between studies and results difficult. Therefore, specialists have an urgent need for techniques that optimize regenerative therapeutic delivery strategies, and thereby improve cardiac function, and bring cardiac regenerative therapy to the next level. Thereby generating a strong 'market pull' from specialists for tools to assist in regenerative therapy and a great opportunity for value creation and commercial exploitation. No other company is currently offering a treatment planning technology platform to standardize the injection strategy. The initial market for the treatment planning and 3D CartBox toolbox, allowing real-time visualization of the border zone during injection procedures, is aimed at clinical trials involving cardiac regenerative therapy. With the positive results so far, now is the time to move from an experimental setting to the clinic, and create a commercial platform to exploit the project results outside academia. CARTcare will provide this.

Mission & vision

Mission The mission of CARTcare is to develop and commercialize products and techniques to improve cardiac regenerative therapy.

Vision In the near future the products of CARTcare will provide a targeted and standardized delivery strategy based on multimodality imaging and thereby significantly contribute to improve the quality of life for many patients.

Business strategy

Valorization of the treatment planning and 3D CartBox toolbox will take place in subsequent phases: (1) core-lab service for treatment planning, and (2) combination of the treatment planning and 3D CartBox toolbox to guide intramyocardial injection procedures in real time.

Core-lab service for treatment planning

As a first product we will set up a commercial core-lab service providing treatment planning for preclinical use to ensure a rapid market introduction. Customers can deliver their imaging

Table 1. Overview of the BMM Smartcare consortium

Prinicipal investigator P.A. Doevendans		
Work package	Aim	Work package leader
1	Define the optimal cell source to generate cardiac tissue	M.J. Goumans
2	Up scaling of CPC and MSC culture under GMP conditions	M.V. Herias
3	Development of biomaterial carrier for cellular therapy	R.P. Sijbesma
4	Define the optimal micro-mechanical environment for cells	C.V.C. Bouten
5	Micro tissue application in large animal models	S.A.J. Chamuleau
6	Development of novel infarct imaging technique using MRI	P.R. Luijten

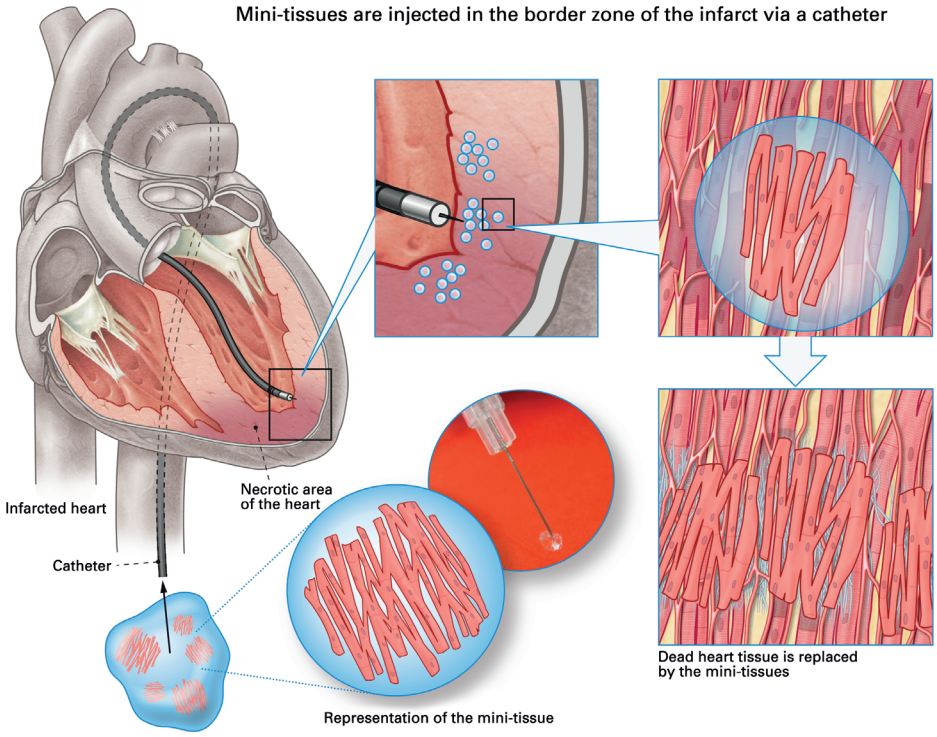

Figure 1. BMM SMARTCARE project. Lodge pieces of heart muscle tissue in a biomaterial carrier so they can be introduced with catheters to targeted sites in the heart.

data via an online service to CARTcare, and receive the injection target area conform standard visualization methods used in cardiology on a fee for service basis. This will familiarize users, cardiologists and research institutions, with a new standardized method compared to current subjective identification of the border zone for injection, and will help establish our technology in the field of cardiac regenerative therapy. In addition, these preclinical studies will provide the necessary data for further testing and validation of the treatment planning algorithm in a clinical setting. Furthermore the core-lab provides the opportunity to test the product at an early stage and accommodate immediate feedback of the consumer to improve the product.

Real-time stand-alone treatment planning and guidance of injections

Through collaboration with catheter companies we will further optimize the treatment planning and 3D CartBox toolbox. Participation in multicenter clinical trials in collaboration with pharmaceutical and catheter companies will be needed for CE registration and FDA approval of the toolbox and enable future use of the toolbox in a clinical setting. In this phase income will be generated from licensing of the toolbox to pharmaceutical and catheter companies, income generated after market entry, government secured loans, and investors. Hereafter we anticipate that CARTcare can be self-supporting.

Marketing strategy

The primary customers of the treatment planning and 3D CartBox toolbox are cardiologists and research institutions performing preclinical trials, and pharmaceutical and catheter companies participating in clinical trials in regenerative medicine. Existing collaborations, sales activities and a strong network will be used to approach these cardiologists and research institutions as potential clients. Present collaborations with catheter companies will be expanded to further develop the treatment planning and 3D CartBox toolbox for use with different catheter systems. The collaborating companies have existing distribution channels, and marketing and sales experience. This will result in a marketing strategy where the toolbox will be licensed to customers, and marketed together with the catheter system and/or therapy.

IP position

In collaboration with the Technology Transfer Office of UMC Utrecht (Utrecht Holdings) we have currently submitted a US provisional patent application entitled: Guidance of intramyocardial catheters. (EFS ID: 16716266; Application Number: 61871320) to protect our treatment planning technology (filing date 29th of August 2013).

Future developments

Since HF patients often carry an ICD or pacemaker, and these devices are not eligible for MRI, the abovementioned treatment planning algorithm cannot be used for a large population of HF patients. For this reason we are currently adapting the treatment planning tool for perfusion data obtained from SPECT/CT. Another application of the treatment planning and 3D CartBox toolbox might be the use during catheter based diagnostic biopsies in non-ischemic cardiomyopathies.

Acknowledgements

The business plan of CARTcare has been rewarded with the BMM valorization grant of €200.000,-. In addition the Netherlands Heart Institute ICIN Incentives grant of €50.000,- and the UMC Utrecht Octopus grant for stimulation of valorization of cardiovascular research of €90.000,- were obtained to enable further optimization of the treatment planning and 3D CartBox toolbox.

References

1. Go AS, Mozaffarian D, Roger VL, Benjamin EJ, Berry JD, Borden WB, Bravata DM, Dai S, Ford ES, Fox CS, Franco S, Fullerton HJ, Gillespie C, Hailpern SM, Heit JA, Howard VJ, Huffman MD, Kissela BM, Kittner SJ, Lackland DT, Lichtman JH, Lisabeth LD, Magid D, Marcus GM, Marelli A, Matchar DB, McGuire DK, Mohler ER, Moy CS, Mussolino ME, Nichol G, Paynter NP, Schreiner PJ, Sorlie PD, Stein J, Turan TN, Virani SS, Wong ND, Woo D, Turner MB. Heart disease and stroke statistics--2013 update: a report from the American Heart Association. Circulation. 2013;127:e6-e245
2. www.marketresearch.com. www.marketresearch.com. online. 2013
3. Laflamme MA, Murry CE. Heart regeneration. Nature. 2011;473:326-335
4. Selem S, Hatzistergos KE, Hare JM. Cardiac stem cells: Biology and therpeutic applications. In: Atala A, Lanza R, Thomson JA, (Eds). Principles of Regenerative Medicine. San Diego, CA: Elsevier Inc; 2011:327-346.
5. Williams AR, Trachtenberg B, Velazquez DL, McNiece I, Altman P, Rouy D, Mendizabal AM, Pattany PM, Lopera GA, Fishman J, Zambrano JP, Heldman AW, Hare JM. Intramyocardial stem cell injection in patients with ischemic cardiomyopathy: functional recovery and reverse remodeling. Circulation research. 2011;108:792-796
6. Orlic D, Kajstura J, Chimenti S, Jakoniuk I, Anderson SM, Li B, Pickel J, McKay R, Nadal-Ginard B, Bodine DM, Leri A, Anversa P. Bone marrow cells regenerate infarcted myocardium. Nature. 2001;410:701-705
7. clinicaltrials.gov. clinicaltrials.gov. online. 2013
8. Suncion VY, Schulman IH, Hare JM. Concise review: the role of clinical trials in deciphering mechanisms of action of cardiac cell-based therapy. Stem cells translational medicine. 2012;1:29-35

PART THREE

Advanced assessment of local cardiac function

Frebus J. van Slochteren[1], Tycho I.G. van der Spoel[1], Hendrik H.G. Hansen[2], Peter H.M. Bovendeerd[3], Pieter A. Doevendans[1,4], Joost P.G. Sluijter[1,4], Steven A.J. Chamuleau*[1,4], Chris L. de Korte*[2]

* Authors contributed equally to the manuscript

[1] Department of Cardiology, University Medical Centre Utrecht, the Netherlands
[2] Medical UltraSound Imaging Centre, Department of Radiology, Radboud University Nijmegen Medical Centre, Nijmegen, the Netherlands
[3] Department of Biomedical Engineering, Eindhoven University of Technology, the Netherlands
[4] Interuniversity Cardiology Institute of the Netherlands (ICIN), Utrecht, the Netherlands

CHAPTER 7

Layer specific radio frequency ultrasound based strain analysis in a porcine model of ischemic cardiomyopathy validated by a geometrical model

Published in Ultrasound in Medicine and Biology, September 2013

Abstract

Local layer specific myocardial deformation after myocardial infarction (MI) has not been studied extensively although the subendocardium is more vulnerable to ischemia, and interstitial fibrosis deposition. Radio frequency (RF) ultrasound based analysis could provide superior layer specific radial strain estimation compared to clinically available deformation imaging techniques. In this study we used RF based myocardial deformation measurements to investigate layer specific differences between healthy and damaged myocardium in a porcine model of chronic MI. RF data were acquired epicardially in healthy (n=21), and infarcted (n=5) regions of a porcine chronic MI model 12 weeks post MI. Radial and longitudinal strains were estimated in the subendocardial, midwall, and subepicardial layers of the left ventricle (LV). Collagen content was quantified in three layers of healthy and infarcted regions in five pigs. An analytical geometrical model of the LV was used to theoretically underpin the radial deformation estimated in different myocardial layers. Mean ± se values of the peak radial strain estimates of the subendocardial, midwall, and subepicardial layers of the healthy and infarcted tissue were: 82.7 ± 5.2 % vs. 39.9 ± 10.8 % (p=0.002), 63.6 ± 3.3 % vs. 38.8 ± 7.7 % (p=0.004), and 34.3 ± 3.0 % vs. 35.1 ± 5.2 % (p=0.9) respectively. The radial strain gradient between the subendocardium and the subepicardium had decreased 12 weeks after MI and histological examination showed most collagen increase in the subendocardial and midwall layers. Comparable normal peak radial strain values were found by geometrical modeling when input values were derived from the *in vivo* measurements and literature. In conclusion, the estimated strain values are realistic, and show that subendocardial radial strain in healthy tissue can amount to 80%. This high value can be explained by the cardiac geometry as was shown by geometrical modeling. After MI, the subendocardial and midwall layers show decreased strain values and increased collagen content. Layer specific peak radial strain can be assessed by RF strain estimation and shows a clear difference between healthy and infarcted tissue. Although the relation between tissue stiffness and tissue strain is not strictly local, this novel technique provides a valuable way to assess layer specific regional cardiac function in a variety of myocardial diseases.

Introduction

The use of regional deformation assessment has been proposed to accurately select heart failure patients for local therapy based on local pathological myocardial deformation. This may be the case for arrhythmogenic cardiomyopathy[1] or ischemic heart disease[2-5]. Another field of application can be the assessment of changes in the myocardium induced by cardiac regenerative therapies[6,7] aiming at local enhancement of vasculogenesis, cardiomyogenesis, or matrix enhanced myocardium stabilization. Besides providing information about the local pathological changes in the myocardium, this can help to identify dominant therapeutic mechanisms[8]. Currently used techniques to assess layer specific myocardial deformation have limited spatial and temporal resolution (MRI tagging and ultrasound speckle tracking), require alignment of the ultrasound beam with the direction of motion (tissue Doppler imaging), or use mathematical techniques and physiological assumptions[9,10]. These limitations particularly prevent reliable assessment of radial strain in a specific area[11]. RF based deformation imaging techniques might be applicable to assess local layer specific radial deformation since they are angle independent (compared to tissue Doppler imaging (TDI) methods), and higher spatial resolutions can be achieved. Classically B-mode images and speckle based deformation imaging only make use of the envelope data of the ultrasound signal. In contrast RF data is composed of the envelope, but also includes the phase information. This difference is illustrated in Figure 1. Therefore the strain can be determined with high resolution and accuracy along the ultrasound line (axial direction). Typically a 10 times better accuracy is obtained with RF-based strain estimation techniques with respect to envelope based strain estimation methods[12]. The RF-based techniques used in this study are validated using simulation data and phantom experiments[13]. The combination of a linear array probe and an ultrasound frequency of 8.7 MHz leads to an optimal field of view and a spatial resolution for the strain estimate of approximately 0.2 mm whereas the spatial resolution of speckle tracking based strain images is limited to approximately 2 mm. In contrast, the spatial resolution of the gold standard MRI tagging deformation assessment is even limited to the tagline distance which is often set to 5mm in large animal studies. In the aforementioned pathologies cardiac contractility and myocardial stiffness are altered. Consequently local tissue deformation changes accordingly and can be used to monitor subtle changes. The local extracellular matrix deposition alters tissue stiffness and deformation layer specific since the subendocardium is more vulnerable to increased wall stress, ischemia, and interstitial fibrosis. We therefore hypothesized that layer specific peak strain estimations reflect sub-clinical changes in regional LV performance. In this study we investigated the differences between healthy and damaged myocardium in a porcine model of chronic MI by RF based myocardial strain estimations.

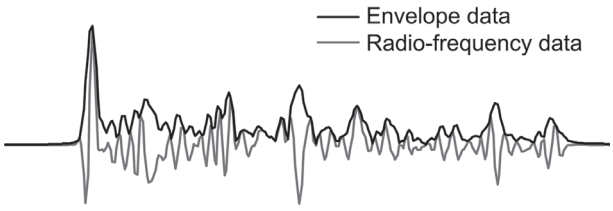

Figure 1. B-mode images are created from the envelope data (black) withdrawn from the RF data. This only represents the amplitude of the signal (reflected energy), while the phase information in the RF signal (grey) directly reflects the position of acoustic impedance transitions in the tissue.

Local radial and longitudinal peak strain and local collagen content and collagen cross linking were quantified in the subepicardial, midwall, and subendocardial layers of the healthy and infarcted myocardium using a linear array ultrasound probe. Measurements were done in three layers to account for the transmural mechanical differences in the myocardium[14]. A simplified analytical geometrical model of the LV based on a range of input values derived from the *in vivo* measurements and literature was used to theoretically underpin radial deformation in the different myocardial layers when assuming ventricular geometry and tissue incompressibility[15].

Materials and Methods

Porcine myocardial infarction model

Twenty-one female Dalland Landrace pigs (weighing 69 ± 4 kg) received care in accordance with the *Guide for the Care and Use of Laboratory Pigs* prepared by the Institute of Laboratory Animal Resources. Experiments were approved by the Animal Experimentation Committee of the Utrecht University, the Netherlands. Closed-chest MI was created in 5 pigs by a percutaneous balloon of equivalent size to the proximal left circumflex artery (LCX). Prior to MI all animals received an oral dose of amiodarone (400 mg/day; start 10 days prior to MI) and clopidogrel (75 mg/day; start 3 days prior to MI, Sanofi Aventis, Gouda, the Netherlands). A bolus of 500 mg acetylic salicylic acid (Centrafarm, Etten-Leur, the Netherlands) was given the day before the occlusion. The balloon was inflated for 75 minutes at 5-8 atm[16]. Complete occlusion of the LCX was confirmed by angiography. To prevent ventricular arrhythmias, 300 mg amiodarone (Centrafarm, Etten-Leur, the Netherlands) was given intravenously. External defibrillation (150-200 Joules) was used if ventricular fibrillation occurred. After the procedure, coronary angiography was performed to confirm vessel patency. After recovery, the animals received an oral dose of 50 mg metoprolol, 400 mg amiodarone, 75 mg clopidogrel, and 160 mg acetylic salicylic acid daily, until euthanasia to prevent thrombosis and arrhythmias.

Experimental protocol

Twelve weeks after MI, a thoracotomy was performed for epicardial measurements of ultrasound RF data in long-axis cross sections from the LV lateral and anterior wall as depicted in Figure 2. Data recorded from the LCX territory of the lateral wall are hereafter

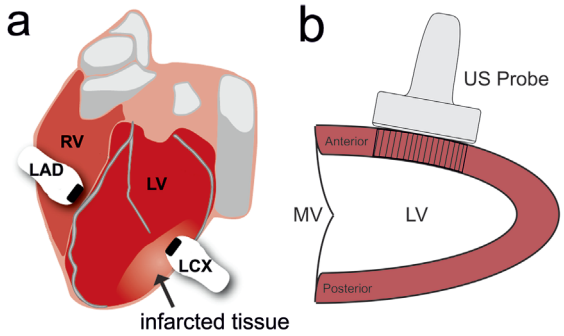

Figure 2. Measurement positions at the infarcted left ventricular lateral (LCX) and healthy anterior (LAD) wall on the left ventricle (LV) illustrated by the two probes (a). Schematic overview of the probe orientation during the LAD measurements (b). MV = Mitral valve, LV = Left ventricle.

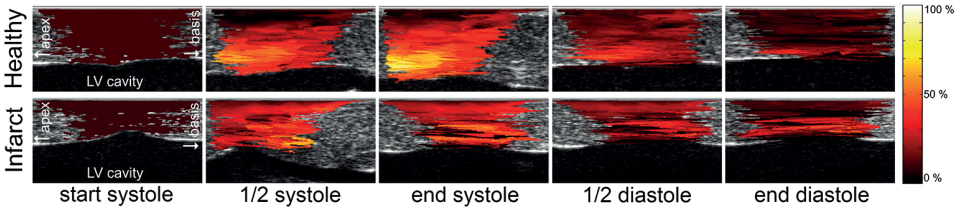

Figure 3. Epicardially acquired RF ultrasound recordings during the cardiac cycle. The left and right sides of the images respectively correspond to the apical and basal directions of the left ventricle. The dark area is the ventricular cavity. Colors indicate the regional radial strain values.

referred to as infarcted. Since the left anterior descending coronary artery (LAD) is untreated, data recorded from the anterior wall are referred to as healthy. Locations where data was recorded were marked by epicardial stitches. To avoid errors in deformation estimation caused by motion of the heart in a direction perpendicular to the ultrasound imaging plane (out of plane motion), the apex was loosely fixed by a Starfish Cardiac Positioner (Medtronic Inc., Minneapolis, MN, USA), and the ultrasound probe was manually moved with the tissue. After data acquisition, hearts were excised and tissue samples marked by the stitches were taken for collagen quantification.

Functional parameters

End diastolic and end systolic volumes, and ejection fraction (EF) were measured before the ischemia reperfusion procedure (baseline) and after twelve weeks by PV loop measurements as described before[17].

RF echocardiographic data acquisition

RF data were acquired with a Medison Accuvix V10 ultrasound scanner (Samsung Medison, South Korea) with a radiofrequency data interface in combination with a 3.8 cm wide linear array probe (L5-13) with a center frequency of 8.7 MHz. The RF data were digitized at a sampling rate of 61.6 MHz. A 2D cross correlation algorithm was used to calculate the tissue displacements in the axial and lateral directions of the ultrasound beam, in the subendocardial, midwall, and subepicardial layers as illustrated in Figure 5. These directions respectively align with the radial and longitudinal cardiac strain. This lead to the recordings depicted in Figure 3.

RF based deformation estimation

To assign reference timing at end diastole, the minimum wall thickness was determined by an M-mode measurement in the central region of the acquisition. This was done because no external ECG could be recorded by the used ultrasound scanner, and the aortic valve was not in the imaging plane during data acquisition. To estimate the tissue motion (displacement) from one ultrasound frame to the next, an iterative cross-correlation based search algorithm was used[13]. Both the motion in the direction of the ultrasound beam (radial tissue direction) as well as perpendicular to the ultrasound beam (longitudinal tissue direction) was determined. In each of five iterations RF data for a certain tissue region in one ultrasound frame were shifted over the RF data within a larger tissue region (search region) in the next ultrasound frame and the 2D cross-correlation value was calculated.

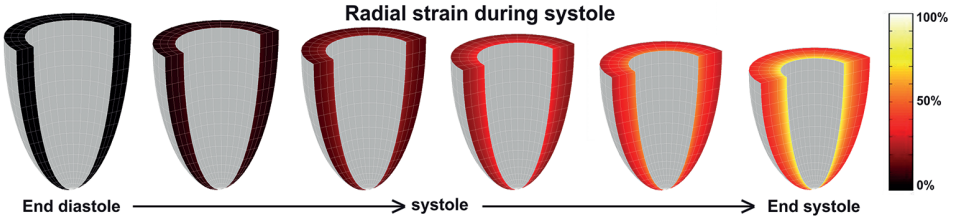

Figure 4. The geometrical model in different systolic phases. Colors indicate the distribution of the radial strain in the left ventricular wall.

The 2D shift that resulted in the highest cross-correlation value (best match) was a value for the occurred 2D motion for that part of the tissue. The accuracy of the motion estimates was increased in each iteration. In the first four iterations this was achieved by halving the window sizes of both the initial window and the search window. In the final iteration, the motion estimates were improved by sub sample aligning of the RF data of the initial window and search window[13,18]. The motion estimates of preceding iterations were used as a starting point for the search in each new iteration. In the first iteration the cross-correlations were calculated using the envelope of the RF data to get a robust initial motion estimate. After each iteration motion estimates were median filtered to remove outliers. The window size of the median filter was 9 × 9 motion estimate values. The iterative procedure resulted in motion estimates for tissue segments of 0.125 mm x 0.200 mm. To derive the radial and longitudinal strains a 2D least-squares strain estimator (LSQSE) was applied to the radial and longitudinal motion field, respectively[19,20]. The derived displacement values were also used to track all segments over the cardiac cycle[21]. Strain values were averaged by drawing equally sized regions of interest in three myocardial layers: subendocardial, midwall, and subepicardial.

Analytical strain

Analytical modeling was done to explain radial strain values that were estimated in the different myocardial layers. For the analytical modeling we assumed that myocardial tissue is composed of incompressible spongy solid material filled with incompressible intracoronary blood as defined by Huyghe[15]. Based on the conservation of volume, tissue deformations in the three orthogonal directions of the cardiac coordinate system are directly related. The dimensions of the truncated ellipsoidal geometrical model were based on the mean baseline (healthy) dimensions of 5 animals used during the experiments. Longitudinal model

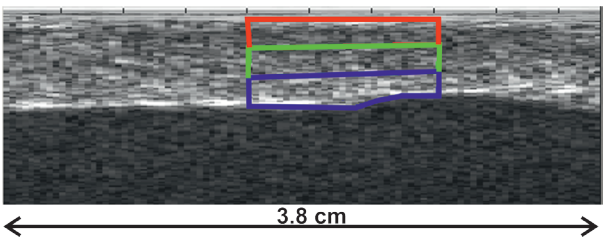

Figure 5. B-mode ultrasound image of infarcted tissue used for RF data analysis. Regions where deformation is assessed, and collagen content and density are quantified are depicted by the colored edges: subendocardium (blue), midwall (green), subepicardium (red).

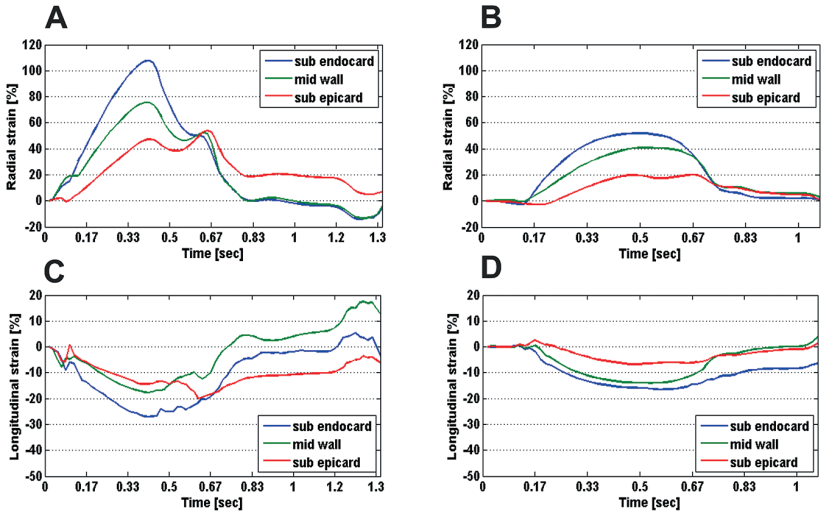

Figure 6. Radial (A, B) and longitudinal (C, D) strain curves of healthy (A and C) and infarcted (B and D) tissue.

deformation was uniformly imposed to the model according to the peak values measured *in vivo* ranging from -16% to -26%. Epicardial circumferential strain was varied between 0 and -10%[22]. Output parameters of the geometrical model are the layer specific radial and circumferential peak strains. These parameters are irrespective of the complex underlying cardiac fiber orientation, and activation sequence. An overview of the model parameters is presented in more detail in Table 2. In Figure 4 different systolic phases of the geometrical model are illustrated. The mathematics of the geometrical model is discussed in more detail in the supplementary section.

Histology

After euthanasia, tissue samples of the exact areas that were used for RF data acquisition were taken from the infarcted and remote regions of the heart (n=5). Samples were fixed in 4% formalin, and embedded in paraffin. Sections of 5 micrometer were cut, and collagen content was quantified by picrosirius red staining with circularly polarized light and digital image microscopy as described before[23]. Multiple images of the infarcted and healthy tissue were obtained at 1.25x magnification, and merged together to reconstruct the exact tissue area that was used for RF data acquisition (Figure 5). After conversion into grey value images the image intensity was quantified in the subendocardial, midwall, and subepicardial layers by CellP software version 2.8 build 1235. Collagen content was used as a measure of the distribution of the collagen throughout the myocardium, and was indicated as a fraction of the total area of each layer containing collagen. Collagen density reflects the amount of cross linking between the collagen fibers, and was calculated in each myocardial layer by the formula:

$$Collagen\ density = \frac{area\ fraction \cdot mean\ intensity}{area\ of\ total\ tissue\ section}\left[\text{mean gray value}/_{\text{mm}^2}\right].^{23}$$

To restrict the analysis to replacement fibrosis, collagen in the adventitial and medial layers of blood vessels, gaps in the tissue, and the intraluminal areas of blood vessels were excluded from the analysis.

Statistics

Data are presented as mean ± se. A paired student t-test was used to compare baseline and follow up measurements, and an independent student t-test was used to compare parameters measured from healthy and infarcted tissue for each layer. P values < 0.05 were considered significant.

Results

Myocardial infarction reduced the EF of the pigs from 68.6 ± 3.6 % at baseline to 54.0 ± 3.5 % (p=0.03) after twelve weeks. End systolic volume increased from 29.7 ± 4.8 ml at baseline to 41.1 ± 3.8 ml (p=0.2) after 12 weeks, and end diastolic volume did not change 88.3 ± 12.0 ml vs. 90.7 ± 8.6 ml (p=0.9). Mean heart rate during measurements was 51 ± 7 beats per minute.

RF based strain estimation

Typical strain curves measured from healthy and infarcted tissue are shown in Figure 6. Both in healthy and infarcted tissue a difference exists between the subendocardial, midwall, and subepicardial strain. The mean values of the radial and longitudinal strain of

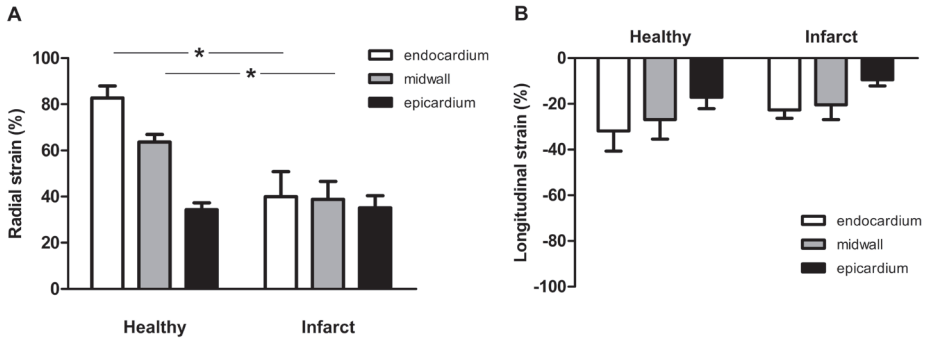

Figure 7. Peak radial (A) and longitudinal (B) strain values. Data is presented as mean ± se. * p < 0.05.

Table 1. Radial and longitudinal strain in subendocardial, midwall, and subepicardial layers and the difference between the subendocardial and subepicardial layers.

	Peak radial strain			Peak longitudinal strain		
	Infarct (n=5)	Healthy (n=21)	p	Infarct (n=5)	Healthy (n=21)	p
Subendocard	39.9 ± 10.8%	82.7 ± 5.2%	0.002	-22.7 ± 3.5%	-31.9 ± 3.8%	0.27
Midwall	38.8 ± 7.7%	63.6 ± 3.3%	0.004	-20.4 ± 6.4%	-26.9 ± 3.7%	0.44
Subepicard	35.1 ± 5.2%	34.3 ± 3%	0.9	-9.5 ± 2.6%	-17.1 ± 2.1%	0.12
Difference	4.8 ± 11.8%	48.4 ± 4.8%	0.001	13.2 ± 4.4%	14.8 ± 2.9%	0.8

the complete wall in healthy tissue respectively are 54.8 ± 2.7% and -33.6 ± 2.7 %. Mean RF based peak strain values of 21 healthy, and 5 infarcted areas are shown in Figure 7 and Table 1. Mean peak radial strain values of the healthy subendocardial, midwall, and subepicardial layers of all pigs respectively are: 82.7 ± 5.2 %, 63.6 ± 3.3 %, and 34.3 ± 3.0 %. The transmural difference between the subendocardium and the subepicardium is 48.4 ± 4.8 %. In the infarcted wall the mean peak radial strain values are: 39.9 ± 10.8 %, 38.8 ± 7.7 %, and 35.1 ± 5.2 % respectively. The difference between the subendocardium and the subepicardium is 4.8 ± 11.8 %. The mean peak radial strain values in the subendocardial and mid wall regions are lower, and the difference between the subendocardium and the subepicardium is decreased 12 weeks after MI. Mean peak longitudinal strain values of the healthy subendocardial, midwall, and subepicardial layers are: -31.9 ± 3.8 %, -26.9 ± 3.7 %, and -17.1 ± 2.1 % respectively, with a transmural difference of -14.8 ± 2.9%. Smaller strain values and a smaller transmural difference were observed in comparison to the peak radial strain values. In infarcted regions the mean peak longitudinal strain values respectively are: -22.7 ± 3.5 %, -20.4 ± 6.4 %, and -9.5 ± 2.6 % with a transmural difference of -13.2 ± 4.4%. Both the mean peak longitudinal strain values and the transmural difference are diminished 12 weeks after MI.

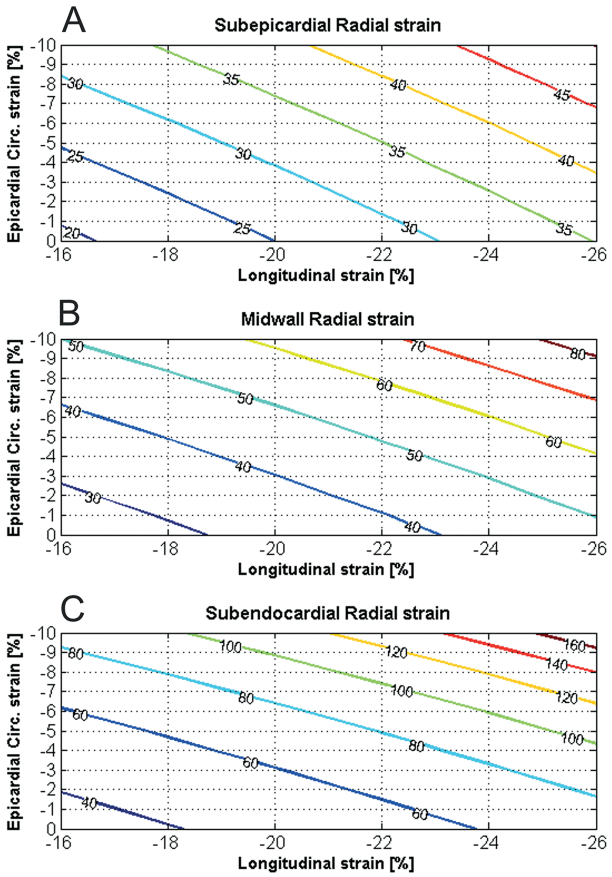

Figure 8. Simulated peak radial strain values resulting from different combinations of longitudinal strain and epicardial circumferential strain in the subepicardial (A), midwall (B), and subepicardial (C) layers.

Analytical Solution

The relations between the input values: peak longitudinal, and epicardial peak circumferential strain, and the layer specific output parameters: peak radial strain, and peak circumferential strain are shown in Figure 8 and 9 respectively. From Figure 8 it can be observed that the simulated peak radial strain values in the subendocardial, midwall, and subepicardial layers are similar to the estimated healthy peak radial strain values. More specifically, with a longitudinal peak strain of -22% (horizontal axis Figure 8C), and an epicardial circumferential strain of -5% (vertical axis Figure 8C), the subendocardial radial strain in healthy tissue theoretically can amount to approximately 80%. In Figure 8A a longitudinal strain of -22%, and an epicardial circumferential strain of -5% lead to a sub-epicardial peak radial strain of approximately 35%. Theoretically the abovementioned strain values lead to a transmural difference between the subendocardium and the subepicardium of 45%. However not estimated *in vivo*, the relation between the input values: peak longitudinal, and peak epicardial circumferential strain, and the resulting layer specific peak circumferential strain is shown Figure 9 to completely describe the model.

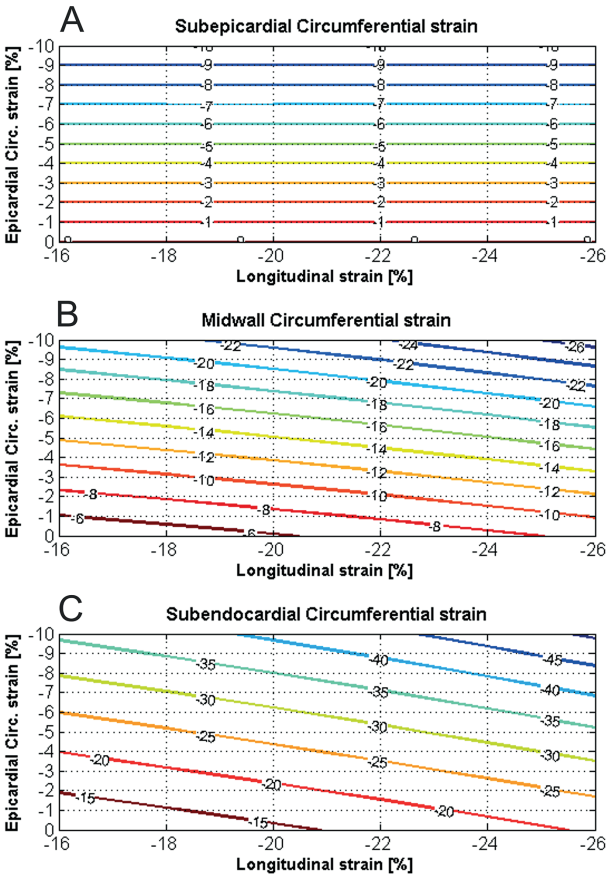

Figure 9. Simulated circumferential radial strain values resulting from different combinations of longitudinal strain and epicardial circumferential strain in the subepicardial (A), midwall (B), and subepicardial (C) layers.

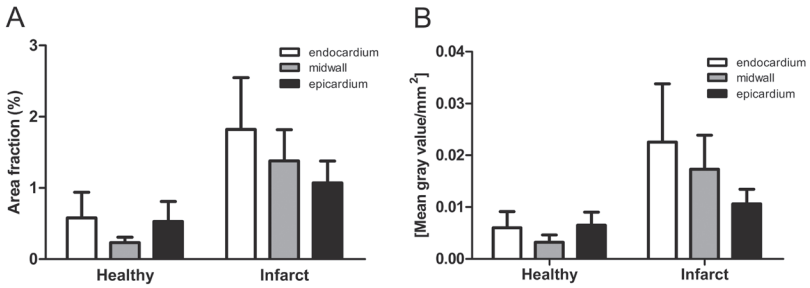

Figure 10. Collagen area fraction (A) and collagen density (B) of the healthy and infarcted myocardial layers.

Table 2. Parameters of the geometrical model. Static input parameters are fixed in all simulations. Dynamic input parameters are chosen within a clinically relevant range.

Static input parameters (measured)	Symbol	Value
End diastolic inner diameter	D_{edi}	4.5 cm
End diastolic outer diameter	D_{edo}	6.5 cm
End diastolic length	l_{ed}	7.5 cm
Dynamic input parameters (measured & literature)		
Longitudinal peak strain	ε_{long}	-16 % to -26 %
Epicardial circumferential peak strain	ε_{circ_epi}	0 to -10 %
Output parameters		
Layer specific radial peak strain	ε_{rad}	Figure 8
Layer specific circumferential peak strain	ε_{circ}	Figure 9

Histology

No significant differences were found between healthy and infarcted tissue in terms of collagen content in the subendocardial, midwall, and subepicardial layers. In the healthy subendocardial, midwall, and subepicardial layers collagen content was: 0.60 ± 0.36 %, 0.23 ± 0.08 %, and 0.53 ± 0.28 %, whereas in the subendocardial, midwall, and subepicardial layers of the infarcted myocardium collagen content was: 1.82 ± 0.73 %, 1.40 ± 0.44 %, and 1.0 ± 0.3. Moreover in healthy tissue collagen densities [mean gray value/mm^2] were (6.0 ± 6.0)·10^{-3} , (3.0 ± 2.8)·10^{-3}, (6.5 ± 5.0)·10^{-3}, in subendocardial, midwall, and subepicardial layers respectively, and in infarcted tissue (22.5 ± 22.5)·10^{-3}, (17.3 ± 13.1)·10^{-3} and (10.6 ± 5.6)·10^{-3}. These values are depicted in Figure 10 A and B respectively. The most increase of collagen content and collagen density was found in the subendocardial and midwall layers of the infarcted tissue.

Discussion

In this study, both RF measurements and geometric modeling showed that a transmural difference exists in the radial and longitudinal strain of healthy tissue. The average values are consistent with previously reported values using clinically available techniques[24].

Secondly, the transmural difference is diminished after MI. Thirdly, it was shown for the first time by RF based strain estimation that radial strain in the subendocardium can amount to 80%. The peak radial strain values in the three transmural layers that were estimated *in vivo* with this analysis were in the same order of magnitude as the peak strain values obtained from geometrical modeling.

Healthy tissue

The measured transmural difference in peak radial and longitudinal strain values was most pronounced between the subepicardial and the subendocardial layers of healthy tissue. This difference is caused by cardiac physiology and cardiac specific deformation as demonstrated by the geometrical modeling. Diffusion tensor imaging[14], and electrocardiography-based shear wave imaging[25,26] studies showed that the myofibers in the myocardial wall are predominantly oriented longitudinally in the subendocardium, and subepicardium, and predominantly circumferential in the midwall region. Radial strain therefore results from shortening of the longitudinally and circumferentially oriented myofibers and tissue incompressibility in, and in the vicinity of the measured regions. As a consequence the estimated peak longitudinal strain values are lower compared to the peak radial strain values.

Infarcted tissue

In the infarcted tissue both the strain values, and the transmural difference in peak radial and longitudinal strain values were much lower since the contractile function of the myocytes in this tissue is worse. During MI tissue perfusion is most severely impaired in the subendocardium and midwall layers, leading to cell death, and most pronounced collagen deposition and cross linking in these layers as shown in Figure 10 A and B respectively. In the present study non transmural infarcts, and multiple infarct patches were created by the use of the myocardial ischemia-reperfusion technique in contrast to the permanent ligation technique[27]. This allows a distinction between the responses of different myocardial layers to MI in terms of collagen deposition, cross linking, and deformation. It is known that extracellular matrix deposition enhances tissue stiffening and impairs deformation, and consequently reduces radial strain[28]. Although it is tempting to suggest a causal relation between local collagen content and local deformation, the relation between tissue stiffening and deformation cannot be strictly local: stiffening of either the subendocardial, midwall or subepicardial layers will affect strain in all layers, due to mechanical tethering of these layers. We found that subendocardial peak radial strain was highest in healthy tissue, and affected strongest upon infarction in terms of collagen deposition and deformation. But since tissue is a continuous material, and strain inevitably decreases from the endocardium to the epicardium, subendocardial strain is affected by collagen deposition in all myocardial layers. Suggesting a layer specific relation between collagen deposition and deformation is therefore not correct. The final radial and longitudinal strain in all three transmural layers results from the combination of local stiffness and tethering to adjacent tissue. This basic concept of tissue deformation must always be kept in mind when interpreting deformation imaging.

High subendocardial peak radial strain

The extraordinary spatial resolution of approximately 0.2mm of the RF technique uniquely revealed that radial strain can be as high as 80% in the subendocardial layer whilst the

average radial strain of all layers corresponded to values found in literature (50 - 55%)[24]. In the study by Yingchoncharoen et al. clinically available speckle tracking techniques are used, that are less accurate in estimating layer specific radial strain[11]. To the best of our knowledge these high values have not been measured before using RF based techniques. Validation by geometrical modeling revealed that the 80% peak radial strain value can be explained by the thick walled truncated ellipsoidal geometry of the ventricle. Both the range of the peak strain values that were used as an input of the model, as the range of the peak strain values resulting from the model corresponded to values found in literature[24,29]. The choice to use only the longitudinal peak strain and the epicardial peak circumferential strain as input parameters of the model was done to simplify the parameterization procedure of the model, and thereby keep the model as straightforward as possible. Consequently, the use of a clinically relevant range of input values in the simulation, resulted in a clinically relevant range of output values as shown in Figure 8 and 9. It is most likely that the midwall radial, and circumferential strain values were underestimated due to the lacking active circumferentially oriented active shortening in the midwall layer. However, the message that the transmural radial strain gradient (i.e. 80.5 % to 34.9 %) inevitably results from the geometry and the incompressibility of the cardiac muscle can be derived from this model. The assumption of 100% tissue incompressibility is a slight over simplification since this neglects the squeezing of blood from the tissue during systole[30].

Limitations

The purpose of this study was to investigate the use of RF ultrasound based deformation estimation to assess differences between normal and infarcted myocardium. There were some limitations to the methods used. The 3.8 cm wide linear array ultrasound probe used during this study requires epicardial imaging and prevented RF data acquisition from the circumferential direction of the heart due to an insufficient contact plane between the probe and the contracting heart in the circumferential direction and consequently air entrapment underneath the probe. We could not overcome this problem by applying ultrasound gel. It therefore was not possible to obtain tissue deformation in all three directions of the cardiac coordinate system. Positioning of the ultrasound probe on the epicardium might have influenced the measurements. The resulting peak strain values were however normal and very consistent. Most likely the Starfish Cardiac Positioner prevented apical motion while not constraining cardiac deformation. Reference timing based on the minimal wall thickness of the M-mode images might have affected the resulting peak strain value. However since this is done in a standardized way, we believe that this effect was small. The longitudinal strain curves contained the most irregularities and drift, as can be observed in Figure 6. The irregularities most likely were caused by the lack of phase information available for tissue tracking in this direction. The drift was primarily caused by the fast tissue motion during the early filling phase. The radial peak strain values used in this study were unaffected by this. Besides local contractility, peak strain values can also be influenced by confounding factors like preload, afterload, and tethering by adjacent tissue. Although we did not measure these factors, we believe that they have not influenced the results severely since measured strain profiles were very consistent. The geometrical model did not include active circumferential shortening, and can therefore not be used to predict local tethering effects induced by layer specific myocardial stiffness alterations. For this purpose a finite element modeling technique is available[31]. To omit unnecessary complicated modeling the finite element technique was not used in this study.

RF ultrasound in the future

Although the described method cannot be applied clinically, the present pre-clinical study has shown that contrary to speckle tracking techniques[11], RF ultrasound based strain analysis can accurately detect radial and longitudinal strain in subendocardial, midwall, and subepicardial layers. Besides present applications in pre-clinical research, this technique can become applicable in clinical applications when incorporated in a transthoracic probe[32,33]. In addition to the detection of regional layer specific subtle changes of cardiac mechanics in patients treated with e.g. cardiac regenerative therapy, this assessment is also of interest to detect viable myocardium in patients with stable angina pectoris or ischemic cardiomyopathy, or to diagnose other cardiomyopathies. As an extension of this technique angular compounding ultrasound can be used[34]. This approach makes use of the possibility of deriving motion in any desired direction in a 2D plane, by combining the motion estimates from acquisitions in which the ultrasound beam is transmitted at multiple angles. Since motion is estimated more accurately in the beam direction, the lateral motion and consequently the longitudinal deformation estimated by angular compounding is more accurate[35].

Conclusion

Layer specific radial and longitudinal strain can be accurately assessed by RF strain estimation. Thereby this technique uniquely enables accurate assessment of layer specific radial deformation in a myocardial region. In healthy tissue our data showed a transmural gradient of radial strain from 82.7% in the subendocardium to 34.3% in the subepicardium, and a clear difference between healthy and infarcted tissue. Healthy peak radial strain values were confirmed by geometrical modeling. This novel technique offers a valuable way to assess layer specific regional cardiac function in a variety of myocardial diseases.

Supplementary Data

Supplementary data contains the theoretical explanation of the analytical model, and the RF cross correlation algorithm used for the strain estimation.

Acknowledgements

We gratefully acknowledge Cees Verlaan, Merel Schurink, Marlijn Jansen, Maringa Emons, Joyce Visser, Sanne Jansen of Lorkeers and René van Es for excellent technical assistance and animal care.This work was supported by the Netherlands Heart Foundation '[2003B07304 and 2010T025]', BSIK program "Dutch Program for Tissue Engineering", '[grant 6746]', and a Bekalis price (PD). This research is part of the Project P1.04 SMARTCARE of the research program of the BioMedical Materials institute, co-funded by the Dutch Ministry of Economic Affairs and the Nederlandse Hartstichting.

References

1. Astrom Aneq M, Engvall J, Brudin L, Nylander E. Evaluation of right and left ventricular function using speckle tracking echocardiography in patients with arrhythmogenic right ventricular cardiomyopathy and their first degree relatives. Cardiovascular ultrasound. 2012;10:37-37
2. Adamu U, Schmitz F, Becker M, Kelm M, Hoffmann R. Advanced speckle tracking echocardiography allowing a three-myocardial layer-specific analysis of deformation parameters. European Journal of Echocardiography. 2009;10:303-308
3. Becker M, Ocklenburg C, Altiok E, Füting A, Balzer J, Krombach G, Lysyansky M, Kühl H, Krings R, Kelm M, Hoffmann R. Impact of infarct transmurality on layer-specific impairment of myocardial function: a myocardial deformation imaging study. European heart journal. 2009;30:1467-1476
4. Leitman M, Lysiansky M, Lysyansky P, Friedman Z, Tyomkin V, Fuchs T, Adam D, Krakover R, Vered Z. Circumferential and longitudinal strain in 3 myocardial layers in normal subjects and in patients with regional left ventricular dysfunction. Journal of the American Society of Echocardiography. 2010;23:64-70
5. Sarvari SI, Haugaa KH, Zahid W, Bendz B, Aakhus S, Aaberge L, Edvardsen T. Layer-Specific Quantification of Myocardial Deformation by Strain Echocardiography May Reveal Significant CAD in Patients With Non-ST Elevation Acute Coronary Syndrome. Journal of the American College of Cardiology: Cardiovascular imaging. 2013;6:535-544
6. Tendera M, Wojakowski W. How to measure the effects of the intracoronary stem cell therapy? European Journal of Echocardiography. 2010;11:438-439
7. Traverse JH, Henry TD, Moye LA. Is the measurement of left ventricular ejection fraction the proper end point for cell therapy trials? An analysis of the effect of bone marrow mononuclear stem cell administration on left ventricular ejection fraction after ST-segment elevation myocardia. American heart journal. 2011;162:671-677
8. van Slochteren FJ, Teske AJ, van der Spoel TIG, Koudstaal S, Doevendans PA, Sluijter JPG, Cramer MJM, Chamuleau SAJ. Advanced measurement techniques of regional myocardial function to assess the effects of cardiac regenerative therapy in different models of ischaemic cardiomyopathy. European Journal of Cardiovascular Imaging. 2012;13:10
9. Bogaert J, Rademakers FE. Regional nonuniformity of normal adult human left ventricle Regional nonuniformity of normal adult human left ventricle. American Journal Of Physiology Heart and Circulation Physiology. 2001;280:610-620
10. Hashimoto I, Li X, Bhat AH, Jones M, Zetts AD, Sahn DJ. Myocardial Strain Rate Is a Superior Method for Evaluation of Left Ventricular Subendocardial Function Compared With Tissue Doppler Imaging. Journal of the American College of Cardiology. 2003;42:16-20
11. Koopman LP, Slorach C, Hui W, Manlhiot C, McCrindle BW, Friedberg MK, Jaeggi ET, Mertens L. Comparison between different speckle tracking and color tissue Doppler techniques to measure global and regional myocardial deformation in children. Journal of the American Society of Echocardiography. 2010;23:919-928
12. Varghese T, Ophir J. Characterization of elastographic noise using the envelope of echo signals. Ultrasound in medicine & biology. 1998;24:543-555
13. Lopata RGP, Nillesen MM, Hansen HHG, Gerrits IH, Thijssen JM, de Korte CL. Performance evaluation of methods for two-dimensional displacement and strain estimation using ultrasound radio frequency data. Ultrasound in medicine & biology. 2009;35:796-812
14. Geerts L, Bovendeerd P, Nicolay K, Arts T. Characterization of the normal cardiac myofiber field in goat measured with MR-diffusion tensor imaging. American journal of physiology. Heart and circulatory physiology. 2002;283:H139-145
15. Huyghe JM, Arts T, Campen DHV, Reneman RS. Porous medium finite element model of the beating left ventricle Porous medium finite element model of the beating left ventricle. American Journal Of Physiology Heart and Circulation Physiology. 1992;262:1256-1267

16. van der Spoel TIG, Vrijsen KR, Koudstaal S, Sluijter JPG, Nijsen JFW, de Jong HW, Hoefer IE, Cramer MJM, Doevendans PA, van Belle E, Chamuleau SAJ. Transendocardial cell injection is not superior to intracoronary infusion in a porcine model of ischemic cardiomyopathy: A study on delivery efficiency. Journal of cellular and molecular medicine. 2012:2768-2776
17. Timmers L, Henriques JPS, de Kleijn DPV, Devries JH, Kemperman H, Steendijk P, Verlaan CWJ, Kerver M, Piek JJ, Doevendans PA, Pasterkamp G, Hoefer IE. Exenatide reduces infarct size and improves cardiac function in a porcine model of ischemia and reperfusion injury. Journal of the American College of Cardiology. 2009;53:501-510
18. Alam SK, Ophir J. Reduction of signal decorrelation from mechanical compression of tissues by temporal stretching: applications to elastography. Ultrasound in medicine & biology. 1997;23:95-105
19. Kallel F, Ophir J. A least squares strain estimator for elastograpy. Ultrasonic Imaging. 1997;19:195-208
20. Lopata RGP, Hansen HHG, Nillesen MM, Thijssen JM, de Korte CL. Comparison of One-Dimensional and Two-Dimensional Least-Squares Strain Estimators for Phased Array Displacement Data. Ultrasonic Imaging. 2009;16:1-16
21. Lopata RGP, Nillesen MM, Gerrits IH, Hansen HHG, Kapusta L, Thijssen JM, Korte CLD. 3D Cardiac Strain Imaging using a Novel Tracking Method. Abstract European Congress of the International Federation for Medical and Biological Engineering. 2008:697-700
22. Emilsson K, Brudin L, Wandt B. The mode of left ventricular pumping: is there an outer contour change in addition to the atrioventricular plane displacement? Clinical physiology. 2001;21:437-446
23. Sluijter JPG, Smeets MB, Velema E, Pasterkamp G, de Kleijn DPV. Increase in Collagen Turnover But Not in Collagen Fiber Content Is Associated with Flow-Induced Arterial Remodeling. Journal of Vascular Research. 2004;41:546-555
24. Yingchoncharoen T, Agarwal S, PopovićZB, Marwick TH. Normal ranges of left ventricular strain: a meta-analysis. Journal of the American Society of Echocardiography. 2013;26:185-191
25. Lee W, Larrat B, Pernot M, Tanter M. Ultrasound elastic tensor imaging: comparison with MR diffusion tensor imaging in the myocardium. Physics in Medicine and Biology. 2012;57:20
26. Lee W, Pernot M, Couade M, Messas E, Bruneval P, Bel A, Hagege A, Fink M, Tanter M. Abstract Mapping myocardial fiber orientation using echocardiography-based shear wave imaging. IEEE Translations Medical Imaging. 2012;31:8
27. Holmes JW, Nunez JA, Covell JW. Functional implications of myocardial scar structure. American Journal Of Physiology Heart and Crculation Physiology. 1997;41:2123-2130
28. Holmes JW, Borg TK, Covell JW. Structure and Mechanics of Healing Myocardial Infarcts. Annual Reviews of Biomedical Engineering. 2005;7:223-253
29. Rosner A, Bijnens B, Hansen M, How OJ, Aarsæther E, Sutherland GR, Myrmel T. Left ventricular size determines tissue Doppler-derived longitudinal strain and strain rate. European Journal of Echocardiography. 2009;10:271-277
30. Spaan JA. Coronary diastolic pressure-flow relation and zero flow pressure explained on the basis of intramyocardial compliance. Circulation Research. 1985;56:293-309
31. Bovendeerd PHM, Arts T, Delhaas T, Huyghe JM, Campen DHVAN, Reneman RS. Regional numerical wall mechanics in the ischemic left ventricle: modeling and dog experiments. American Journal Of Physiology Heart and Crculation Physiology. 1996;270:398 410-398 410
32. Lopata RGP, Nillesen MM, Thijssen JM, Kapusta L, de Korte CL. Three-dimensional cardiac strain imaging in healthy children using RF-data. Ultrasound in Medicine & Biology. 2011;37:1399-1408
33. Lopata RGP, Nillesen MM, Verrijp CN, Singh SK, Lammens MMY, van der Laak JAWM, van Wetten HB, Thijssen JM, Kapusta L, de Korte CL. Cardiac biplane strain imaging: initial in vivo experience. Physics in Medicine and Biology. 2010;55:963-979
34. Hansen HHG, Lopata RGP, de Korte CL. Noninvasive carotid strain imaging using angular compounding at large beam steered angles: validation in vessel phantoms. IEEE transactions on medical imaging. 2009;28:872-880
35. Hansen HHG, Lopata RGP, Idzenga T, de Korte CL. Full 2D displacement vector and strain tensor estimation for superficial tissue using beam-steered ultrasound imaging. Physics in Medicine and Biology. 2010;55:3201-3218

Supplementary data

The Geometrical model

A geometrical LV shape with dimensions similar to the average values measured from five animals used during the experiments was constructed from two truncated ellipsoids (Supplementary Figure 1). Volumes of the truncated ellipsoidal shapes are calculated by means of

$$V = \frac{2}{3} \cdot \pi \cdot \left({}^{D}/_{2}\right)^{2} \cdot l \qquad \text{[A1]}$$

The initial end diastolic, and end systolic lengths l_{ed} and l_{es}, and end diastolic inner and outer diameters D_{edi}, D_{edo} are set to appropriate values (Table 2). Hereafter the enclosed volume (myocardial tissue) can be calculated. When this is held constant during longitudinal shortening (ε_l) induced (length) changes, diameter changes at different transmural locations can be calculated by setting D to different transmural values (D_{esi}, D_{eso} in Supplementary Figure 1). The assumption of tissue incompressibility allows the longitudinal (λ_l) and circumferential (λ_c) stretch ratios to be calculated by

$$\lambda_l = \frac{l_{es}}{l_{ed}} \qquad \text{[A2]}$$

and

$$\lambda_c = \frac{D_{end\ systole}}{D_{end\ diastole}} = \left(\frac{V_{end\ diastole} \cdot l_{end\ systole}}{V_{end\ systole} \cdot l_{end\ diastole}}\right)^{-1/2} \qquad \text{[A3]}$$

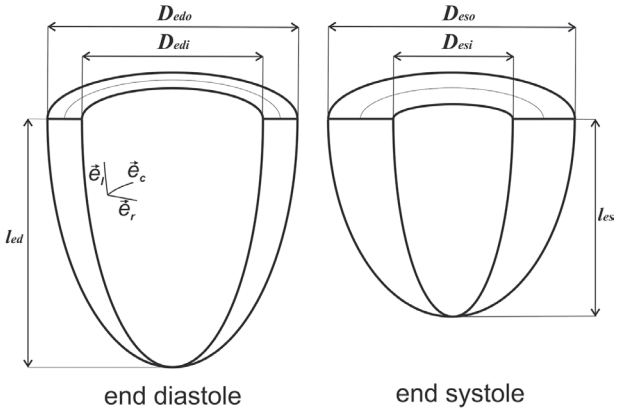

Supplementary figure 1.
Geometrical model with the essential parameters for the analytical determination of layer specific radial strain values. Values for D_{edi}, D_{edo}, l_{ed}, l_{es} (εl) are derived from the experiments, values for D_{esi}, D_{eso} follow from the simulations.

For the epicardial border an additional circumferential shortening $\lambda_{c,epi}$ is applied as is suggested by Emilsson[22]. Now the fixed relation between the stretch ratios results in the radial (λ_r) stretch ratio via

$$\lambda_r = \frac{1}{\lambda_l \cdot \lambda_c}. \qquad \text{[A4]}$$

Finally linear radial strain is expressed in percentages by the parameter ε calculated from

$$\varepsilon = (\lambda - 1) \cdot 100\%. \qquad \text{[A5]}$$

The values for D_{edi}, D_{edo}, l_{ed}, ε_l are derived from the experiments and are listed in Table 2.

PART THREE

Advanced assessment of local cardiac function

Frebus J. van Slochteren[1], Hendrik H.G. Hansen[2], Maartje M. Nillesen[2], Peter H.M. Bovendeerd[3], Pieter A. Doevendans[1,4], Steven A.J. Chamuleau*[1,4], Chris L. de Korte*[2]

* Authors contributed equally to the manuscript

[1] Department of Cardiology, University Medical Centre Utrecht, the Netherlands
[2] Medical UltraSound Imaging Centre, Department of Radiology, Radboud University Medical Centre, Nijmegen, the Netherlands
[3] Department of Biomedical Engineering, Eindhoven University of Technology, the Netherlands
[4] Interuniversity Cardiology Institute of the Netherlands (ICIN), Utrecht, the Netherlands

CHAPTER 8

Radiofrequency compounding to estimate layer specific cardiac deformation. Technical note

Submitted

Abstract

By using the radiofrequency ultrasound signal the local tissue displacement and deformation can be quantified more accurately than by using the B-mode data. However, this only holds for deformations in the direction of the ultrasound beam (axial, zero degrees) and not for deformations in the direction perpendicular to the ultrasound beam (lateral). To overcome this problem, a new technique (compounding) was developed in which ultrasound transmissions in different angles with respect to the tissue are combined. Hereby an improved accuracy for the displacement estimation in the lateral direction can be obtained as was determined in a vascular imaging study. Since the cardiac displacement velocity is high and ultrasound acquisition at multiple angles reduces the acquisition rate of the data available, there will be a trade-off between the benefit of compound strain imaging and the reduced acquisition rate. To investigate the possibility to estimate cardiac displacement and deformation using compounding radiofrequency ultrasound acquisitions we have used a finite element model of left ventricular mechanics. We have acquired ultrasound radio frequency datasets using this model and a linear array probe using FieldII ultrasound simulation software. Initial *in vivo* measurements were performed in the healthy areas perfused by the left anterior descending coronary artery of 2 pigs. From the simulations it was found that axial displacements are best estimated by zero degrees analysis. Whether lateral displacement is best estimated by zero degrees or compounding analysis depends on the phase of the cardiac cycle. An inverse relation was found between the accuracy of the displacement estimation and the displacements in the direction perpendicular to the ultrasound plane. We believe that the use of a finite element model of left ventricular mechanics provides a highly accurate reference of the complex cardiac biomechanics, and can excellently be used to assess the performance of displacement estimation techniques. Based on the simulations the *in vivo* strain data could be interpreted better. Representative axial strain curves were measured *in vivo*. Lateral strain estimation was less accurate by both the zero degrees and compounding analysis. This is respectively caused by the lack of phase information in the zero degrees analysis and the reduced frame rate during the compounding analysis. Future studies should focus on using a matrix array probe to allow extracorporeal data acquisition applicable for clinical practice, and the use of plane wave imaging techniques to increase the frame rate of the acquisitions.

Introduction

Strain analysis can be used to distinguish diseased from healthy cardiac tissue. Besides the clinically available tissue Doppler imaging (TDI) and speckle tracking (STE) techniques, Radio Frequency (RF) based strain estimation can be used. A drawback of TDI and STE is the necessity to align the ultrasound beam in the direction of tissue deformation (TDI), or the relatively low spatial resolution (STE). These drawbacks can be overcome by using RF based strain estimation. Whereas for speckle tracking the envelope (amplitude) of the ultrasound signal is used for image creation and processing, the RF data contains both phase and envelope information, allowing a more accurate estimation of the deformation. Typically a 10 times better accuracy is obtained with RF-based strain estimation techniques with respect to envelope based strain estimation methods in the axial direction[1]. When the cross-correlation algorithm is applied to the lateral direction of the axial recordings, lateral displacements can also be estimated, albeit with a lower accuracy since the phase information is lacking in this direction. In addition to RF data transmitted in the axial direction, RF-compounding was introduced. This technique rapidly records RF data at multiple angles with respect to the tissue. After combining the recorded data from the multiple angles a displacement vector can be calculated, and tissue deformation can be assessed with very high accuracy[2]. Due to the fact that a large footprint of the transducer is required since the tissue has to be imaged at different angles, only linear array probes are capable to perform this technique. Current applications of this latter technique have been limited to vascular imaging. We already have shown that RF based strain estimation can be used to assess local myocardial deformation in healthy and chronically ischemic hearts[3].We now hypothesized that the use of RF-compounding might be beneficial to assess local deformation of the myocardium in more detail, and can be used to specify both extensional and shear strains more accurately. This is of interest to unravel the complex cardiac biomechanics and to assess local pathologies, or locally oriented therapies. In this article we describe our findings with the RF based deformation assessment using RF in the axial direction, and RF-compounding in a finite element model of left ventricular mechanics[4]. Based on the simulations the data recorded from the healthy anterior walls of 2 pigs with chronic myocardial infarction of the lateral wall can be interpreted more thoroughly.

Materials and Methods

For the simulation of the interaction between the ultrasound signal and the myocardium during deformation we have used the Field II simulation program[5]. Field II requires the user to define transducer properties, a scanning sequence and a matrix representing the three-dimensional coordinates of scatterers with respect to the transducer surface. First, the definition of the 'scatterer' matrices for the myocardial deformation will be described, followed by a description of the transducer and other imaging settings, and the *in vivo* experiments.

Finite element model

To obtain physiologically relevant data we have used the data obtained by the ACT simulation as defined by[4] using the finite element model (FEM) of left ventricular mechanics as described by[6]. From the model we have extracted 63 nodal positions which together

form a block with dimensions of 1 x 2 x 2 cm^3 (Figure 1). To simulate ultrasound data of the FEM we have loaded this block with $2.5 \cdot 10^6$ scatterers which positions were calculated relative to the nodal positions throughout the 80 simulated time increments using three dimensional (3D) shape functions. During the simulation the probe position was moved according to the nodes at the center of the tissue sample to mimic the *in vivo* data acquisition procedure. Figure 1 shows an illustration of the FEM with the scatterers positions in the volume used for the ultrasound simulations and the location and orientation of the ultrasound plane. In the simulation, eight cardiac cycles, consisting of 80 time increments were computed to obtain a cyclic steady state. The last cycle was used for the analysis.

Ultrasound simulation

All transducer properties were maintained for the 80 deformation states. A linear array transducer was simulated with a center frequency (f_c) of 8.8MHz and 192 physical elements. The element pitch was 200 μm and the element height 4 mm. Each physical element was subdivided into 10 × 10 mathematical elements to improve the accuracy of the simulations. During the simulations the sampling frequency was set to 123.2 MHz. Afterwards, the simulated RF data were down sampled to 61.6 MHz to match the sampling frequency used in the experiments: each sample with a sample number that was not a multiple of two was deleted. The two times higher sampling rate during the simulations was chosen, because Field II uses digitally sampled versions of the excitation and impulse responses, which are continuous signals in reality. For a higher sampling frequency the discrepancy between Field II and reality is smaller, and thus, more realistic ultrasound signals were simulated. In the axial–lateral direction, 12 elements were simultaneously active. No apodization was applied in transmit. A fixed transmit focus of 0.6 cm was used. In receive, dynamic focusing was applied with an F-number of 0.875. The maximum number of simultaneously active elements was restricted to 128. Hamming apodization was applied in receive. In the axial–elevational direction, a fixed focus of 2.0 cm was set and Hamming apodization was used in both transmit and receive. Displacements in both the axial and

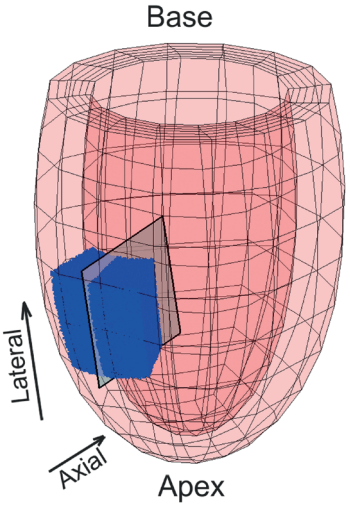

Figure 1. Finite element model of the left ventricle. The blue markers are the scatterers used to simulate the interference of ultrasound with biological tissue. The gray plane illustrates the ultrasound plane used during the simulation.

transverse directions of the ultrasound beam were estimated using both the ultrasound transmitted solely axially[7], and under the three beam steering angles[2,8]. These acquisitions are respectively referred to as zero degrees, and compounding. RF data of the FEM were simulated in all 80 deformation states for zero degrees, and two times 27 deformation states for the two beam steering angles of –20◦ and +20◦ for compounding. During the compounding data acquisition the sampling frequency is reduced to one-third of the sampling frequency of the zero degrees acquisition because three acquired angulated frames are combined for displacement estimation of one compounding frame. For comparison of displacements and strains estimated by both techniques to the ground truth displacements of the FEM we have down sampled the ground truth by a factor of 3. Zero degree results were cumulated over 3 frames using bilinear interpolation. The error of the displacement calculation is expressed in the root of the mean squared error (RMSE)[7]. The axial and lateral directions respectively align with the radial and the longitudinal direction of the cardiac coordinate system. Engineering axial (εAA), lateral (εLL) and shear (εAL) strains were assessed in the subendocardial, midwall and subepicardial layers. The simulations, and the *in vivo* acquisitions are done similarly to allow comparison between the simulations and *in vivo* acquired data. For optimal tracking of the tissue during the displacement estimation it is essential that the tissue remains in the field of view of the ultrasound aperture during the complete cardiac cycle. The position of the ultrasound probe therefore was moved with the nodal displacements of the contact area in the FEM during simulations. This allows free displacement of the FEM in all directions of the cardiac coordinate system and reliable estimation of displacements and strains.

Animal experiments

In vivo data were recorded in two female Dalland Landrace pigs receiving care in accordance with the *Guide for the Care and Use of Laboratory Pigs* prepared by the Institute of Laboratory Animal Resources. Experiments were approved by the Animal Experimentation Committee of the Utrecht University, the Netherlands. Closed-chest MI was created in the pigs by a percutaneous balloon of equivalent size to the proximal left circumflex artery (LCX). Prior to MI all animals received an oral dose of amiodarone (400 mg/day; start 10 days prior to MI) and clopidogrel (75 mg/day; start 3 days prior to MI, Sanofi Aventis, Gouda, the Netherlands). A bolus of 500 mg acetylic salicylic acid (Centrafarm, Etten-Leur, the Netherlands) was given the day before the occlusion. The balloon was inflated for 75 minutes at 5-8 atm[9]. Complete occlusion of the LCX was confirmed by angiography.

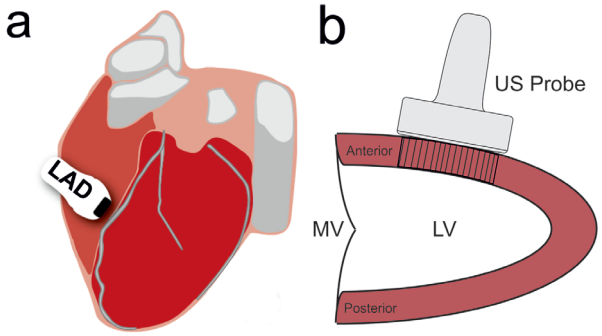

Figure 2. In vivo data acquisition

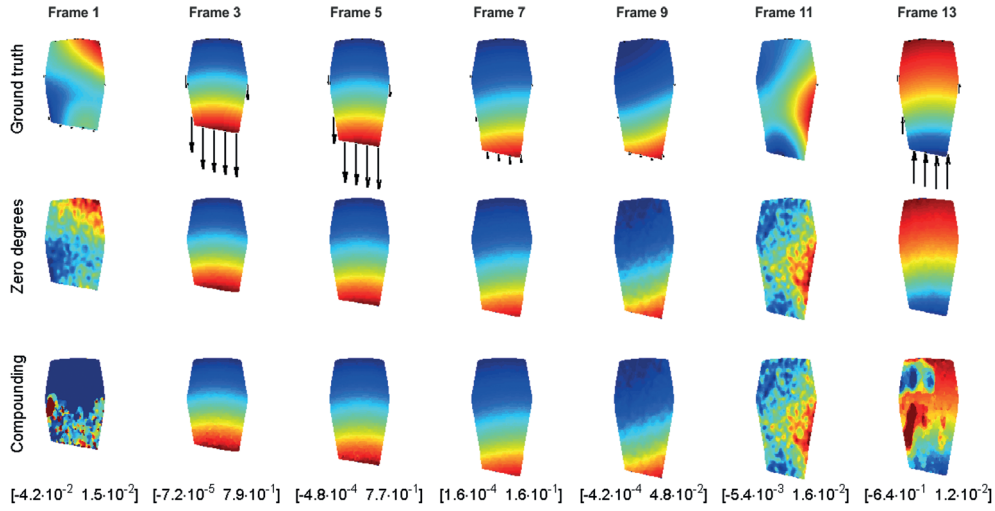

Figure 3. Axial interframe displacements of the imaged plane in 13 subsequent frames throughout the cardiac cycle that result from a single simulation. Frame 1 represent begin systole and frame 25 represents end diastole. The axial displacement values of the FEM and the values estimated by the zero degrees RF and compounding RF ultrasound analysis are respectively shown in the top, middle, and bottom rows. The top of each plane represents the epicardium. The colors represent the axial inter-frame displacements, the used color bar is represented on the right. The numbers underneath the bottom row represent the color scale limits of the corresponding column of three figures [min max]. The arrows in the top row represent the absolute value and the direction of the displacements. Displacements towards the probe (upward direction) are shown as negative values and vice versa. In frames where no arrows are visible, the absolute values of the displacements are correspondingly low.

To prevent ventricular arrhythmias, 300 mg amiodarone (Centrafarm, Etten-Leur, the Netherlands) was given intravenously. External defibrillation (150-200 Joules) was used if ventricular fibrillation occurred. After the procedure, coronary angiography was performed to confirm vessel patency. After recovery, the animals received an oral dose of 50 mg metoprolol, 400 mg amiodarone, 75 mg clopidogrel, and 160 mg acetylic salicylic acid daily, until euthanasia to prevent thrombosis and arrhythmias.

Experimental protocol

Twelve weeks after MI, a thoracotomy was performed for epicardial measurements of ultrasound RF data in long-axis cross sections from the LV anterior wall as depicted in Figure 2. Since the left anterior descending coronary artery (LAD) is untreated, data recorded from the anterior wall are referred to as healthy. To minimize errors in deformation estimation caused by motion of the heart in a direction perpendicular to the ultrasound imaging plane (out of plane motion), the apex was loosely fixed by a Starfish Cardiac Positioner (Medtronic Inc., Minneapolis, MN, USA), and the ultrasound probe was manually moved with the tissue during the acquisition.

RF echocardiographic data acquisition and deformation estimation

RF data were acquired with a Medison Accuvix V10 ultrasound scanner (Samsung Medison, South Korea) with a radiofrequency data interface in combination with a 3.8 cm wide linear

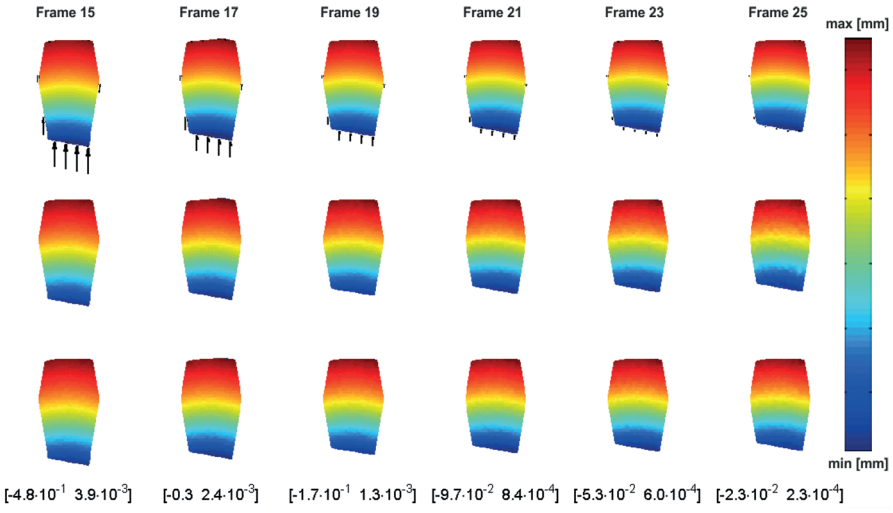

Figure 3. Continued

array probe (L5-13) with a center frequency of 8.7 MHz. The RF data were digitized at a sampling rate of 61.6 MHz. For the *in vivo* acquisitions beam steering angles of −28◦ and +28◦ were used.

Results

Figure 3 and 4 respectively show the axial and lateral interframe displacements of the imaged plane in 13 subsequent frames throughout the cardiac cycle that result from a single simulation. The arrows represent the absolute value and direction of the displacements for the corresponding column of figures. The arrow size of Figure 3 and 4 are independent from each other. Because the absolute displacements vary greatly between the frames, the color scale is altered for each frame to be able to maximally visualize the differences between the different techniques. The numbers below the figures represent the color scale limits of each column of figures. From comparison of the ranges in Figure 3 and 4 it can be observed that the axial interframe displacements are larger than the lateral interframe displacements, and that the zero degrees and compounding estimation both have difficulties to correctly estimate the axial and lateral interframe displacements for some parts of the cardiac cycle. RMSE values of the zero degrees and compounding estimations are illustrated in Figure 5.

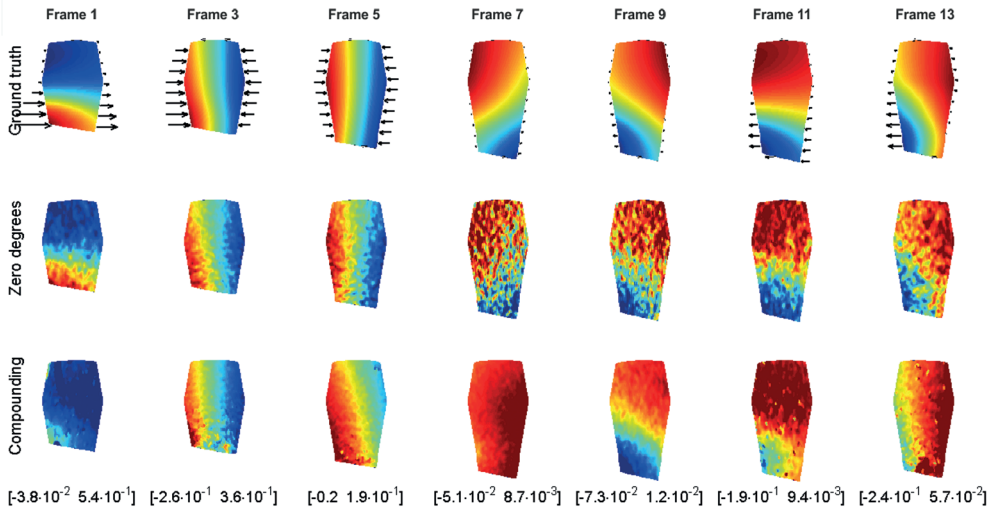

Figure 4. Lateral interframe displacements of the imaged plane in 13 subsequent frames throughout the cardiac cycle that result from a single simulation. Frame 1 represent begin systole and frame 25 represents end diastole. The lateral displacement values of the FEM and the values estimated by the zero degrees RF and compounding RF ultrasound analysis are respectively shown in the top, middle, and bottom rows. The top of each plane represents the epicardium. The colors represent the lateral inter-frame displacements, the used color bar is represented on the right. The numbers underneath the bottom row represent the color scale limits of the corresponding column of three figures [min max]. The arrows in the top row represent the absolute value and the direction of the displacements. Displacements from left to right are shown as positive values and vice versa. In frames where no arrows are visible, the absolute values of the displacements are correspondingly low.

Based on the RMSE the zero degrees has the most difficulties to estimate the axial displacements in frame 3-5 and 13, and compounding estimation has the most difficulties to estimate the axial displacements in frame 1 and 12-13. The lateral displacement estimation by both the zero degrees and compounding analysis have a higher RMSE throughout the complete cardiac cycle compared to the axial displacement estimations. Compounding analysis has the most problematic lateral displacement estimation in frames 1-6, 11-14. The green line in Figure 5 represents the absolute inter frame elevational displacements perpendicular to, and in the center of the imaging plane. In all analysis the highest RMSE coincides with the highest elevational displacement. The axial, lateral, and axial/lateral shear strains estimated in the subendocardial, midwall and subepicardial layers are shown in Figure 6. In all directions strains are best estimated by the zero degrees analysis. Best performance of the compounding analysis is found for the axial strains in the subendocardial layer. The errors in the axial, midwall and subepicardial strains of the compounding analysis already arise in the first frame. This coincides with the highest displacement estimation errors in Figure 3 and 5A. The error in the lateral strains of the compounding arise in frame 1-6, and 11-14, coinciding with the highest displacement estimation errors in Figure 4 and 5B. After frame 2 the axial and lateral strain curves show similarities with the simulations. From the frames represented along the x-axis of Figure 6 it can be observed that for the compounding analysis only one out of three frames is available for displacement and strain estimation since it only uses the reconstruction from

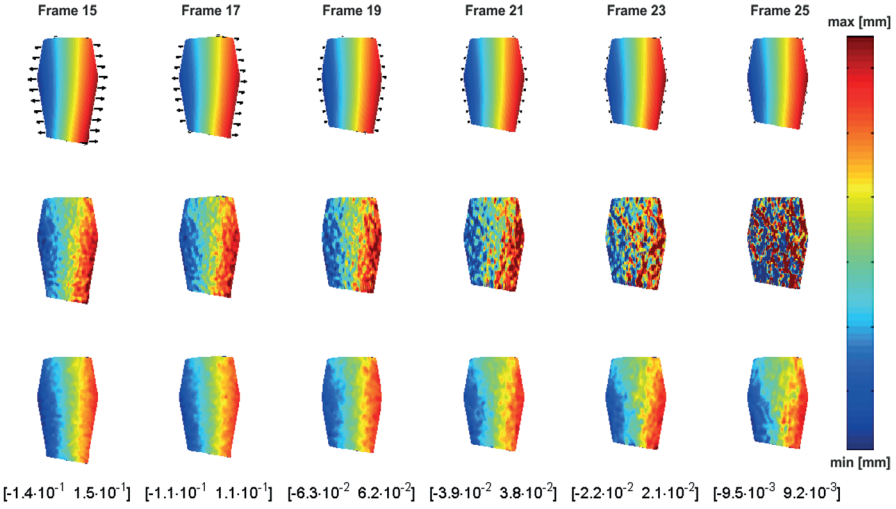

Figure 4. Continued

the angularly transmitted ultrasound. To demonstrate that these techniques can also be applied *in vivo* and not only by using the FEM, strains were also estimated from two *in vivo* datasets. In figures 7 and 8 axial, lateral, and shear strain curves calculated from the zero degrees analysis of data acquired in two healthy porcine LAD regions are shown. Large differences exist between the strain curves of the simulations and the *in vivo* data. The lateral and shear strain curves are noisy, however the absolute strain values of the lateral strain are in the physiological range[3]. The gradient between the subendocardial and subepicardial strain is not observed in all datasets.

Discussion

In this study we have used a finite element model of left ventricular mechanics to simulate the estimation of displacements and strains by RF ultrasound. The use of a FEM allowed us to calculate the ground truth displacements in the plane used for ultrasound simulations. Quantification of the error between the simulated and estimated displacements was done by RMSE. When interpreting RMSE it must be kept in mind that a very small area with a very high offset between the simulated and the estimated values causes a very high RMSE. However dynamic phenomena as 'post-systolic' deformation and inertia induced passive tissue deformation present the *in vivo* data are not available in the simulations, the FEM

does represent the layer specific features of cardiac deformation and the resulting torsion. Hereby an accurate comparison can be made between the ground truth and estimations by different ultrasound acquisitions and analysis methods. The choice to use a 3.8 cm wide linear array probe (L5-13) with a center frequency of 8.7 MHz during simulations and *in vivo* epicardial acquisitions was motivated by the possibility to have optimal ultrasound resolution and a large field of view. Epicardial acquisitions allowed to move the probe with the tissue to assure optimal tissue tracking during post processing.

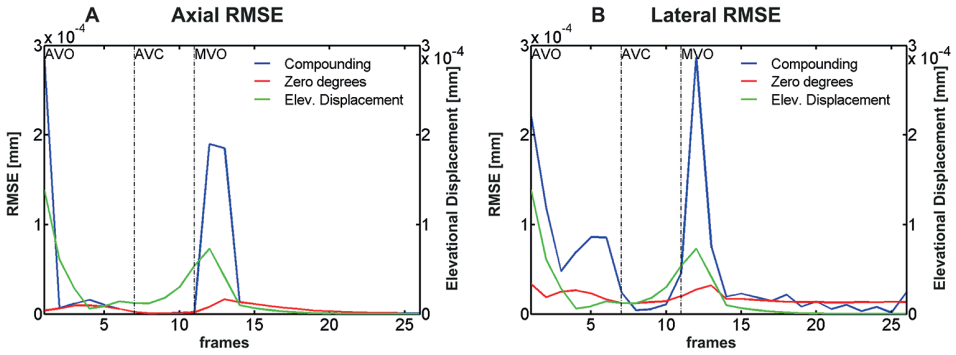

Figure 5. RMSE of four simulations. Axial (red) and compounding (blue) RF ultrasound derived axial displacements vs. the analytically determined axial displacements (A). Axial (red) and compounding (blue) RF ultrasound derived lateral displacements vs. the analytically determined lateral displacements (B). The green line represents the absolute elevational inter-frame displacements of the scatterers from the imaging plane due to circumferential motion caused by torsion of the myocardium. AVO indicates aortic valve opening, AVC indicates aortic valve closure, MVO indicates mitral valve opening.

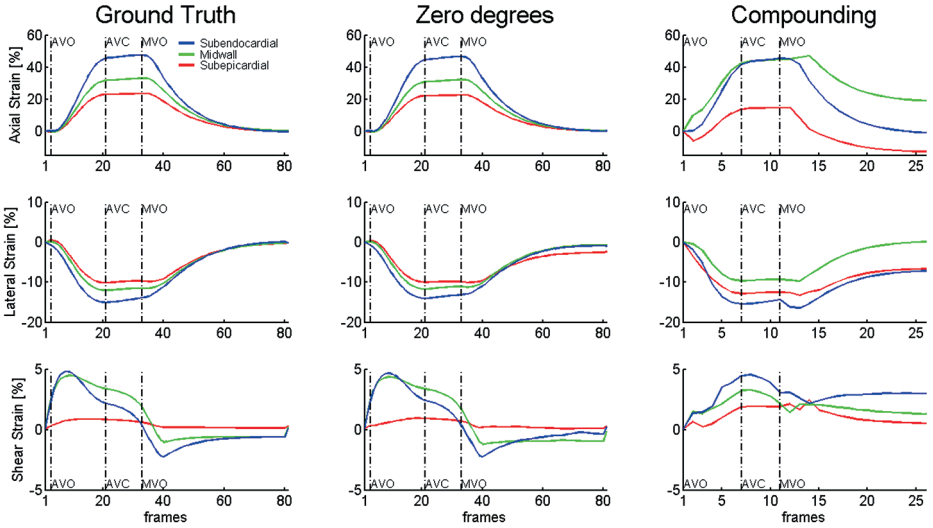

Figure 6. Strain curves calculated from the simulated displacements (left) and strain curves calculated from displacements estimated by axial (mid) and compounding (right) RF ultrasound analysis. AVO indicates aortic valve opening, AVC indicates aortic valve closure, MVO indicates mitral valve opening. The shear strain is the axial/lateral shear strain.

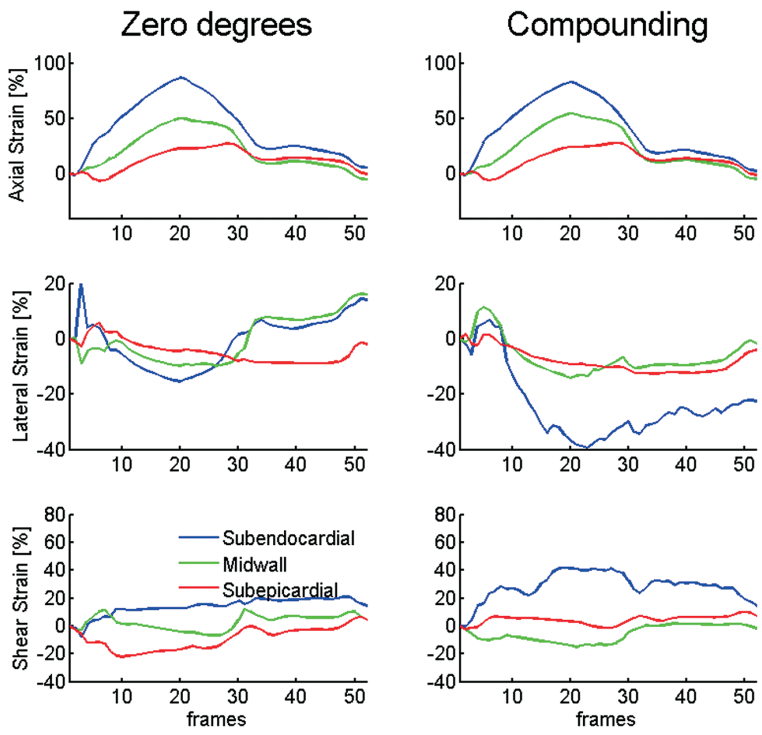

Figure 7. Strain curves measured from a healthy porcine anterior wall. Axial, lateral, and axial/lateral shear strains are calculated by means of axial (left) and compounding (right) RF ultrasound analysis.

Displacements

The axial displacements shown in Figure 3 and the RMSE of the axial displacements in Figure 5A clearly indicate that there is a relation between the elevational displacements of the scatterers and the accuracy of the axial displacement estimation. This effect is most pronounced in the compounding analysis. Since the frame rate during the compounding analysis in the axial direction is one-third of the frame rate of the zero degrees analysis it is more affected by scatterer displacements in the elevational direction. This erroneous tracking induced displacement estimation error peaks in frame 1 and 12-13. The lateral displacements shown in Figure 4, and the RMSE of the lateral displacements in Figure 5B also show a relation between the elevational displacements of the scatterers and the accuracy of the displacement estimation. In these parts of the heart cycle, compounding displacement estimation is inferior to zero degrees lateral displacement estimation. However, in phases with low elevational displacement , the velocity of the displacement is the dominant factor to determine the RMSE as can be observed in frame 3-7 in Figure 5B and by the displacement values in Figure 4. The compounding analysis in the lateral direction using a frame rate of one-third of the frame rate of the zero degrees analysis only leads to a superior displacement estimation in the lateral direction in frames where both the elevational displacements of the scatterers and the velocity of the scatterers is minimal. In conclusion the zero degrees analysis performs best in displacement estimation in both the axial and the lateral direction of the simulated data. This is due to the higher frame rate,

leading to optimal tracking during fast motion of the scatterers and displacements in a direction perpendicular to the ultrasound plane.

Strains

From the strain curves derived from the FEM in Figure 6 it can be observed that although a high RMSE was found between the simulated and estimated displacements as shown in Figure 3, 4 and 5, the strain curves of the simulation and the zero degrees and compounding estimations show a high similarity. This is caused by the fact that the strains were calculated in the subendocardial, midwall, and subepicardial layers. Each area covered one-third of the myocardial area measured. In case of the zero degrees analysis the averaging over the area resulted in a correct strain estimation. The errors in the compounding analysis in both the axial and lateral strain estimations reveals that regional averaging does not compensate the strain in the compounding frames with a high RMSE as can also be observed from Figure 3 and 4. The errors in the strain arising in the first frames with high RMSE persist throughout the complete cardiac cycle. The accumulation of errors from the axial and lateral direction cause the axial/lateral shear strain estimation by compounding analysis to be unreliable.

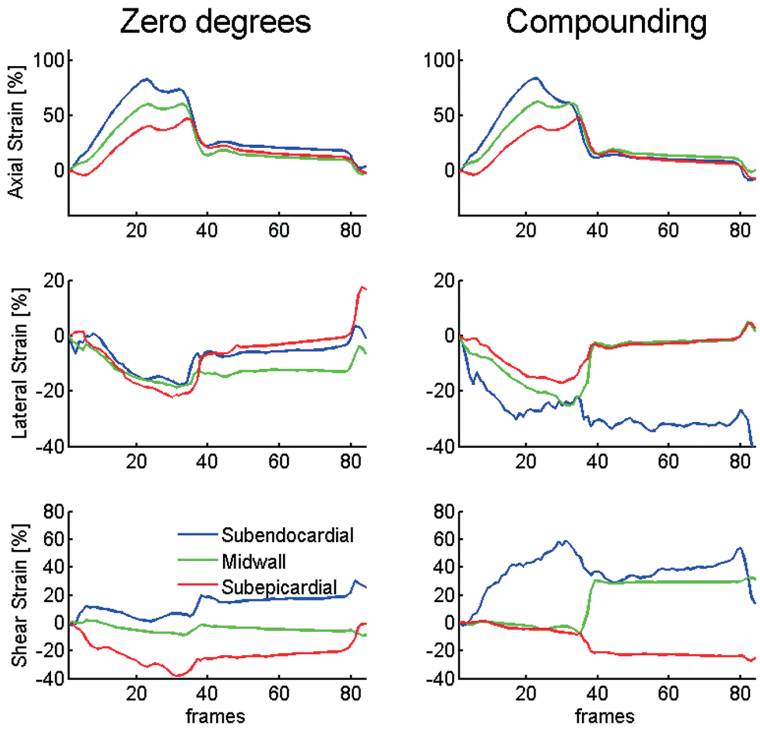

Figure 8. Strain curves measured from a healthy porcine anterior wall. Axial, lateral, and axial/lateral shear strains are calculated by means of axial (left) and compounding (right) RF ultrasound analysis.

In vivo data

We have shown that the best results are obtained from the zero degrees data. Fore completeness we present the *in vivo* results of both the zero degrees and the compounding analysis in two acquisitions in two pigs where the elevational displacement of the tissue was minimal, and displacements could be estimated. Unfortunately, we were not able to acquire simultaneous electrocardiograms or valvular movements to use as a time reference in the *in vivo* datasets. Therefore reference timing was done based on the M-mode data. The moment with the thinnest wall was used as reference timing at t=0. Although the tissue was optimally followed by the probe during data acquisition in the two *in vivo* datasets, it can clearly be observed that all strain curves have different morphologies. Based on the FEM analysis we now can state that the amount of tissue displacement in the direction perpendicular to the ultrasound plane and the velocity of the tissue displacements determine the accuracy of the displacement estimation. During the *in vivo* acquisitions we have attempted to minimize the elevational motion by moving the probe with the tissue to prohibit tissue displacement in the direction perpendicular to the ultrasound plane. The axial strain curves reveal that the combination of both the displacement estimation and the averaging of each myocardial layer leads to a reliable strain estimation. Anomalies of the axial strain from the expected absolute radial strain values and transmural gradients[3] are therefore caused by altered acquisition locations, capturing of the papillary muscles, or possibly biological variation. The combination of displacement estimation and averaging of each myocardial layer is insufficient to correctly determine the lateral strain by both the zero degrees and compounding analysis. In the clinical scanner the zero degrees acquisition rate is decreased to the same value as the compounding acquisition rate. In combination with larger *in vivo* displacements the low frame rate causes the *in vivo* lateral strains by the zero degrees analysis to be unreliable. Overall it can be stressed that in this experimental setup displacements were so high that only the axial strain could be reliably estimated from the *in vivo* epicardial acquisitions.

Limitations

The epicardial use of a linear array probe caused an optimal ultrasound resolution, a large field of view, and the ability to move with the tissue during acquisitions. However the effects were most likely minimal, the epicardial measurement affected the tissue deformation. Moreover, the linear array probe made it impossible to examine the tissue displacements in the direction perpendicular to the probe. We were therefore not able to completely derive the complex deformation of the heart *in vivo*. Use of a matrix array probe and transthoracic acquisition might have prevented this. We have shown that the ultrasound acquisition rate dominates the accuracy of the displacement estimation. Although it was already shown that the results for beam steering angles between 20◦ and 30◦ were approximately the same 10, we have not examined its combined effect with the large tissue displacements and velocities.

Conclusion

In this study we have used a finite element model of left ventricular mechanics to simulate the estimation of displacements and strains by RF ultrasound. The ground truth displacements and strains of the finite element model could be estimated by RF ultrasound analysis using both the zero degrees and the compounding analysis. We found that the

displacement estimation error is dominantly affected by the mismatch between the ultrasound acquisition rate and the velocity of the tissue in the imaging plane, and the motion perpendicular to the imaging plane. Consequently, due to the higher frame rate, the best results are found for the zero degrees analysis. Compounding only improved displacement estimates in parts of the heart cycle with the lowest tissue displacement. Due to the high tissue velocity and limited frame rate *in vivo* strains could only be reliably estimated in the axial direction.

Acknowledgements
We gratefully acknowledge Cees Verlaan, Merel Schurink, Marlijn Jansen, Maringa Emons, Joyce Visser, Sanne Jansen of Lorkeers and René van Es for excellent technical assistance and animal care.This work was supported by the Netherlands Heart Foundation '[2003B07304 and 2010T025]', BSIK program "Dutch Program for Tissue Engineering", '[grant 6746]', and a Bekalis price (PD). This research is part of the Project P1.04 SMARTCARE of the research program of the BioMedical Materials institute, co-funded by the Dutch Ministry of Economic Affairs and the Nederlandse Hartstichting.

References

1. Varghese T, Ophir J. Characterization of elastographic noise using the envelope of echo signals. Ultrasound in Medicine & Biology. 1998;24:543-555
2. Hansen HHG, Lopata RGP, Idzenga T, de Korte CL. Full 2D displacement vector and strain tensor estimation for superficial tissue using beam-steered ultrasound imaging. Physics in Medicine and Biology. 2010;55:3201-3218
3. Van Slochteren FJ, Van der Spoel TIG, Hansen HHG, Bovendeerd PHM, Doevendans PA, Sluijter JPG, Chamuleau SAJ, de Korte CL. Layer-Specific Radiofrequency Ultrasound-Based Strain Analysis in a Porcine Model of Ischemic Cardiomyopathy Validated by a Geometric Model. Ultrasound in Medicine & Biology. 2013:1-11
4. Bovendeerd PHM, Kroon W, Delhaas T. Determinants of left ventricular shear strain. American Journal of Physiology. Heart and Circulatory Physiology. 2009;297:H1058-1068
5. Jensen JA. Field: A Program for Simulating Ultrasound Systems, Paper presented at the 10th Nordic-Baltic Conference on Biomedical Imaging. Medical & Biological Engineering & Computing. 1996;34:351-353
6. Kerckhoffs RCP, Bovendeerd PHM, Kotte JCS, Prinzen FW, Smits K, Arts T. Homogeneity of Cardiac Contraction Despite Physiological Asynchrony of Depolarization: A Model Study. Annals of Biomedical Engineering. 2003;31:536-547
7. Lopata RGP, Nillesen MM, Hansen HHG, Gerrits IH, Thijssen JM, de Korte CL. Performance evaluation of methods for two-dimensional displacement and strain estimation using ultrasound radio frequency data. Ultrasound in Medicine & Biology. 2009;35:796-812
8. Hansen HHG, Richards MS, Doyley MM, de Korte CL. Noninvasive vascular displacement estimation for relative elastic modulus reconstruction in transversal imaging planes. Sensors. 2013;13:3341-3357
9. Van der Spoel TIG, Vrijsen KR, Koudstaal S, Sluijter JPG, Nijsen JFW, de Jong HW, Hoefer IE, Cramer MJM, Doevendans PA, van Belle E, Chamuleau SAJ. Transendocardial cell injection is not superior to intracoronary infusion in a porcine model of ischemic cardiomyopathy: A study on delivery efficiency. Journal of Cellular and Molecular Medicine. 2012:2768-2776
10. Hansen HHG, Idzenga T, De Korte CL. Band-pass filtering for optimal displacement estimation in the presence of grating lobes at large beam steering angles. Ultrasonics Symposium (UIS) 2012 IEEE international. 2012:2559 - 2562

PART FOUR

Summary and discussion

CHAPTER 9

Summary, general discussion and future perspectives

The therapeutic options for patients suffering from ischemic heart disease (IHD) are limited, and worldwide 23 million patients suffer from heart failure[1,2]. Therefore there is a strong need for alternative therapies for IHD. Since cardiac regenerative therapies have shown promising results in basic science studies[3,4], the attention for cardiac regenerative therapy has been overwhelming in the last decade[5-7]. Nevertheless the clinical benefits are still modest, and do not always prevent progression of the disease towards end stage HF. The appealing promise of cardiac regenerative therapy to be readily available as a low cost and effective treatment is once more accelerated by the enormous developments in the field of bio-technology in combination with a strong scientific competition. Besides the medical and biological aspects of the therapy, topics concerning the optimal injection strategy and the optimal endpoints to assess the therapy have been underexposed. Standard clinical techniques have been used, whereas specialized techniques might be more effective and better suited in the crucial phase of further development of a promising therapy. As discussed in the introduction efficient development, introduction and valorization of new techniques are the specialized skills of a medial engineer. In the summary and general discussion part the major findings, conclusions, and future perspectives of the solutions investigated in this thesis are discussed.

The major topics of this thesis are presented in three parts. In the first part the technical challenges of cardiac regenerative therapy are addressed. The second part covers the development of the optimal injection technique for application of cardiac regenerative therapy. In the third part advanced measurement techniques of local cardiac function are studied in order to establish constructive feedback for optimizing cardiac regenerative therapy. The major findings of this thesis are:

1. Infarct transmurality measured by the gold standard late gadolinium enhancement MRI can be co-visualized during the injection procedure using the clinical standard NOGA®XP intramyocardial injection system based on electromechanical mapping (EMM).
2. The target area selection based on the gold standard imaging technique of infarct transmurality provides valuable additional information during the injection procedure.
3. Respiratory induced cardiac motion affects electromechanical mapping datasets and can be corrected for in order to obtain an anatomical correct map or allow optimal registration on respiratory gated imaging data.
4. Cardiac deformation assessment based on radiofrequency ultrasound analysis can be used to accurately measure myocardial strain, and provides new insights in cardiac biomechanics. It's relation to the local effects of cardiac regenerative therapy needs further investigation.

Summary

PART ONE
ADDRESSING THE TECHNICAL CHALLENGES OF CARDIAC REGENERATIVE THERAPY

Since evolution of the therapy in both preclinical and clinical research has been rather slow over the last decade, a different approach is required[8]. In **Chapter 2** we present a review of current measurement techniques used to assess the effects of cardiac regenerative therapy. We observed that the measurement techniques used to assess the therapy might lack the level of detail necessary to provide optimal feedback to re-design the therapy. The reviewed invasive and non-invasive quantitative techniques and their derivatives reflect different aspects of cardiac function. Direct distinct relations between the measures, effects, and mechanisms of cardiac regenerative therapy however do not exist. As a new approach to measure the local effects of cardiac regenerative therapy we have suggested relations between *in vivo* measurable parameters and the three typical mechanisms of cardiac regenerative therapy: vasculogenesis, cardiomyogenesis, and matrix assisted myocardium stabilization. As a starting point we used preexisting knowledge about natural myocardial healing[9-12]. Since cardiac biomechanics reflects cellular function and all physiological determinants of deformation are targeted by stem cell therapy, we have advocated cardiac deformation to be used as a surrogate measure of the local effects of cardiac regenerative therapy. Since deformation imaging is affected by multiple confounders[13], a comprehensive approach is required to allow distinction between the physiological determinants and confounders[14]. When applied properly it can provide a unique insight in the therapy induced alterations of deformation.

PART TWO
ADVANCED DELIVERY

Clinical available delivery techniques used for the administration of biologics in the context of cardiac regenerative therapy are all suboptimal. Surgical application and endoscopic guided pericardial injections require a highly demanding surgical procedure. All percutaneous approaches like intracoronary infusion and intramyocardial injection and also surgical approaches are associated with low cell retention of approximately 10% after 4 hours[15]. In cardiac regenerative therapies focusing on stem cells as a biologic, the transplantation is the final stage of an expensive and time consuming process in which stem cells need to be extracted, expanded, cultured, or biomaterials need to be made and prepared for transplantation. The transplantation techniques however received least attention over the last years. Besides the expensive, time consuming and operator dependent treatment planning based on electromechanical mapping (EMM) by the NOGA®XP intramyocardial injection system[16], other injection/infusion techniques do not provide treatment planning[17]. Provided that the effects of cardiac regenerative therapy are low, and that multiple administration strategies are currently used, there is a strong need for standardization of the injection strategy. Standardization facilitates comparison between studies and enables optimization of the injection strategy and improve the therapeutic effects. In Part Two we describe the in-house development and the first

experiences of an easy to use operator independent standardized injection strategy which is least demanding for the patient.

In **Chapter 3** the development and initial experiences with the treatment planning and 3D CartBox software toolbox to perform multimodality infarct identification for optimal image guided intramyocardial stem cell injections are described. The software for this toolbox is developed in this thesis project in cooperation with three subsequent MSc students of the University of Twente. The treatment planning algorithm assigns the border zone of regions with a distinct infarct transmurality based on the gold standard technique to quantify infarct transmurality: late gadolinium enhancement magnetic resonance imaging (LGE-MRI). In combination with the 3D CartBox image integration toolbox the assigned border zone can be visualized during the catheter mapping procedure using the NOGA®XP catheter navigation system to guide injections. The three main findings of this study were: 1) real-time use of the toolbox was feasible. 2) A visual mismatch was found between infarct assessment by EMM and LGE-MRI. And 3) The 3D CartBox toolbox can be of additional value for infarct assessment during cardiac stem cell injection procedures. Thereby the hypothesis that infarct transmurality measured by the gold standard imaging technique can be co-visualized during the injection procedure using the clinical standard intramyocardial injection system based on EMM is adopted. In **Chapter 4** the treatment planning and 3D CartBox toolbox is retrospectively applied to a dataset of 17 pigs from two cohorts of different models of chronic myocardial infarction. In contrast to earlier studies using a manual segmental comparison[18], this technique enabled an accurate in depth analysis of the electromechanical properties of infarct areas. The four main findings of this study were: 1) The overlap between infarct areas identified by EMM and infarct areas identified by LGE-MRI is poor. 2) Unipolar voltage (UV) and bipolar voltage (BV) do distinguish infarcted and healthy tissue, but lack the sensitivity to make a distinction between different infarct transmurality values. 3) Linear local shortening (LLS) and wall thickening (WT) are differently affected by infarct transmurality. 4) Our treatment planning algorithm can be used to identify the true infarct border zone in an easy and practical way. Based on **Chapter 4** the hypothesis that the target area selection can be assisted during the injection procedure by the gold standard imaging technique of infarct transmurality is adopted. Crucial element of 3D CartBox is the registration of the EMM data and the MRI data based on the anatomy of the LV. Within the NOGA®XP system there is no compensation of the respiration induced cardiac motion. From literature it is known that respiratory induced motion of the heart can be as high as 1 cm in various directions and this might lead to registration errors[19-21]. In **Chapter 5** we present the initial results of an in-house developed technique to perform respiratory motion correction of the NOGA®XP catheter during the mapping procedure. The potential of our solution as a standardized injection strategy for cardiac regenerative therapy has created an opportunity for valorization and value creation. In **Chapter 6** we present the outline of our business plan written for the commercial exploitation of the treatment planning and image integration toolbox presented in Chapter 3, and rewarded with the BMM valorization grant of €200.000,-. The treatment planning and 3D CartBox toolbox will be commercialized by the newly founded spin-off company called "CARTcare: Technical solutions to improve cardiac regenerative therapy".

PART THREE
ADVANCED ASSESSMENT OF LOCAL CARDIAC FUNCTION

In **Chapter 2** of this thesis the specific use of measures of local cardiac function for optimal feedback of cardiac regenerative therapy was advocated. Measuring cardiac function locally can however be done using different techniques. In Part Three of this thesis we investigated the use of radio frequency (RF) ultrasound for local cardiac deformation estimation, as a novel approach for this purpose. In **Chapter 7**, both RF measurements and geometric modeling showed that a transmural difference exists in the radial and longitudinal strain of healthy tissue. Secondly, the transmural difference was diminished after MI. Thirdly, it was shown for the first time by RF based strain estimation that radial strain in the subendocardium can amount to 80%. The peak radial strain values in the three transmural layers that were estimated in vivo with this analysis were in the same order of magnitude as the peak strain values obtained from geometrical modeling. In this work the existing theories about cardiac biomechanics were confirmed via RF ultrasound based cardiac deformation estimation. RF compounding, and improved 2D deformation imaging technique was evaluated in an ultrasound simulation study based on a finite element model of left ventricular mechanics[22] described in **Chapter 8**. The main reasons for the difficulties to estimate cardiac deformation by RF ultrasound were investigated. The mismatch between the tissue velocity and the frame rate of the RF data acquisition, and the directions of the displacements with respect to the imaging plane play a major role in the accuracy of the cardiac deformation estimation. Both the orientation and activation sequence of the cardiac muscle fibers throughout the myocardial wall cause the complex three dimensional deformation pattern of the myocardium[23]. When acquiring ultrasound data in a single plane, only the two dimensional component of the deformation is measured. The so-called through plane or elevational motion (the third dimension) causes tissue tracking difficulties during the post processing, which cannot be compensated for. When the frame rate of the RF data acquisition is sufficient the tracking algorithm can accurately calculate the displacements of the tissue. However, when the frame rate is lowered because recordings are done using multiple angles during compounding, displacement estimation becomes problematic in phases of the cardiac cycle where the tissue velocity is high. In phases of the cardiac cycle where the tissue velocity is low compounding leads to superior displacement estimation in the direction perpendicular to the ultrasound beam. During in vivo acquisitions the displacements were so high that only the axial strain could be reliably estimated from the *in vivo* epicardial acquisitions.

General discussion and future perspective

PART ONE
ADDRESSING THE TECHNICAL CHALLENGES OF CARDIAC REGENERATIVE THERAPY

Our attempt to assign clinically available measures of local cardiac function to measure the local effects of cardiac regenerative therapy has also been suggested by other groups[24]. The pre-clinical studies using local measures of cardiac function did not apply the comprehensive approach suggested in chapter 2, and did not show an advantage of local measures of cardiac function over the standard endpoints[25]. Although this might be interpreted as a disappointing result, we believe that a study to assess the most optimal surrogate endpoint of cardiac regenerative therapy requires dedication, persistence and collaboration between the researchers involved. More than the technical challenges this new methodology therefore requires a paradigm shift of the research community from the current believe that via a trial and error approach ultimately the therapy most affecting LVEF will evolve, towards a methodology in which in depth measurements of local cardiac function are used to optimize the therapy. Technically special attention should be paid to the technique used to measure strain. Although the need for standardization of strain imaging technologies has been addressed[26], myocardial strain imaging currently is strongly affected by the vendors of the ultrasound equipment using different algorithms to calculate strain[27,28], and excessive post processing to acquire the most smooth results[29]. For the assessment of the local effects of cardiac regenerative therapy it is desirable to use the most raw measurement data to circumvent issues concerning the strain calculation algorithm and the effects of the excessive post processing. In Part Three of this thesis raw radio frequency based ultrasound analysis was used to quantify local layer specific cardiac function. Through a collaboration with the development team of the used technology this technique meets all the requirements stated above, and did provide new insights in cardiac biomechanics.

PART TWO
ADVANCED DELIVERY

Starting point for the development of an advanced delivery technique was the difficulty to accurately target the area for the injection of cardiac stem cell therapy using the NOGA®XP system. In both animal studies and patients, EMM often did not show a distinct delineation of the infarct area based on electromechanical characterization while other infarct assessment techniques clearly showed an infarcted area. In clinical practice, the injections are therefore often performed based on incomplete mapping and the a priori knowledge of the physician about the infarct location and severity. The lack of a technique to accurately perform targeted injections has even forced physicians and researchers to go back to the paradigm that the injection location is irrelevant since the mechanisms of action are purely paracrine and don't require localized administration[30]. Hereby ignoring the fact that paracrine signaling might also be more effective when targeted to a specific region of the myocardium. The suboptimal injection technique described above has inspired us to develop the treatment planning and 3D CartBox toolbox to assign and guide to the optimal injection location for cardiac regenerative therapy based on the gold standard infarct transmurality

assessment technique. Our solution comprises a patient friendly, operator independent, accurate and safe technique to guide intramyocardial injections. Because the challenges to develop this toolbox were of both technical and medical nature, the specialized skills of a medical engineer were most suitable for an efficient development process. The treatment planning toolbox can be used to assign the border zone of the infarct, and potentially dangerous areas for injections based on LGE-MRI. However, whether the border zone is the optimal area for stem cell injections, and how the border zone is characterized however only has been investigated to a limited extent[31]. Alternatively, the use of other imaging modalities might also be of interest to guide intramyocardial injections. Our treatment planning algorithm defines the border zone by a user definable wide border over the isolines of infarct transmurality at any percentage between 0 and 100% infarct transmurality. By definition it can therefore excellently be used to further establish the definition of infarct border zone and the most optimal injection location. Conclusive evidence for the optimal injection location must be investigated in future studies in which besides the accuracy of the border zone targeting also local and global cardiac function must be assessed. An important aspect of the accuracy of the border zone targeting is the registration of the NOGA®XP catheter on the cine MRI images. A registration error can cause erroneous targeting of the border zone during the injection procedure. Respiratory induced motion of the heart during the EMM procedure can affect the registration error[32]. We demonstrated that our respiratory motion correction algorithm worked in case of a phantom experiment, but showed no improvement of the registration error in the *in vivo* porcine experiments. This most likely was caused by the minimal respiratory induced motion of the porcine heart. The effects of our respiratory motion correction algorithm in humans must be further investigated. An alternative method to assess respiratory induced motion would be the introduction of a dedicated electrode which is mounted in the heart via a screw, and serves as a reference of respiratory induced motion. Since this requires both a soft- and hardware modification of the equipment we did not investigate the option of a reference electrode. The paradigm of the border zone of the infarction to be the most appropriate area for cardiac regenerative therapy injections has driven us to develop the treatment planning based on infarct transmurality derived from LGE-MRI. In future applications the use of perfusion, or viability imaging by SPECT/CT might be more suitable since it can be performed in patients with an ICD or a pacemaker. On-going developments in MR imaging techniques[33,34]make MRI a very advanced and desirable technique to use for treatment planning. For example the use of MR tagging to quantify local tissue deformation, or diffusion tensor imaging to assess the local orientation of the myofibers might further improve treatment planning. Both cardiac deformation and the local orientation of the myofibers provide information about the local remodeling status of the myocardium[10] which might importantly determine the success of cardiac regenerative therapy. After small adaptations of the treatment planning and 3D CartBox toolbox mentioned above, alternative treatment planning strategies can become available for pre-clinical studies. Besides the use of the toolbox to perform injections in the context of cardiac regenerative therapy, it might also be of interest to guide diagnostic myocardial biopsies in non-ischemic cardiomyopathies. Another development initiated by the development of the treatment planning and 3D CartBox toolbox is the development of a MRI compatible injection catheter. This specific catheter would enable real-time image guided injections in the MRI scanner. Thereby a new injection platform is generated for the recent developments of cardiac regenerative therapeutics and MRI imaging techniques to visualize endogenous contrast of fibrotic tissue.

An advantage of injections in the MRI scanner is the real time imaging of the catheter for feedback, and prevention of tissue perforation, and the possibility to have direct feedback of the success of injections. The project to develop a MRI compatible catheter was granted by the Life Sciences Health Impulse grant.

Valorization in spin-off company 'CARTcare'

The strong need for technical co-operation in the field of cardiac regenerative therapy has led to the awarding of the business plan written to commercialize the treatment planning and 3D CartBox toolbox. With the BMM spin-off company CARTcare we aim to provide technical solutions to improve cardiac regenerative therapies. With our first product we aim to become the gold standard injection platform for cardiac regenerative therapy. This ambition is founded by the observation that cardiac regenerative therapy currently is the most promising and evolving new therapy for IHD, and therefore will remain of key interest in the upcoming years. Moreover, current developments in biological therapeutics are maturing, but a standardized way to administer the therapeutics is lacking. With our solution we are able to deliver any therapeutic at any desired location in the myocardium in a standardized way. The business plan in chapter 6 of this thesis is based on the scientific work performed for chapter 4, and thereby illustrates the complementary roles of science and valorization. Furthermore, this also emphasizes that the current opinion in medical science that only high impact publications are valuable does not always hold for technological developments. Key to success in this project most likely has been, and will be, the creativity and persistence of the people involved to find the most optimal solution to a problem. Up to now the challenges according to the development of the optimal injection technique in the context of cardiac regenerative therapy have mainly been of an engineering nature. However, in the next phase of the valorization process business development will become more important, requiring different skills. We look forward to this exciting new phase of this project.

PART THREE
ADVANCED ASSESSMENT OF LOCAL CARDIAC FUNCTION

Current application of RF ultrasound based deformation imaging in the field of cardiology is limited to deformation estimation of coronary[35,36] and carotid[37] arteries in patients suffering from a plaque in the respective artery. Before a study was designed to quantify the local effects of cardiac regenerative therapy using local measures of cardiac function, it therefore was important to investigate the use of RF ultrasound to estimate the deformation of the *in vivo* myocardium. The resulting studies reported in chapter 7 and 8 therefore respectively focus on the physiological interpretation of the estimated deformation and on the technical difficulties arising when estimating cardiac deformation by compounding RF ultrasound. Modeling is a strong tool to generate insight into the theoretical explanation of the *in vivo* measurements of cardiac physiology and allows to investigate the causal relations between different parameters of the model and the results. The geometrical model used in chapter 7 was chosen because it most simply reflected the aspects of cardiac motion that we were interested in. The use of a finite element model[22] to investigate the technical difficulties arising when estimating cardiac deformation by RF ultrasound was chosen since it inherits a clinically relevant cardiac deformation pattern, and allowed us to simulate the interaction between cardiac deformation and the ultrasound signal[38]. Moreover since authors were

familiar with the finite element model, the construction of a new analytical model consisting of the complex cardiac deformation pattern for this purpose would have been more laborious. The goal of Part Three of the thesis to develop a technique applicable to measure the local effects of cardiac regenerative therapy was not completely achieved. Main reason for this were the interpretation of the measurement results from healthy tissue, and difficulties to standardize the epicardial data acquisition. The use of RF ultrasound to assess the local effects of cardiac regenerative therapy requires a highly standardized data acquisition setup. The hypothesis that cardiac deformation assessment based on radiofrequency ultrasound analysis can be used to accurately measure myocardial strain, and provided new insights in cardiac biomechanics regarding to the local effects of cardiac regenerative therapy can therefore only be partially adopted. Overall future use of RF ultrasound to measure cardiac biomechanics, and more specifically the local effects of cardiac regenerative therapy is possible, but needs improvement. When using conventional (focused transmission) ultrasound, the frame rate of the acquisitions is the bottleneck for deformation estimation. A solution for the future is the use of plane wave transmission techniques[39]. Via this novel ultrasound principle images can be reconstructed with frame rates up to 10 times higher due to a smart choice of plane wave strategies and ultrafast ultrasound systems. To measure the local effects of cardiac regenerative therapy the use of shear wave imaging might be even more interesting since it directly measures local tissue viscoelasticity[40,41] resembling cardiac contractility in healthy tissue, and tissue stiffness in the remodeled areas. To overcome the problems clarified in chapter 8 a three dimensional matrix array probe should be used as already done in a study by Lopata et al.[42].

Taken together the work presented in this thesis shows how a medical engineer can be of importance to translate scientific questions into technical challenges and develop technical solutions. In the field of advanced delivery techniques a solution was developed to standardize intramyocardial injections by 3D image guided interventions. Besides that, an advanced assessment technique of local cardiac function was investigated to maximize the feedback of cardiac regenerative therapy studies to optimize the therapy. Both techniques investigated in this thesis have great potential to improve cardiac regenerative therapies. Besides technological development, this thesis accentuates that valorization of the results are highly needed to implement the findings in clinical practice. Indeed, these results have led to set up our spin off company, CARTcare. We really look forward to the near future.

References

1. Bui AL, Horwich TB, Fonarow GC. Epidemiology and risk profile of heart failure. Nat Rev Cardiol. 2011;8:30-41
2. Roger VL. Epidemiology of heart failure. Circ Res. 2013;113:646-659
3. Orlic D, Kajstura J, Chimenti S, Bodine DM, Leri A, Anversa P. Bone marrow stem cells regenerate infarcted myocardium. Nature. 2001;410:701-705
4. Smits AM, Laake LWV, Ouden KD, Schreurs C, Szuhai K, van Echteld CJ, Mummery CL, Doevendans PA, Goumans M-J. Human cardiomyocyte progenitor cell transplantation preserves long-term function of the infarcted mouse myocardium. Cardiovascular Research. 2009;83:527-535
5. van der Spoel TIG, Jansen of Lorkeers SJ, Agostoni P, van Belle E, Gyöngyösi M, Sluijter JPG, Cramer MJ, Doevendans PAFM, Chamuleau SAJ. Human relevance of pre-clinical studies in stem cell therapy: systematic review and meta-analysis of large animal models of ischaemic heart disease. Cardiovascular research. 2011;91:649-658
6. Jeevanantham V, Butler M, Saad A, Abdel-Latif A, Zuba-Surma EK, Dawn B. Adult Bone Marrow Cell Therapy Improves Survival and Induces Long-Term Improvement in Cardiac Parameters: A Systematic Review and Meta-Analysis. Circulation. 2012:551-568
7. Zimmet H, Porapakkham P, Porapakkham P, Sata Y, Haas SJ, Itescu S, Forbes A, Krum H. Short- and long-term outcomes of intracoronary and endogenously mobilized bone marrow stem cells in the treatment of ST-segment elevation myocardial infarction: a meta-analysis of randomized control trials. European journal of heart failure. 2011
8. Bursac N. Stem Cell Therapies for Heart Disease: Why Do We Need Bioengineers? IEEE Engineering in Medicine and Biology Magazine. 2007;26:76-79
9. Fomovsky GM, Rouillard AD, Holmes JW. Regional mechanics determine collagen fiber structure in healing myocardial infarcts. Journal of molecular and cellular cardiology. 2012;52:1083-1090
10. Holmes JW, Borg TK, Covell JW. Structure and mechanics of healing myocardial infarcts. Annual review of biomedical engineering. 2005;7:223-253
11. Holmes JW, Nunez JA, Covell JW. Functional implications of myocardial scar structure. American Journal Of Physiology Heart and Crculation Physiology. 1997;41:2123-2130
12. Holmes JW, Yamashita H, Waldman LK, Covell JW. Scar Remodeling and Transmural Deformation After Infarction in the Pig. Circulation. 1994;90:410-420
13. Bijnens B, Claus P, Weidemann F, Strotmann J, Sutherland GR. Investigating cardiac function using motion and deformation analysis in the setting of coronary artery disease. Circulation. 2007;116:2453-2464
14. Ferferieva V, Van den Bergh A, Claus P, Jasaityte R, Veulemans P, Pellens M, La Gerche a, Rademakers F, Herijgers P, D'hooge J. The relative value of strain and strain rate for defining intrinsic myocardial function. American journal of physiology. Heart and circulatory physiology. 2012;302:H188-195
15. van der Spoel TIG, Vrijsen KR, Koudstaal S, Sluijter JPG, Nijsen JFW, de Jong HW, Hoefer IE, Cramer MJM, Doevendans PA, van Belle E, Chamuleau SAJ. Transendocardial cell injection is not superior to intracoronary infusion in a porcine model of ischemic cardiomyopathy: A study on delivery efficiency. Journal of cellular and molecular medicine. 2012:2768-2776
16. Psaltis PJ, Worthley SG. Endoventricular Electromechanical Mapping - The Diagnostic and Therapeutic Utility of the NOGA ® XP Cardiac Navigation System. Journal of Cardiovascular Translational Research. 2008;2:48-62
17. Kumar A, Haralampus CA, Hughes M, Rouy D, Cresswell N, Braun R, Turner D, Amrani D, Motlagh D, Schaer GL. Assessment of safety, accuracy, and human CD34+ cell retention after intramyocardial injections with a helical needle catheter in a porcine model. Catheterization and Cardiovascular Interventions. 2013;81:970-977
18. Gyöngyösi M, Dib N. Diagnostic and prognostic value of 3D NOGA mapping in ischemic heart disease. Nature Reviews Cardiology. 2011;8:393-404
19. Holland AE, Goldfarb JW, Edelman RR. Diaphragmatic and cardiac motion during suspended breathing: preliminary experience and implications for breath-hold MR imaging. Radiology. 1998;209:483-489

20. Shechter G, Ozturk C, Resar JR, McVeigh ER. Respiratory motion of the heart from free breathing coronary angiograms. IEEE Trans Med Imaging. 2004;23:1046-1056
21. Jagsi R, Moran JM, Kessler ML, Marsh RB, Balter JM, Pierce LJ. Respiratory motion of the heart and positional reproducibility under active breathing control. International Journal of Radiation Oncology, Biology, Physics. 2007;68:253-258
22. Bovendeerd PHM, Kroon W, Delhaas T. Determinants of left ventricular shear strain. American journal of physiology. Heart and circulatory physiology. 2009;297:H1058-1068
23. Sengupta PP, Korinek J, Belohlavek M, Narula J, Vannan MA, Jahangir A, Khandheria BK. Left ventricular structure and function: basic science for cardiac imaging. Journal of the American College of Cardiology. 2006;48:1988-2001
24. Tendera M, Wojakowski W. How to measure the effects of the intracoronary stem cell therapy ? European Journal of Echocardiography. 2010;11:438-439
25. Herbots L, D'hooge J, Eroglu E, Thijs D, Ganame J, Claus P, Dubois C, Theunissen K, Bogaert J, Dens J, Kalantzi M, Dymarkowski S, Bijnens B, Belmans A, Boogaerts M, Sutherland G, Van de Werf F, Rademakers F, Janssens S. Improved regional function after autologous bone marrow-derived stem cell transfer in patients with acute myocardial infarction: a randomized, double-blind strain rate imaging study. European heart journal. 2009;30:662-670
26. Nelson MR, Hurst RT, Raslan SF, Cha S, Wilansky S, Lester SJ. Echocardiographic measures of myocardial deformation by speckle-tracking technologies: the need for standardization? J Am Soc Echocardiogr. 2012;25:1189-1194
27. Koopman LP, Slorach C, Hui W, Manlhiot C, McCrindle BW, Friedberg MK, Jaeggi ET, Mertens L. Comparison between different speckle tracking and color tissue Doppler techniques to measure global and regional myocardial deformation in children. Journal of the American Society of Echocardiography. 2010;23:919-928
28. Koopman LP, Slorach C, Manlhiot C, McCrindle BW, Friedberg MK, Mertens L, Jaeggi ET. Myocardial tissue Doppler velocity imaging in children: comparative study between two ultrasound systems. Journal of the American Society of Echocardiography. 2010;23:929-937
29. Negishi K, Lucas S, Negishi T, Hamilton J, Marwick TH. What is the primary source of discordance in strain measurement between vendors: imaging or analysis? Ultrasound in medicine & biology. 2013;39:714-720
30. Arsalan M, Dhein S, Aupperle H, Rastan AJ, Barten MJ, Walther T, Mohr FW, Garbade J. The reverse remodeling effect of mesenchymal stem cells is independent from the site of epimyocardial cell transplantation. Innovations. 2013;8:433-439
31. Duran JM, Taghavi S, Berretta RM, Makarewich CA, Sharp III T, Starosta T, Udeshi F, George JC, Kubo H, Houser SR. Characterization and Targeting of the Infarct Border Zone in a Swine model of Myocardial Infarction. Clinical and Translational Science. 2012;5:416-421
32. Roujol S, Anter E, Josephson ME, Nezafat R. Characterization of respiratory and cardiac motion from electro-anatomical mapping data for improved fusion of MRI to left ventricular electrograms. PLOS ONE. 2013;8:e78852-e78852
33. Witschey WRT, Pilla JJ, Ferrari G, Koomalsingh K, Haris M, Hinmon R, Zsido G, Gorman JH, Gorman RC, Reddy R. Rotating frame spin lattice relaxation in a swine model of chronic, left ventricular myocardial infarction. Magnetic Resonance in Medicine. 2010;64:1453-1460
34. Wang VY, Lam HI, Ennis DB, Cowan BR, Young AA, Nash MP. Modelling passive diastolic mechanics with quantitative MRI of cardiac structure and function. Medical Image Analysis. 2009;13:773-784
35. Nair A, Kuban BD, Tuzcu ME, Schoenhagen P, Nissen SE, Vince GD. Coronary Plaque Classification With Intravascular Ultrasound Radiofrequency Data Analysis. Circulation. 2002;106:2200-2206
36. Goderie TPM, van Soest G, Garcia-Garcia HM, Gonzalo N, Koljenović S, van Leenders GJLH, Mastik F, Regar E, Oosterhuis JW, Serruys PW, van der Steen AFW. Combined optical coherence tomography and intravascular ultrasound radio frequency data analysis for plaque characterization. Classification accuracy of human coronary plaques in vitro. The International Journal of Cardiovascular Imaging. 2010;26:843-850

37. Hansen HHG, Lopata RGP, de Korte CL. Noninvasive carotid strain imaging using angular compounding at large beam steered angles: validation in vessel phantoms. IEEE transactions on medical imaging. 2009;28:872-880
38. Jensen JA, Lyngby D, Medical P, Engineering B, Technology I. Field: A Program for Simulating Ultrasound Systems, Paper presented at the 10th Nordic-Baltic Conference on Biomedical Imaging. Medical & biological engineering & computing. 1996;34:351-353
39. Park S, Aglyamov SR, Scott WG, Emelianov SY. Strain imaging using conventional and ultrafast ultrasound imaging: numerical analysis. IEEE Trans Ultrason Ferroelectr Freq Control. 2007;54:987-995
40. Couade M, Pernot M, Messas E, Bel A, Ba M, Hagege A, Fink M, Tanter M. In vivo quantitative mapping of myocardial stiffening and transmural anisotropy during the cardiac cycle. IEEE transactions on medical imaging. 2011;30:295-305
41. Pernot M, Couade M, Mateo P, Crozatier B, Fischmeister R, Tanter M. Real-time assessment of myocardial contractility using shear wave imaging. Journal of the American College of Cardiology. 2011;58:65-72
42. Lopata RGP, Nillesen MM, Thijssen JM, Kapusta L, de Korte CL. Three-dimensional cardiac strain imaging in healthy children using RF-data. Ultrasound in Medicine & Biology. 2011;37:1399-1408

PART FOUR

Summary and discussion

CHAPTER **10**

Nederlandse samenvatting

Het openscheuren van een intra arteriële plaque in een kransslagader kan leiden tot een trombo-embolische occlusie met als gevolg dat zuurstoftekort optreedt in een deel van de hartspier. In de acute fase leidt deze ischemie tot het afsterven van contractiele hartspiercellen (cardiomyocyten). Wanneer de bloedtoevoer tijdig wordt hersteld door een interventie uit te voeren om de occlusie op te heffen kan de schade worden beperkt, maar nooit helemaal worden opgeheven. Om het verlies aan cardiomyocyten te compenseren, en de functie van het hart om voldoende bloed door het lichaam te pompen te continueren, wordt er littekenweefsel gevormd op de plek van het myocardinfarct. Deze natuurlijke cardiale remodellering leidt echter ook tot een verder verlies van cardiomyocyten en tot progressie van de ziekte naar een chronische vorm en uiteindelijk tot hartfalen[1]. Met medicijnen kunnen de klinische symptomen van de ziekte worden onderdrukt, maar het littekenweefsel kan hiermee niet worden vervangen door gezonde cardiomyocyten. Jaarlijks overlijden wereldwijd meer dan 7 miljoen mensen aan ischemische hartspierziekten (internetpagina WHO Juli 2013). Met de groeiende blootstelling aan risicofactoren wordt verwacht dat het aandeel van ischemische hartziekten in de toekomst verder zal toenemen. De ontwikkeling van alternatieve therapieën om ischemische hartziekten te behandelen is daarom noodzakelijk. Met de ontwikkelingen van de kennis en technieken op het gebied van de biotechnologie zijn nieuwe behandelmethoden voor ischemische hartziekten ontstaan. Deze nieuwe therapieën maken gebruik van stamcellen en de biologisch actieve stoffen die stamcellen uitscheiden. Deze hebben een beschermende werking op de cardiomyocyten en bevorderen biologische processen zoals vasculogenese om de remodellering te beperken[2]. In de meest wenselijke situatie worden de verloren cardiomyocyten vervangen door nieuwe. Dit aanzetten tot herstel van het lichaam wordt regeneratie therapie genoemd en richt zich op het aanzetten van het herstelvermogen van het lichaam na schade. Het vinden van de juiste stamcellen en door stamcellen uitgescheiden factoren voor deze therapie is een uitdaging op het gebied van de biologie. Naast de biologie is er bij de ontwikkeling en toepassing van de therapie ook een belangrijke rol weggelegd voor klinische cardiologen om de translatie tussen de preklinische onderzoeken en klinische toepassing te verzorgen. Naast deze biologische en medische inbreng is er een derde aspect welke betrekking heeft op de technieken om de therapie uit te voeren en de effecten van de therapie te meten[3]. Dit laatste is van belang omdat in de ontwikkelfase van de therapie de te verwachten therapeutische effecten nog onbekend zijn en het eveneens nog onbekend is of met standaard klinische technieken voldoende terugkoppeling kan worden gegenereerd om de therapie efficiënt te kunnen optimaliseren. In dit proefschrift worden twee nieuwe technieken geïntroduceerd om regeneratieve therapie voor ischemische hartziekten te verbeteren:

1. Ontwikkeling van een techniek om de optimale injectielocatie voor cardiale regeneratieve therapie te bepalen en uit te voeren met behulp van een beeld gestuurde katheter injectie techniek.
2. Ontwikkeling van een meettechniek van de lokale hartspierfunctie om de meest optimale terugkoppeling te bewerkstelligen om cardiale regeneratieve therapie te optimaliseren.

Dit proefschrift bevat drie delen waarin deze technieken worden gepresenteerd. **Deel Eén** betreft een overzichtsstudie van alternatieve technieken die kunnen worden gebruikt om de effecten van regeneratieve therapie voor het hart te meten. In **Deel Twee** wordt een nieuwe beeld gestuurde injectietechniek beschreven. In **Deel Drie** wordt een nieuwe

echocardiografie techniek geïntroduceerd om het lokale effect van regeneratieve therapie voor het hart te meten. Naast het wetenschappelijke en sociale belang om inzicht te verkrijgen in het werkingsmechanisme van cardiale stamcel therapie en stamcel therapie te verbeteren wordt in dit proefschrift een derde aspect naar voren gebracht. Dit betreft het sociale en economische belang om de kennis en technieken die zijn ontwikkeld in de wetenschap te exploiteren in een vanuit de universiteit opgericht bedrijf. In dit proefschrift wordt in hoofdstuk 6 een bedrijfsplan gepresenteerd om de techniek die wordt beschreven in hoofdstuk 3 te exploiteren. Dit businessplan is gewaardeerd met de BMM valorization grant.

DEEL ÉÉN
DE TECHNISCHE KANT VAN REGENERATIEVE THERAPIE VOOR HET HART

Cardiale regeneratieve therapie bij ischemische hartziekten richt zich op het beperken van het verlies van cardiomyocyten na een myocardinfarct en het vormen van nieuwe cardiomyocyten. De werkingsmechanismen van de stamcellen en door stamcellen uitgescheiden factoren zijn: 1) vasculogenesis, 2) cardiomyogenesis, en 3) support van de extracellulaire matrix. De effecten van deze mechanismen op de lokale hartspierfunctie kunnen echter niet direct gemeten worden. In de preklinische en klinische studies die tot nu toe zijn uitgevoerd zijn daarom verschillende methoden gebruikt om de therapeutische effecten te kwantificeren. De meest gebruikte methode om therapeutische effecten aan te tonen is door de linker ventrikel (LV) ejectie fractie te meten (LVEF), maar het is de vraag of deze globale maat een goede indruk geeft van de lokale effecten van regeneratieve therapie. In **hoofdstuk 2** wordt een overzicht gegeven van studies waarin naast LVEF alternatieve lokale invasieve en niet invasieve metingen van de hartspierfunctie zijn gedaan om de lokale effecten van de therapie te meten. In deze studie hebben wij op basis van de data uit de studies, en de bestaande kennis over de natuurlijke processen na een myocardinfarct, relaties afgeleid tussen de gemeten parameters en de werkingsmechanismen van regeneratieve therapie. Conclusie van deze studie was dat de verschillende parameters afzonderlijk een beperkte indruk geven van de afzonderlijke werkingsmechanismen. Door een combinatie van metingen te gebruiken kan wel een indruk worden verkregen van de dominante werkingsmechanismen. Omdat de biomechanica van het hart beïnvloedt wordt door de beoogde werkingsmechanismen van regeneratieve therapie, hebben wij geconcludeerd dat het meten van de relatieve vervorming van het hartspierweefsel als maat kan worden gebruikt om de effecten van regeneratieve therapie voor het hart te kwantificeren. Omdat hartspier vervorming ook door andere factoren wordt beïnvloedt zoals de vullingsstatus, tegendruk, en inotrope status is het erg belangrijk om deze te meten en hiervoor te corrigeren[4,5]. Wanneer zo een alomvattende meting wordt toegepast kan een goed inzicht worden verkregen van de therapeutische effecten van cardiale regeneratieve therapie en kan de therapie optimaal worden bijgestuurd teneinde een zo groot mogelijk therapeutisch effect te behalen.

DEEL TWEE
DE INJECTIETECHNIEK

Om regeneratieve therapie voor het hart uit te voeren dienen de stamcellen of de door stamcellen uitgescheiden factoren in de omgeving van het myocardinfarct te worden getransplanteerd. De beschikbare technieken hiervoor beperken zich tot drie routes: 1) chirurgisch, 2) intra-coronair, en 3) intra-myocardiaal. Om chirurgische injecties uit te voeren dient een externe toegang tot het hart te worden gecreëerd. Dit kan via een endoscopie of via een sternotomie. Beide manieren zijn erg belastend voor de patiënt. Intra-coronaire infusie betreft het inspuiten van de cellen in een kransslagader met behulp van een katheter. Hiervoor dient de kransslagader toegankelijk te zijn. Bij intra-myocardiale injecties wordt een katheter in het LV gebracht om injecties in de hartspier te doen. Vanwege de minimaal invasieve toegang tot het hart worden de laatste twee technieken het meest toegepast. Voor het succes van regeneratieve therapie is het erg belangrijk dat er voldoende cellen rondom het infarct gebied aanwezig zijn. Bij alle genoemde technieken is de retentie van de cellen na 4 uur ongeveer 10%[6]. Om de effecten van regeneratieve therapie te maximaliseren is het daarom van belang dat deze 10% in ieder geval op de juiste locatie geïnjecteerd wordt. Ten opzichte van intra-coronaire infusie kan bij intra-myocardiale injectie de injectie locatie door de interventiecardioloog vrij worden gekozen in de wand van het LV. Het meest gebruikte intra-myocardiale injectiesysteem is het NOGA®XP systeem[7]. Met dit systeem kunnen door middel van een katheter lokale metingen worden gedaan van de elektrische geleiding en van de lokale deformatie van het hart. Omdat in het infarct gebied de elektrische en mechanische activiteit is verminderd, kan deze informatie worden gebruikt om injectielocaties te bepalen. Omdat deze techniek voorafgaand aan de injecties veel metingen met speciale katheters verreist, is deze methode duur, tijdrovend, en moeilijk te standaardiseren. De gouden standaard techniek om de grootte en locatie van het infarct te meten is MRI waarbij gebruik wordt maakt van het contrastmiddel Gadolinium[8]. Door de MRI metingen te gebruiken om het infarct en de randgebieden van het infarct te visualiseren en deze tijdens de injectie procedure te gebruiken om de katheter naar de juiste locatie te sturen, kunnen injecties beter gestandaardiseerd worden waardoor de therapie efficiënter kan worden geoptimaliseerd. In **hoofdstuk 3** worden de ontwikkeling en de eerste resultaten van de treatment planning en 3D CartBox software toolbox in een diermodel beschreven. Deze software toolbox is ontwikkeld tijdens dit promotietraject. Het treatment planning algoritme kan worden gebruikt om de (rand) gebieden van het infarct met een relatieve infarctdikte tussen 0 en 100% van de totale lokale dikte van de hartspier te bepalen. Met behulp van de 3D CartBox beeld registratie toolbox kunnen de randgebieden op een 3D model van het hart worden geprojecteerd. De katheter wordt ook met dit 3D model gefuseerd om beeld gestuurde intra-myocardiale injecties mogelijk te maken. De conclusies van deze studie waren dat 1) De nauwkeurigheid van de 3D CartBox beeld registratie methode voldoende is voor klinische toepassing. 2) De infarctlocatie en transmuraliteit die wordt bepaald met het NOGA®XP systeem niet altijd in overeenstemming is met de gouden standaard MRI techniek. En 3) De treatment planning in combinatie met 3D CartBox van complementaire waarde kan zijn tijdens injectie procedures in het kader van regeneratieve therapie voor het hart. Na deze eerste studie om deze techniek te testen is deze techniek toegepast op een dataset van 17 varkens met een chronisch myocardinfarct. In **hoofdstuk 4** hebben wij onderzocht in welke mate de met NOGA®XP gemeten parameters gerelateerd zijn aan de lokale eigenschappen van de infarctgebieden die met

behulp van de gouden standaard MRI techniek zijn gediagnosticeerd. De conclusies uit deze studie waren dat 1) De overlap tussen infarct gebieden bepaald door NOGA®XP en MRI beperkt is. 2) De elektrische signalen gemeten met NOGA®XP wel in staat zijn om infarct en gezond weefsel te onderscheiden, maar geen goede indicatie geven van de relatieve dikte van het infarct ten opzichte van de dikte van de hartspier. 3) De mechanische parameter gemeten met NOGA®XP niet overeenkomt met de verdikking van de wand gemeten met MRI. En 4) het treatment planning algoritme goed in staat is om het (rand) gebied van een infarct met een relatieve infarctdikte te bepalen. Om deze informatie te gebruiken tijdens de injectieprocedure moet de injectie katheter gefuseerd worden met de MRI data met behulp van 3D CartBox. 3D CartBox maakt hiervoor gebruik van de eind diastolische opnames van de MRI en van de eind diastolische opnames van de katheter posities. Echter, de MRI opnames worden gemaakt tijdens maximale uitademing van de patiënt, en tijdens de katheter procedure kan de patiënt gewoon doorademen. Dit heeft een verplaatsing van het hart in de thorax tot gevolg van ongeveer 1 cm in verschillende richtingen[9]. Het resultaat hiervan is dat de registratie niet optimaal geschiedt waardoor foutieve injectielocaties kunnen worden benaderd. Om deze fout te minimaliseren beschrijven wij in **hoofdstuk 5** een ademhalingscorrectie techniek waarmee de katheter posities kunnen worden gecorrigeerd voor beweging veroorzaakt door de ademhaling, en worden weergegeven op de eind diastolische locatie. Het principe van deze techniek hebben wij met goed resultaat kunnen aantonen met behulp van een fantoom. Daarnaast hebben wij in een kleine dierstudie eveneens aangetoond dat het principe werkt, maar zagen wij geen verbetering van de registratie. Dit werd hoofdzakelijk veroorzaakt omdat de respiratie slechts een geringe beweging van het hart veroorzaakt in het gekozen varkens model. In **hoofdstuk 6** wordt een bedrijfsplan beschreven om de in hoofdstuk 3 ontwikkelde techniek te commercialiseren. Dit bedrijfsplan is gewaardeerd met de BMM valorisatie subsidie van € 200.000,- waarmee de spin-off company "CARTcare" zal worden opgericht met als doel om nieuwe technieken te ontwikkelen om regeneratieve therapie voor het hart te verbeteren.

DEEL DRIE
HET METEN VAN DE LOKALE THERAPEUTISCHE EFFECTEN

Eén van de alternatieve parameters die kan worden gebruikt om het effect van regeneratieve therapie op het hart te bepalen, is door het meten van de lokale vervorming van de hartspier. Hiervoor zijn verschillende technieken beschikbaar. In **hoofdstuk 7** wordt een studie beschreven waarin het gebruik van radio frequent (RF) ultrageluid voor dit doel is onderzocht. Bij RF ultrageluid worden geluidsgolven met een hoge frequentie (8.7 MHz) in het weefsel gestuurd, door het weefsel gereflecteerd, en weer gemeten. Door de teruggekaatste signalen op achtereenvolgende tijdspunten met elkaar te vergelijken met behulp van een kruiscorrelatie functie kan de vervorming van het weefsel worden berekend[10]. In de studie in **hoofdstuk 7** is gebruik gemaakt van proefdieren met een chronisch myocardinfarct waarbij metingen zijn uitgevoerd in het gezonde en in het infarct weefsel. Daarnaast is een geometrisch model gebruikt om de resultaten van deze metingen theoretisch te onderbouwen. De conclusies uit deze studie waren dat de vervorming van het gezonde weefsel zowel in de radiale als de longitudinale richting van de hartspier een transmurale gradiënt heeft. Deze gradiënt was verminderd in het myocardinfarct. Uit de metingen is

verder gebleken dat relatieve radiale vervorming (verdikking) van het endocardiaal gelegen myocard kan oplopen tot 80%. Het geometrische model is afgeleid van de afmetingen en de vervormingen van de harten die zijn gebruikt bij de experimenten, en daarnaast gebaseerd op de niet compressibiliteit van het hartspierweefsel. De piekwaarden die zijn gemeten in de experimenten zijn eveneens in het geometrische model waargenomen. Op deze manier is bevestigd dat de vervormingsmetingen op basis van RF ultrageluid in samenspraak zijn met de bestaande theorie over cardiale biomechanica. In **hoofdstuk 8** zijn wij met stapje verder gegaan met RF ultrageluid. Door de geluidsgolven intermitterend onder hoeken van +20, 0, en -20 graden het weefsel in te zenden kunnen de vervormingen in de richting loodrecht op de stand van de ultrasound transducer ook worden berekend. Om te onderzoeken of deze compounding techniek van toegevoegde waarde is om de vervorming van de hartspier te meten, en welke factoren hierop van invloed zijn hebben we deze techniek in **hoofdstuk 8** onderzocht met behulp van simulaties en een diermodel. Voor de simulaties is hiervoor gebruik gemaakt van een eindige elementen model van LV mechanica[11]. Uit deze studie is naar voren gekomen dat de combinatie van weefselsnelheid en opname frequentie van het ultrageluid, en de beweging in de richting loodrecht op het beeldvlak bepalen of de RF analyse en in het bijzonder de RF compounding analyse succesvol is. De oriëntatie en de activatie van de hartspiercellen zorgt voor een complexe drie dimensionale vervorming van het hart. Bij opnames in een enkel vlak zoals tijdens deze studie is gedaan kan dan slechts de twee dimensionale vervorming worden gemeten. De beweging in de richting loodrecht op dit vlak bemoeilijkt de analyse en leidt tot een grotere fout van de berekende weefsel verplaatsingen. Door bij compounding opnames ultrageluid onder 3 hoeken in het weefsel te zenden, wordt de opname frequentie met een factor 3 verlaagd. Dit leidt tot verkeerd berekende weefsel verplaatsingen in de fases van de hartcyclus waar de weefsel verplaatsingen het grootst zijn. RF compounding presteert alleen beter dan de 0 graden RF analyse bij het berekenen van de longitudinale verplaatsingen in de fases van de hartcyclus waar de weefsel verplaatsingen het laagst zijn. De hoge snelheid van het weefsel in het diermodel veroorzaakte dat alleen de axiale strain correct kon worden berekend.

Toekomstvisie

Regeneratieve therapie voor het hart richt zich op de bescherming en herstel van cardiomyocyten na een hartinfarct. Omdat na een hartinfarct altijd blijvende schade optreedt kan het beperken van deze schade grote verbetering van de hartfunctie veroorzaken. Vijftien jaar geleden werden de eerste basale studies gepubliceerd waarin regeneratie van het hart werd beschreven[12]. Bij deze studies werden de eenvoudig te isoleren beenmerg stamcellen direct in het randgebied van het infarct geïnjecteerd. Omdat de effecten in die eerste studie klein waren en niet altijd konden worden gereproduceerd, zijn er sindsdien vele stappen gezet om de therapie te verbeteren. Deze ontwikkelingen hebben zich in eerste instantie beperkt tot het type cel dat werd geïnjecteerd, de injectietechniek, en het moment van injecteren. De laatste tijd ontstaat er meer interesse in het combineren van de biologische materialen (cellen en de door cellen uitgescheiden factoren) met biomaterialen. Biomaterialen zijn biologisch inerte materialen die kunnen worden aangepast om de optimale condities voor zowel de cellen als voor het hart te creëren. Van cruciaal belang voor alle toekomstige ontwikkelingen blijven echter: 1) het injecteren van de therapeutische media op de optimale plaats in het hart, en 2) het meten van de effecten van de therapie op de lokale hartspierfunctie. Door de ontwikkeling van nieuwe technologieën op deze

twee gebieden kan regeneratieve therapie voor het hart in de toekomst efficiënt worden verbeterd. De twee technieken die in dit proefschrift worden beschreven kunnen daarmee van grote waarde worden voor cardiale regeneratieve therapie. Met het opzetten van het bedrijf 'CARTcare' hebben wij als doel om de optimale injectielocatie voor een grote groep gebruikers beschikbaar te maken en de eerste stap te zetten richting standaardisatie van de therapie. Hiermee behouden de gebruikers de vrijheid om zelf het therapeutische medium te ontwikkelen en zo in de toekomst maximale therapeutische effecten te bewerkstelligen. Omdat zowel ultrasound als MRI de mogelijkheid bieden om zowel de optimale injectielocatie te bepalen, als de lokale functie te meten, zullen in de toekomst technieken beschikbaar komen waarin de twee bovengenoemde aspecten verder geïntegreerd worden. De biologische, medische, en technologische ontwikkelingen zullen tezamen een geheel nieuwe cardiale regeneratieve therapie voortbrengen waarin het therapeutische effect gemaximaliseerd is. Hiermee kan regeneratieve therapie voor het hart in de toekomst doorgroeien naar een standaard klinische therapie.

References

1. Holmes JW, Borg TK, Covell JW. Structure and mechanics of healing myocardial infarcts. Annual review of biomedical engineering. 2005;7:223-253
2. Dimmeler S, Zeiher AM, Schneider MD. Review series Unchain my heart: the scientific foundations of cardiac repair. 2005;115
3. Bursac N. Stem Cell Therapies for Heart Disease: Why Do We Need Bioengineers? IEEE Engineering in Medicine and Biology Magazine. 2007;26:76-79
4. Bijnens B, Claus P, Weidemann F, Strotmann J, Sutherland GR. Investigating cardiac function using motion and deformation analysis in the setting of coronary artery disease. Circulation. 2007;116:2453-2464
5. Ferferieva V, Van den Bergh A, Claus P, Jasaityte R, Veulemans P, Pellens M, La Gerche a, Rademakers F, Herijgers P, D'hooge J. The relative value of strain and strain rate for defining intrinsic myocardial function. American journal of physiology. Heart and circulatory physiology. 2012;302:H188-195
6. van der Spoel TIG, Vrijsen KR, Koudstaal S, Sluijter JPG, Nijsen JFW, de Jong HW, Hoefer IE, Cramer MJM, Doevendans PA, van Belle E, Chamuleau SAJ. Transendocardial cell injection is not superior to intracoronary infusion in a porcine model of ischemic cardiomyopathy: A study on delivery efficiency. Journal of cellular and molecular medicine. 2012:2768-2776
7. Ben-Haim SA, Osadchy D, Schuster I, Gepstein L, Hayam G, Josephson ME. Nonfluoroscopic, in vivo navigation and mapping technology. Nature Medicine. 1996;2:1393-1395
8. McNamara MT, Higgins CB, Ehman RL, Revel D, Sievers R, Brasch RC. Acute myocardial ischemia: magnetic resonance contrast enhancement with gadolinium-DTPA. Radiology. 1984;153:157-163
9. Jagsi R, Moran JM, Kessler ML, Marsh RB, Balter JM, Pierce LJ. Respiratory motion of the heart and positional reproducibility under active breathing control. International Journal of Radiation Oncology, Biology, Physics. 2007;68:253-258
10. Lopata RGP, Nillesen MM, Hansen HHG, Gerrits IH, Thijssen JM, de Korte CL. Performance evaluation of methods for two-dimensional displacement and strain estimation using ultrasound radio frequency data. Ultrasound in medicine & biology. 2009;35:796-812
11. Bovendeerd PHM, Kroon W, Delhaas T. Determinants of left ventricular shear strain. American journal of physiology. Heart and circulatory physiology. 2009;297:H1058-1068
12. Orlic D, Kajstura J, Chimenti S, Bodine DM, Leri A, Anversa P. Bone marrow stem cells regenerate infarcted myocardium. Nature. 2001;410:701-705

PART FIVE

Appendices

Dankwoord/ Acknowledgments

Curriculum Vitae

List of publications

Dankwoord/ Acknowledgments

Dit proefschrift is het resultaat van ruim 4 jaren werk in het UMC Utrecht. Vier jaren werk op het grensvlak van geneeskunde, biologie en engineering. Een grensvlak dat volop in ontwikkeling is en waar veel mogelijkheden zijn. Het zijn ook drie vakgebieden met ieder hun eigen unieke benadering van het probleem waarover dit proefschrift gaat: chronische ischemische hartziekten. Het was een voorrecht om met mensen uit de verschillende disciplines te werken, en van ze te leren. Dit heeft geresulteerd in een groot aantal mensen die allemaal grote en kleine bijdragen hebben geleverd aan dit proefschrift. Allemaal persoonlijke contacten die naast de hulp bij de totstandkoming dit boekje mij een zeer prettige werkomgeving hebben bezorgd de afgelopen jaren. Bedankt allemaal!

Prof. dr. P.A.F.M. Doevendans, Beste **Pieter**, Innoveren, patenteren, entrepreneuren! Hoewel het laatste geen correct werkwoord is zou jij deze volgorde graag bij alle nieuwe projecten aanhouden. Iedereen weet natuurlijk dat dat onmogelijk is, en in sommige gevallen ook onwenselijk, maar ik ben met je eens dat het absoluut geen kwaad kan om af en toe als entrepreneur naar de projecten te kijken. Ik heb dan ook erg genoten van de brainstorm sessies die we gezamenlijk en met het hele stamcel lab hebben gehouden. Misschien is het deze insteek waardoor ik nu bezig ben om mijn idee voor een nieuwe beeld gestuurde injectietechniek te commercialiseren. Naast onze gezamenlijke passie voor innovaties houden we beide erg van fietsen. Zo heb ik persoonlijk ook mooie herinneringen aan de bewuste tocht in de Ardennen waarbij ik jou tijdens het beklimmen van de Wanneranval ongeveer 20 meter voor mij zag rijden. Ik moet eerlijk zeggen dat ik even had ingehouden voordat ik je met twee vingers in de neus kwam inhalen, maar de blik op jou gezicht was onvergetelijk! Bedankt voor de mooie samenwerking, ik denk dat we nog mooie uitvindingen gaan doen!

Dr. S.A.J. Chamuleau, Beste **Steven**, Jij was net begonnen als Cardioloog in het UMC toen je de eindpresentatie van mijn master thesis bijwoonde. Ik moet een goede indruk hebben gemaakt want een week later hadden we een afspraak en nog wat later was ik de derde promovendus onder jou hoede. Een engineer in het stamcel team. Een nieuwe ervaring voor mij, maar zeker ook voor jou. Door je toewijding aan het onderzoek, en je openheid voor nieuwe dingen heb ik vier jaar met veel plezier met je samengewerkt. Je enthousiasmerende begeleiding werkte altijd aanstekelijk en heeft me meer dan eens geholpen om door de onvermijdbare dalen van mijn promotie te geraken. Naast het professionele vlak kunnen we het op het persoonlijke vlak ook goed vinden samen. De grappen en lachsalvo's tijdens onze besprekingen zijn talrijk, en creëren een ontspannen sfeer. Hierin zorgen onze verschillende expertises voor een mooie complementaire samenwerking wat al heeft geresulteerd in het binnenhalen van twee mooie subsidies. Ik denk dat we nog mooie dingen gaan doen!

Dr. C.L. de Korte, Beste **Chris**, Je publicaties op het gebied van ultrageluid elastografie waren me al een tijdje opgevallen en toen ik de kans kreeg om met je te gaan samenwerken heb ik die meteen gegrepen. Bij het Radboud UMC in Nijmegen heb je met MUSIC (Medical Ultraound Imaging Centre) een mooie groep opgebouwd. Dat vind ik een perfect voorbeeld van het combineren van technisch onderzoek en ontwikkeling in de kliniek. Door jouw enthousiasme en kennis op het gebied van ultrageluid hebben

we mooi onderzoek kunnen doen waarmee ik al op meerdere congressen succes heb geboekt. Op de dagen dat ik bij jullie in Nijmegen was heb ik genoten van de rustige werksfeer, de gezellige koffiepauzes, en de constructieve discussies. Naast de professionele en persoonlijke contacten houden we elkaar ook op sportief gebied goed in de gaten. Als ik weer een fietstocht op Strava heb geüpload duurt het meestal niet zo lang tot jij een reactie geeft. Bij jou ben ik er maar mee gestopt want die schier oneindige stroom aan uploads van je hardloop rondjes was niet meer bij te houden. Als het weer mooi weer is gaan we een keer fietsen!

Dr, J.P.G. Sluijter, Beste **Joost**, Als hoofd van de stam cel groep van de afdeling cardiologie kreeg je ineens een engineer in je team en bij de wekelijkse bespreking. Met mijn volledig andere benadering van het hart met behulp van modellen heb ik je wenkbrauwen menigmaal doen fronsen. Maar je stond altijd open voor mijn input en gaf constructieve feedback. Dat was voor mij heel erg nuttig. In het lab heb je een mooie groep opgebouwd en de BBQs bij jou thuis zijn echt heel gezellig. Bedankt voor de fijne samenwerking!

Dr. Ir. P.H.M. Bovendeerd, Beste **Peter**, Jouw passie om cardiale biomechanica te onderzoeken en te onderwijzen heeft op mij aanstekelijk gewerkt. Als engineer in de kliniek zag ik het ook als doel om de theoretische kennis op dit gebied toe te passen in de kliniek. Toen ik enigszins de kans kreeg om het eindige elementen model van de LV mechanica in mijn promotie te incorporeren heb ik dat gedaan. Toen ik aan het begin van mijn promotie de behoefte had om de technisch aspecten van mijn onderzoek, of de zaken waar ik als engineer in de kliniek tegenaan liep te bespreken kon ik bij jou terecht. Heel erg bedankt daarvoor.

De leden van de lees commissie, **prof dr. W.P.T.M. Mali, prof. dr. G. Pasterkamp, prof. dr. P.R. Luijten, prof. dr. J. D'hooge, prof. dr. F.W. Prinzen**, bedankt voor de bereidheid zitting te nemen in de beoordelingscommissie van mijn proefschrift.

De staf van de afdeling experimentele cardiologie, Beste **Gerard, Imo**. Mede dankzij jullie draait de afdeling als een goed geoliede machine. Bedankt voor jullie inhoudelijke inbreng bij mijn projecten, en het delen van jullie ervaring om de basale resultaten te valoriseren.

Dr. S. Koudstaal, Beste **Stefan**, Ko, Ik heb maar vast Dr. Voor je naam gezet want ten tijde van het verschijnen van dit proefschrift ben jij al een tijdje gepromoveerd. Het was een tijdje een nek aan nek race tussen ons wie het eerste klaar zou zijn, maar eigenlijk ook niet. Met het plan om cardioloog te worden zat jij reeds vanaf het begin in de 'fast track'. In het begin zaten we met 3 man op 3 vierkante meters in 'de bunker'. Het was soms afzien, maar ook heel gezellig. Na onze verhuizing naar 'de villa' kregen we meer ruimte en bleef het gezellig. Ik heb erg genoten van onze uitstapjes naar Liverpool en New York, en onze discussies over het werk en privézaken, en wens je heel veel succes bij je verdere carrière. Ik weet zeker dat we elkaar in de toekomst blijven spreken en samen nog veel hamburgers gaan bakken. Ik vind het erg leuk dat je mijn paranimf bent.

Beste I**ng Han**, Gho, Wij hebben maar kort samen in 'de bunker' gezeten toch zijn mijn herinneringen aan die tijd levendig. Het moet zijn omdat het in deze fase erg gezellig was en het 'Gho-Slo-Ko' trio is ontstaan. Het was een mooi moment toen jij het vaste lunch telefoontje opnam met deze woorden. Met je rustige uitstraling en je slimme inbreng in

onze discussies heb je me erg geholpen tijdens mijn promotie en ben je van grote waarde voor het team. Ook buiten het werk hebben we al veel dingen samen gedaan. Naast onze trip naar Liverpool om Stefan te bezoeken proberen we ons allebei te bekwamen in het schaatsen. Dat is leuk, en ook erg gezellig. Gelukkig hebben we na een vliegende start op de golfbaan ook allebei ingezien dat de golfsport niet onze roeping is. Ik vind het erg leuk dat je mijn paranimf bent.

Beste Tycho, Jij zat in je eentje in 'de bunker' toen ik, en later Stefan erbij kwamen. Ineens had je nog maar 1/3 deel van een toch al te kleine ruimte. Daarover heb ik je nooit horen klagen. Ik bewonder je werklust en denk dat je daarmee in je huidige opleiding en je carrière in de cardiologie een mooie toekomst tegemoet gaat. Naast het werken samen heb ik ook mooie herinneringen aan onze deelname aan de estafetteloop naar Parijs. De fysieke inspanning in een veranderend landschap met mooie lichteffecten, een surrealistische ervaring. Mooi om mee te maken.

Beste René, Sanne, Cheyenne, De nieuwe harde kern van de Chamuleau stamcel groep. René, je begon als Technisch Geneeskunde student op het beeld gestuurde injectie project. Mede dankzij jou is hiervoor mooie software ontwikkeld wat aan de basis heeft gestaan van het spin-off bedrijf CARTcare. Je 'out of the box' manier om dingen aan te pakken heeft meer dan eens geleidt tot een alternatieve aanpak en is daarmee ook van grote waarde voor het team. Onze samenwerking is gelukkig nog niet ten einde, maar als we in de toekomst nog eens samen gaan vliegen moeten we proberen om het vliegtuig niet te missen! Beste Sanne, je kwam binnen als de studente van Tycho met die interessante achternaam. Soms zaten we dan met vier man in 'de bunker'. Niets aan de hand. Daarna, tijdens het optimaliseren en interpreteren van de analyses voor het HMR project heb ik erg genoten van onze discussies over de coronaire fysiologie. Dat was leuk en nuttig. Onze recente trip naar stamcel congres in New York was ook erg gezellig! Vooral het bezoek aan de basketbal wedstrijd van de New York Knicks staat in mijn geheugen gegrift! High-fiven met onze buren uit de Bronx! Wauw! Beste Cheyenne, Jij bent de jongste aanwinst voor het stamcel team, maar met je enthousiaste instelling heb je je plekje al helemaal veroverd. Ik kijk uit naar onze samenwerking in de toekomst.

Het stamcel lab van de afdeling cardiologie. Beste Krijn, Alain, Marish, Dries, Zhiyong, Hamid, Jia, Esther, Corina, Judith, Peter Paul, Vera, Roberto, als ik af en toe weer eens de voortgang mijn projecten bij de stamcel besprekingen presenteerde kon ik na een tijdje aan jullie gezichten zien waar mijn boodschap strandde. Erg handig, want zo kon ik steeds beter inspelen op jullie vragen. Andersom was het ook vaak zo dat ik op mijn beurt jullie projecten op het gebied van de moleculaire biologie en werk met transgene muizen maar moeilijk te begrijpen vond. Maar uiteindelijk werken we toch allemaal aan de oplossing van hetzelfde probleem en hebben jullie me veel geleerd over de biologie en jullie werk en jullie oplossingen door me gewoon mee te laten kijken. Ik heb met heel veel plezier met jullie samengewerkt!

De mensen van het Medical Ultrasound Imaging Centre. Beste Rik, Maartje, Jan, Stein, Anne, Gert, Tim, in jullie kantoortuin in het UMC st Radboud heerste altijd een bijna serene rust. Heerlijk. Op mijn werkplek in het UMC Utrecht heb ik dit vaak gemist, en als ik bij jullie was kon ik dan ook altijd goed werken. Als we dan even gingen koffie drinken, waar

in mijn herinnering altijd iets lekkers bij was, of gingen lunchen was het altijd ook erg gezellig. Na afronding van mijn promotie kom ik dan ook zeker nog eens langs met iets lekkers voor bij de koffie!

Alle onderzoekers van de afdeling cardiologie. Beste **Geert, Margot, Marieke, Willemien, Roos, Mariam, Martine, Freek, Jetske, Marloes, Mieke, Manon, Remco, Cas, Judith, Thomas, Gijs**, waar aan het begin van mijn promotie 3 onderzoekers op de afdeling cardiologie gestationeerd waren, zijn dat er dus nu 14, en is er een grote kans dat ik daarbij nog wel iemand vergeten ben. Met zijn allen roulerend over de spaarzame werkplekken hebben we er het beste van gemaakt en was het ook altijd erg gezellig tijdens de lunch, congressen, en het eten van taart vanwege alweer een verjaardag. Ik wens jullie allemaal veel succes bij jullie eigen promoties.

Alle stafleden van de afdeling cardiologie. Bedankt voor jullie kleine en grote bijdragen aan mijn onderzoek. Beste **Tamara, Sylvia, Jantiene**, bedankt voor de gezelligheid in jullie kamer en alle zaken die jullie voor mij geregeld hebben.

Experimentele cardiologie medewerkers in het GDL. Beste **Merel, Cees, Joyce, Ben, Marlijn, Maringa, Grace, Gerard, Martijn, Evelyn**, Heel erg bedankt voor de prettige werksfeer en jullie vakkundigheid en inzet bij het uitvoeren van de experimenten voor dit proefschrift. Het meedoen met het mudmasters spektakel was een passende afsluiting en zal ik nooit vergeten!

Lieve (al dan niet fietsende) vrienden, **Wannes, Eltjo, Paul, Bram de V, Bram vd H, Geert, Gert, Rob, Sander, Dirk, Mats, Frank, Wilbert, Suzanne**. Het contact is de laatste tijd niet met iedereen even frequent geweest, maar altijd als ik bij jullie was en we iets leuks gingen doen was het meteen weer als vanouds. Het is heel erg mooi om jullie als vrienden te hebben.

Lieve Familie, **Pap, Mam, Geesje, Karam, Hilde, Elise** wat fijn dat jullie mijn familie zijn. Lieve **Pap en Mam** bedankt voor jullie onvoorwaardelijke steun bij alles wat ik doe. Hoe bochtige mijn levenspad ook lijkt: studeren, werken, studeren, promoveren, op jullie kan ik altijd rekenen. Behalve onze gedeelde zorg voor levende wezens lijkt jullie werk op de boerderij ogenschijnlijk in niets op mijn werk in het ziekenhuis, de essentie heb ik toch wel van jullie geleerd: een open en geïnteresseerde levenshouding in combinatie met hard werken. Het is mooi om te zien hoe jullie hiermee nog steeds nieuwe dingen ontdekken en ook veel plezier hebben! Jullie zijn me lief. Lieve **Geesje en Karam**, het is erg mooi om te zien hoe leuk jullie het samen hebben in Amsterdam. Ik vind het altijd fijn om bij jullie te zijn en te praten over de dingen die ons bezighouden. Als jullie daarbij van die heerlijke gerechten op tafel blijven zetten overweeg ik om ook naar Amsterdam te verhuizen! Bedankt voor jullie steun en ik wens jullie heel veel geluk samen. Lieve **Hilde**, We zien elkaar niet zo vaak, maar gelukkig is er de telefoon. Altijd als ik je spreek is het goed en merk ik hoeveel we gemeenschappelijk hebben. Bedankt voor al je steun. Lieve **Elise**, gezellig dat je ook in onze familie bent gekomen. Met je vrolijke en sportieve natuur pas je er goed bij! Je hebt als fysio al menig advies kunnen gegeven, iets wat in de toekomst nog wel vaker voor gaat komen vrees ik. Ik wens jullie heel veel geluk samen.

Frebus

Curriculum Vitae

Frebus Jan van Slochteren was born on September 3rd 1977 in Oldekerk, the Netherlands and was raised in Niekerk. At the age of 10 the family moved to the neighboring village Faan to live on a farm. At the age of 14 Frebus graduated from lower general secondary education (MAVO) and continued with secondary vocational education (MTS) in Groningen to study mechanical engineering. After graduation and at the age of 19 Frebus moved to Utrecht to study Industrial Automation and Control Systems Engineering at the University of applied Sciences. At the age of 24 Frebus received his MSc degree and started working as a Robot Application Engineer. Shortly thereafter the medical field appeared to be more interesting and Frebus changed to a job as a Biomedical Engineer at the University Medical Center Utrecht. After 2 years of working Frebus decided to study Medical Engineering at the Eindhoven University of Technology. At the age of 31 Frebus received his second MSc degree after finishing his Master Thesis at the department of Cardiology of the University Medical Center Utrecht. During the Master Thesis project Frebus studied the electromechanical behavior of the left ventricle in healthy hearts and hearts with WPW pathology by means of an finite element model of the left ventricle. The master thesis project was supervised by Dr. B.W.L. De Boeck and Dr. Ir. P.H.M. Bovendeerd. During the master thesis Frebus' attention was drawn to research and in 2010 he started as a PhD student in the department of Cardiology of the University Medical Center Utrecht. This PhD study was performed as a part of the BMM SMARTCARE project granted to prof. dr. P.A.F.M. Doevendans. In this project new regenerative therapies are developed for ischemic heart disease. As a part of the project Frebus (co-)authored multiple peer-reviewed papers and presented his work at national and international congresses. Under supervision of Dr S.A.J. Chamuleau and Dr. Ir. C.L de Korte the project resulted in the PhD thesis entitled 'Technical solutions to improve cardiac regenerative therapy'. Besides the PhD thesis, the work performed to optimize the injection technique used for cardiac regenerative therapy got granted with the BMM valorization grant. This will lead to the founding of the spin-off company 'CARTcare' with the mission to develop technical solutions to improve cardiac regenerative therapy. In the upcoming years Frebus will continue working in the department of Cardiology of the University Medical Center Utrecht to proceed with the developments that have been deployed.

List of publications

Bastings MM, Koudstaal S, Kieltyka RE, Nakano Y, Pape AC, Feyen DA, **van Slochteren FJ**, Doevendans PA, Sluijter JP, Meijer EW, Chamuleau SAJ, Dankers PY.
A Fast pH-Switchable and Self-Healing Supramolecular Hydrogel Carrier for Guided, Local Catheter Injection in the Infarcted Myocardium.
Adv Healthc Mater. 2014;3:70-78

Grundeman PF, van der Spoel TI, Steendijk P, **van Slochteren FJ**, Cramer MJ, Doevendans PA, Pasterkamp G.
Surgical left ventricular radius enlargement by patch insertion on the beating heart: a new experimental aneurysm model.
Interact Cardiovasc Thorac Surg. 2012;15:10-13

Koudstaal S, Bastings MM, Feyen DA, Waring CD, **van Slochteren FJ**, Dankers PY, Torella D, Sluijter JP, Nadal-Ginard B, Doevendans PA, Ellison GM, Chamuleau SA.
Sustained delivery of insulin-like growth factor-1/hepatocyte growth factor stimulates endogenous cardiac repair in the chronic infarcted pig heart.
J Cardiovasc Transl Res. 2014;7:232-241

Koudstaal S, Jansen of Lorkeers SJ, Gaetani R, Gho JMIH, **van Slochteren FJ**, Sluijter JPG, Doevendans PA, Ellison GM, Chamuleau SAJ.
Concise Review: Heart Regeneration and the Role of Cardiac Stem Cells.
Stem cells translational medicine. 2013;2:0-0

Koudstaal S, Jansen Of Lorkeers SJ, **van Slochteren FJ**, van der Spoel TI, van de Hoef TP, Sluijter JP, Siebes M, Doevendans PA, Piek JJ, Chamuleau
SA. Assessment of coronary microvascular resistance in the chronic infarcted pig heart.
J Cell Mol Med. 2013;17:1128-1135

Stecher D, **van Slochteren FJ**, Hoefer IE, Pasterkamp G, Tulleken CA, van Herwerden LA, Buijsrogge MP.
The nonocclusive laser-assisted coronary anastomotic connector in an off-pump porcine bypass model.
J Thorac Cardiovasc Surg. 2013

van Slochteren FJ, Teske AJ, van der Spoel TI, Koudstaal S, Doevendans PA, Sluijter JP, Cramer MJ, Chamuleau SA.
Advanced measurement techniques of regional myocardial function to assess the effects of cardiac regenerative therapy in different models of ischaemic cardiomyopathy.
Eur Heart J Cardiovasc Imaging. 2012;13:808-818

van Slochteren FJ, van der Spoel TI, Hansen HH, Bovendeerd PH, Doevendans PA, Sluijter JP, Chamuleau SA, de Korte CL.
Layer-specific radiofrequency ultrasound-based strain analysis in a porcine model of ischemic cardiomyopathy validated by a geometric model.
Ultrasound Med Biol. 2014;40:378-388